

# CELL JOURNAL

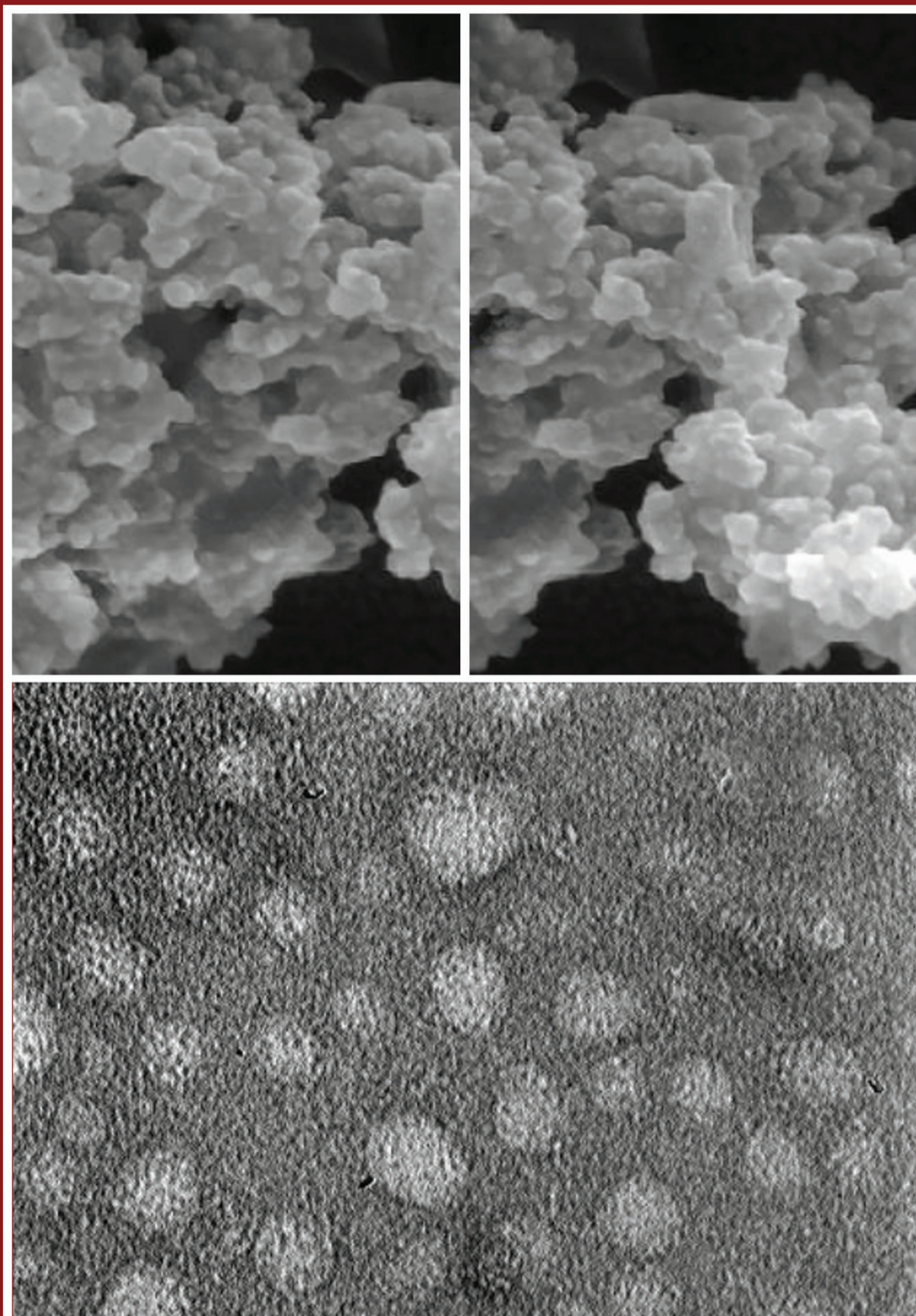
(Yakhteh)

Vol 26, No 1, January 2024, Serial Number: 120  
Pages: 1-90

ISSN: 2228-5806

eISSN: 2228-5814

[www.celljournal.org](http://www.celljournal.org)



A monthly publication of the Royan Institute



پژوهشگاه رویان

**Aims and Scope:** The "Cell Journal (Yakhteh)" is a peer review and monthly English publication of Royan Institute of Iran. The aim of the journal is to disseminate information by publishing the most recent scientific research studies based on medical and developmental biology including cell therapy and regenerative medicine, stem cell biology reproductive medicine, medical genetics, immunology, oncology, clinical biochemistry, neuroscience, and tissue engineering. **Cell J**, has been certified by the Ministry of Culture and Islamic Guidance since 1999 and accredited as a scientific and research journal by HBI (Health and Biomedical Information) Journal Accreditation Commission since 2000 which is an open access journal. **This journal holds the membership of the Committee on Publication Ethics (COPE).**

### 1. Types of articles

The articles in the field of Cellular and Molecular can be considered for publications in **Cell J**. These articles are as below:

#### A. Original articles

Original articles are scientific reports of the original research studies. The article consists of English Abstract (structured), Introduction, Materials and Methods, Results, Discussion, Conclusion, Acknowledgements, Author's Contributions, and References (**Up to 40**).

#### B. Review articles

Review articles are the articles written by well experienced authors and those who have excellence in the related fields. The corresponding author of the review article must be one of the authors of at least three published articles appearing in the references. The review article consists of English Abstract (unstructured), Introduction, Conclusion, Author's Contributions, and References (**Up to 90**).

#### C. Systematic Reviews

Systematic reviews are a type of literature review that collect and critically analyzes multiple research studies or papers. The Systematic reviews consist of English Abstract (unstructured), Introduction, Materials and Methods, Results, Discussion, Conclusion, Acknowledgements, Author's Contributions, and References (**Up to 90**).

#### D. Short communications

Short communications are articles containing new findings. Submissions should be brief reports of ongoing researches. The short communication consists of English Abstract (unstructured), the body of the manuscript (should not hold heading or sub-heading), Acknowledgements, Author's Contributions, and References (**Up to 30**).

#### E. Case reports

Case reports are short discussions of a case or case series with unique features not previously described which make an important teaching point or scientific observation. They may describe novel techniques or use equipment, or new information on diseases of importance. It consists of English Abstracts (Unstructured), Introduction, Case Report, Discussion, Acknowledgements, Author's Contributions, and References (**Up to 30**).

#### F. Commentary

Commentaries are short articles containing a contemporary issue that is relevant to the journal's scope and also expressing a personal opinion or a new perspective about existing research on a particular topic. The Commentary consists of English Abstract (unstructured), the body of the manuscript (should not hold heading or subheading), Acknowledgements, Author's Contributions, and References (**Up to 30**).

#### G. Editorial

Editorials are articles should be written in relevant and new data of journals' filed by either the editor in chief or the editorial board.

#### H. Imaging in biology

Images in biology should focus on a single case with an interesting illustration such as a photograph, histological specimen or investigation. Color images are welcomed. The text should be brief and informative.

#### I. Letter to the editors

Letter to the editors are in response to previously published **Cell J** articles, and may also include interesting cases that do not meet the requirement of being truly exceptional, as well as other brief technical or clinical notes of general interest.

#### J. Debate

Debates are articles which show a discussion of the positive and negative view of the author concerning all aspect of the issue relevant to scientific research.

## 2. Submission process

It is recommended to see the guidelines for reporting different kinds of manuscripts. This guide explains how to prepare the manuscript for submission. Before submitting, we suggest authors to familiarize themselves with **Cell J** format and content by reading the journal via the website ([www.celljournal.com](http://www.celljournal.com)). The corresponding author ensures that all authors are included in the author list and agree with its order, and they must be aware of the manuscript submission.

### A. Author contributions statements

It is essential for authors to include a statement of responsibility in the manuscript that specifies all the authors' contributions. This participation must include: Conceptualization, Methodology, Software, Validation, Formal analysis, Investigation, Resources, Data Curation, Writing - Original Draft, Writing - Review & Editing, Visualization, Supervision, Project administration, and Funding acquisition. Authors who do not meet the above criteria should be acknowledged in the Acknowledgments section.

### B. Cover letter and copyright

Each manuscript should be accompanied by a cover letter, signed by all authors specifying the following statement: "The manuscript has been seen and approved by all authors and is not under active consideration for publication. It has neither been accepted for publication nor published in another journal fully or partially (except in abstract form). **Also, no manuscript would be accepted in case it has been pre-printed or submitted to other websites.** I hereby assign the copyright of the enclosed manuscript to **Cell J.**" The corresponding author must confirm the proof of the manuscript before online publishing. It is needed to suggest three peer reviewers in the field of their manuscript.

### C. Manuscript preparation

Authors whose first language is not English encouraged to consult a native English speaker in order to confirm his manuscripts to American or British (not a mixture) English usage and grammar. It is necessary to mention that we will check the plagiarism of your manuscript by iThenticate Software. The manuscript should be prepared in accordance with the "International Committee of Medical Journal Editors (ICMJE)". Please send your manuscript in two formats word and PDF (including: title, name of all the authors with their degree, abstract, full text, references, tables and figures) and also send tables and figures separately in the site. The abstract and text pages should have consecutive line numbers in the left margin beginning with the title page and continuing through the last page of the written text. Each abbreviation must be defined in the abstract and text when they are mentioned for the first time. Avoid using abbreviation in the title. Please use the international and standard abbreviations and symbols

It should be added that an essential step toward the integration and linking of scientific information reported in published literature is using standardized nomenclature in all fields of science and medicine. Species names must be italicized (*e.g.*, *Homo sapiens*) and also the full genus and species written out in full, both in the title of the manuscript and at the first mention of an organism in a paper.

It is necessary to mention that genes, mutations, genotypes, and alleles must be indicated in italics. Please use the recommended name by consulting the appropriate genetic nomenclature database, *e.g.*, HUGO for human genes. In another words; if it is a human gene, you must write all the letters in capital and italic (*e.g.*, *OCT4*, *c-MYC*). If not, only write the first letter in capital and italic (*e.g.*, *Oct4*, *c-Myc*). **In addition, protein designations are the same as the gene symbol but are not italicized.**

**Of note, Cell J** will only consider publishing genetic association study papers that are novel and statistically robust. Authors are advised to adhere to the recommendations outlined in the STREGA statement (<http://www.strega-statement.org>). The following criteria must be met for all submissions:

1. Hardy-Weinberg Equilibrium (HWE) calculations must be carried out and reported along with the P-values if applicable [see Namipashaki et al. 2015 (Cell J, Vol 17, N 2, Pages: 187-192) for a discussion].
2. Linkage disequilibrium (LD) structure between SNPs (if multiple SNPs are reported) must be presented.
3. Appropriate multiple testing correction (if multiple independent SNPs are reported) must be included.

Submissions that fail to meet the above criteria will be rejected before being sent out for review.

Each of the following manuscript components should begin in the following sequence:

**Authors' names** and order of them must be carefully considered (full name(s), highest awarded academic degree(s), email(s), and institutional affiliation(s) of all the authors in English. Also, you must send mobile number and full postal address of the corresponding author).

**Changes to Authorship** such as addition, deletion or rearrangement of author names must be made only before the manuscript has been accepted in the case of approving by the journal editor. In this case, the corresponding author must explain the reason of changing and confirm them (which has been signed by all authors of the manuscript). If the manuscript has already been published in an online issue, an erratum is needed. Please contact us via [info@celljournal.org](mailto:info@celljournal.org) in case of any changes (corrections, retractions, erratum, etc.).

**Title** is providing the full title of the research (do not use abbreviations in title).

**Running title** is providing a maximum of 7 words (no more than 50 characters).

**Abstract** must include Objective, Materials and Methods, Results, and Conclusion (no more than 300 words).

**Keywords**, three to five, must be supplied by the authors at the foot of the abstract chosen from the Medical Subject Heading (MeSH). Therefore; they must be specific and relevant to the paper.

The following components should be identified after the abstract:

**Introduction:** The Introduction should provide a brief background to the subject of the paper, explain the importance of the study, and state a precise study question or purpose.

**Materials and Methods:** It includes the exact methods or observations of experiments. If an apparatus is used, its manufacturer's name and address should be stipulated in parenthesis. If the method is established, give reference but if the method is new, give enough information so that another author can perform it. If a drug is used, its generic name, dose, and route of administration must be given. Standard units of measurements and chemical symbols of elements do not need to be defined.

**Statistical analysis:** Type of study and statistical methods should be mentioned and specified by any general computer program used.

**Ethical considerations:** Please state that informed consent was obtained from all human adult participants and from the parents or legal guardians of minors and include the name of the appropriate institutional review board that approved the project. It is necessary to indicate in the text that the maintenance and care of experimental animals complies with National Institutes of Health guidelines for the humane use of laboratory animals, or those of your Institute or agency.

**Clinical trial registration:** All of the Clinical Trials performing in Iran must be registered in Iranian Registry of Clinical Trials ([www.irct.ir](http://www.irct.ir)). The clinical trials performed abroad, could be considered for publication if they register in a registration site approved by WHO or [www.clinicaltrials.gov](http://www.clinicaltrials.gov). If you are reporting phase II or phase III randomized controlled trials, you must refer to the CONSORT Statement for recommendations to facilitate the complete and transparent reporting of trial findings. Reports that do not conform to the CONSORT guidelines may need to be revised before peer-reviewing.

**Results:** They must be presented in the form of text, tables, and figures. Take care that the text does not repeat data that are presented in tables and/or figures. Only emphasize and summarize the essential features of the main results. Tables and figures must be numbered consecutively as appeared in the text and should be organized in separate pages at the end of the manuscript while their location should be mentioned in the main text.

**Tables and figures:** If the result of your manuscript is too short, it is better to use the text instead of tables & figures. Tables should have a short descriptive heading above them and also any footnotes. Figure's caption should contain a brief title for the whole figure and continue with a short explanation of each part and also the symbols used (no more than 100 words). All figures must be prepared based on cell journal's guideline in color (no more than 6 Figures and Tables) and also in TIF format with 300 DPI resolution.

**Of Note: Please put the tables & figures of the result in the results section not any other section of the manuscript.**

**Supplementary materials** would be published on the online version of the journal. This material is important to the understanding and interpretation of the report and should not repeat material within the print article. The amount of supplementary material should be limited. Supplementary material should be original and not previously published and will undergo editorial and peer review with the main manuscript. Also, they must be cited in the manuscript text in parentheses, in a similar way as when citing a figure or a table. Provide a caption for each supplementary material submitted.

**Discussion:** It should emphasize the present findings and the variations or similarities with other researches done by other researchers. The detailed results should not be repeated in the discussion again. It must emphasize the new and important aspects of the study.

**Conclusion:** It emphasizes the new and important aspects of the study. All conclusions are justified by the results of the study.

**Acknowledgements:** This part includes a statement thanking those who contributed substantially with work relevant to the study but does not have authorship criteria. It includes those who provided technical help, writing assistance and name of departments that provided only general support. You must mention financial support in the study. Otherwise; write this sentence "There is no financial support in this study".

**Conflict of interest:** Any conflict of interest (financial or otherwise) and sources of financial support must be listed in the Acknowledgements. It includes providers of supplies and services from a commercial organization. Any commercial affiliation

must be disclosed, regardless of providing the funding or not.

**Of Note:** If you have already any patent related to the subject of your manuscript, or you are going to apply for such a patent, it must be mentioned in this part.

**References:** The references must be written based on the Vancouver style. Thus the references are cited numerically in the text and listed in the bibliography by the order of their appearance. The titles of journals must be abbreviated according to the style used in the list of Journals Indexed in PubMed. Write surname and initials of all authors when there are six or less. In the case of seven or more authors, the names of the first six authors followed by "et al." must be listed. You can download Endnote file for Journal references style: endnote file

The reference of information must be based on the following order:

**Article:**

Surname(s) and first letter of name & middle name(s) of author(s) .Manuscript title. Journal title (abbr).publication date (year); Volume & Issue: Page number.

Example: Manicardi GC, Bianchi PG, Pantano S, Azzoni P, Bizzaro D, Bianchi U, et al. Presence of endogenous nicks in DNA of ejaculated human spermatozoa and its relationship to chromomycin A3 accessibility. Biol Reprod. 1995; 52(4): 864-867.

**Book:**

Surname(s) and first letter of name & middle name(s) of author(s).Book title. Edition. Publication place: publisher name; publication date (year); Page number.

Example: Edelman CL, Mandle CL. Health promotion throughout the lifespan. 2<sup>nd</sup> ed. ST Louis: Mosby; 1998; 145-163.

**Chapter of book:**

Surname(s) and first letter of name & middle name(s) of author(s).Chapter title. In: Surname(s) and first letter of name & middle name(s) of editor(s), editors. Book title. Edition. Publication place: publisher name; publication date (year); Page number.

Example: Phillips SJ, Whisnant JP. Hypertension and stroke. In: Laragh JH, Brenner BM, editors. Hypertension: pathophysiology, diagnosis, and management. 2<sup>nd</sup> ed. New York: Raven Press; 1995; 465-478.

**Abstract book:**

Example: Amini rad O.The antioxidant effect of pomegranate juice on sperm parameters and fertility potential in mice. Cell J. 2008;10 Suppl 1:38.

**Thesis:**

Name of author. Thesis title. Degree. City name. University. Publication date (year).

Example: Eftekhari Yazdi P. Comparison of fragment removal and co-culture with Vero cell monolayers on development of human fragmented embryos. Presented for the Ph.D., Tehran. Tarbiyat Modarres University. 2004.

**Internet references**

**Article:**

Example: Jahanshahi A, Mirnajafi-Zadeh J, Javan M, Mohammad-Zadeh M, Rohani M. Effect of low-frequency stimulation on adenosineA1 and A2A receptors gene expression in dentate gyrus of perforant path kindled rats. Cell J. 2008; 10 (2): 87-92. Available from: <http://www.celljournal.org>. (20 Oct 2008).

**Book:**

Example: Anderson SC, Poulsen KB. Anderson's electronic atlas of hematology.[CD-ROM]. Philadelphia: Lippincott Williams & Wilkins; 2002.

**D. Proofs** are sent by email as PDF files and should be checked and returned within 72 hours of receipt. It is the authors' responsibility to check that all the text and data as contained in the page proofs are correct and suitable for publication. **We are requested to pay particular attention to author's names and affiliations as it is essential that these details be accurate when the article is published.**

**E. Pay for publication:** Publishing an article in **Cell J** requires Article Processing Charges (APC) that will be billed to the submitting author following the acceptance of an article for publication. For more information please see [www.celljournal.org](http://www.celljournal.org).

**F. Ethics of scientific publication:** Manuscripts that have been published elsewhere with the same intellectual material will

refer to duplicate publication. If authors have used their own previously published work or work that is currently under review, as the basis for a submitted manuscript, they are required to cite the previous work and indicate how their submitted manuscript offers novel contributions beyond those of the previous work. Research and publication misconduct is considered a serious breach of ethics.

The Journal systematically employs iThenticate, plagiarism detection and prevention software designed to ensure the originality of written work before publication. Plagiarism of text from a previously published manuscript by the same or another author is a serious publication offence. Some parts of text may be used, only where the source of the quoted material is clearly acknowledged.

### 3. General information

**A.** You can send your manuscript via online submission system which is available on our website. If the manuscript is not prepared according to the format of **Cell J**, it will be returned to authors.

**B.** The order of article appearance in the Journal is not demonstrating the scientific characters of the authors.

**C.** **Cell J** has authority to accept or reject the manuscript.

**D.** Corresponding authors should send the manuscripts via the Online Manuscript Submission System. All submissions will be evaluated by the associated editor in order to check scope and novelty. If the manuscript suits the journal criteria, the associated editor would select the single-blind peer-reviewers. The reviewers of the manuscript must not share information about the review with anyone without permission of the editors and authors. If three reviewers pass their judgments on the manuscript, it will be presented to the associated editor of **Cell J**. In the case of having a favorable judgment on the manuscript, reviewers' comments will be presented to the corresponding author (the identification of the reviewers will not be revealed). After receiving the revision, the associated editor would choose the final reviewer among the previous ones. The final decision will be taken by editor-in-chief based on the final reviewer's comments. The review process takes between 2 to 4 months in **Cell J**. The executive member of journal will contact the corresponding author directly within 3-4 weeks by email. If authors do not receive any reply from journal office after the specified time, they can contact the journal office. Finally, the executive manager will respond promptly to authors' request.

After receiving the acceptance letter, the abstract of the paper would be published electronically. The paper will be in a queue to be published in one Cell J. At last, the corresponding author should verify a proof copy of the paper in order to be published.

### The Final Checklist

The authors must ensure that before submitting the manuscript for publication, they have to consider the following parts:

1. The first page of manuscript should contain title, name of the author/coauthors, their academic qualifications, designation & institutions they are affiliated with, mailing address for future correspondence, email address, phone, and fax number.
2. Text of manuscript and References prepared as stated in the "guide for authors" section.
3. Tables should be on a separate page. Figures must be sent in color and also in JPEG (Jpg) format.
4. Cover Letter should be uploaded with the signature of all authors.
5. An ethical committee letter should be inserted at the end of the cover letter.

*The Editor-in-Chief: Ahmad Hosseini, Ph.D.*

*Cell Journal*<sub>(Yakhteh)</sub>

*P.O. Box: 16635-148, Iran*

*Tel/Fax: + 98-21-22510895*

*Emails: info@celljournal.org*

*journals@celljournal.org*





## IN THE NAME OF GOD

### Gone But not Forgotten

In the memory of the late Director of Royan Institute, Founder of Stem Cells Research in Iran and Chairman of *Cell Journal* (Yakhteh). May he rest in peace.

**Dr. Saeed Kazemi Ashtiani**

### OWNED:

Royan Institute, Iranian Academic Center for Education Culture and Research (ACECR)

### CHAIRMAN:

Hamid Gourabi, Ph.D., (Professor, Royan Institute, Tehran, Iran)

### EDITOR IN CHIEF:

Ahmad Hosseini, Ph.D., (Professor, Shahid Beheshti Medical University, Tehran, Iran)

### SECTION EDITORS:

Saeid Abroun, Ph.D., Professor, Tarbiat Modares University, Tehran, Iran  
Masoud Vosough, M.D., Ph.D., Associate Professor, Royan Institute, Iran  
Hoda Madani, M.D., Ph.D., Royan Institute, Iran  
Marzieh Ebrahimi, Ph.D., Professor, Royan Institute, Tehran, Iran  
Sara Soudi, Ph.D., Associate Professor, Tarbiat Modares University, Tehran, Iran  
Sharif Moradi, Ph.D., Assistant Professor, Royan Institute, Tehran, Iran  
Sara Pahlavan, Ph.D., Assistant Professor, Royan Institute, Tehran, Iran  
Sadaf Vahdat, Ph.D., Assistant Professor, Tarbiat Modares University, Tehran, Iran  
Amir Amiri-Yekta, Ph.D., Assistant Professor, Royan Institute, Tehran, Iran  
Afagh Alavi, Ph.D., Associate Professor, University of Social Welfare and Rehabilitation Sciences, Tehran, Iran  
Seyed Javad Mirnajafi-Zadeh, Ph.D., Assistant Professor, Tarbiat Modares University, Tehran, Iran  
Sahar Kiani, Ph.D., Associate Professor, Royan Institute, Tehran, Iran  
Marjan Sabaghian, Ph.D., Associate Professor, Royan Institute, Tehran, Iran  
Seyyed Abolghasem Ghadami, Ph.D., Alzahra University, Tehran, Iran  
Mohammad Kazemi Ashtiani, Ph.D., Royan Institute, Tehran, Iran  
Hamed Daemi, Ph.D., Assistant Professor, Royan Institute, Tehran, Iran  
Fatemeh Hassani, Ph.D., Assistant Professor, Royan Institute, Tehran, Iran  
Mahshid Bazrafkan, Ph.D., Assistant Professor, Avicenna Fertility Center, Karaj, Iran  
Alireza Soltanian, Ph.D., Professor, University of Medical Sciences, Hamadan, Iran

### EDITORIAL BOARDS:

Saeid Abroun, Ph.D., (Professor, Tarbiat Modares University, Tehran, Iran)  
Kamran Alimoghadam, M.D., (Associate Professor, Tehran Medical University, Tehran, Iran)  
Alireza Asgari, Ph.D., (Professor, Baghyatallah University, Tehran, Iran)  
Mohammad Kazem Aghaee Mazaheri, D.D.S., (Assistant Professor, ACECR, Tehran, Iran)  
Mohamadreza Baghaban Eslaminejad, Ph.D., (Professor, Royan Institute, Tehran, Iran)  
Gila Behzadi, Ph.D., (Professor, Shahid Beheshti Medical University, Tehran, Iran)  
Hossein Baharvand, Ph.D., (Professor, Royan Institute, Tehran, Iran)  
Marzieh Ebrahimi, Ph.D., (Professor, Royan Institute, Tehran, Iran)  
Mary Familiar, Ph.D., (Senior Lecturer, University of Melbourne, Melbourne, Australia)  
Hamid Gourabi, Ph.D., (Professor, Royan Institute, Tehran, Iran)  
Jurgen Hescheler, M.D., (Professor, Institute of Neurophysiology of University Zu Koln, Germany)  
Ghasem Hosseini Salekdeh, Ph.D., (Professor, Agricultural Biotechnology Research Institute, Karaj, Iran)  
Esmail Jabbari, Ph.D., (Associate Professor, University of South Carolina, Columbia, USA)  
Suresh Jesuthasan, Ph.D., (Associate Professor, National University of Singapore, Singapore)  
Bahram Kazemi, Ph.D., (Professor, Shahid Beheshti Medical University, Tehran, Iran)  
Saadi Khochbin, Ph.D., (Professor, Inserm/Grenoble University, France)  
Ali Khademhosseini, Ph.D., (Professor, Harvard Medical School, USA)  
Navid Manuchehrabadi, Ph.D., (Angio Dynamics, Marlborough, USA)  
Hosseinali Mehrani, Ph.D., (Professor, Baghyatallah University, Tehran, Iran)  
Marcos Meseguer, Ph.D., (Clinical Embryology Laboratory IVI Valencia, Valencia, Spain)  
Seyed Javad Mowla, Ph.D., (Professor, Tarbiat Modares University, Tehran, Iran)  
Mohammad Hossein Nasr Esfahani, Ph.D., (Professor, Royan Institute, Tehran, Iran)  
Toru Nakano, M.D., Ph.D., (Professor, Osaka University, Osaka, Japan)  
Donald Newgreen, Ph.D., (Professor, Murdoch Children Research Institute, Melbourne, Australia)  
Mojtaba Rezazadeh Valojerdi, Ph.D., (Professor, Tarbiat Modares University, Tehran, Iran)  
Mohammad Hossein Sanati, Ph.D., (Associate Professor, National Institute for Genetic Engineering and Biotechnology, Tehran, Iran)  
Eimei Sato, Ph.D., (Professor, Tohoku University, Sendai, Japan)  
Andreas Serra, M.D., (Professor, University of Zurich, Zurich, Switzerland)  
Abdolhossein Shahverdi, Ph.D., (Professor, Royan Institute, Tehran, Iran)  
Michele Catherine Studer, Ph.D., (Institute of Biology Valrose, IBV University of Nice Sophia-Antipolis, France)

Peter Timashev, Ph.D., (Sechenov University, Moscow, Russia)  
Daniela Toniolo, Ph.D., (Head, Unit of Common Disorders, San Raffaele Research Institute, Milano, Italy)  
Christian van den Bos, Ph.D., Managing Director MARES Ltd, Greven, Germany  
Catherine Verfaillie, Ph.D., (Professor, Katholie Universiteit Leuven, Leuven, Belgium)  
Gianpaolo Zerbin, M.D., Ph.D., (San Raffaele Scientific Institute, Italy)  
Shubing Zhang, Ph.D., (Associate Professor, Central South University, China)  
Daniele Zink, Ph.D., (Institute of Bioengineering and Nanotechnology, Agency for Science Technology & Science, Singapore)

**EXECUTIVE MANAGER:**

Farideh Malekzadeh, M.Sc., (Royan Institute, Tehran, Iran)

**EXECUTIVE BOARDS:**

Parvaneh Afsharian, Ph.D., (Royan Institute, Tehran, Iran)  
Reza Azimi, B.Sc., (Royan Institute, Tehran, Iran)  
Reza Omani-Samani, M.D., (Royan Institute, Tehran, Iran)  
Elham Amirchaghmaghi, M.D., Ph.D., (Royan Institute, Tehran, Iran)  
Leila Daliri, M.Sc., (Royan Institute, Tehran, Iran)  
Mahdi Lottipannah, M.Sc., (Royan Institute, Tehran, Iran)  
Faezeh Shekari, Ph.D., (Royan Institute, Tehran, Iran)

**ENGLISH EDITORS:**

Mitra Amiri Khabooshan, Ph.D., (Monash University, Victoria, Australia)  
Sima Binaafar, M. Sc., (Royan Institute, Tehran, Iran)  
Saman Eghtesad, Ph.D., (Royan Institute, Tehran, Iran)  
Jane Elizabeth Ferrie, Ph.D., (University College of London, London, UK)  
Vahid Ezzatizadeh, Ph.D., (Royan Institute, Tehran, Iran)  
Farnaz Shapouri, Ph.D., (Memphasys Limited, NSW, Australia)  
Kim Vagharfard, M.Sc., (Royan Institute, Tehran, Iran)  
Maryam Vatani, M.Sc., (University of Calgary, Canada)

**GRAPHIST:**

Laleh Mirza Ali Shirvani, B.Sc., (Royan Institute, Tehran, Iran)

**PUBLISHED & SPONSORED BY:**

Publication of Royan Institute (ACECR)

**Indexed in:**

1. Thomson Reuters (ISI)
2. PubMed
3. PubMed Central (PMC)
4. National Library Medicine (NLM)
5. Biosis Preview
6. Index Medicus for the Eastern Mediterranean Region (IMEMR)
7. Regional Information Center for Sciences and Technology (RICEST)
8. Index Copernicus International
9. Cambridge Scientific Abstract (CSA)
10. EMBASE
11. Scopus
12. Cinahl Database
13. Google Scholar
14. Chemical Abstract Service (CAS)
15. Proquest
16. Directory of Open Access Journals (DOAJ)
17. Open Academic Journals Index (OAJI)
18. Directory of Research Journals Indexing (DRJI)
19. Scientific Information Database (SID)
20. Iranmedex
21. Islamic World Science Citation Center (ISC)
22. Magiran
23. Science Library Index
24. Biological Abstracts
25. Essential Science Indicators
26. EuroPub

**ACECR**

**Copyright and license information:**

The **Cell Journal**<sup>(Yakhteh)</sup> is an open access journal which means the articles are freely available online for any individual author to download and use the providing address. The journal is licensed under a Creative Commons Attribution-Non Commercial 3.0 Unported License which allows the author(s) to hold the copyright without restrictions that is permitting unrestricted non-commercial use, distribution, and reproduction in any medium provided the original work is properly cited.

**Editorial Office Address (Dr. Ahmad Hosseini):**

Royan Institute, P.O.Box: 16635-148,  
Tehran, Iran  
Tel & Fax: (+9821)22510895  
Website: [www.celljournal.org](http://www.celljournal.org)  
Emails: [info@celljournal.org](mailto:info@celljournal.org)  
[journals@celljournal.org](mailto:journals@celljournal.org)

**Printing Company:**

Naghsh e Johar Co.  
No. 103, Fajr alley, Tehranpars Street,  
Tehran, Iran.





CONTENTS

**Systematic Review**

- **Clinical Implications and Prognostic Value of Leucine-Rich G Protein-Coupled Receptor 5 Expression as A Cancer Stem Cell Marker in Malignancies: A Systematic Review and Meta-Analysis**

Sepideh Ghobakhloo, Mehri Khoshhali, Nasimeh Vatandoost, Sima Jafarpour, Anoosha Niazmand, Reza Nedaeinia, Rasoul Salehi ..... 1

**Original Articles**

- **Identification and Functional Characterization of PI3K/Akt/mTOR Pathway-Related lncRNAs in Lung Adenocarcinoma: A Retrospective Study**

Jiaqi Zhong, Ying Kong, Ruming Li, Minghan Feng, Liming Li, Xiao Zhu, Lianzhou Chen ..... 13

- **Effect of Exosomes Derived from Bone Marrow Mesenchymal Stem Cells on Ovarian Granulosa Cells of Immature NMRI Mice**

Sajad Farrokhyar, Javad Baharara, Akram Eidi, Nasim Hayati Roodbari ..... 28

- **A Mutational Hotspot in The *LAMP2* Gene: Unravelling Intrafamilial Phenotypic Variation and Global Distribution of The c.877C>T Variant: A Descriptive Study**

Saeideh Kavousi, Mohammad Dalili, Bahareh Rabbani, Mehrdad Behmanesh, Mehrdad Noruzinia, Nejat Mahdieh ..... 39

- **Candidate Biomarkers for Targeting in Type 1 Diabetes; A Bioinformatic Analysis of Pancreatic Cell Surface Antigens**

Hamed Dabiri, Mahdi Habibi-Anbouhi, Vahab Ziaei, Zahra Moghadasi, Majid Sadeghizadeh, Ensiyeh Hajizadeh-Saffar ..... 51

- **The Neuroprotective Effects of Curcumin Nanoparticles on The Cerebral Ischemia-Reperfusion Injury in The Rats-The Roles of The Protein Kinase RNA-Like ER Kinase/Extracellular Signal-Regulated Kinase and Transcription Factor EB proteins**

Yalda Saghari, Monireh Movahedi, Majid Tebianian, Maliheh Entezari ..... 62

- **Fabrication of Rosuvastatin-Incorporated Polycaprolactone -Gelatin Scaffold for Bone Repair: A Preliminary *In Vitro* Study**


Maliheh Gharibshahian, Morteza Alizadeh, Mohammad Kamalabadi Farahani, Majid Salehi ..... 70

- **Effects of Streptozotocin Induced Diabetes on One-Carbon Cycle and Sperm Function**

Farnaz Pouriayevali, Marziyeh Tavalae, Fatemeh Kazeminasab, Maurizio Dattilo, Mohammad Hossein Nasr-Esfahani ..... 81

- **Front page of Cell Journal<sub>(Yakhteh)</sub>: Figure 2 D, E, F, Page: 32**

# Clinical Implications and Prognostic Value of Leucine-Rich G Protein-Coupled Receptor 5 Expression as A Cancer Stem Cell Marker in Malignancies: A Systematic Review and Meta-Analysis

Sepideh Ghobakhloo, M.Sc.<sup>1,2</sup>, Mehri Khoshhali, Ph.D.<sup>3</sup>, Nasimeh Vatandoost, M.Sc.<sup>1,2</sup>, Sima Jafarpour, Ph.D.<sup>1,2</sup>,  
Anoosha Niazmand, B.Sc.<sup>1</sup>, Reza Nedaeinia, Ph.D.<sup>2</sup>, Rasoul Salehi, Ph.D.<sup>1,2\*</sup> 

1. Department of Genetics and Molecular Biology, School of Medicine, Isfahan University of Medical Sciences, Isfahan, Iran  
2. Pediatric Inherited Diseases Research Center, Research Institute for Primordial Prevention of Non-Communicable Diseases, Isfahan University of Medical Sciences, Isfahan, Iran  
3. Child Growth and Development Research Center, Research Institute for Primordial Prevention of Non-Communicable Disease, Isfahan University of Medical Sciences, Isfahan, Iran

## Abstract

Leucine-rich G protein-coupled receptor 5 (*LGR5*) is a marker of cancer stem cells (CSCs) in various cancers. Based on different studies, conflicting reports exist on correlation between *LGR5* expression and poor prognosis/clinicopathological parameters in cancer patients. Therefore, our purpose in conducting this study was to investigate correlation between *LGR5* expression and outcomes of cancer patients under study through a systematic review and meta-analysis. Relevant articles were searched and collected using EMBASE, PubMed, Science Direct, and Scopus databases until December 21, 2022. This study was conducted to examine correlation between *LGR5* expression and different clinical outcomes, such as recurrence-free survival (RFS), disease-free survival (DFS), overall survival (OS), and clinicopathological characteristics of the included cancer patients. To achieve this, hazard ratios (HRs) with 95% confidence intervals (CIs) and odds ratios (ORs) with 95% CIs were used as statistical measures. A meta-analysis was conducted using STATA 12.0 software. Finally, 53 studies including 9523 patients met the inclusion criteria. Significantly, high-level expression of *LGR5* was related to poor prognosis in terms of OS, higher tumor stage, presence of distant metastasis, and presence of lymph node metastasis. It was discovered through subgroup analysis that several factors, including the study area, evaluation method, and type of cancer, can influence the correlation between *LGR5* expression and negative prognosis in cancer patients. According to the results of our study, *LGR5* overexpression was related to poor OS in cancer patients. In addition, clinicopathological data indicated an unfavorable prognosis in cancer patients with high *LGR5* expression. In conclusion, *LGR5* may serve as a potential prognostic marker for predicting survival in certain cancer types.

**Keywords:** Cancer Stem Cells, Clinicopathological Features, *LGR5*, Prognostic Marker

**Citation:** Ghobakhloo S, Khoshhali M, Vatandoost N, Jafarpour S, Niazmand A, Nedaeinia R, Salehi R. Clinical implications and prognostic value of leucine-rich g protein-coupled receptor 5 expression as a cancer stem cell marker in malignancies: a systematic review and meta-analysis. Cell J. 2024; 26(1): 1-12. doi: 10.22074/CELLJ.2023.2010157.1396

This open-access article has been published under the terms of the Creative Commons Attribution Non-Commercial 3.0 (CC BY-NC 3.0).

## Introduction

Cancer remains a leading cause of death globally and a significant public health issue (1). Despite extensive studies in recent decades and progress in new systemic treatments, cancer treatment faces many challenges, including resistance to treatment and the existence of cancer stem cells (CSCs) (2). These challenges contribute to tumor recurrence, tumor progression, and mortality. Therefore, to effectively treat cancer and address the issues of invasion and metastasis and thus improve patient outcomes, it is essential to identify prognostic markers and new treatment options (3).

The CSCs theory is supported by data from various tumors and malignancies, indicating that CSCs have

the potential to re-establish an entire tumor (4). These cells play a critical role in tumor development, spread, progression, metastasis, recurrence, and resistance to treatment due to their ability to self-renew, be flexible, and differentiate into heterogeneous cell lineages (5). Various factors regulate CSCs (6). Signaling pathways similar to those found in normal stem cells are also present in CSCs (7). Consequently, targeting the signaling pathways and genes involved in regulating CSCs is highly effective in eliminating these cells and preventing treatment failure, adverse outcomes, and side effects (8). Moreover, investigation of CSC markers could potentially provide prognostic information and new therapeutic targets (9).

*LGR5*, a G-protein coupled receptor, is encoded by the

Received: 30/August/2023, Revised: 08/November/2023, Accepted: 18/November/2023

\*Corresponding Address: P.O.Box: 8174673461, Department of Genetics and Molecular Biology, School of Medicine, Isfahan University of Medical Sciences, Isfahan, Iran

Email: [r\\_salehi@med.mui.ac.ir](mailto:r_salehi@med.mui.ac.ir)



Royan Institute  
Cell Journal (Yakhteh)

gene located on chromosome 12. This receptor contains a leucine-rich repeat and is also referred to as GPR49, which belongs to the G-protein-coupled receptor family (10). *LGR5* is a Wnt target gene and it has been identified as a CSC marker in intestinal cells (11). Its ability to maintain CSCs and promote cancer progression has been observed in various types of cancer, including breast, colorectal, hepatocellular, gastric, and ovarian cancers (12-15). Recent studies showed that *LGR5* expression levels could predict prognosis, recurrence, and survival rates in some cancer types (16, 17). High expression of *LGR5* has been linked to shorter survival rates and advanced clinicopathological features in several studies (14, 18-20).

This suggests that *LGR5* may serve as a potential prognostic biomarker as well as a therapeutic target for tumors. Moreover, *LGR5* expression has been shown to cause resistance to 5-FU-based chemotherapy and tumor recurrence. Therefore, checking *LGR5* expression may help identify cancer patients with poor clinical outcomes (21). Therapies targeting pathways related to *LGR5* signaling are important strategies to improve the efficacy of cancer treatment (22).

This study aimed to comprehensively evaluate prognostic significance of *LGR5* expression in various cancers, given the conflicting research on its association with poor prognosis (18, 23, 24). To accomplish this, a meta-analysis of 53 studies with 9523 patients was conducted, in order to investigate potential role of *LGR5* as a clinical and prognostic marker and clarify its relationship with clinical pathological parameters in different cancers.

## Materials and Methods

### Study strategy

This study was conducted according to PRISMA guidelines (PRISMA Checklist) (25). Two researchers independently searched databases including EMBASE, Science Direct, PubMed, and Scopus up to December 21, 2022. In this study, we used the following medical terms to search: ("Cancer" OR "Carcinoma" "Neoplasm" OR "Tumor") AND ("*LGR5*" OR "G-protein coupled receptor 67" OR "G-protein coupled receptor 49" AND "prognosis"). We first gathered the publication's summary and title, then carefully reviewed all selected articles to ensure they contained the necessary information. Any discrepancy was discussed with another researcher to reach a consensus.

### Selection criteria

Eligibility criteria for inclusion in our study were as follows: i. Articles published in English, ii. Diagnosis of any type of cancer or malignancy in patients was confirmed by pathological identification, iii. Investigation of *LGR5* expression in human tissue samples were evaluated by any technique, iv. Studies in

which the correlation of *LGR5* expression with overall survival (OS), recurrence-free survival (RFS), disease-free survival (DFS), and/or clinicopathological data of cancers were investigated and patients were separated into two groups (positive and negative, or high and low) according to *LGR5* expression, and v. Articles that calculated ORs for pathologic clinical features hazard ratios (HRs) for prognostic outcomes. The study excluded book chapters, letters, reviews, or conference abstracts, as they lacked sufficient data, as well as articles on animals, cell lines, or blood samples, as well as studies that did not have sufficient useful information.

### Data extraction

Two researchers (S.G.H. and A.N.) independently assessed each eligible article and extracted data from qualifying publications. The study collected data from each publication, settling disagreements through conversation and using the Newcastle-Ottawa quality evaluation scale to appraise available studies. The most commonly collected data items included author, cancer type, sample size, detection method, publication year, nation, recruitment time, outcomes, HR acquire method, and Newcastle-Ottawa scale (NOS) score (26). S.J. and R.N. verified the all data.

### Quality assessment

Two authors (S.G.H. and S.J.) independently assessed quality of the articles using the NOS rating system, which rates articles on a scale of zero to nine stars, as shown in Table S1 (See Supplementary Online Information at [www.celljournal.org](http://www.celljournal.org)). Articles scoring six or higher were deemed of good quality, and any disagreements were resolved through discussion.

### Statistical analysis

The effect sizes of HR from each original article were extracted directly in Meta-analysis. Cochran's test evaluated heterogeneity and expressed it with the  $I^2$  index. Pooled results used a random effects model. Subgroup analysis was conducted based on cancer type, ethnicity, and diagnosis method. To assess robustness of the results, sensitivity analysis was conducted by excluding one study or group of studies at a time. All statistical analysis was conducted using STATA software (version 12.0; STATA Corp, USA). Publication bias was assessed using Egger's test and funnel plots.

## Results

### Literature search

As shown in Figure 1, initially 958 articles were recognized using the primary search based on PRISMA guidelines. After removing overlapping studies, 695 studies were selected, and then the titles and abstracts of the selected studies were independently assessed by two authors to remove unrelated items. The authors examined

the remaining 322 articles carefully. 269 studies were excluded from our review for the following reasons: letters (n=6), reviews (n=21), blood samples (n=4), non-cancer studies (n=103), abstract of the meeting and congress (n=19), animal studies (n=61), cell line studies (n=23), and studies that do not have enough information (n=32). As a result, 53 articles met our inclusion criteria. Of these 53 selected studies, 27 articles were demonstrated from China, 10 papers were reported from Japan, five and four experiments were respectively obtained from Korea and USA, two articles from Germany, two papers from Taiwan, and the remaining experiments were reported from Sweden, Iran, and Egypt. The included studies contained twelve types of cancer: colorectal cancer (n=19), gastric cancer (n=8), breast cancer (n=6), head and neck cancer (n=6), liver cancer (n=4), lung cancer (n=3), ovarian cancer (n=2), cholangiocarcinoma (n=1), intrahepatic cholangiocarcinoma (n=1), cervical carcinoma (n=1), small intestinal adenocarcinoma (n=1),

and pancreatic ductal carcinoma (n=1). *LGR5* expression level was investigated by immunohistochemistry (IHC) in 40 studies, by RNA in situ hybridization (ISH) in seven studies, by quantitative polymerase chain reaction (qRT-PCR) in five studies, and by western blot in one study. Due to different definitions, cut-off values for *LGR5* expression varied among the studies. Out of the 53 studies that were collected, in 48 studies, *LGR5* expression was analyzed in relation to clinicopathological features. Additionally, in 27 of 53 studies, *LGR5* expression was evaluated in relation to survival rates, including OS (n=24), DFS (n=3), and RFS (n=4), in cancer patients.

### Study quality

In the selected studies, the NOS score ranged from six to eight. Results of the quality assessment of each study and further details about the papers are summarized in Table 1.

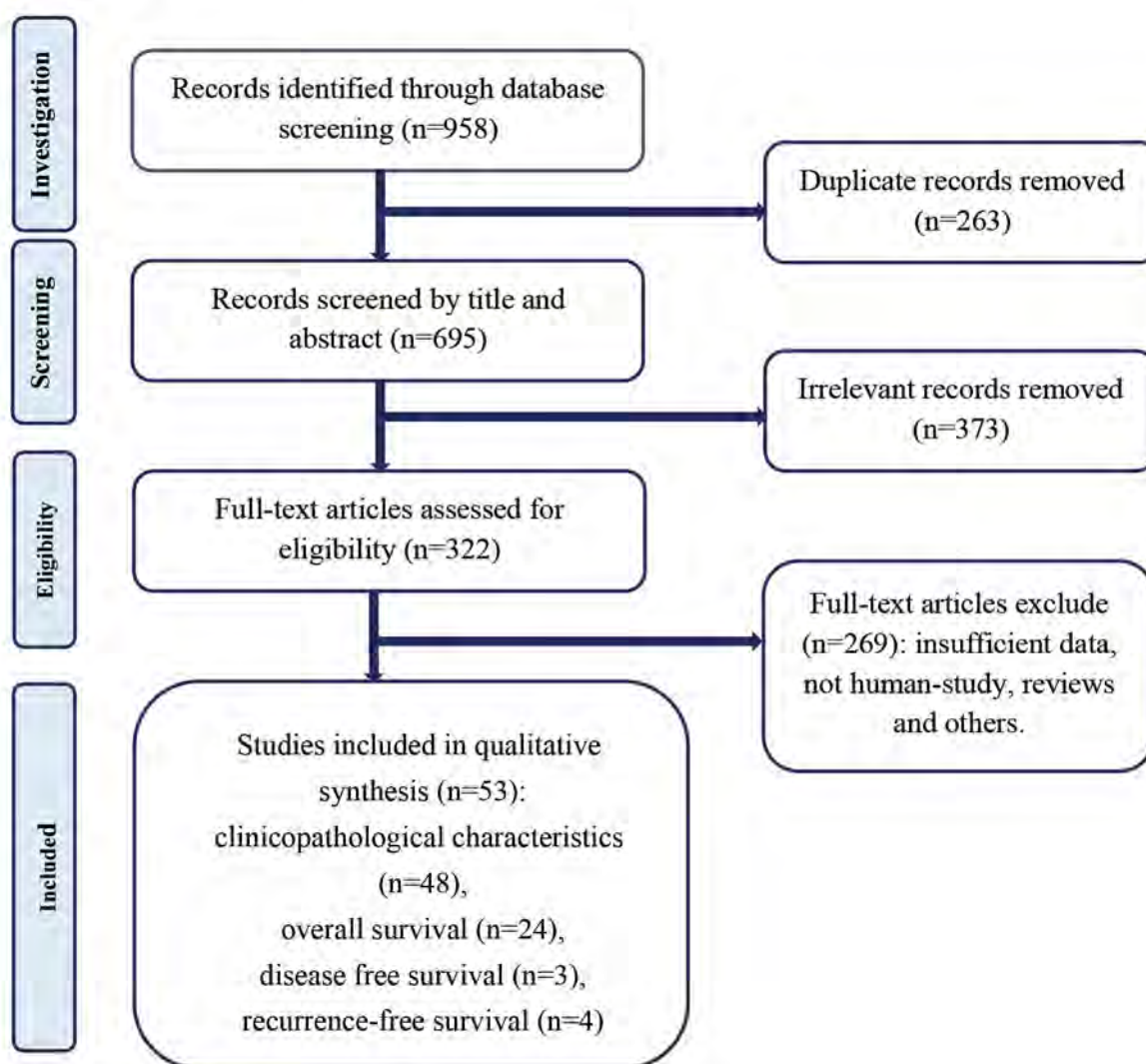


Fig.1: Flowchart for the study selection process.

**Table 1:** Characteristic of the included studies

Study	Year	Country	Cancer type	Sample size	Follow-up (month)	Detection method	Cut-off value	Evaluation of LGR5 expression (H or L/+ or -)	NOS score	Expression associated with poor prognosis	Clinical feature	Outcome
Yoshizawa et al. (20)	2022	Japan	Cholangiocarcinoma	25	NA	IHC	NA	High/low	6	Low	Yes	NA
AbdelMageed et al. (27)	2021	Sweden	CRC	121	144	qRT-PCR	Median	Positive/Negative	6	High	No	DFS
Lee et al. (28)	2021	South Korea	TNBC	293	NA	IHC	NA	Positive/Negative	7	Positive	Yes	NA
Xu et al. (14)	2021	China	CRC	98	60	Western blot	Median	High/low	8	High	Yes	NA
Kawasaki et al. (29)	2021	Japan	ICC	59	NA	IHC	≥ 4	High/low	6	High	Yes	RFS
Abdelrahman et al. (30)	2021	Egypt	Colon cancer	60	40.8	IHC	NA	High/low	7	High	Yes	NA
Ehara et al. (16)	2021	Japan	GAS	41	NA	RNA-ISH	NA	High/low	6	High	Yes	OS
Hagerling et al. (31)	2020	USA	Breast cancer ER+	401	106	IHC	NA	High/low	6	High	Yes	OS
Ogasawara et al. (19)	2020	Japan	Breast carcinoma	43	NA	RNA-ISH	NA	High/low	6	High	Yes	OS
Kang et al. (32)	2020	China	CRC stage I, II	92	NA	IHC	≥ 4	High/low	7	High	Yes	OS, RFS
Zhang et al. (33)	2020	China	ESCC	45	48	IHC	Mean	Positive/Negative	7	NO relation	Yes	OS
Nagashima et al. (34)	2020	Japan	NSCLC	360	66	IHC	NA	High/low	7	High	Yes	OS, RFS
Ihemelandu et al. (35)	2019	USA	CRC	49	62.4	IHC	NA	High/low	8	Low	Yes	OS
Shen et al. (36)	2019	China	Breast carcinoma	112	3	IHC	Mean	Positive/Negative	7	High	Yes	NA
Shekarriz et al. (24)	2019	Iran	CRC	40	NA	IHC	Median	High/low	7	High	Yes	NA
Liu et al. (13)	2019	China	GC	100	56	IHC	NA	High/low	7	High	No	OS
Freiin Grote et al. (37)	2019	Germany	Gastric carcinoma	236	29.5	IHC	Median	High/Low	6	High	Yes	NA
Ko et al. (38)	2019	Taiwan	HCC	352	27	IHC	Median	High/Low	7	High	Yes	OS
Ma et al. (39)	2019	China	HCC	100	NA	IHC	Median	High/Low	7	High	Yes	OS
Rot et al. (40)	2019	Germany	OSCC	78	44.9	qRT-PCR	Median	High/Low	7	High	Yes	OS
Yu et al. (15)	2019	China	Epithelial ovarian cancer	210	NA	IHC	NA	Positive/Negative	7	High	Yes	NA
Kuraishi et al. (18)	2019	Japan	Pancreatic ductal	78	NA	RNA-ISH	NA	High/low	7	Low	Yes	NA
Hou et al. (41)	2018	Taiwan	Breast cancer	126	NA	IHC	Median	High/Low	6	High	Yes	NA
Jang et al. (42)	2018	Korea	CRC	788	NA	RNA-ISH	NA	Positive/Negative	7	High	Yes	OS
Kim et al. (43)	2018	Korea	CRC	337	NA	IHC	NA	High/Low	7	High	Yes	OS, DFS
Chen et al. (12)	2018	China	HCC	66	NA	IHC	NA	High/Low	7	High	Yes	OS
Harada et al. (44)	2017	Japan	Low rectal cancer	61	69.5	IHC	NA	Positive/Negative	6	High	Yes	NA
Lv et al. (45)	2017	China	ESCC	280	NA	IHC	NA	Positive/Negative	6	High	Yes	NA

Table 1: Continued

Study	Year	Country	Cancer type	Sample size	Follow-up (month)	Detection method	Cut-off value	Evaluation of <i>LGR5</i> expression (H or L /+ or -)	NOS score	Expression associated with poor prognosis	Clinical feature	Outcome
Liu et al. (46)	2017	China	HCC	139	31.15	IHC	NA	High/Low	8	High	Yes	NA
Wu et al. (47)	2017	China	OSCC	190	NA	IHC	NA	Positive/Negative	7	High	Yes	NA
Wu et al. (48)	2016	China	CRC	80	60	qRT-PCR	Median	High/Low	8	High	No	OS
Jang et al. (49)	2016	Korea	Gastric carcinomas	603	NA	RNA-ISH	NA	Positive/Negative	6	NA	Yes	NA
Sun et al. (50)	2015	China	Cervical carcinoma	94	46	qRT-PCR	NA	High/Low	7	High	Yes	OS, RFS
Yang et al. (51)	2015	China	Breast cancer	134	NA	IHC and TMA	NA	High/Low	7	High	Yes	NA
Gao et al. (52)	2015	China	Lung cancer	85	15.2	IHC	Median	Positive/Negative	7	High	Yes	OS
Sun et al. (53)	2015	China	Ovarian cancer	100	NA	IHC	NA	High/Low	7	High	Yes	NA
Wang et al. (54)	2015	China	Small intestinal adenocarcinomas	38	NA	IHC	NA	Positive/Negative	6	High	Yes	NA
Gao et al. (55)	2014	China	CRC stage IV	42	NA	IHC	Mean	Positive/Negative	6	High	Yes	NA
Liu et al. (56)	2014	China	CRC	366	NA	IHC	NA	Positive/Negative	7	High	Yes	NA
He et al. (57)	2014	China	CRC	53	48	IHC	Median	High/Low	7	High	Yes	OS
Chen et al. (58)	2014	China	SCCE	44	11.1	IHC	SI >4	High/Low	7	High	Yes	OS
Xi et al. (59)	2014	China	GC	318	NA	IHC	NA	High/Low	7	High	Yes	OS
Hsu et al. (60)	2013	China	CRC	218	28.3	IHC	NA	High/Low	7	High	Yes	DFS
Jang et al. (61)	2013	Korea	GC	159	NA	RNA-ISH	NA	Positive/Negative	6	High	Yes	NA
Zheng et al. (62)	2013	China	Gastric carcinoma	180	NA	IHC	NA	Positive/Negative	6	High	Yes	NA
Ryuge et al. (63)	2013	Japan	Lung adenocarcinoma	266	88	IHC	NA	Positive/Negative	7	High	Yes	OS
Bu et al. (64)	2013	China	GC stage I, II	257	NA	IHC	NA	Positive/Negative	7	High	Yes	NA
Wu et al. (65)	2012	China	Colorectal carcinoma	192	NA	IHC	NA	Positive/Negative	7	High	Yes	OS
Ziskin et al. (66)	2012	USA	Colorectal adenocarcinomas	891	NA	RNA-ISH	NA	High/Low	7	High	No	OS
Takahashi et al. (67)	2011	Japan	Colon and rectum	180	35.16	qRT-PCR	NA	High/Low	6	High	Yes	NA
Takeda et al. (68)	2011	Japan	CRC	60	NA	IHC	Median 5%	High/Low	6	High	Yes	NA
Becker et al. (69)	2010	USA	Barrett's esophagus and esophageal adenocarcinoma dote	81	32	IHC	SI >5	High/Low	6	High	No	OS
Fan et al. (70)	2010	China	CRC	102	NA	IHC	NA	Positive/Negative	7	Positive	Yes	NA

NOS; Newcastle-Ottawa scale, NA; Not available, CRC; Colorectal cancer, TNBC; Triple negative breast cancer, ICC; Intrahepatic cholangiocarcinoma, GAS; Gastric adenocarcinoma, ESCC; Esophageal squamous cell carcinoma, NSCLC; Non-small cell lung cancer, GC; Gastric cancer, HCC; Hepatocellular carcinoma, SCCE; Small cell carcinoma of the esophagus, IHC; Immunohistochemistry, qRT-PCR; Real-Time quantitative reverse transcription PCR, ISH; In situ Hybridization, TMA; tissue microarray, SI; Staining intensity, DFS; Disease-free survival, RFS; Relapse-free survival, and OS; Overall survival.

### Relationship between the expression of the *LGR5* gene and overall survival

Among the 24 studies, including 4956 patients, correlation between *LGR5* expression and OS was significant. Therefore, meta-analysis of the total data of 24 studies using the random effect model revealed a positive and significant correlation between the expression of *LGR5* and OS [pooled HR (95% CI): 1.33 (1.02, 1.74, Fig.2A)]. There was a high and significant level of heterogeneity found among the studies ( $I^2=82.50%$ ,  $P<0.001$ ). Table 2 shows results of the subgroup meta-analysis according to cancer type, detection method, ethnicity, and model type. The association between OS and *LGR5* expression was significant for colorectal cancer groups [pooled HR (95%

CI): 1.70 (1.06, 2.72);  $I^2=88.20%$ ,  $P<0.001$ ], detection method of qRT-PCR [pooled HR (95% CI): 2.68 (1.27, 5.65);  $I^2=65.20%$ ,  $P=0.056$ ], and multiple models [pooled HR (95% CI): 1.35 (1.01, 1.81);  $I^2=84.10%$ ,  $P<0.001$ ). The funnel plots showed symmetry (Fig.2B). Upon analysis, no evidence of publication bias was detected among the studies. ( $P$  for Egger's test=0.963). Meta-regression was used to determine how the effect sizes (HRs) were affected by the sample size and year of publication. The year of publication was a significant factor ( $\beta=-0.11$ ,  $SE=0.05$ ,  $P=0.048$ ) that may have contributed to heterogeneity between the studies. However, sensitivity analysis revealed that the exclusion of individual studies did not affect the overall effect size (HR).

**Table 2:** Subgroup analysis of the correlation between *LGR5* expression and OS

Cancer type	Number of studies	Pooled HR (95% CI)	P value	Heterogeneity	
				$I^2$	P value
Overall	24	1.33 (1.02, 1.74)	0.038	82.50%	<0.001
Cancer type					
Colorectal	8	1.70 (1.06, 2.72)	0.029	88.20%	<0.001
Gastric	3	1.17 (0.34, 4.04)	0.805	90.90%	<0.001
Breast	2	0.77 (0.53, 1.13)	0.189	0.00%	0.742
Head and neck	4	1.43 (0.69, 2.99)	0.337	56.50%	0.075
Lung	3	1.34 (0.71, 2.53)	0.368	63.60%	0.064
Liver	3	0.78 (0.19, 3.10)	0.719	93.00%	<0.001
Other	1	2.13 (0.81, 5.56)			
Detection method					
IHC	17	1.23 (0.85, 1.77)	0.273	82.10%	<0.001
qRT-PCR	3	2.68 (1.27, 5.65)	0.01	65.20%	0.056
RNA-ISH	4	1.03 (0.69, 1.54)	0.883	75.40%	0.007
Ethnicity					
Asian	19	1.29 (0.90, 1.83)	0.167	84.40%	<0.001
Non-Asian	5	1.35 (0.88, 2.08)	0.173	70.00%	0.01
Model type					
Multiple	21	1.35 (1.01, 1.81)	0.045	84.10%	<0.001
Univariate	3	1.15 (0.60, 2.20)	0.679	57.60%	0.094

HR; Hazard ratio, OS; Overall survival, CI; Confidence interval, IHC; Immunohistochemistry, qRT-PCR; Real-Time quantitative reverse transcription PCR, and ISH; In situ hybridization.

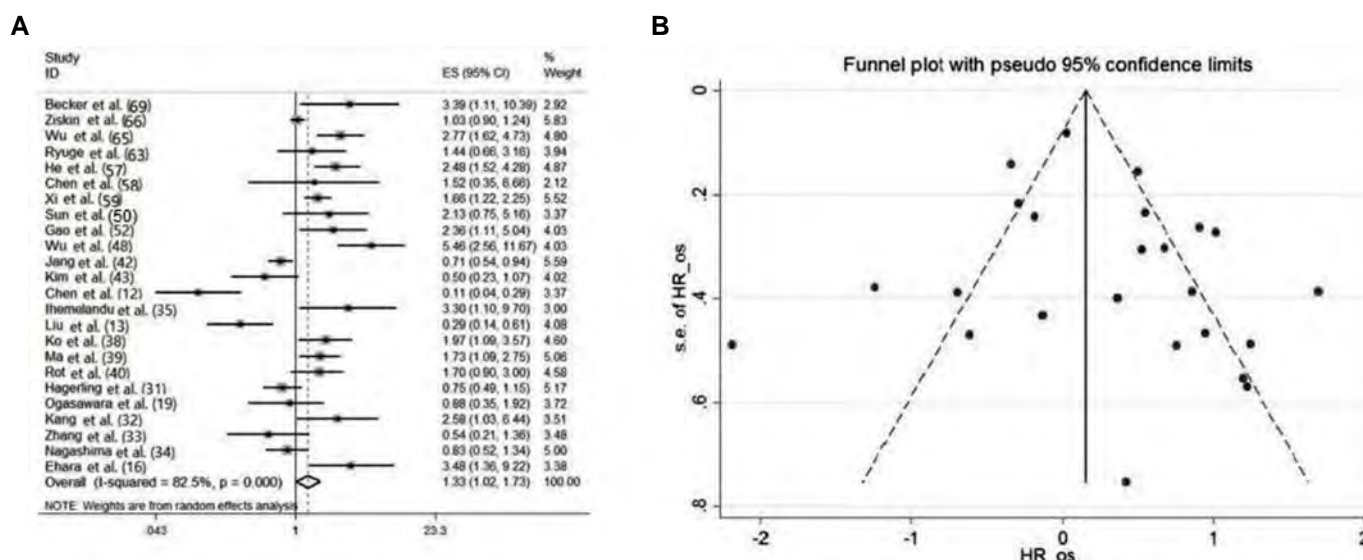


Fig.2: Relationship between the expression of the *LGR5* gene and OS. A. Forest plot and B. Funnel plots.

### Relationship between the expression of *LGR5* gene and disease-free survival

Three studies, involving several colorectal cancer models, which included a total of 676 patients, reported a correlation between *LGR5* expression and DFS. Using the random effects model, meta-analysis of data from three studies did not reveal any significant correlation between *LGR5* expression level and DFS [pooled HR; (95% CI): 1.45 (0.54, 3.94); ( $I^2=88.5%$ ,  $P<0.001$ , Fig.3A)]. None of the studies exhibited publication bias ( $P$  for Egger's test=0.105). Meta-regression analysis indicated that sample size and publication year were not the primary sources of heterogeneity ( $P>0.05$ ). The sensitivity analysis revealed that upon excluding non-Asian studies that used qRT-PCR, the pooled hazard ratio for Asian studies detected by IHC was not statistically significant (pooled HR=1.12 (95% CI: 0.31, 4.01);  $I^2=89.9%$ ,  $P=0.002$ ).

### Relationship between the expression of the *LGR5* gene and relapse-free survival

Four studies, all from Asia including 573 patients, reported a correlation between *LGR5* expression and RFS. Therefore, a meta-analysis of the total data of four studies using the random effect model did not find any significant correlation between high or positive *LGR5* expression and RFS [pooled HR; (95% CI): 2.20 (0.91, 5.33); ( $I^2=70.6%$ ,  $P<0.017$ , Fig.3B)]. None of the studies showed any evidence of publication bias ( $P$  for Egger's test=0.963). Meta-regression analysis found that neither the publication year nor sample size were a significant source of heterogeneity ( $P>0.05$ ). Sensitivity analysis indicated that excluding the study by Nagashima et al. (34) did not alter the results with the univariate model, while the pooled HR for multiple models was significant

[pooled HR=3.62 (95% CI: 1.86, 7.06);  $I^2=1.1%$ ,  $P=0.364$ ]. However, by excluding the study with the detection method of qRT-PCR (Sun et al. 50), the pooled HR on studies with the detection method of IHC was not significant [pooled HR=1.79 (95% CI: 0.60, 5.36);  $I^2=68.1%$ ,  $P=0.043$ ].

### Correlation between *LGR5* expression and clinicopathological features

A total of 48 studies, including 8250 patients, investigated relationship between *LGR5* expression level and clinical pathological features. Table 3 shows correlation between *LGR5* expression and clinicopathological characteristics in cancer patients. Results of the studies revealed that there was no correlation between the expression level of *LGR5* with gender [pooled OR (95% CI): 1.10 (0.97, 1.25), Fig.S1, See Supplementary Online Information at [www.celljournal.org](http://www.celljournal.org)], age [pooled OR (95% CI): 1.26 (0.98, 1.62), Fig.S2A, See Supplementary Online Information at [www.celljournal.org](http://www.celljournal.org)], tumor grade [pooled OR (95% CI): 1.42 (0.40, 5.03); Fig.S2B, See Supplementary Online Information at [www.celljournal.org](http://www.celljournal.org)] and tumor size [pooled OR (95% CI): 1.05 (0.74, 1.48), Fig.S3, See Supplementary Online Information at [www.celljournal.org](http://www.celljournal.org)]. According to results of the study, high expression of *LGR5* is significantly correlated with the advanced stage of tumor [pooled OR (95% CI): 1.91 (1.31, 2.79), Fig.S4A, See Supplementary Online Information at [www.celljournal.org](http://www.celljournal.org)], distant metastasis [pooled OR (95% CI): 1.80 (1.15, 2.83), Fig.S4B, See Supplementary Online Information at [www.celljournal.org](http://www.celljournal.org)] and presence of lymph node metastasis [pooled OR (95% CI): 1.37 (1.02, 1.85), Fig.S5, See Supplementary Online Information at [www.celljournal.org](http://www.celljournal.org)]. The study did not identify any publication bias ( $P$  for Egger's test  $>0.05$ ).



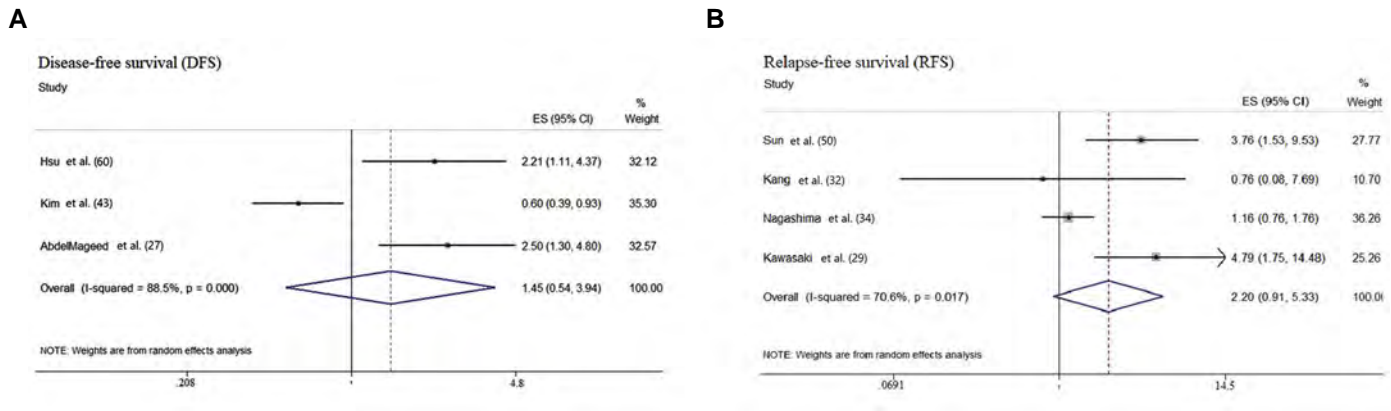


**Fig.3:** Forrest plot of HR. **A.** Forest plot for relationship between the expression of *LGR5* gene and DFS. **B.** Forest plot for relationship between the expression of *LGR5* gene and RFS. HR; Hazard ratio, ES; Effect Size, and CI; Confidence interval.

**Table 3:** Meta-analysis of *LGR5* expression and clinicopathological characteristics

Characteristics	Number of studies	Number of patients	Pooled OR (95%CI)	P value	Heterogeneity		Publication bias (Egger's test)
					I <sup>2</sup> (%)	P value	
Gender (male vs. female)	37	6340	1.10 (0.97, 1.25)	0.134	5.40	0.377	0.768
Age (old vs. young)	11	2472	1.26 (0.98, 1.62)	0.076	46.4	0.045	0.551
Tumor grade (high vs. low)	7	586	1.42 (0.40, 5.03)	0.584	84.70	<0.001	0.506
Tumor size (large vs. small)	21	2888	1.05 (0.74, 1.48)	0.786	67.3	<0.001	0.393
Tumor stage (high vs. low)	32	5929	1.91 (1.31, 2.79)	0.001	87.3	<0.001	0.936
Distant metastasis (present vs. absent)	15	2241	1.80 (1.15, 2.83)	0.011	57.4	0.003	0.089
Lymph node metastasis (present vs. absent)	32	5951	1.37 (1.02, 1.85)	0.036	78.6	<0.001	0.671

OR; Odds ratio and CI; Confidence interval.

## Discussion

As an enhancer of the Wnt signaling pathway, *LGR5* has a crucial functional role in both normal development and cancer (71). *LGR5* has been identified as a marker of CSCs in colorectal, ovarian, esophageal, hepatocellular, and gastric cancers (72, 73). There has been extensive research on the role of *LGR5* in development of tumors, and its correlation with patient survival has been investigated in numerous studies. *LGR5* is overexpressed in gastric cancer, brain cancer, ovarian cancer, and esophageal cancer (74). Several studies have explored the connection between *LGR5* expression and cancer patient outcomes. Although high *LGR5* expression is generally associated with poor prognosis, conflicting findings in some cancers suggested the need for further research. These findings suggested that increased expression of *LGR5* is a negative prognostic factor in multiple types of human cancers

(30, 33). On the contrary, some other reports suggested no significant correlation between *LGR5* expression and tumor outcomes (23, 75).

*LGR5* is now regarded as a recognized marker for breast, and pancreatic CSCs (51, 76). Based on the gradually accumulating scientific evidences on various organs, limited population of stem cells started to demonstrate overexpression of *LGR5*, which may gain other prerequisites and complete their developmental steps to become CSCs (51). It has been shown that in squamous cell carcinoma of the skin, *LGR5* interacted with R-spondin in canonical Wnt receptors and modulated Wnt/ $\beta$ -catenin. Additionally, *LGR5*-Wnt receptor complex internalization caused a delay in endosomal degradation processes (76). In breast cancer, activation of Wnt/ $\beta$ -catenin signaling pathways by *LGR5* promoted growth and invasion in stem-like cells and it

was necessary for maintaining CSCs (77). In contrast, *LGR5* expression did not substantially correlate with tumor characteristics in patients with triple-negative breast cancer (78). Moreover, the results of Kim et al. (79) showed that expression of *LGR5* in ovarian cancer patients during disease progression to invasive cancer was significantly associated with improved outcomes.

Previous studies on gastric cancers have yielded inconsistent results. *LGR5*-positive patients showed considerably shorter survival periods than *LGR5*-negative patients (59). *LGR5* mRNA expression is not regarded as a prognostic predictor in GC, despite the increased *LGR5* expression in tumors following neoadjuvant chemotherapy. These findings demonstrated that *LGR5* expression was not a reliable prognostic indicator for GC. However, it was a negative prognostic marker when restricted to GC with nuclear catenin expression (80).

For many tumors, chemotherapy is the initial line of treatment that kills cancer cells. Recent research demonstrated a correlation between chemotherapy resistance and *LGR5* expression. *LGR5* has been linked to outcome and therapy resistance in GC. It is well documented that experimental overexpression of *LGR5* in spheroids developed from the GC cell line, caused proliferation, enhanced migration as well as development of resistance towards chemotherapy drugs (81). High *LGR5* expression in GC patients was a marker of bad prognosis and demonstration of resistance to the platinum drugs and 5-FU (16). Clark-Corrigall et al. (82) reported correlation between *LGR5* expression and neuroblastoma (NB) resistance to chemotherapy. Ma et al. (39) reported that *LGR5* acted as a tumor initiator to increase cell migration and induced epithelial mesenchymal transitions (EMT) in HCC cells, thereby increasing resistance to doxorubicin. These results showed that *LGR5* was involved in tumorigenesis.

*LGR5* expression was increased with glioma progression and it was connected to negative outcomes (83). Canonical Wnt target genes were overexpressed in the NB tumor taken from patients with advanced disease. High level of Wnt target genes in these tumors accompanied by *LGR5* overexpression was interpreted as Wnt dysregulation in NB (84). Vicari et al. (85) studied *LGR5* activity in NB and concluded that *LGR5* acted as a main hub for Wnt and MEK/ERK signalling regulation in NB. In papillary thyroid carcinoma, there has been a correlation between tumor aggressiveness indicators and *LGR5* overexpression (86).

Substantial evidence highlighted important role of *LGR5* in the pathogenesis of CRC (27, 30). *LGR5* expression is closely associated with tumorigenesis, chemotherapy resistance, and CRC recurrence. However, conflicting results were reported by Jang et al. (42), who found that *LGR5* overexpression reduced proliferation, migration, and colony formation in the late stages of CRC progression. A recent study demonstrated that loss of *LGR5* expression was associated with enhanced resistance to therapy (87).

Therefore, conclusions regarding *LGR5* expression and its clinical outcomes are debated and controversial. To address this issue, we performed a comprehensive meta-analysis of eligible studies to assess prognostic value and clinicopathological characteristics of *LGR5* expression in the various cancers.

Our findings revealed a positive association between *LGR5* expression and OS, with *LGR5* overexpression commonly indicating poor prognosis in cancers. The sub-group analysis result based on cancer type found a significant correlation between expression of *LGR5* and OS in the groups of patients with colorectal cancer, including 2482 patients, which is consistent with the previous study (88). However, this relationship was not observed in another cancer type that was included in the study. This result may show different clinical characteristics and biological behaviors of the *LGR5* in different types of cancer. Relationships between high *LGR5* expression and poor OS were significant in the studies that employed the qRT-PCR method but not IHC, according to the results of a subgroup analysis by this method. These results showed that use of different methods to measure expression of *LGR5* was effective in the final result (23). However, our result found no significant relationship between *LGR5* expression with DFS and RFS. It could be due to the small number of samples. Similar to this result, Ihemelandu et al. (35) observed a negative association between *LGR5* expression and patient survival outcomes, and the small sample size was cited as a limitation of the study. Expression of *LGR5* was influenced by various factors in different cancers. *LGR5* was also present in normal stem cells which governs tissue homeostasis. Potentially these *LGR5*-positive cells are amenable to oncogenic transformation (89). The positive results of *LGR5* expression in cancer are related to its basal level in different organs. *LGR5* is very low in breast and stomach tissue and it may not be expressed at all. But, healthy tissue of the colorectum is more expressive. Probably, lack of *LGR5* in homeostatic state of the cells can lead to its low positivity in some cancers (28). *LGR5* expression may vary in different tumor stages. In Kim et al.'s (90) study, GC was divided into three categories based on the expression pattern of several stem cell markers: basic, focal and scattered patterns. The findings demonstrated that *LGR5* expression was elevated during the baseline state and sustained during the initial phases of GCs. Furthermore, presence of different molecular subgroups in the tumor can affect expression of *LGR5*. In the study of Hagerling et al. (31), it was shown that prognostic value of *LGR5* in patients with ER positive BC patients was different compared to ER negative BC patients, and *LGR5* in BCER negative type has the prognostic value.

Correlation between increased expression of *LGR5* and clinical implications was investigated in several different cancers. In epithelial ovarian cancer, there was a correlation of the positive rate of tumor stage and lymph node metastasis with an elevated expression of *LGR5* (15). A study by Rot et al. (40) on oral squamous cell carcinoma

showed that *LGR5* expression was associated with lymph node metastasis. Abdelrahman et al. (30) showed that there was a relationship of the increased expression of *LGR5* and lymph node metastasis with advanced stage of the tumor in colon cancer. In another study, Liu et al. (13) showed no correlation between *LGR5* expression and age, gender, tumor stage, and lymph node metastasis in gastric cancer. Our findings indicated that *LGR5* expression was linked to pathological variables including tumor stage, distant metastasis and lymph node metastasis, which was consistent with the previous studies and emphasized its potential as a prognostic factor. Our study found no significant association between *LGR5* expression and patient age, sex, tumor size, or grade, contradicting the previous research (37).

This meta-analysis was the first to assess predictive importance of *LGR5* expression in different cancer types. The present study found no evidence of publication bias. However, the study does have limitations. Firstly, it should be noted that all studies included were in English, potentially introducing selection bias. Secondly, the included studies were those which used different cut-off values and detection methods for measuring *LGR5* expression. Thirdly, the limited number of studies evaluating RFS and DFS may have led to further bias. Fourthly, our finding might be most relevant to Asian patients, as the majority of the included studies were conducted in Asia. Fifthly, to ensure the credibility of our findings, we only considered publications providing HR with 95% CI directly and did not estimate HR through Kaplan-Meier curves.

## Conclusion

Our study demonstrated a strong correlation between high *LGR5* expression and poor OS, distant metastasis, tumor stage, and lymph node metastasis in cancer patients. These findings suggested that *LGR5*, a marker for CSCs, could serve as a valuable prognostic indicator and a promising therapeutic target for cancer treatment. However, to verify these findings, well-designed studies with larger populations and more diverse ethnic groups are necessary.

## Acknowledgements

Financial support by the Iran National Science Foundation (INSF) through Grant No. 99025071 is gratefully acknowledged. All authors agree with the content of the article and declare that there is no conflict of interest.

## Authors' Contributions

R.S., S.J.; Conceptualization. S.Gh., S.J.; Methodology and Data curation. S.Gh., A.N.; Investigation and Visualization. S.J., R.N., N.V.; Validation of data. M.Kh., S.Gh., S.J.; Formal analysis. S.Gh., N.V., S.J.; Writing the original draft. R.S., S.Gh.; Review and editing. R.S.; Supervision. All authors read and approved the final

manuscript for submission.



## References

- Sung H, Ferlay J, Siegel RL, Laversanne M, Soerjomataram I, Jemal A, et al. Global cancer statistics 2020: GLOBOCAN estimates of incidence and mortality worldwide for 36 cancers in 185 countries. *CA Cancer J Clin.* 2021; 71(3): 209-249.
- Li Y, Wang Z, Ajani JA, Song S. Drug resistance and cancer stem cells. *Cell Commun Signal.* 2021; 19(1): 19.
- Kelley RK, Wang G, Venook AP. Biomarker use in colorectal cancer therapy. *J Natl Compr Canc Netw.* 2011; 9(11): 1293-1302.
- Hung KF, Yang T, Kao SY. Cancer stem cell theory: are we moving past the mist? *J Chin Med Assoc.* 2019; 82(11): 814-818.
- Marzagalli M, Fontana F, Raimondi M, Limonta P. Cancer stem cells-key players in tumor relapse. *Cancers (Basel).* 2021; 13(3): 376.
- Lathia JD, Mack SC, Mulkearns-Hubert EE, Valentim CL, Rich JN. Cancer stem cells in glioblastoma. *Genes Dev.* 2015; 29(12): 1203-1217.
- Carnero A, Garcia-Mayea Y, Mir C, Lorente J, Rubio IT, Lleonart ME. The cancer stem-cell signaling network and resistance to therapy. *Cancer Treat Rev.* 2016; 49: 25-36.
- Xu H, Li W, Song X, Zhang H, Wang H, Wang J, et al. Expression and prognostic value of Lgr5 in patients with recurrent nasopharyngeal carcinoma. *Int J Gen Med.* 2023; 16: 2023-2034.
- Walcher L, Kistenmacher AK, Suo H, Kitte R, Dluczek S, Strauß A, et al. Cancer stem cells-origins and biomarkers: perspectives for targeted personalized therapies. *Front Immunol.* 2020; 11: 1280.
- Haegebarth A, Clevers H. Wnt signaling, lgr5, and stem cells in the intestine and skin. *Am J Pathol.* 2009; 174(3): 715-721.
- de Lau W, Peng WC, Gros P, Clevers H. The R-spondin/Lgr5/Rnf43 module: regulator of Wnt signal strength. *Genes Dev.* 2014; 28(4): 305-316.
- Chen W, Fu Q, Fang F, Fang J, Zhang Q, Hong Y. Overexpression of leucine-rich repeat-containing G protein-coupled receptor 5 predicts poor prognosis in hepatocellular carcinoma. *Saudi J Biol Sci.* 2018; 25(5): 904-908.
- Liu XS, Lin XK, Mei Y, Ahmad S, Yan CX, Jin HL, et al. Regulatory T cells promote overexpression of Lgr5 on gastric cancer cells via TGF-beta1 and confer poor prognosis in gastric cancer. *Front Immunol.* 2019; 10: 1741.
- Xu N, Gao K, Luo H, Wu Y, Shen B, Liu K. Correlation of Lgr5 expression with clinicopathological features of colorectal cancer and its diagnostic and prognostic values. *J BUON.* 2021; 26(1): 87-92.
- Yu L, Mao X, Wu S, Zhou L, Song W, Gong X, et al. The correlation of the expressions of WWOX, LGR5 and vasohibin-1 in epithelial ovarian cancer and their clinical significance. *Int J Clin Exp Pathol.* 2019; 12(1): 327-336.
- Ehara T, Uehara T, Nakajima T, Kinugawa Y, Kobayashi S, Iwaya M, et al. LGR5 expression is associated with prognosis in poorly differentiated gastric adenocarcinoma. *BMC Cancer.* 2021; 21(1): 228.
- Sato K, Uehara T, Nakajima T, Iwaya M, Miyagawa Y, Watanabe T, et al. Inverse correlation between PD-L1 expression and LGR5 expression in tumor budding of stage II/III colorectal cancer. *Ann Diagn Pathol.* 2021; 52: 151739.
- Kuraishi Y, Uehara T, Kobayashi Y, Nakajima T, Watanabe T, Shimizu A, et al. Correlation of clinicopathological features and leucine-rich repeat-containing G-protein-coupled receptor 5 expression in pancreatic ductal adenocarcinoma. *Pathol Res Pract.* 2019; 215(11): 152623.
- Ogasawara S, Uehara T, Nakajima T, Iwaya M, Maeno K, Tsuchiya S, et al. Correlation of clinicopathological features and LGR5 expression in triple-negative breast cancer. *Ann Diagn Pathol.* 2020; 46: 151491.
- Yoshizawa T, Uehara T, Iwaya M, Asaka S, Kobayashi S, Nakajima T, et al. Correlation of LGR5 expression and clinicopathological features in intrahepatic cholangiocarcinoma. *Pathol Res Pract.* 2022; 232: 153832.
- Nagata H, Ishihara S, Kishikawa J, Sonoda H, Murono K, Emoto S, et al. CD133 expression predicts post-operative recurrence in patients with colon cancer with peritoneal metastasis. *Int J Oncol.* 2018; 52(3): 721-732.
- Cao W, Li M, Liu J, Zhang S, Noordam L, Verstegen MMA, et al. LGR5 marks targetable tumor-initiating cells in mouse liver cancer. *Nat Commun.* 2020; 11(1): 1961.
- Sato K, Uehara T, Iwaya M, Nakajima T, Miyagawa Y, Ota H, et al.

- Correlation of clinicopathological features and LGR5 expression in colon adenocarcinoma. *Ann Diagn Pathol.* 2020; 48: 151587.
24. Shekarriz R, Montazer F, Alizadeh-Navaei R. Overexpression of cancer stem cell marker Lgr5 in colorectal cancer patients and association with clinicopathological findings. *Caspian J Intern Med.* 2019; 10(4): 412-416.
  25. Liberati A, Altman DG, Tetzlaff J, Mulrow C, Gøtzsche PC, Ioannidis JP, et al. The PRISMA statement for reporting systematic reviews and meta-analyses of studies that evaluate healthcare interventions: explanation and elaboration. *BMJ.* 2009; 339: b2700.
  26. Stang A. Critical evaluation of the Newcastle-Ottawa scale for the assessment of the quality of nonrandomized studies in meta-analyses. *Eur J Epidemiol.* 2010; 25(9): 603-605.
  27. AbdelMageed M, Ismail HTH, Olsson L, Lindmark G, Hammarström ML, Hammarström S, et al. Clinical significance of stem cell biomarkers EpCAM, LGR5 and LGR4 mRNA levels in lymph nodes of colon cancer patients. *Int J Mol Sci.* 2021; 23(1): 403.
  28. Lee HJ, Myung JK, Kim HS, Lee DH, Go HS, Choi JH, et al. Expression of LGR5 in mammary myoepithelial cells and in triple-negative breast cancers. *Sci Rep.* 2021; 11(1): 17750.
  29. Kawasaki K, Kuboki S, Furukawa K, Takayashiki T, Takano S, Ohtsuka M. LGR5 induces  $\beta$ -catenin activation and augments tumour progression by activating STAT3 in human intrahepatic cholangiocarcinoma. *Liver International.* 2021; 41(4): 865-881.
  30. Abdelrahman AE, El-Azony A, Elsebai E, Ibrahim HM. Prognostic impact of LGR5, Prox1, and Notch1 biomarkers in stage II to III colon cancer. *Appl Immunohistochem Mol Morphol.* 2022; 30(2): 126-135.
  31. Hagerling C, Owyong M, Sitarama V, Wang C-Y, Lin C, Van Den Bijgaart R J, et al. LGR5 in breast cancer and ductal carcinoma in situ: a diagnostic and prognostic biomarker and a therapeutic target. *BMC Cancer.* 2020; 20(1): 542.
  32. Kang XL, He LR, Chen YL, Wang SB. Role of doublecortin-like kinase 1 and leucine-rich repeat-containing G-protein-coupled receptor 5 in patients with stage II/III colorectal cancer: cancer progression and prognosis. *World J Gastroenterol.* 2020; 26(43): 6853-6866.
  33. Zhang X, Yuan A, Zhao X, Li Z, Cui G. Tumoral expression of CD166 in human esophageal squamous cell carcinoma: implications for cancer progression and prognosis. *Cancer Biother Radiopharm.* 2020; 35(3): 214-222.
  34. Nagashima T, Oshima T, Hiroshima Y, Yokose T, Woo T, Rino Y, et al. Clinical significance of tumour CD44v and MIST1 expression in patients with non-small-cell lung cancer. *Anticancer Res.* 2020; 40(11): 6407-6416.
  35. Ihemelandu C, Naeem A, Parasido E, Berry D, Chaldeckas K, Harris BT, et al. Clinicopathologic and prognostic significance of LGR5, a cancer stem cell marker in patients with colorectal cancer. *Colorectal Cancer.* 2019; 8(4): CRC11.
  36. Shen R, Wu T, Huang P, Shao Q, Chen M. The clinicopathological significance of ubiquitin-conjugating enzyme E2C, leucine-rich repeated-containing G protein-coupled receptor, WW domain-containing oxidoreductase, and vasculogenic mimicry in invasive breast carcinoma. *Medicine (Baltimore).* 2019; 98(16): e15232.
  37. Freiin Grote A, Halske C, Behrens HM, Krüger S, Wilhelm F, Egberts JH, et al. Expression of LGR5, FZD7, TROY, and MIST1 in perioperatively treated gastric carcinomas and correlation with therapy response. *Dis Markers.* 2019; 2019: 8154926.
  38. Ko CJ, Li CJ, Wu MY, Chu PY. Overexpression of LGR-5 as a predictor of poor outcome in patients with hepatocellular carcinoma. *Int J Environ Res Public Health.* 2019; 16(10): 1836.
  39. Ma Z, Guo D, Wang Q, Liu P, Xiao Y, Wu P, et al. Lgr5-mediated p53 repression through PDCD5 leads to doxorubicin resistance in hepatocellular carcinoma. *Theranostics.* 2019; 9(10): 2967-2983.
  40. Rot S, Kaune T, Taubert H, Greither T, Kotrba J, Güttler A, et al. Prognostic impact of mRNA levels of LGR5 transcript variants in OSCC patients. *BMC Cancer.* 2019; 19(1): 155.
  41. Hou MF, Chen PM, Chu PY. LGR5 overexpression confers poor relapse-free survival in breast cancer patients. *BMC Cancer.* 2018; 18(1): 219.
  42. Jang BG, Kim HS, Chang WY, Bae JM, Kim WH, Kang GH. Expression profile of LGR5 and its prognostic significance in colorectal cancer progression. *Am J Pathol.* 2018; 188(10): 2236-2250.
  43. Kim YJ, Kang DH, Song GJ, Ahn TS, Son MW, Lee MS, et al. Clinical relevance of Lgr5 expression in colorectal cancer patients. *Korean J Clin Oncol.* 2018; 14(2): 76-82.
  44. Harada Y, Kazama S, Morikawa T, Murono K, Yasuda K, Otani K, et al. Leucine-rich repeat-containing G protein-coupled receptor 5 and CD133 expression is associated with tumor progression and resistance to preoperative chemoradiotherapy in low rectal cancer. *Oncol Lett.* 2017; 14(6): 7791-7798.
  45. Lv Z, Yu JJ, Zhang WJ, Xiong L, Wang F, Li LF, et al. Expression and functional regulation of stemness gene Lgr5 in esophageal squamous cell carcinoma. *Oncotarget.* 2017; 8(16): 26492-26504.
  46. Liu J, Yu GZ, Cheng XK, Li XD, Zeng XT, Ren XQ. LGR5 promotes hepatocellular carcinoma metastasis through inducing epithelial-mesenchymal transition. *Oncotarget.* 2017; 8(31): 50896-50903.
  47. Wu Z, Song W, Cheng Z, Yang D, Yu L. Expression of LGR5 in oral squamous cell carcinoma and its correlation to vasculogenic mimicry. *Int J Clin Exp Pathol.* 2017; 10(11): 11267-11275.
  48. Wu W, Cao J, Ji Z, Wang J, Jiang T, Ding H. Co-expression of Lgr5 and CXCR4 characterizes cancer stem-like cells of colorectal cancer. *Oncotarget.* 2016; 7(49): 81144-81155.
  49. Jang BG, Lee BL, Kim WH. Prognostic significance of leucine-rich-repeat-containing G-protein-coupled receptor 5, an intestinal stem cell marker, in gastric carcinomas. *Gastric Cancer.* 2016; 19(3): 767-777.
  50. Sun B, Ye X, Li Y, Zhang W. Lgr5 is a potential prognostic marker in patients with cervical carcinoma. *Int J Clin Exp Pathol.* 2015; 8(2): 1783-1789.
  51. Yang L, Tang H, Kong Y, Xie X, Chen J, Song C, et al. LGR5 promotes breast cancer progression and maintains stem-like cells through activation of Wnt/ $\beta$ -catenin signaling. *Stem Cells.* 2015; 33(10): 2913-2924.
  52. Gao F, Zhou B, Xu JC, Gao X, Li SX, Zhu GC, et al. The role of LGR5 and ALDH1A1 in non-small cell lung cancer: Cancer progression and prognosis. *Biochem Biophys Res Commun.* 2015; 462(2): 91-98.
  53. Sun Y, Jia X, Wu X. High expressions of Lgr5 and ALDH1 in primary epithelial ovarian cancer correlate with advanced tumor stage and grade as well as poor prognosis of the patients. *Gynecol Obstet Invest.* 2015 (ahead of print)
  54. Wang Y, Jiang CQ, Fan LF. Correlation of Musashi-1, Lgr5, and pEGFR expressions in human small intestinal adenocarcinomas. *Tumour Biol.* 2015; 36(8): 6075-6082.
  55. Gao FJ, Chen JY, Wu HY, Shi J, Chen M, Fan XS, et al. Lgr5 overexpression is positively related to the tumor progression and HER2 expression in stage pTNN IV colorectal cancer. *Int J Clin Exp Pathol.* 2014; 7(4): 1572-1579.
  56. Liu Z, Dai W, Jiang L, Cheng Y. Over-expression of LGR5 correlates with poor survival of colon cancer in mice as well as in patients. *Neoplasia.* 2014; 61(2): 177-185.
  57. He S, Zhou H, Zhu X, Hu S, Fei M, Wan D, et al. Expression of Lgr5, a marker of intestinal stem cells, in colorectal cancer and its clinicopathological significance. *Biomed Pharmacother.* 2014; 68(5): 507-513.
  58. Chen WW, Wang F, Zhang DS, Luo HY, Wang ZQ, Wang FH, et al. Primary small cell carcinoma of the esophagus: clinicopathological study of 44 cases. *BMC Cancer.* 2014; 14: 222.
  59. Xi HQ, Cai AZ, Wu XS, Cui JX, Shen WS, Bian SB, et al. Leucine-rich repeat-containing G-protein-coupled receptor 5 is associated with invasion, metastasis, and could be a potential therapeutic target in human gastric cancer. *Br J Cancer.* 2014; 110(8): 2011-2020.
  60. Hsu HC, Liu YS, Tseng KC, Hsu CL, Liang Y, Yang TS, et al. Over-expression of Lgr5 correlates with resistance to 5-FU-based chemotherapy in colorectal cancer. *Int J Colorectal Dis.* 2013; 28(11): 1535-1546.
  61. Jang BG, Lee BL, Kim WH. Distribution of LGR5+ cells and associated implications during the early stage of gastric tumorigenesis. *PLoS One.* 2013; 8(12): e82390.
  62. Zheng ZX, Sun Y, Bu ZD, Zhang LH, Li ZY, Wu AW, et al. Intestinal stem cell marker LGR5 expression during gastric carcinogenesis. *World J Gastroenterol.* 2013; 19(46): 8714-8721.
  63. Ryuge S, Sato Y, Jiang SX, Wang G, Kobayashi M, Nagashio R, et al. The clinicopathological significance of Lgr5 expression in lung adenocarcinoma. *Lung Cancer.* 2013; 82(1): 143-148.
  64. Bu Z, Zheng Z, Zhang L, Li Z, Sun Y, Dong B, et al. LGR5 is a promising biomarker for patients with stage I and II gastric cancer. *Chin J Cancer Res.* 2013; 25(1): 79-89.
  65. Wu XS, Xi HQ, Chen L. Lgr5 is a potential marker of colorectal carcinoma stem cells that correlates with patient survival. *World J Surg Oncol.* 2012; 10: 244.
  66. Ziskin JL, Dunlap D, Yaylaoglu M, Fodor IK, Forrest WF, Patel R, et al. In situ validation of an intestinal stem cell signature in colorectal cancer. *Gut.* 2013; 62(7): 1012-1023.
  67. Takahashi H, Ishii H, Nishida N, Takemasa I, Mizushima T, Ikeda M, et al. Significance of Lgr5(+ve) cancer stem cells in the colon and rectum. *Ann Surg Oncol.* 2011; 18(4): 1166-1174.

68. Takeda K, Kinoshita I, Shimizu Y, Matsuno Y, Shichinohe T, Dosaka-Akita H. Expression of LGR5, an intestinal stem cell marker, during each stage of colorectal tumorigenesis. *Anticancer Res.* 2011; 31(1): 263-270.
69. Becker L, Huang Q, Mashimo H. Lgr5, an intestinal stem cell marker, is abnormally expressed in Barrett's esophagus and esophageal adenocarcinoma. *Dis Esophagus.* 2010; 23(2): 168-174.
70. Fan XS, Wu HY, Yu HP, Zhou Q, Zhang YF, Huang Q. Expression of Lgr5 in human colorectal carcinogenesis and its potential correlation with beta-catenin. *Int J Colorectal Dis.* 2010; 25(5): 583-590.
71. Hsu SY, Liang SG, Hsueh AJ. Characterization of two LGR genes homologous to gonadotropin and thyrotropin receptors with extracellular leucine-rich repeats and a G protein-coupled, seven-transmembrane region. *Mol Endocrinol.* 1998; 12(12): 1830-1845.
72. Leng Z, Xia Q, Chen J, Li Y, Xu J, Zhao E, et al. Lgr5+CD44+EpCAM+ strictly defines cancer stem cells in human colorectal cancer. *Cell Physiol Biochem.* 2018; 46(2): 860-872.
73. Wang X, Wang X, Liu Y, Dong Y, Wang Y, Kassab MA, et al. LGR5 regulates gastric adenocarcinoma cell proliferation and invasion via activating Wnt signaling pathway. *Oncogenesis.* 2018; 7(8): 57.
74. Xu L, Lin W, Wen L, Li G. Lgr5 in cancer biology: functional identification of Lgr5 in cancer progression and potential opportunities for novel therapy. *Stem Cell Res Ther.* 2019; 10(1): 219.
75. Vaquero J, Guedj N, Clapéron A, Nguyen Ho-Bouidoires TH, Paradis V, Fouassier L. Epithelial-mesenchymal transition in cholangiocarcinoma: From clinical evidence to regulatory networks. *J Hepatol.* 2017; 66(2): 424-441.
76. Liu S, Gong Z, Chen M, Liu B, Bian D, Wu K. Lgr5-positive cells are cancer stem cells in skin squamous cell carcinoma. *Tumour Biol.* 2014; 35(11): 11605-11612.
77. Trimboli AJ, Fukino K, de Bruin A, Wei G, Shen L, Tanner SM, et al. Direct evidence for epithelial-mesenchymal transitions in breast cancer. *Cancer Res.* 2008; 68(3): 937-945.
78. Montazer F, Boozari B, Alizadeh-Navaei R. Evaluation of LGR5 cancer stem cell marker expression in breast cancer and its relationship with hormonal profile and clinical pathological features. *Asian Pac J Cancer Prev.* 2023; 24(2): 467-470.
79. Kim H, Lee DH, Park E, Myung JK, Park JH, Kim DI, et al. Differential epithelial and stromal LGR5 expression in ovarian carcinogenesis. *Sci Rep.* 2022; 12(1): 11200.
80. Bauer L, Langer R, Becker K, Hapfelmeier A, Ott K, Novotny A, et al. Expression profiling of stem cell-related genes in neoadjuvant-treated gastric cancer: a NOTCH2, GSK3B and  $\beta$ -catenin gene signature predicts survival. *PLoS One.* 2012; 7(9): e44566.
81. Jia Y, Li Z, Cheng X, Wu X, Pang F, Shi J, et al. Depletion of death-associated protein-3 induces chemoresistance in gastric cancer cells through the  $\beta$ -catenin/LGR5/Bcl-2 axis. *J Investig Med.* 2019; 67(5): 856-861.
82. Clark-Corrigan J, Myssina S, Michaelis M, Cinatl J Jr, Ahmed S, Carr-Wilkinson J. Elevated expression of LGR5 and WNT signaling factors in neuroblastoma cells with acquired drug resistance. *Cancer Invest.* 2023; 41(2): 173-182.
83. Nakata S, Phillips E, Goidts V. Emerging role for leucine-rich repeat-containing G-protein-coupled receptors LGR5 and LGR4 in cancer stem cells. *Cancer Manag Res.* 2014; 6: 171-180.
84. Liu X, Mazanek P, Dam V, Wang Q, Zhao H, Guo R, et al. Downregulated Wnt/ $\beta$ -catenin program in high-risk neuroblastomas without MYCN amplification. *Oncogene.* 2008; 27(10): 1478-1488.
85. Vicari L, Colarossi C, Giuffrida D, De Maria R, Memeo L. Cancer stem cells as a potential therapeutic target in thyroid carcinoma. *Oncol Lett.* 2016; 12(4): 2254-2260.
86. Michelotti G, Jiang X, Sosa JA, Diehl AM, Henderson BB. LGR5 is associated with tumor aggressiveness in papillary thyroid cancer. *Oncotarget.* 2015; 6(33): 34549-34560.
87. Posey TA, Jacob J, Parkhurst A, Subramanian S, Francisco LE, Liang Z, et al. Loss of LGR5 through therapy-induced downregulation or gene ablation is associated with resistance and enhanced MET-STAT3 signaling in colorectal cancer cells. *Mol Cancer Ther.* 2023; 22(5): 667-678.
88. Yang L, Lin Y, Liu Z, Li Y, Liu Y, Liang R. Impact of LGR5 in colorectal cancer on overall and progression-free survival: a systematic review and meta-analysis. *Int J Clin Exp Med.* 2016; 9(9): 10537-10543.
89. Sigal M, Rothenberg ME, Logan CY, Lee JY, Honaker RW, Cooper RL, et al. *Helicobacter pylori* activates and expands Lgr5(+) stem cells through direct colonization of the gastric glands. *Gastroenterology.* 2015; 148(7): 1392-1404. e21.
90. Kim HS, Song HJ, Kim HU, Jeong IH, Koh HM, Shin JH, et al. Expression profile of intestinal stem cell and cancer stem cell markers in gastric cancers with submucosal invasion. *Pathol Res Pract.* 2021; 218: 153336.

# Identification and Functional Characterization of PI3K/Akt/mTOR Pathway-Related lncRNAs in Lung Adenocarcinoma: A Retrospective Study

Jiaqi Zhong, B.Sc.<sup>1#</sup>, Ying Kong, M.Sc.<sup>2#</sup>, Ruming Li, B.Sc.<sup>1</sup>, Minghan Feng, B.Sc.<sup>1</sup>, Liming Li, B.Sc.<sup>1</sup>,  
Xiao Zhu, Ph.D.<sup>1\*</sup> , Lianzhou Chen, M.D.<sup>3\*</sup> 

1. The Marine Biomedical Research Institute of Guangdong Zhanjiang, School of Ocean and Tropical Medicine, Guangdong Medical University, Zhanjiang, China
2. Department of Clinical Laboratory, The Third People's Hospital of Hubei Province, Wuhan, China
3. Laboratory of General Surgery, The First Affiliated Hospital, Sun Yat-sen University, Guangzhou, China

## Abstract

**Objective:** This paper aimed to investigate the PI3K/Akt/mTOR signal-pathway regulator factor-related lncRNA signatures (PAM-SRFLncSigs), associated with regulators of the indicated signaling pathway in patients with lung adenocarcinoma (LUAD) undergoing immunotherapy.

**Materials and Methods:** In this retrospective study, we employed univariate Cox, multivariate Cox, and least absolute shrinkage and selection operator (LASSO) regression analyses to identify prognostically relevant long non-coding RNAs (lncRNAs), construct prognostic models, and perform Gene Ontology (GO) and Kyoto Encyclopedia of Genes and Genomes (KEGG) analyses. Subsequently, immunoassay and chemotherapy drug screening were conducted. Finally, the prognostic model was validated using the Imvigor210 cohort, and tumor stem cells were analyzed.

**Results:** We identified seven prognosis-related lncRNAs (*AC084757.3*, *AC010999.2*, *LINC02802*, *AC026979.2*, *AC024896.1*, *LINC00941* and *LINC01312*). We also developed prognostic models to predict survival in patients with LUAD. KEGG enrichment analysis confirmed association of LUAD with the PI3K/Akt/mTOR signaling pathway. In the analysis of immune function pathways, we discovered three good prognostic pathways (Cytolytic activity, Inflammation-promoting, T\_cell\_co-inhibition) in LUAD. Additionally, we screened 73 oncology chemotherapy drugs using the "pRRophetic" algorithm.

**Conclusion:** Identification of seven lncRNAs linked to regulators of the PI3K/Akt/mTOR signaling pathway provided valuable insights into predicting the prognosis of LUAD, understanding the immune microenvironment and optimizing immunotherapy strategies.

**Keywords:** Immunotherapy, lncRNAs, Lung Adenocarcinoma, Prognosis, Tumor Microenvironment

**Citation:** Zhong J, Kong Y, Li R, Feng M, Li L, Zhu X, Chen L. Identification and functional characterization of PI3K/Akt/mTOR pathway-related lncRNAs in lung adenocarcinoma: a retrospective study. *Cell J.* 2024; 26(1): 13-27. doi: 10.22074/CELLJ.2023.2007918.1378

This open-access article has been published under the terms of the Creative Commons Attribution Non-Commercial 3.0 (CC BY-NC 3.0).

## Introduction

Lung cancer is the malignancy with the highest morbidity and mortality worldwide. The main type of non-small cell lung cancer (NSCLC) is LUAD. PI3K/Akt/mTOR signaling pathway, as a crucial regulator of various cellular processes including cell proliferation, growth, survival, migration, apoptosis, translation, glucose metabolism and DNA repair, plays a pivotal role in essential cellular activities (1). The primary objective of regulating PI3K-AKT pathway is to stimulate cellular growth and proliferation. However, excessive activation of this signaling pathway leads to an overstimulation of cells, resulting in abnormal cell proliferation, such

as tumorigenesis, as well as involvement in tumor erosion and metastasis. Dysregulation of this pathway is commonly observed in cancer, exerting control over multiple cancer-related features. It has been shown that aberrant activation or inhibition of the intracellular PI3K/Akt/mTOR pathway has been identified as a major contributor to cancer cell resistance against antitumor therapies (2). Notably, patients with EGFR mutations accompanied with PI3K pathway activation exhibited shorter progression-free survival (PFS) and overall survival (OS) (3). Activation of the PI3K/Akt/mTOR signaling pathway has been demonstrated to be prevalent in diffuse gliomas and escalated with tumor grade (4).

Received: 31/July/2023, Revised: 08/October/2023, Accepted: 18/November/2023

#These authors contributed equally in this study.

\*Corresponding Addresses: The Marine Biomedical Research Institute of Guangdong Zhanjiang, School of Ocean and Tropical Medicine, Guangdong Medical University, Zhanjiang, China  
Laboratory of General Surgery, The First Affiliated Hospital, Sun Yat-sen University, Guangzhou, China

Emails: xzhu@gdmu.edu.cn, chlianzhou@mail.sysu.edu.cn



Excessive activation of the PI3K/Akt/mTOR pathway can detrimentally impact the patient's prognosis. In the selected preclinical and initial clinical trials, targeted therapeutic intervention through inhibition of PI3K/Akt/mTOR signaling has been contemplated as a viable strategy due to its intimate correlation with tumorigenesis and disease progression (5).

Many individuals diagnosed with lung cancer are unfortunately diagnosed in the advanced stages of the disease, either with locally progressed tumors or metastatic spread. This delayed diagnosis, coupled with the absence of suitable therapeutic targets, contributed to the unfavorable prognosis experienced by patients (6, 7). Consequently, it becomes imperative to investigate potential biomarkers that can aid in the early detection and treatment of LUAD, enabling intervention at an earlier stage. Through our research, we identified some lncRNAs as diagnostic biomarkers for LUAD patients (7-9). Despite their inability to encode proteins, lncRNAs play a pivotal role in gene transcription and expression. Numerous studies have demonstrated the involvement of lncRNAs in the various diseases, influencing critical cellular functions, such as chromatin modification, gene expression regulation, cell differentiation, and cell cycle progression. Additionally, lncRNAs can exert their effects by acting as competing RNAs, thereby impacting expression of the target genes (10, 11). In general, lncRNAs carry out their functions by interacting with various biomolecules, including DNA, RNA and proteins. They play a crucial role in regulation of gene expression, which significantly impacts tumorigenesis and disease progression. Nevertheless, specific roles of these lncRNAs in lung adenocarcinoma (LUAD) and their precise association with the PI3K/AKT/mTOR signaling pathway remained largely unknown.

Overall, the PI3K/AKT/mTOR pathway serves as a vital coordinator of cellular responses to internal and external stimuli, thereby influencing key processes associated with carcinogenesis (12). Hence, investigating the expression patterns of lncRNAs associated with the PI3K/AKT/mTOR signaling pathway in LUAD, in addition to comprehending their diverse expressions and functions in LUAD can furnish us with a more profound comprehension of LUAD. Furthermore, this exploration can unveil pivotal regulatory factors in the mechanism of LUAD development, as well as the biological mechanisms of drug resistance, thereby offering novel prospects for prevention, diagnosis and treatment of LUAD. In our investigation, we meticulously scrutinized and sieved through PAM-SRFLncSig to construct a prognostic risk model tailored specifically for LUAD patients. Through this approach, we delved into the intricate interplay between PAM-SRFLncSig and LUAD prognosis, as well as its impact on the immune microenvironment and potential implications for immunotherapy. Additionally, we identified promising molecular markers and potential drug targets, thus presenting a fresh research strategy for LUAD immunotherapy.

## Materials and Methods

### Databases

The flow chart of this study is shown in Figure S1A (See Supplementary Online Information at [www.celljournal.org](http://www.celljournal.org)). The Molecular Signature Database (MSigDB) is a comprehensive resource housing numerous annotated gene sets, meticulously categorized into human and mouse collections. In this investigation, we initially procured four gene sets associated with the PI3K/Akt/mTOR signaling pathway from MSigDB. The database can be accessed at <https://www.gsea-msigdb.org/gsea/msigdb/index.jsp> website. Specifically, we focused on the WikiPathways gene set labeled as CP (canonical pathways) within the human gene C2 (curated gene sets) in MSigDB. The downloaded gene sets were as follows: "WP\_FOCAL\_ADHESIONPI3KAKTMTORSIGNALING\_PATHWAY (n=309)", "WP\_PI3KAKTMTOR\_SIGNALING\_PATHWAY\_AND\_THERAPEUTIC\_OPPORTUNITIES (n=30)" and "WP\_PI3KAKTMTOR\_VITD3\_SIGNALING (n=22)". The "HALLMARK\_PI3K\_AKT\_MTOR\_SIGNALING" gene set (n=105) was subsequently acquired from the H (hallmark gene sets) category, focusing on the genes up-regulated upon activation of the PI3K/AKT/mTOR pathway. After eliminating duplicate genes from the four gene sets, a final set of 399 genes associated with the PI3K/Akt/mTOR signaling pathway was obtained and included in the subsequent analysis (Fig.S1B, Table S1, See Supplementary Online Information at [www.celljournal.org](http://www.celljournal.org)). The data for this study encompassed mRNA transcription data (n=19508), lncRNA transcription data (n=13481), corresponding clinical information files (Table S2, See Supplementary Online Information at [www.celljournal.org](http://www.celljournal.org)), and prognostic data from 494 patients with LUAD, which were obtained from The Cancer Genome Atlas (TCGA; <https://portal.gdc.cancer.gov/>), as a collaborative resource established by the National Cancer Institute and the National Human Genome Research Institute, which provides comprehensive cancer genomic data, including mutation, mRNA expression and methylation data. Patient data from the IMVigor210 clinical trial were also downloaded from the "IMVigor210CoreBiologies" R package.

### Extracting expression matrix of lncRNAs co-expressed with the gene sets

For data analysis, we utilized the "R software (version 4.1.3)". Initially, we extracted expression matrix of the lncRNAs co-expressed with the PI3K/AKT/mTOR gene set using the "limma" package. The data were processed and subjected to a Pearson correlation test, and a total of 3610 lncRNA associated with LUAD were identified ( $|\text{cor}| > 0.4$ ,  $P < 0.0001$ ). The resulting genome-lncRNA associations were visualized using a Sankey diagram. Then, we constructed a prognostic model for genome-associated lncRNAs using the "limma" package.

### Construction of the correlated lncRNAs prognostic model with Cox regression analysis

We conducted univariate Cox regression analysis to identify significant lncRNAs ( $P < 0.05$ ) and established correlation of lncRNA expression with patient survival. To streamline our model, we employed LASSO regression, which incorporated a penalty function into the commonly used multiple linear regression, continuously compressing the coefficients to prevent covariance and overfitting (13). Risk factor for each gene was calculated using the following formula (7-9):

$$\text{PAM-SRFLncSig} = \sum I = \ln \text{Coef}(i) \times \text{Expr}(i)$$

Subsequently, the data was divided, and a total of 494 LUAD patients were randomly assigned to the training cohort ( $n=330$ ) and testing cohort ( $n=164$ ). If all p-values between the two groups were non-significant, it indicated that there was no statistical difference in the various clinical indicators of the randomized groups, ensuring well-grouped data without any statistical bias.

### Analysis and validation of a clinically independent prognostic model for patients with LUAD

The LUAD patients in the training cohort were divided into high-risk and low-risk subgroups, based on the median risk score. OS in the both subgroups was analyzed using Kaplan-Meier survival curves ( $P < 0.001$ ). Furthermore, a Cox regression ( $P < 0.001$ ) risk model was established to determine prognosis of clinicopathological factors, including age, gender, race, American Joint Committee on Cancer (AJCC) stage, primary tumor (T), distant metastasis (M), regional lymph nodes (N), and risk score. We developed a mathematical model using the Cox regression risk model. Clinical receiver operating characteristic (ROC) curves and survival time ROC curves were used for this assessment. In addition, we constructed column line plots to predict one, three and five year(s) OS in LUAD patients. These column line plots were created using the “rms” package in the “R software”. Nomograms were employed to visualize parameters related to patient survival. Consistency index (C-index) and calibration curves were used to explore performance of the column line plots and the predicted versus actual survival probabilities.

### GO and KEGG enrichment analysis

To unravel the profound biological implications of PAM-SRFLncSig in LUAD, we embarked on an enrichment analysis employing the GO database and the KEGG pathway to delve into the genes encoding co-expressed proteins of prognostic lncRNAs. By comparing expression of lncRNAs in LUAD patients, we meticulously screened and identified 418 differentially expressed lncRNAs (logFC filter=1, FDR < 0.05), employing the false discovery rate (FDR), as a stringent filter. Subsequently, we subjected these lncRNAs to Gene Ontology (GO) and Kyoto Encyclopedia of Genes and Genomes (KEGG)

analyses, unveiling the enriched p-values for specific GO annotations and KEGG pathways, thereby illuminating the synergistic correlation of the functions of all lncRNAs. We deemed a corrected P value FDR < 0.1, as the significance index for GO enrichment, while  $P < 0.5$  was considered as the significance index for KEGG.

### Immunoassay of PAM-SRFLncSig high- and low-risk subgroups

To assess relative differences in immune profiles between high- and low-risk subgroups, we obtained immunocompetent gene set files and analyzed differential expression of immune checkpoints in these populations. In addition, we performed a single-sample gene set enrichment analysis (ssGSEA) using the “limma”, “GSVA” and “GSEABase” packages in the “R software” to assess the infiltrating immune cells and immune-related functions in LUAD patients. Role of PAM-SRFLncSig in 13 immune functions was assessed and presented in a heat map (14).

### Analysis of TMB and TIDE scores

Tumor mutation burden (TMB), defined as the number of cellular mutations per one million bases, serves as a biomarker for predicting the efficacy of immunotherapy (15). We analyzed differences in TMB and survival between high- and low-risk groups using the “limma” and “ggpubr” packages, and performed a KM survival analysis to explore associations between TMB, risk subgroups, and survival outcomes ( $P < 0.001$ ). To predict patients response to immunotherapy and identify factors related to tumor immune escape mechanisms, we utilized the tumor immune dysfunction and exclusion (TIDE) algorithm. TIDE scoring file was obtained from <http://tide.dfci.harvard.edu/> (16). Furthermore, we analyzed myeloid-derived suppressor cells (MDSC), cancer-associated fibroblasts (CAF), tumor-associated macrophages M2 (TAMM2), microsatellite instability (MSI), Merck18, IFNG, CD274 and cluster of differentiation (CD) (17-20).

### Screening of potential chemotherapeutic agents for oncology

Drug resistance poses a significant obstacle in the field of oncology treatment. We used the “pRRophetic” software package in the “R software” to predict the maximum half inhibitory concentration ( $IC_{50}$ ) of the applicable drugs to high- and low-risk subgroups, in order to evaluate drug sensitivity of the prediction model. This algorithm, which has been extensively employed in the various studies, has been previously published (20).

### Imvigor210 model validated PAM-SRFLncSig model for immunotherapy

We validated prognostic value of the PAM-SRFLncSig model, using an immunotherapy dataset (Imvigor210). This dataset encompassed expression data from human metastatic uroepithelial carcinoma (mUC) samples,



specifically associated with patient response to anti-PD-L1 immunotherapy. Relevant data was obtained from the "IMvigor210CoreBiologies" package (21). While IMvigor210 focused primarily on mUC, it encompassed a broad cohort of patients, many of whom have concurrently suffered from different types of malignancy, including lung cancer, providing valuable insights into the feasibility of immunotherapy in LUAD (22). By examining efficacy of immunotherapy and influence of specific variables on treatment response, this study extends its implications beyond mUC. LUAD patients may have similar expression patterns of immune checkpoint-related genes and TMB as mUC. Consequently, discoveries of IMvigor210 may serve as pivotal cues, inspiring further investigation into the realm of immunotherapeutic approaches for LUAD. Initially, we matched the genes of LUAD patients, obtained through LASSO regression analysis, with the immunotherapy data in the IMvigor210 model. Subsequently, risk scores were assigned for the patients in IMvigor210, using the same formula employed for risk scoring. Finally, based on these risk scores, the patients were categorized into high- and low-risk subgroups, and the differences in survival and immunotherapy response between high- and low-risk patients in IMvigor210 were analyzed using the "survival", "survminer", "caret", "timeROC", "limma" and "ggpubr" packages (14).

### Differential analysis of tumor stem cells

RNA expression-based stemness index (mRNAsi), is a metric that captures the likeness of tumor cells to cancer stem cells (CSCs). To investigate association between genetic characteristics and tumor stemness, we employed the one-class logistic regression (OCLR) algorithm, in order to calculate mRNAsi to measure the degree of similarity between tumor cells and stem cells based on gene expression levels (23). Subsequently, we calculated the mRNAsi of each LUAD patient and categorized them into high- and low-mRNAsi subgroups and performed survival analyses on these subgroups ( $P < 0.001$ ). Lastly, we examined correlation between mRNAsi and clinicopathological factors in the LUAD patients ( $P < 0.001$ ).

### Ethical approval

The work was approved by the Guangdong Medical University committee (Zhanjiang, China, YS2021159).

### Statistical analysis

Statistical analysis of this study was utilized in the "R software (version 4.1.3)". The "limma" package was employed to screen relevant lncRNAs, followed by regression analysis utilizing one-way COX, multi-way COX, and LASSO. Kaplan-Meier (KM) curves were used to compare survival times between high- and low-risk subgroups, as determined by the median risk score, while ROC curves were used to assess quality of clinically independent prognostic models for the LUAD patients. Subsequently, a nomogram was constructed using the

"rms" package of the TCGA dataset, incorporating significant variables identified through multivariate Cox regression. Prognostic accuracy of the nomogram was assessed using the c-index. Prognostic lncRNA co-expression protein coding genes were enriched using the GO database and KEGG pathway. Infiltrating immune cells and immune-related functions in the LUAD patients were evaluated using the "limma", "GSVA", and "GSEABase" packages in the "R software". PAM-SRFLncSig role in immune function was assessed through ssGSEA. Impact of immunotherapy was then evaluated using TMB and TIDE scores. Potential drugs for the LUAD patients were identified using the pRRophetic package in the "R software". Finally, the OCLR algorithm was employed to analyze the correlation of mRNAsi with clinicopathological factors in the LUAD patients.

## Results

### Co-expression relationship between the gene sets and lncRNAs

The Sankey diagram outcome is visually depicted in the Figure S2 (See Supplementary Online Information at [www.celljournal.org](http://www.celljournal.org)). Through univariate Cox regression analysis, a total of 339 lncRNAs exhibited significance ( $P < 0.05$ ), with 31 lncRNAs displayed an even more remarkable  $P < 0.0001$  (Table S3, See Supplementary Online Information at [www.celljournal.org](http://www.celljournal.org)). The latter lncRNAs included *AL606489.1*, *DEPDC1-AS1*, *LINC02323*, *AC084757.3*, *LINC01116*, *LINC01537*, *BZW1-AS1*, *AC021066.1*, *AC034223.1*, *TMPO-AS1*, *LINC02178*, *AP000695.2*, *LINC00519*, *LINC02320*, *LINC02802*, *SMILR*, *AP005137.2*, *MIR193BHG*, *NKILA*, *AC025419.1*, *LINC00941*, *AC009743.1*, *AC108136.1*, *LINC01117*, *ABCA9-AS1*, *LINC00707*, *AC090023.2*, *FLG-AS1*, *AC079949.2*, *AL049836.1*, *LINC01312* and *OGFRP1*.

### Construction of a clinical prognostic model for gene set-associated lncRNAs

A total of 494 patients with LUAD were randomly divided into a training cohort ( $n=330$ ) and a testing cohort ( $n=164$ ). Following validation, comparison of the clinical indicators between the two groups of patients, the difference was not statistically significant ( $P > 0.05$ ), indicating a good grouping. Subsequently, we analyzed the independent clinical prognosis of the training group. We employed one-way Cox analysis and LASSO regression to screen lncRNAs ( $P < 0.05$ , Table S4, See Supplementary Online Information at [www.celljournal.org](http://www.celljournal.org), Fig. 1A, B). Seven differentially expressed PAM-SRFLncSigs were then identified using multivariate Cox regression analysis (significance filtering criteria  $P < 0.05$ ), and the results are presented in Table S5 (See Supplementary Online Information at [www.celljournal.org](http://www.celljournal.org)). In addition, we calculated risk scores for the training cohort and divided them into high-risk ( $n=165$ ) and low-risk ( $n=165$ ) subgroups, based on median risk scores. We also plotted KM survival curves for patients in both subgroups

(Fig.1C). The low-risk subgroup exhibited significantly longer survival time compared to the high-risk subgroup ( $P<0.001$ ). Heat map of the training cohort demonstrated differential expression of the seven risk-related lncRNAs in the high- and low-risk subgroups. Blue color indicated low expression and red color indicated high expression. AC010999.2 [hazard ratios (HR) $<1$ ] and AC026979.2 (HR $<1$ ) appeared as red in the low-risk region, indicating high gene expression and a lower risk of tumor death (Fig.1D). Risk score distribution of the LUAD patients revealed significantly lower survival rate in the high-risk subgroup, compared to the low-risk subgroup (Fig.1E, F). Results of the testing cohort and the entire cohort are depicted in the Fig.S3A-F (See Supplementary Online Information at [www.celljournal.org](http://www.celljournal.org)). KM survival curve plot for the testing cohort patients demonstrated a significantly lower probability of survival in the high-risk subgroup compared to the low-risk subgroup ( $P<0.05$ ). Consistency between results of the training and testing cohorts indicated accurate prediction of the patient survival by the clinical prognostic model for LUAD.

#### **Association of PAM-SRFLncSig with clinical profiles of the LUAD patients**

To comprehend relationship of PAM-SRFLncSig and the clinical profile of the LUAD patients, we visually represented the patient clinical profile and risk scores. The outcomes revealed that M ( $P=0.77$ ), age ( $P=0.59$ ), gender ( $P=0.83$ ), race, stage, T and N ( $P>0.05$ ) exhibited no association with risk scores (Fig.S4A-G, See Supplementary Online Information at [www.celljournal.org](http://www.celljournal.org)). However, the survival status was correlated with the risk score (Fig.S4H, See Supplementary Online Information at [www.celljournal.org](http://www.celljournal.org)). Univariate Cox regression analysis demonstrated that AJCC stage (HR=1.552, 95% confidence interval (CI): 1.303-1.849,  $P<0.001$ ), T (HR=1.481, 95% CI: 1.162 ~ 1.888,  $P=0.001$ ), N (HR=1.827, 95% CI: 1.454 ~ 2.296,  $P<0.001$ ), and risk score (HR=1.269, 95% CI: 1.185 ~ 1.358,  $P<0.001$ ) significantly influenced the survival time of the LUAD patients (Fig.S4I, See Supplementary Online Information at [www.celljournal.org](http://www.celljournal.org)). Furthermore, multifactorial Cox regression analysis revealed that only the risk score (HR=1.210, 95% CI: 1.124 ~ 1.303,  $P<0.001$ ) exhibited a significant association with the survival time of the LUAD patients (Fig.S4J, See Supplementary Online Information at [www.celljournal.org](http://www.celljournal.org)).

#### **Evaluation of the clinically independent prognostic model for patients with LUAD**

We assessed the efficacy of patient clinical prognostic models, through the utilization of clinical ROC curves and survival time ROC curves. Prognostic capacity of these predictive models was evaluated by calculating the area under the curve (AUC) of time-dependent ROC curves. ROC curves were plotted for 1-, 3- and 5-year(s) intervals, with AUC values of 0.717, 0.670 and 0.686, respectively (Fig.S5A, See Supplementary

Online Information at [www.celljournal.org](http://www.celljournal.org)). All AUC values exceeded 0.5, indicating that the model played a critical role in predicting outcomes in the patients with LUAD (24). Figure S5B (See Supplementary Online Information at [www.celljournal.org](http://www.celljournal.org)) displays the clinicopathological indicators for 1-year survival probability, including risk score (AUC=0.717), age (AUC=0.470), gender (AUC=0.554), race (AUC=0.497), AJCC stage (AUC=0.698), T stage (AUC=0.633), M stage (AUC=0.497) and N stage (AUC=0.652). These clinical indicators, except for age, AJCC stage and M stage, were found to be potential predictors of 1-year survival probability for the LUAD patients (AUC $>0.5$ ). Clinicopathological indicators for 3- and 5-years survival probabilities are depicted in the Figure S5C and D (See Supplementary Online Information at [www.celljournal.org](http://www.celljournal.org)). Overall, risk scores exhibited a relatively high AUC value, making them superior predictors of prognosis for the LUAD patients.

Clinical C-index curves can be used to evaluate predictive efficacy and differentiation of clinically independent prognostic models for patients (25). A C-index curve closer to one indicates greater accuracy in the predicted values of the Cox regression model (Fig. S5E, See Supplementary Online Information at [www.celljournal.org](http://www.celljournal.org)). We employed a nomogram based on univariate and multifactorial Cox regression analyses to visually predict patients OS at 1-, 3- and 5-year intervals. The predictive performance of the nomogram was further assessed using the calibration curve method, which demonstrated favorable prediction outcomes (Fig. S5F, G, See Supplementary Online Information at [www.celljournal.org](http://www.celljournal.org)).

#### **Model validation of clinical grouping data for the LUAD patients**

We categorized patients with LUAD into high-risk subgroups and low-risk subgroups, based on their clinical characteristics (age, gender, race, etc.). Our findings revealed that the OS rate of deceased patients was not associated with the risk score ( $P=0.311$ , Fig.S6A, See Supplementary Online Information at [www.celljournal.org](http://www.celljournal.org)). Survival probability of the patients with LUAD over time was 100% (Fig.S6B, See Supplementary Online Information at [www.celljournal.org](http://www.celljournal.org)). Notably, age  $\leq 65$  years ( $P=0.004$ ) and age  $>65$  ( $P=0.005$ ), as well as male patients ( $P=0.022$ ) and female patients ( $P=0.001$ ), black or African American patients ( $P=0.041$ ) and white patients ( $P<0.001$ ), stage I patients ( $P=0.011$ ) and stage II patients ( $P=0.014$ ), stage T2 patients ( $P=0.005$ ) and stage T3 patients ( $P=0.003$ ), stage M0 patients ( $P<0.001$ ), stage N0 patients ( $P=0.003$ ), and stage N1 patients ( $P=0.044$ ) exhibited significant associations with survival (Fig.S6C-J, N, O, Q, S, T, See Supplementary Online Information at [www.celljournal.org](http://www.celljournal.org)). The high-risk subgroup of patients experienced a more rapid decline in survival probability compared to the low-risk subgroup. However, there was no significant correlation between

risk scores and OS rates in the LUAD patients with stage III (P=0.053), stage IV (P=0.743), T1 (P=0.379), T4 (P=0.131), M1 (P=0.743), and N2 (P=0.160, Fig.S6K-M, P, R, U, See Supplementary Online Information at www.celljournal.org). Furthermore, we employed principal component analysis (PCA) to evaluate distinguishability

of the all genes, mRNA, lncRNA, and risk lncRNA between the high and low-risk groups (Fig.S7A-D, See Supplementary Online Information at www.celljournal.org). The results suggested that samples from the two risk subgroups typically had different statuses that can be characterized by lncRNA signatures.

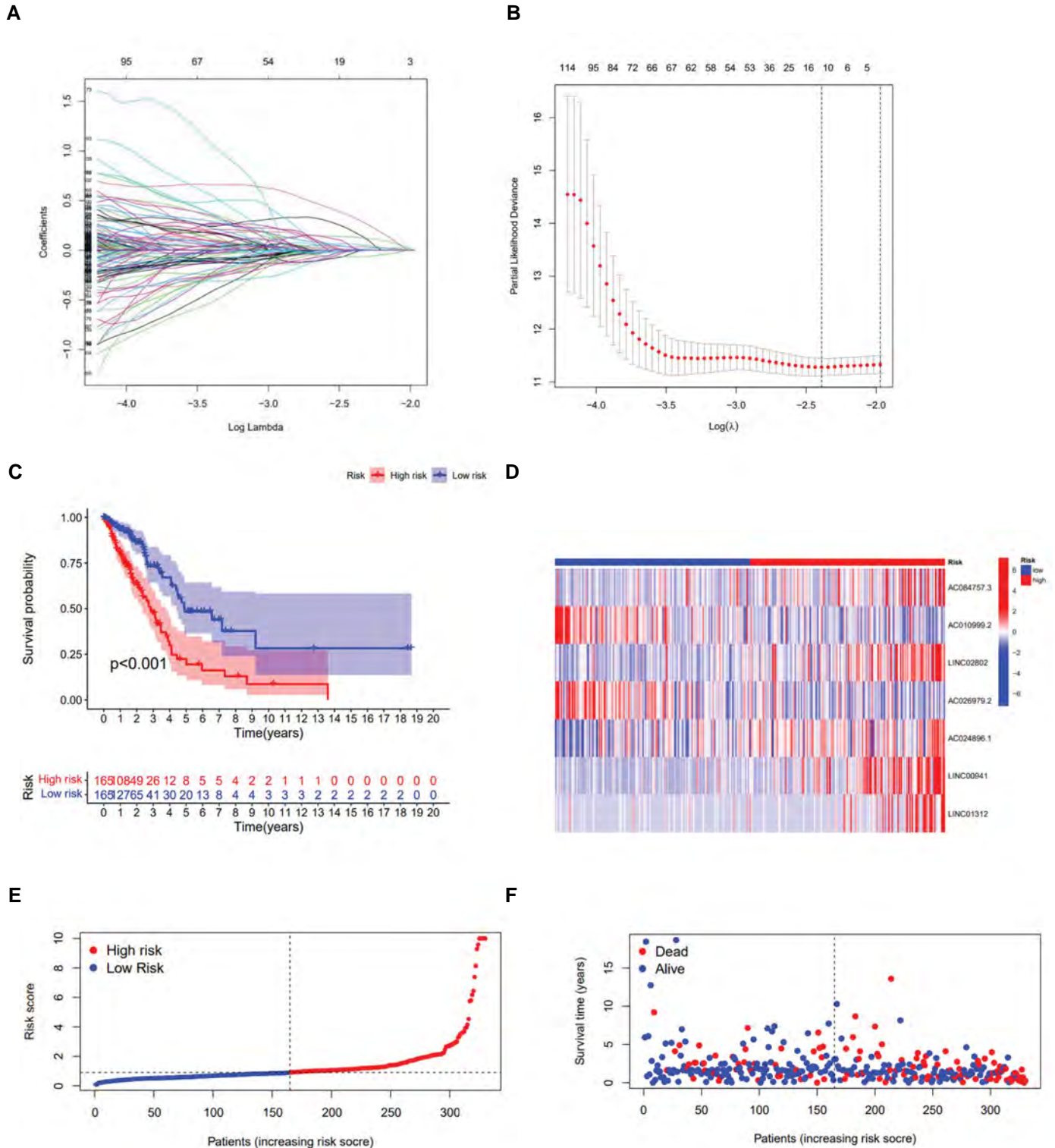


**Fig.1:** Target genes were identified using lasso Cox regression analysis for the construction of seven lncRNA signatures in the training cohort. **A.** Log( $\lambda$ ) versus change in regression coefficient. **B.** Partial-likelihood deviance curve with Log( $\lambda$ ) in Lasso regression. **C.** The probability of survival was significantly lower in the high-risk subgroup than the low-risk subgroup by the Kaplan-Meier test. **D.** *AC010999.2* and *AC026979.2* were highly expressed in the low-risk subgroup, and *AC084757.3*, *LINC02802*, *AC024896.1*, *LINC00941* and *LINC01312* were highly expressed in the high-risk subgroup. **E, F.** Training cohort survival status and risk score for each case.

### Functional enrichment analysis of lncRNA-related pathways in the LUAD patients with a prognosis

We conducted GO enrichment analysis (n=158), based on lncRNAs expression in the LUAD patients and identified lncRNAs (P<0.1) that were closely associated with specific pathways. Among these, a majority of the differentially expressed lncRNAs were found to be particularly relevant to pathways such as collagen-containing extracellular matrix (GO: 0062023), epidermis development (GO: 0008544), cell-cell junction (GO: 0005911) and skin development (GO: 0043588; Fig.2A). Notable examples include *LAMA1*, *LAMA3*, *COL7A1* for collagen-containing extracellular matrix, *GJB5*, *LAMA3*, *COL7A1* for epidermal development, *LAMA1*, *COL7A1*, *GJB3* for cell-cell junction, and *TP63*, *SPRR1*, *GJB3* for skin development. GO analysis of the differentially expressed genes revealed that 20 genes exhibited significant enrichment in the biological process category at a P value of 0.1 (Fig.2B). Furthermore, at P<0.05, KEGG pathway maps also demonstrated significant enrichment of the majority of differentially expressed lncRNAs in pathways such as (hsa04060 cytokine-cytokine receptor interactions) including *IL22RA1*, *MSTN*, *IL1R2*, (hsa04510 foci adhesion) and (hsa05206 microRNAs in cancer; Fig.2C). Functional enrichment chord plot of KEGG highlighted a notable differential expression pattern in the *LAMA1* gene (Fig.2D).

### Immune function study of PAM-SRFLncSig high-risk and low-risk subgroups

The high-risk and low-risk subgroups were visually represented through a heat map, showcasing the expression levels of 13 immune functional pathways. In the training cohort, the low-risk subgroup exhibited high expression levels of Cytolytic activity, Inflammation-promoting, and T\_cell\_co-inhibition pathways, while the high-risk subgroup displayed low expression levels (P<0.05, Fig.2E). This suggests that these pathways are indicators of a low-risk state for LUAD with a better prognosis and lower risk of cancer recurrence. Consistency in immune function pathways was observed in both the testing cohort and the entire cohort, mirroring the findings of the training cohort (Fig.2F, G).

### Analysis of tumor mutation burden of PAM-SRFLncSig

Somatic mutation data from the TCGA database were downloaded to analyze disparities in values and subgroups between the high-risk and low-risk prognostic models. It should be noted that there was no significant difference (P>0.05) in TMB between both of the high-risk and low-risk subgroups (Fig.3A-C). Subsequently, survival analysis was conducted using the “survminer” package, and survival curves were plotted (Fig.3D-F). The combined survival curves of TMB and high/low risk revealed that the H-TMB+ low-risk subgroup exhibited the longest survival in both of the training cohort and the entire cohort (P<0.001).

In contrast, the L-TMB+ high-risk subgroup had the shortest survival (Fig.3G-I).

### Analysis of tumor immune escape and immunotherapy in the high-risk and low-risk subgroups of PAM-SRFLncSig

In the high-risk and low-risk subgroups, analyses of tumor immune escape and immunotherapy were performed using PAM-SRFLncSig, with TIDE scoring showing no significant difference in the training cohort, testing cohort and entire cohort (P>0.05, Fig.4A-C). However, statistically significant differences were observed in MDSC (Fig.4P-R), Exclusion (Fig.5A-C), CAF (Fig.5J-L) and TAMM2 (Fig.5M-O) between the high-risk and low-risk subgroups (P<0.001). On the other hand, other immunomarkers, such as MSI, Merck8, IFNG, CD274 (Fig.4D-O), Dysfunction and CD8 (Fig.5D-I), did not exhibit statistically significant difference between the high-risk and low-risk subgroups (P>0.05).

### Screening of tumor chemotherapy drugs

The pRRophetic algorithm was employed to screen cancer chemotherapy agents within the high-risk and low-risk subgroups of PAM-SRFLncSig. A total of 73 drugs were identified through this algorithm. Upon comparing drug sensitivity, notable variations in IC<sub>50</sub> values were observed between the low-risk and high-risk subgroups for multiple drugs (P<0.05). Notably, the LUAD patients in the high-risk subgroup had increased sensitivity to the various drugs (Bicalutamide, Bleomycin, BMS.509744, BMS.754807, Bortezomib, Bryostatins.1, CGP.082996, CGP.60474, CI.1040, CMK, Dasatinib, Docetaxel and Embelin). Conversely, the low-risk subgroup demonstrated lower IC<sub>50</sub> values for drugs, such as BIRB.0796, CCT007093, and EHT.1864, indicating that the low-risk subgroup was better treated. In this regard, Figure S8A-P (See Supplementary Online Information at [www.celljournal.org](http://www.celljournal.org)) illustrates the top 16 drugs that show potential for dosing in LUAD patients.

### IMvigor210 model validated PAM-SRFLncSig model for immunotherapy

By conducting LASSO regression analysis and aligning the genes obtained from the LUAD patients with immunotherapy data isolated from the IMvigor210 model, we identified the *LINC00941* and *LINC01312* genes. Utilizing a risk scoring formula, patients in the IMvigor210 dataset were assigned scores and subsequently classified into the high-risk and low-risk subgroups (P<0.001). Unfortunately, there was no statistically significant survival between the two subgroups of IMvigor210 bladder cancer target genes (P=0.440, Fig. S9A, See Supplementary Online Information at [www.celljournal.org](http://www.celljournal.org)), indicating poor predictive capability. Subsequently, the PAM-SRFLncSig model was validated using ROC curves, demonstrating improved prediction of

5-years survival in bladder cancer patients (AUC=0.514, Fig.S9B, See Supplementary Online Information at [www.celljournal.org](http://www.celljournal.org)). Furthermore, no significant difference in target gene risk scores, derived from LASSO regression,

was observed among different drug responses to IMvigor210 bladder cancer immunotherapy in the LUAD patients (P=0.092, Fig.S9C, See Supplementary Online Information at [www.celljournal.org](http://www.celljournal.org)).

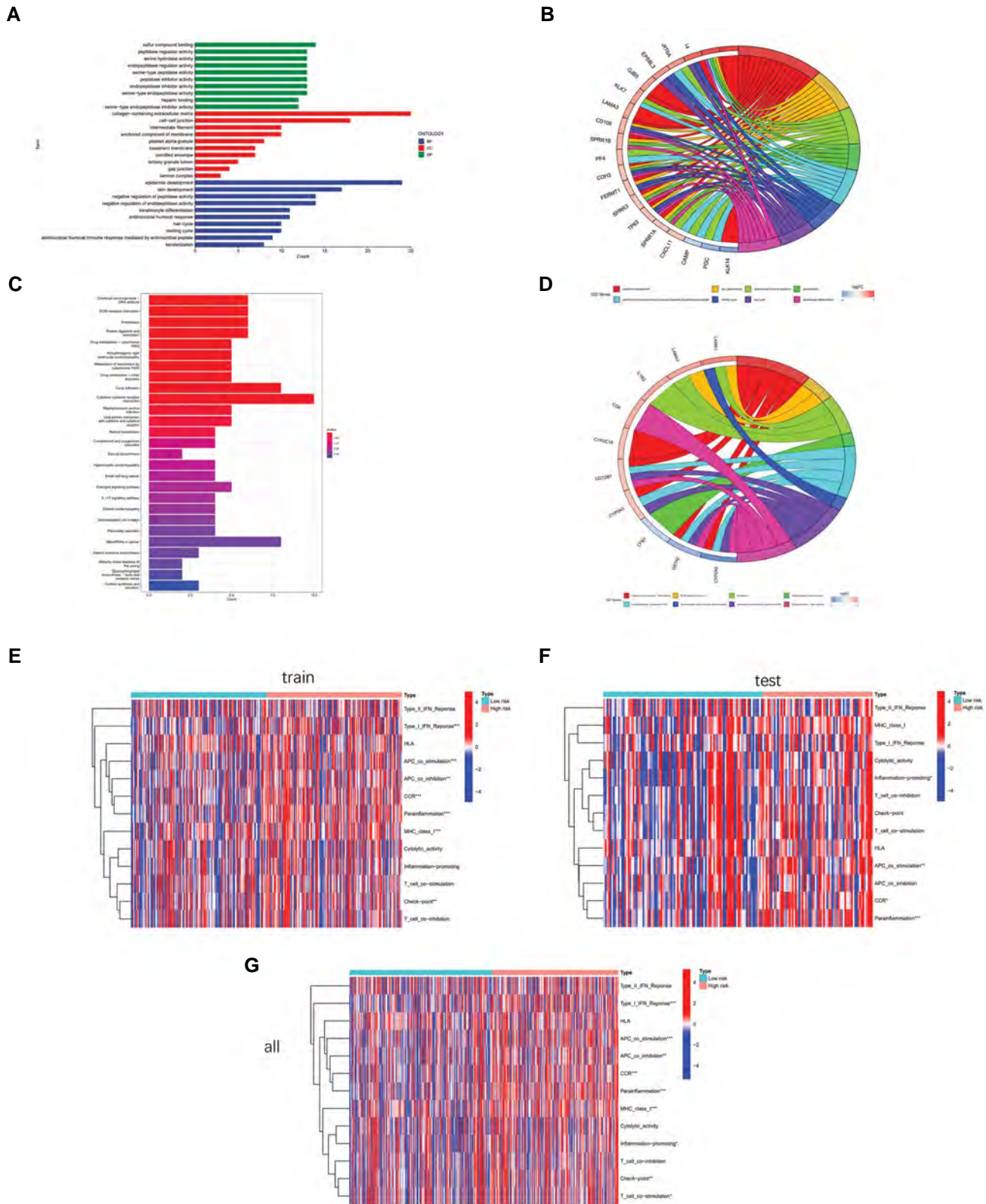


**Fig.2:** GO/KEGG pathway was used for the all differential lncRNAs between the high-risk and low-risk subgroups (n=158) and for 13 immune function pathways in the high- and low-risk subgroups. **A, B.** Results of GO pathway analysis. **C, D.** Results of KEGG pathway analysis. **E.** Thirteen immune function pathways in the training cohort, **F.** Thirteen immune function pathways in the testing cohort and **G.** Thirteen immune function pathways in the entire cohort. GO; Gene ontology and KEGG; Kyoto Encyclopedia of Genes and Genomes.

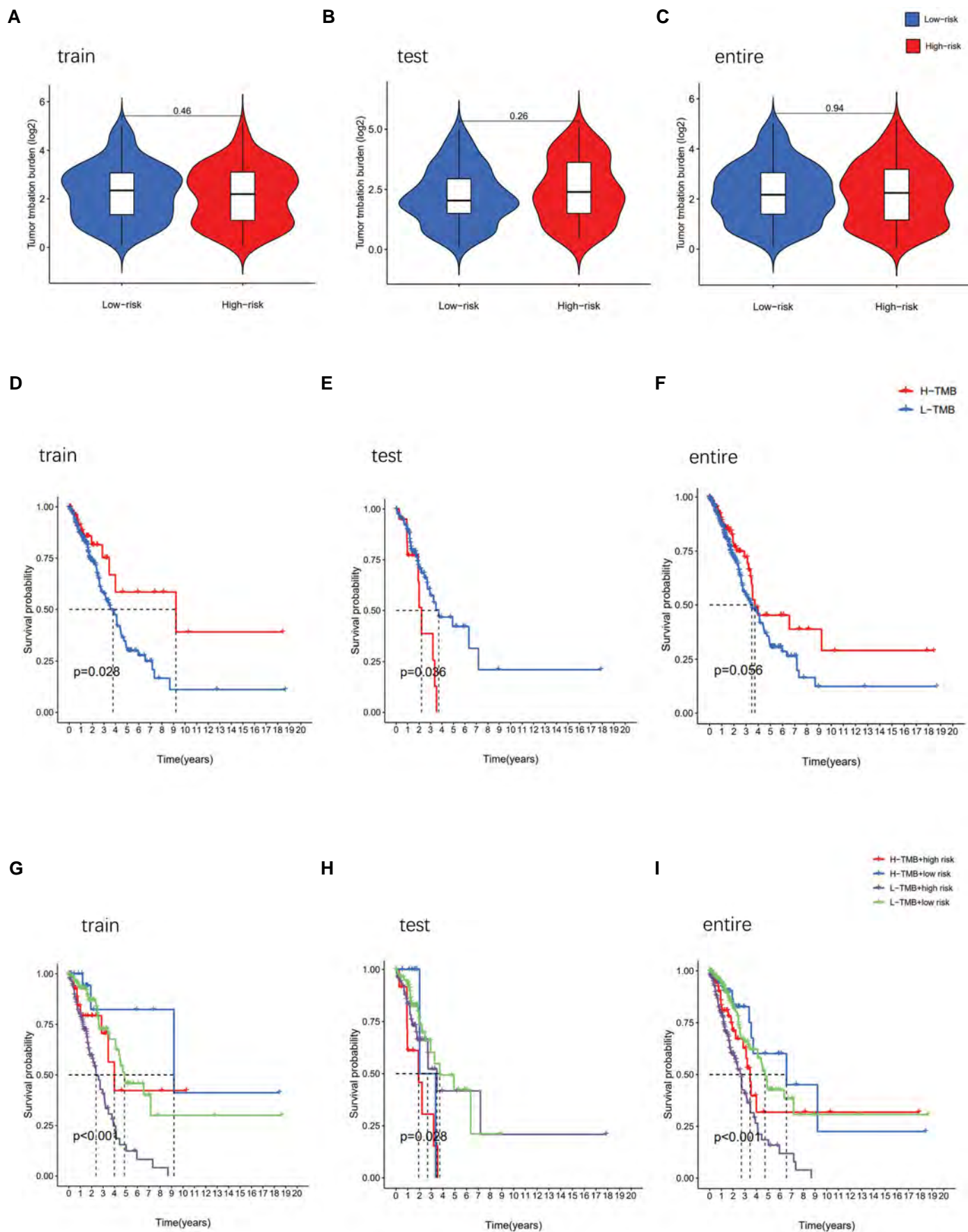


**Fig.3:** Analysis of TMB of PAM-SRFLncSig. Box plots show no significant difference in TMB between the high-risk and low-risk subgroups of the **A**. Training cohort, **B**. Testing cohort and **C**. Entire cohort. KM survival curves show differences in TMB between the high-risk and low-risk subgroups of the **D**. Training cohort, **E**. Testing cohort, **F**. Entirecohort. Survival curve results for TMB combined with high-risk and low-risk of the **G**. Training cohort, **H**. Testing cohort, and **I**. Entire cohort. TMB; Tumor mutation burden.

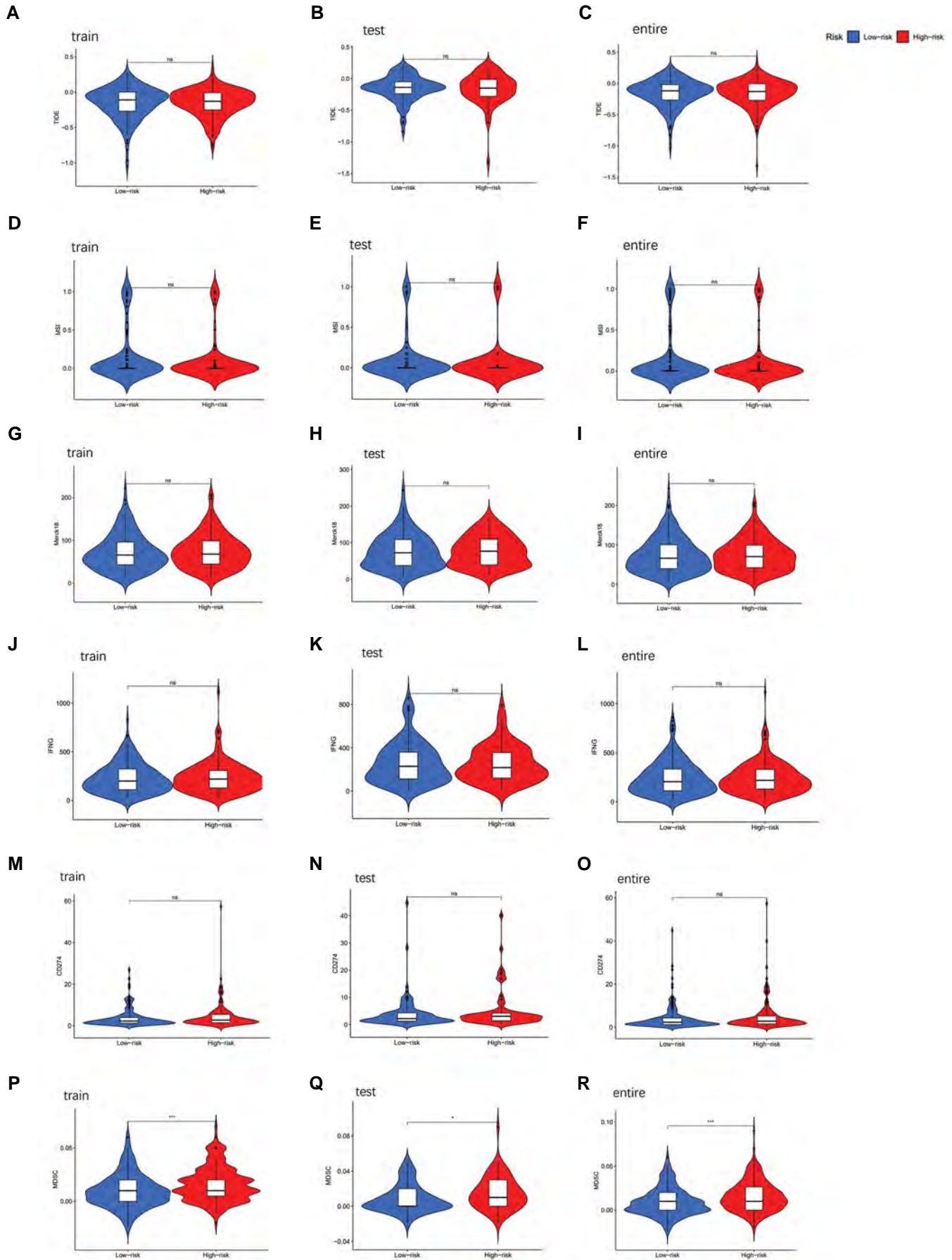


**Fig.4:** Tumor microenvironmental results of PAM-SRFLncSig. Differences in **A-C.** TIDE, **D-F.** MSI, **G-I.** Merck18, **J-L.** IFNG, **M-O.** CD274 and **P-R.** MDSI were analyzed in high- and low-risk subgroups. \*, P<0.05, \*\*, P<0.01, \*\*\*, P<0.001, and ns; No significance.

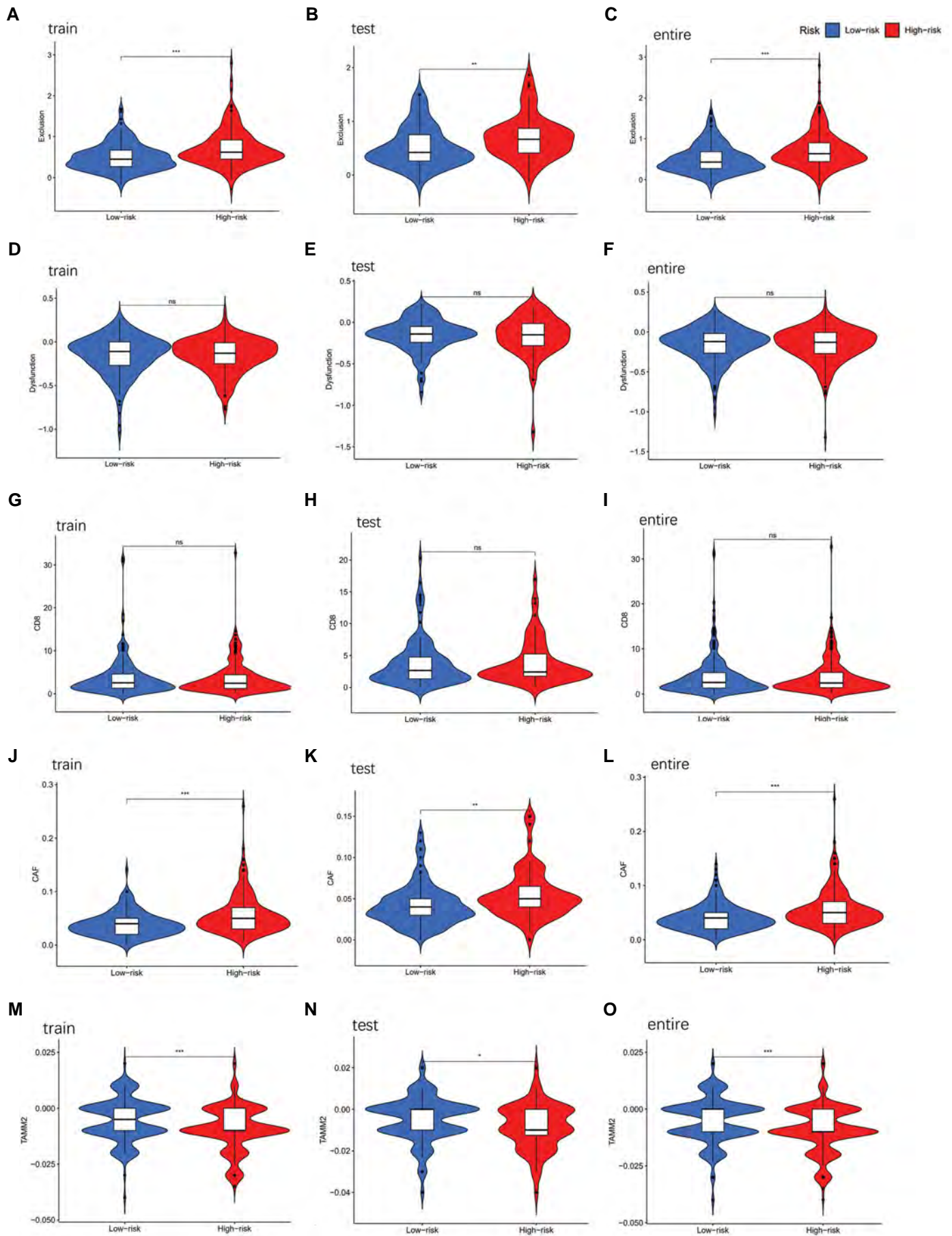


**Fig.5:** Tumor microenvironmental results of PAM-SRFLncSig. Differences in **A-C**. Exclusion, **D-F**. Dysfunction, **G-I**. CD8, **J-L**. CAF and **M-O**. TAMM2 were analyzed in high-risk and low-risk subgroups. \*, P<0.05, \*\*, P<0.01, \*\*\*, P<0.001, and ns; No significance.



### Differential analysis of tumor stem cells

Utilizing the OCLR algorithm, we computed the mRNAsi for each LUAD patient based on their gene expression profiles, yielding indices ranging from 0 to 1. A higher index value signified less differentiated cells, heightened stem cell characteristics and significantly increased aggressiveness. Regrettably, our Kaplan-Meier analysis failed to reveal a significant correlation in OS between the LUAD patients with low mRNAsi and those with high mRNAsi ( $P=0.182$ , Fig.6A). However,

we observed significant differences in mRNAsi levels between the lung cancer tissue group and the normal control group ( $P<0.05$ , Fig.6B). Furthermore, our correlation analysis between mRNAsi and clinicopathological factors in the LUAD patients unveiled a noteworthy association ( $P<0.05$ , Fig.6C-F). Notably, male patients exhibited a higher mRNAsi value compared to female patients, suggesting that males with stronger stem cell characteristics and heightened tumor malignancy tend to possess elevated mRNAsi levels during the later stages of LUAD development.

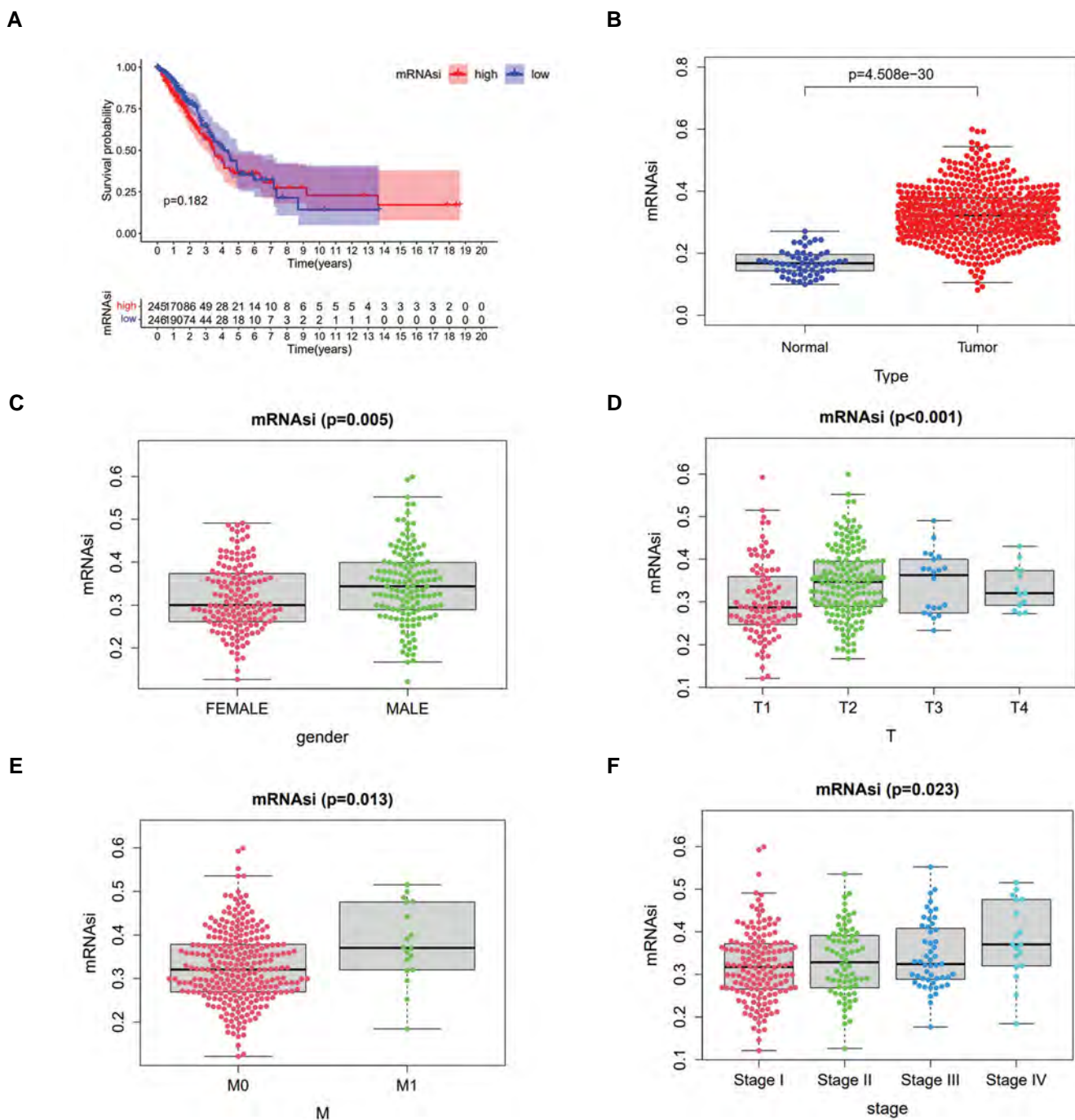


**Fig.6:** Differential analysis of tumor stem cells. **A.** The KM curve showed no significant correlation between OS in the LUAD patients with low mRNAsi and high mRNAsi. **B.** There is a significant difference in mRNAsi between normal and tumor tissues. **C-F.** Significant differences in mRNAsi between clinicopathological factors. KM; Kaplan-Meier, OS; Overall survival, LUAD; Lung adenocarcinoma, M; Metastasis, and T; Primary tumor.

## Discussion

Lung cancer, as the most prevalent and deadliest form of cancer worldwide, claims over one million lives annually (26). Despite the advances in early detection and treatment options for LUAD, the prognosis remains grim, with less than 15% of patients surviving beyond five years (27). Therefore, it is imperative to identify biomarkers and develop targeted therapies specific to LUAD patients to enhance their prognosis.

Numerous studies have demonstrated potential prognostic significance of immune-related lncRNAs in lung adenocarcinoma, highlighting the growing interest in utilizing lncRNAs as prognostic indicators for malignancies (28). lncRNAs may affect the onset and progression of LUAD by regulating the PI3K/Akt/mTOR signaling pathway. The results suggested that lncRNAs could regulate cancer development at many levels, such as TME, tumor growth, invasion, metastasis and recurrence (29). Through a series of bioinformatics analyses, we developed a gene set-associated PAM-SRFLncSig model and identified seven lncRNAs, namely *AC084757.3*, *AC010999.2*, *LINC02802*, *AC026979.2*, *AC024896.1*, *LINC00941* and *LINC01312*, using univariate Cox, LASSO and multivariate Cox regression analyses. Among these lncRNAs, previous studies demonstrated upregulation of *LINC00941* in tumor tissues and plasma of NSCLC patients (30). *LINC00941* is associated with infiltration and lymphatic metastasis of gastric cancer. It also promotes metastasis of papillary thyroid and colorectal cancers (31, 32). Combined with our study, we believe that *LINC00941* plays a crucial role in LUAD and it is highly correlated with tumor development and metastasis. Therefore, *LINC00941* may serve as an important biological marker targeted for immunotherapy and chemotherapy. Survival analysis of the training cohort using these lncRNAs revealed a significant difference in OS between the high-risk and low-risk subgroups, while LUAD patients in the high-risk subgroup exhibiting lower OS rates. Additionally, we observed higher expression levels of *AC010999.2* and *AC026979.2* in the low-risk subgroup, suggesting their potential as protective genes. C-index value, calibration curve verification and ROC curve analysis showed that the model had good predictive ability. Notably, KEGG pathway analysis revealed significant enrichment of the cytokine-cytokine receptor interaction (*hsa04060*), focal adhesion (*hsa04510*) and microRNAs in cancer (*hsa05206*) pathways. Focal adhesion, known to play a crucial role in tumor metastasis and aggressiveness, is primarily influenced by focal adhesion kinase (FAK) and its phosphorylation. FAK serves as a mediator of multiple signaling pathways in cellular signaling and it can activate intracellular PI3K/Akt signaling pathways to regulate cell growth. The PI3K-Akt signaling pathway has emerged as a pivotal pathway for cancer cell survival, orchestrating crucial processes, such as cell proliferation, apoptosis, invasion, metastasis and angiogenesis by modulating activation status of downstream signaling molecules (33). KEGG

enrichment analysis further corroborated association between LUAD and PI3K/Akt/mTOR signaling pathway. Therefore, PI3K/Akt/mTOR signaling pathway is closely related to the pathogenesis and prognosis of LUAD.

In recent years, immunotherapy has exhibited promising initial results in treatment of the various malignancies, including melanoma, lung cancer and others (34). Exploring specific biomarkers for LUAD can facilitate diagnosis and rational treatment choices. In our immune function pathway analysis, we identified Cytolytic activity, Inflammation-promoting and T cell co-inhibition, as good prognostic pathways in LUAD. Notably, our analysis of TMB revealed no statistically significant difference between the high- and low-risk subgroups. Furthermore, when assessing tumor immune escape and immunotherapy using the PAM-SRFLncSig approach, we found no significant difference in TIDE scoring between the high- and low-risk subgroups. However, we did observe statistically significant distinctions in MDSC, Exclusion, CAF and TAMM2 between these subgroups. It is worthy to note that CAF-specific therapy has emerged as a valuable adjunct to immunotherapy, offering substantial clinical benefits for cancer patients (35). Some studies revealed the important regulatory role of the PI3K/Akt/mTOR pathway in transformation of lung cancer growth patterns and chemotherapy resistance (36). In our study, we employed the pRRophetic algorithm to screen 16 potential oncologic chemotherapeutic drugs for LUAD patients. Potential therapeutic agents in the low-risk subgroup are BIRB.0796, CCT007093 and EHT.1864, while potential therapeutic agents in the high-risk subgroup are Bicalutamide, Bleomycin, BMS.509744, BMS.754807, Bortezomib, Bryostatins.1, CGP.082996, CGP.60474, CI.1040, CMK, Dasatinib, Docetaxel and Embelin.

Nevertheless, it is important to acknowledge the limitations of our study. Primarily, utilization of data solely from the TCGA database to construct the PAM-SRFLncSig model introduced the possibility of sample selection bias, potentially stemming from a specific population or region. Consequently, the reliability of our results may be compromised, and the applicability may be limited. Furthermore, absence of alternative databases for additional validation further exacerbated this issue. Additionally, inconsistencies and missing data pertaining to the various molecular features, such as gene expression, mutations or methylation, may also be present. Lastly, exploration of therapeutic efficacy in LUAD patients necessitated implementation of animal and clinical trials. By scrutinizing expression levels of these lncRNAs in patient tissue samples, we can evaluate their impact on survival and disease progression, thereby enabling clinicians to devise more tailored treatment strategies. Further studies are still needed to verify the therapeutic reliability and clinical applicability of PAM-SRFLncSig in LUAD treatment, and the therapeutic modality of combining PI3K/Akt/mTOR signaling pathway inhibitors with other therapeutic agents or targeted drugs is a future

direction of research.

Overall, multivariate COX regression analysis identified seven PAM-SRFLncSigs for the construction of a model for LUAD patients and confirmed the importance of PAM-SRFLncSig-associated lncRNAs in assessment of immunotherapy and prognosis of LUAD patients. The model can also be used to screen chemotherapeutic drugs for lung cancer, which has important clinical applications.

## Conclusion

Based on the samples obtained from 494 LUAD patients, seven differentially expressed PAM-SRFLncSigs with prognostic value were screened, and the PAM-SRFLncSig model was constructed and validated. Validation of LUAD association with the PI3K/Akt/mTOR signaling pathway related lncRNAs through KEGG enrichment analysis. We found that these lncRNAs were associated with tumor immune function, and performed TMB, tumor immune escape and immunotherapy analyses on the high- and low-risk subgroups. Finally, we screened 16 relevant drugs to guide clinical application.

## Acknowledgements

There is no financial support and conflict of interest in this study.

## Authors' Contributions

L.C., X.Z.; Conceptualization, Methodology, Software, and Supervision. J.Z.; Data curation and Writing-Original draft preparation. J.Z., M.F., L.L.; Visualization and Investigation. Y.K., R.L.; Software and Validation. J.Z., Y.K., X.Z., L.C.; Writing-reviewing and editing. All authors read and approved the final version of the manuscript.

## References

- Zou Z, Tao T, Li H, Zhu X. mTOR signaling pathway and mTOR inhibitors in cancer: progress and challenges. *Cell Biosci.* 2020; 10: 31.
- Ren B, Liu H, Yang Y, Lian Y. Effect of BRAF-mediated PI3K/Akt/mTOR pathway on biological characteristics and chemosensitivity of NSCLC A549/DDP cells. *Oncol Lett.* 2021; 22(2): 584.
- Blakely CM, Watkins TBK, Wu W, Gini B, Chabon JJ, McCoach CE, et al. Evolution and clinical impact of co-occurring genetic alterations in advanced-stage EGFR-mutant lung cancers. *Nat Genet.* 2017; 49(12): 1693-1704.
- Mohamed E, Kumar A, Zhang Y, Wang AS, Chen K, Lim Y, et al. PI3K/AKT/mTOR signaling pathway activity in IDH-mutant diffuse glioma and clinical implications. *Neuro Oncol.* 2022; 24(9): 1471-1481.
- Duan Y, Haybaeck J, Yang Z. Therapeutic potential of PI3K/AKT/mTOR pathway in gastrointestinal stromal tumors: rationale and progress. *Cancers (Basel).* 2020; 12(10): 2972.
- Zhang W, Wei C, Huang F, Huang W, Xu X, Zhu X. A tumor mutational burden-derived immune computational framework selects sensitive immunotherapy/chemotherapy for lung adenocarcinoma populations with different prognoses. *Front Oncol.* 2023; 13: 1104137.
- Xiong Z, Han Z, Pan W, Zhu X, Liu C. Correlation between chromatin epigenetic-related lncRNA signature (CELncSig) and prognosis, immune microenvironment, and immunotherapy in non-small cell lung cancer. *PLoS One.* 2023; 18(5): e0286122.
- Lin Q, Zhang M, Kong Y, Huang Z, Zou Z, Xiong Z, et al. Risk score = lncRNAs associated with doxorubicin metabolism can be used as molecular markers for immune microenvironment and immunotherapy in non-small cell lung cancer. *Heliyon.* 2023; 9(3): e13811.
- Xu Y, Tao T, Li S, Tan S, Liu H, Zhu X. Prognostic model and immunotherapy prediction based on molecular chaperone-related lncRNAs in lung adenocarcinoma. *Front Genet.* 2022; 13: 975905.
- Lu T, Wang Y, Chen D, Liu J, Jiao W. Potential clinical application of lncRNAs in non-small cell lung cancer. *Onco Targets Ther.* 2018; 11: 8045-8052.
- Xu S, Liu D, Chang T, Wen X, Ma S, Sun G, et al. Cuproptosis-associated lncRNA establishes new prognostic profile and predicts immunotherapy response in clear cell renal cell carcinoma. *Front Genet.* 2022; 13: 938259.
- Bossler F, Hoppe-Seyler K, Hoppe-Seyler F. PI3K/AKT/mTOR signaling regulates the virus/host cell crosstalk in HPV-positive cervical cancer cells. *Int J Mol Sci.* 2019; 20(9): 2188.
- Zhou D, Liu X, Wang X, Yan F, Wang P, Yan H, et al. A prognostic nomogram based on LASSO Cox regression in patients with alpha-fetoprotein-negative hepatocellular carcinoma following non-surgical therapy. *BMC Cancer.* 2021; 21(1): 246.
- Ye W, Wu Z, Gao P, Kang J, Xu Y, Wei C, et al. Identified gefitinib metabolism-related lncRNAs can be applied to predict prognosis, tumor microenvironment, and drug sensitivity in non-small cell lung cancer. *Front Oncol.* 2022; 12: 939021.
- Lai D, Tan L, Zuo X, Liu D, Jiao D, Wan G, et al. Prognostic ferroptosis-related lncRNA signatures associated with immunotherapy and chemotherapy responses in patients with stomach cancer. *Front Genet.* 2021; 12: 798612.
- Fu J, Li K, Zhang W, Wan C, Zhang J, Jiang P, et al. Large-scale public data reuse to model immunotherapy response and resistance. *Genome Med.* 2020; 12(1): 21.
- Wu Z, Li S, Zhu X. The mechanism of stimulating and mobilizing the immune system enhancing the anti-tumor immunity. *Front Immunol.* 2021; 12: 682435.
- Xu P, Luo H, Kong Y, Lai WF, Cui L, Zhu X. Cancer neoantigen: Boosting immunotherapy. *Biomed Pharmacother.* 2020; 131: 110640.
- Tan S, Li D, Zhu X. Cancer immunotherapy: Pros, cons and beyond. *Biomed Pharmacother.* 2020; 124: 109821.
- Yu J, Lan L, Liu C, Zhu X. Improved prediction of prognosis and therapy response for lung adenocarcinoma after identification of DNA-directed RNA polymerase-associated lncRNAs. *J Cancer Res Clin Oncol.* 2023; 149(14): 12737-12754.
- Powles T, Eder JP, Fine GD, Braiteh FS, Loriot Y, Cruz C, et al. MPDL3280A (anti-PD-L1) treatment leads to clinical activity in metastatic bladder cancer. *Nature.* 2014; 515(7528): 558-562.
- Zhang W, Yao S, Huang H, Zhou H, Zhou H, Wei Q, et al. Molecular subtypes based on ferroptosis-related genes and tumor microenvironment infiltration characterization in lung adenocarcinoma. *Oncoimmunology.* 2021; 10(1): 1959977.
- Sokolov A, Paull EO, Stuart JM. One-class detection of cell states in tumor subtypes. *Pac Symp Biocomput.* 2016; 21: 405-416.
- Gu X, Li H, Sha L, Zhao W. A prognostic model composed of four long noncoding RNAs predicts the overall survival of Asian patients with hepatocellular carcinoma. *Cancer Med.* 2020; 9(16): 5719-5730.
- Zhou ZR, Wang WW, Li Y, Jin KR, Wang XY, Wang ZW, et al. In-depth mining of clinical data: the construction of clinical prediction model with R. *Ann Transl Med.* 2019; 7(23): 796.
- Shen X, Zhi Q, Wang Y, Li Z, Zhou J, Huang J. Hypoxia induces multidrug resistance via enhancement of epidermal growth factor-like domain 7 expression in non-small lung cancer cells. *Chemotherapy.* 2017; 62(3): 172-180.
- Gong T, Cui L, Wang H, Wang H, Han N. Knockdown of KLF5 suppresses hypoxia-induced resistance to cisplatin in NSCLC cells by regulating HIF-1 $\alpha$ -dependent glycolysis through inactivation of the PI3K/Akt/mTOR pathway. *J Transl Med.* 2018; 16(1): 164.
- Qi X, Chen G, Chen Z, Li J, Chen W, Lin J, et al. Construction of a novel lung adenocarcinoma immune-related lncRNA pair signature. *Int J Gen Med.* 2021; 14: 4279-4289.
- Statello L, Guo CJ, Chen LL, Huarte M. Gene regulation by long

- non-coding RNAs and its biological functions. *Nat Rev Mol Cell Biol.* 2021; 22(2): 96-118.
30. Ren MH, Chen S, Wang LG, Rui WX, Li P. LINC00941 promotes progression of non-small cell lung cancer by sponging miR-877-3p to regulate VEGFA expression. *Front Oncol.* 2021; 11: 650037.
  31. Luo C, Tao Y, Zhang Y, Zhu Y, Minyao DN, Haleem M, et al. Regulatory network analysis of high expressed long non-coding RNA LINC00941 in gastric cancer. *Gene.* 2018; 662: 103-109.
  32. Wu N, Jiang M, Liu H, Chu Y, Wang D, Cao J, et al. LINC00941 promotes CRC metastasis through preventing SMAD4 protein degradation and activating the TGF-beta/SMAD2/3 signaling pathway. *Cell Death Differ.* 2021; 28(1): 219-232.
  33. Shen J, Cao B, Wang Y, Ma C, Zeng Z, Liu L, et al. Hippo component YAP promotes focal adhesion and tumour aggressiveness via transcriptionally activating THBS1/FAK signalling in breast cancer. *J Exp Clin Cancer Res.* 2018; 37(1): 175.
  34. Ohaegbulam KC, Assal A, Lazar-Molnar E, Yao Y, Zang X. Human cancer immunotherapy with antibodies to the PD-1 and PD-L1 pathway. *Trends Mol Med.* 2015; 21(1): 24-33.
  35. Saw PE, Chen J, Song E. Targeting CAFs to overcome anticancer therapeutic resistance. *Trends Cancer.* 2022; 8(7): 527-555.
  36. Li X, Li C, Guo C, Zhao Q, Cao J, Huang HY, et al. PI3K/Akt/mTOR signaling orchestrates the phenotypic transition and chemo-resistance of small cell lung cancer. *J Genet Genomics.* 2021; 48(7): 640-651.
-

# Effect of Exosomes Derived from Bone Marrow Mesenchymal Stem Cells on Ovarian Granulosa Cells of Immature NMRI Mice

Sajad Farrokhyar, M.Sc.<sup>1</sup>, Javad Baharara, Ph.D.<sup>2\*</sup> , Akram Eidi, Ph.D.<sup>1</sup>, Nasim Hayati Roodbari, Ph.D.<sup>1</sup>

1. Department of Biology, Science and Research Branch, Islamic Azad University, Tehran, Iran

2. Department of Biology and Research Center for Animal Development Applied Biology, Mashhad Branch, Islamic Azad University, Mashhad, Iran

## Abstract

**Objective:** In recent years, *in vitro* maturation (IVM) has become the focus of fertility maintenance, and infertility treatment. The aim of this study is development of oocytes during folliculogenesis and oogenesis is greatly influenced by the presence of *BMP-7*, *BMP-15*, and *GDF-9* genes, which are present in exosomes generated from bone marrow stem cells.

**Materials and Methods:** In the experimental study, we investigated how exosomes obtained from bone marrow stem cells affected development and expansion of ovarian granulosa cells (GCs) in NMRI mice. In this *in vitro* experiment, bone marrow stem cells were isolated from mice's bone marrow, and after identification, exosomes were recovered. Exosome doses of 100, 50, and 25 µg/ml were applied to GCs before using MTT assay to measure survival rates and quantitative reverse-transcription polymerase chain reaction (PCR) to measure expression of the *BMP-7*, *BMP-15*, and *GDF-9* genes.

**Results:** The results showed that the GCs treated with exosomes concentrations of 25, 50, and 100 µg/ml significantly increased bioavailability, growth and proliferation and it also increased expression level of *BMP-7*, *BMP-15* and *GDF-9* genes compared to the controls.

**Conclusion:** Findings of this study indicated that exosomes derived from bone marrow stem cells improved growth of GCs in NMRI mice and they were a good candidate for further clinical studies to improve quality of the assisted reproductive techniques.

**Keywords:** Annexin, Exosomes, Granulosa Cells, Stem Cells

**Citation:** Farrokhyar S, Baharara J, Eidi A, Hayati Roodbari N. Effect of exosomes derived from bone marrow mesenchymal stem cells on ovarian granulosa cells of immature NMRI mice. Cell J. 2024; 26(1): 28-38. doi: 10.22074/CELLJ.2023.2002520.1307

This open-access article has been published under the terms of the Creative Commons Attribution Non-Commercial 3.0 (CC BY-NC 3.0).

## Introduction

In the recent years, new mechanisms were proposed for cell-to-cell communications. Studies strongly showed that vesicles, such as exosomes and other microparticles cells were formed, the cells entered them into the cellular microenvironment. By sending information via vesicles, the cells might be able to influence behavior of the target cells (1). Some papers also suggested exosomes or microparticle carriers in the follicular fluid as a potential alternative mechanism for the paracrine and autocrine actions in the ovarian follicles.

The findings of this research can aid in our understanding of the many communication routes, which are crucial for early fertility and it have potential clinical implications (2, 3). In fact, extracellular carrier identification can aid in the diagnosis of reproductive disorders and offer biological indicators of oocyte quality in assisted reproductive technology (ART) (4). The Pathogenic process of many diseases, including endometriosis, which

is brought on by the intercellular movement of molecules including miRNAs, RNAs, and proteins, can be described by exosomes as cell-to-cell linkers (5).

Exosomes' participation in cell-cell communications, a crucial aspect of folliculogenesis, should also be a major concern in reproductive biology (6). The primary elements of follicles are theca, granulosa cells (GCs), and oocytes (7). GCs are the most important cells in the ovary that undergo serious changes morphologically and physiologically during the processes of follicular proliferation, differentiation, ovulation, lutenization and atresia (8). GCs affect growth and maturation of oocytes. The main function of GCs is to induce production of sex hormones and various peptides required for folliculogenesis and ovulation (9).

Some reports showed that different growth factors can stimulate GCs proliferation or steroidogenesis *in vitro* (10). For example, *GDF9*- stimulated proliferation of mouse

Received: 16/May/2023, Revised: 24/October/2023, Accepted: 30/October/2023

\*Corresponding Address: P.O.Box: 9183897194, Department of Biology and Research Center for Animal Development Applied Biology, Mashhad Branch, Islamic Azad University, Mashhad, Iran

Email: baharara@mshdiau.ac.ir



Royan Institute  
Cell Journal (Yakhteh)

GCs, but prevented secretion of estradiol and progesterone by suppressing follicle-stimulating hormone (FSH). On the other hand, *BMP15*- stimulated proliferation of mouse GCs and then decreased FSH levels, while *BMP4*- and *BMP7*- both potentiated FSH-stimulating function in the production of estradiol and progesterone from mouse GCs. Growth factor *BMP15*- was secreted by oocytes (11). As two primary tissues, brain and ovary expressed *BMP15*-. After that, a research based on fertility traits was carried out, and it was discovered that *BMP15*- was crucial for growth of the early follicular phase (12). Effect of *BMP7*- on GCs proliferation and progesterone synthesis, which played an important role in controlling effects of gonadotropins and IGF-1 on follicular differentiation, was reported in the other laboratory studies (13). The present study investigated stem cell-derived exosomes in GCs of mice.

We aimed to isolate and characterize exosomes from bone marrow mesenchymal stem cells (MSCs) to examine therapeutic potential of these exosomes as effective paracrine mediators on ovarian GCs.

## Materials and Methods

### Exosome preparation

#### Preparation of bone marrow mesenchymal stem cells

In the animal compartment, NMRI mice were housed according to industry standards with 12 hours of lightness and 12 hours of darkness at a temperature of 25°C. Islamic Azad University-Mashhad Branch Institutional Research Ethics Committee guidelines were followed throughout the entire experimental process (IR.IAU.MSHD.REC.1398.194).

In this experimental study NMRI mice were sacrificed via cervical vertebra dislocation, and the femur was taken out in order to conduct the research. Two ends of the femur were then cut and the contents of the bone marrow were transferred to a cell culture flask by a syringe containing the culture medium (DMEM, Bio Idea, Iran). After changing the culture medium containing, 10% fetal bovine serum (FBS, Gibco, USA), and 5% antibiotic (Gibco, USA) several times and removing the waste material, the bone marrow stem cells began to proliferate and become pure.

#### Bone marrow mesenchymal stem cells identification by flow cytometry

To identify bone marrow MSCs, specific surface markers of CD 73 (Antibodies, UK) and CD 105 (Antibodies, UK) and CD 45 (Antibodies, UK) and CD 34 (Antibodies, UK) and CD 31 (Antibodies, UK) stem cells were used by flow cytometry.

#### Bone marrow mesenchymal stem cells identification by osteogenic differentiation

Bone marrow MSCs were cultured in tissue culture

polystyrene flasks in Dulbecco's Modified Eagle's Medium (DMEM, with 1g/l glucose and Gluta MAX; Bio Idea, Iran) supplemented with 10% FBS (Gibco, USA), as well as 1% of 100 U/ml penicillin and 100 µg/ml streptomycin (P/S, Gibco, USA) at 37°C in 5% CO<sub>2</sub>. At 80% confluency MSCs were trypsinized (Bio Idea, Iran) for three minutes at 37°C and resuspended in DMEM with 10% FBS and 1% P/S. after passage five MSCs were seeded at 3,000 cells/ cm<sup>2</sup> in cell culture plates. The Cells were allowed to attach for 24 hours before changing the medium to either control medium (DMEM, with 4.5 g/l glucose and Gluta MAX Bio Idea, Iran) with 10% FBS and 1% P/S, or osteogenic induction medium (additionally supplemented with 0.1 µM dexamethasone (Sigma-Aldrich, UK), 10 mM β-glycerophosphate (Sigma-Aldrich, UK) and 0.1 mM L-ascorbic acid 2-phosphate (Sigma-Aldrich, UK) (14). Quantitative reverse transcription polymerase chain reaction (qRT-PCR) was used to test expression levels of osteocalcin and osteopontin as key genes involved in the process of osteogenic differentiation.

### Isolation and purification of exosomes

MSCs were cultivated in serum (FBS) free DMEM medium DMEM (Bio Idea, Iran) for 24 to 48 hours after removing the culture medium when their density reached to 70 to 80% of the flask (about 800,000 cells). The exosomes were separated from the supernatant using ultracentrifugation (Beckman, USA) at 100,000 g for one hour in central research laboratory of Mashhad university of medical sciences (15). Exosomes were frozen at -20°C after suspending them in phosphate-buffered saline (PBS, Sigma, USA) (16).

### Exosome identification by atomic force microscopy

To prepare sample for analyzing with the atomic force microscopy (AFM, JPK, Germany), in accordance with published protocols 3 µl of the samples were taken and fixed with 100 µl of 2% paraformaldehyde solution (Sigma, Germany). After that, a little solution drop comprising exosome samples was deposited on the slide, and after 30 minutes the samples were dried and pertinent AFM investigations were carried out (17).

### Exosome identification by Scanning electron microscope

To evaluate the exosome shape and size ,the purified exosomes were fixed with 2.5% glutaraldehyde and rinsed with PBS. The samples were then dewatered with ethanol, and covered with a thin layer of gold on a dry glass surface and examined by scanning electron microscope (SEM, TESCAN, USA) (18).

### Exosome identification by Transmission electron microscopy

Transmission electron microscopy (TEM) was used to examine morphology of the exosomes. After incubating for 15 minutes at room temperature with a 15 µl exosome suspension on a copper grid, the samples were rinsed

with sterile distilled water and dab any remaining liquid was removed by absorbent paper. The filter paper was then removed and the samples were dried for two minutes under an incandescent light after exposing to 15  $\mu$ l of 2% uranyl acetate for one minute on the copper grid. TEM was used to examine the copper mesh, and images were taken at 80 Kv (19).

### Exosome identification by dynamic light scattering method

Quick and simple measurements by dynamic light scattering (DLS) are non-imaging methods used to identify exosomes. All experiments were performed in 1: 1 dilution and performed by Zetasizer (Horiba, Japan) (20).

### Determination of exosome concentrations

Bradford method was used to determine the exosome concentration. To determine the concentration of an isolated exosome, its protein was determined using Bradford solution and standard diagram using successive dilutions of BCA protein (Sigma, UK) with specific concentration.

### Identification of granulosa cells

#### FSHR and AMH immunocytochemistry

After fixing in 4% paraformaldehyde for 15 minutes, the cells were rinsed three times with PBS for a total time of three minutes. The cells were then treated in a 3% hydrogen peroxide ( $H_2O_2$ ) solution while they were incubated at room temperature for 10 minutes. They were rinsed with PBS three times for five minutes to stop peroxidase. The cells were then cultured for 30 minutes at room temperature with 5% bovine serum albumin (BSA) added to the petri dish. FSHR and AMH Primary antibodies (Bioss, USA) were treated with GCs at a concentration of 1/100 in PBS. The secondary FITC goat anti-rabbit antibody (Bioss, USA) against FSHR and AMH were incubated for 30 minutes with the primary antibodies after washing with PBS. The slides were then air-dried, 90% glycerol mounted, and examined under a fluorescence microscope (21, 22).

### Effects of exosomes on granulosa cells

Animals: Immature NMRI mice aged approximately 14 to 21 days were obtained from Research Center for Animal Development Applied Biology (Mashhad, Iran)

GCs extraction: Ovary follicles of 21-days-old mice were subjected to puncture with 25-gauge needle. Follicles were separated and transferred to the other petri dish (4, 24). The follicles were punctured again to release GCs. GCs were then aspirated aseptically in new media and cultured in  $\alpha$ -MEM (Bio Idea, Iran) medium containing FBS (Gibco, USA), ITS (Gibco, USA) and FSH (Cinnal-F, Iran). After 4 days, GCs were treated with doses of 25, 50

and 100  $\mu$ g / ml (23).

### Cellular uptake by PKH26-labeled exosomes

Lipophilic dyes such as the PKH family have been widely used to label a range of cell types like MSCs (24). Since exosomes have a lipid bilayer structure similar to that of the cell plasma membrane, PKH dye family have been adapted for EV labeling (25).

GCs treated with bone marrow-derived exosomes were labeled with fluorescent red PKH26 (Sigma, UK). Exosomes were diluted in 1 ml of Delionnet C solution (Sigma, UK), then 1 ml of Delionnet C solution was diluted with 4 ml of PKH26. This solution was combined with the exosome suspension, and the mixture was incubated with a 1% BSA solution for five minutes. The tagged exosomes were then centrifuged at 100000 g for 70 minutes. The generated tiny stain in the tube was then gradually resuspended in PBS and recentrifuged after the supernatant had been removed (21). Finally, GCs were incubated on a slip cover with exosomes labeled PKH26 at 37°C for 24 hour and then evaluated by confocal fluorescence microscopy (26).

### Effect of exosomes on the viability of granulosa cells

GCs with a density of  $5 \times 10^5$  cell per well were cultured in 12 well plates at 37°C with 5%  $CO_2$  and then the cells were incubated with exosomes for 24 and 48 hours. MTT assay was then performed to evaluate survival of GCs (23).

### Tracking and quantifying apoptosis and necrosis

Annexin-V-PI diagnostic kit (Abcam, UK) was used to track and quantify GCs that underwent apoptosis and necrosis (27). For this purpose, the cells were cultured, and treated using a flow cytometer (BD, USA) and Annexin-V-PI kit according to the manufacturer's instructions.

### Evaluation of changes in *BMP7*, *BMP15* and *GDF9* expression levels by quantitative reverse transcription polymerase chain reaction

qRT-PCR was used to evaluate the expression levels of *GDF-9*, *BMP-15*, and *BMP-7* as key genes in the process of folliculogenesis 48 hours after the treatment of GCs at concentrations of 25, 50, and 100 g/ml exosome. Table S1 (See Supplementary Online Information at [www.celljournal.org](http://www.celljournal.org)) lists the primers used in the current study.

According to the manufacturer's instructions (Scientific Thermo Fisher, USA), total RNA was extracted from the treated and untreated groups. Using a cDNA synthesis kit from Scientific Thermo Fisher (USA), the cDNA was created. qRT-PCR was performed using (BIORAD CFX 96 PCR instrument (BIORAD, USA) (29). This method made use of the Sybergreen fluorescent stain (Pars Tous, Iran).

### Statistical analysis

The trials were run at least three times, and all data

were provided as mean ± standard deviation (SD). One-way ANOVA and the Tukey post hoc tests were both used to analyze variations means in each trial. GraphPad Prism 8 software (GraphPad Software, USA) was used for the statistical analysis. The statistically significant level was set at P<0.05.

## Results

### Confirmation of the cultured bone marrow mesenchymal stem cells by flow cytometry

Positive CD73 and CD105 markers, and negative CD45 and CD34 and CD31 markers, were investigated.

According to the findings, CD73 was expressed by more than 99.9% of the cells, CD105 was expressed by more than 92.4%, but CD45 was only present in 6.92% of these cells. CD34 was only present in 0.2% and CD31 was only present in 3%. Consequently, the stem cells were verified (Fig.1A-E).

### Results of osteocalcin and osteopontin expression in bone marrow mesenchymal stem cells

In the groups treated with osteogenic induction medium, the osteocalcin and osteopontin expression levels were increased significantly (P<0.001) compared to the control group. (Fig.1F, G)

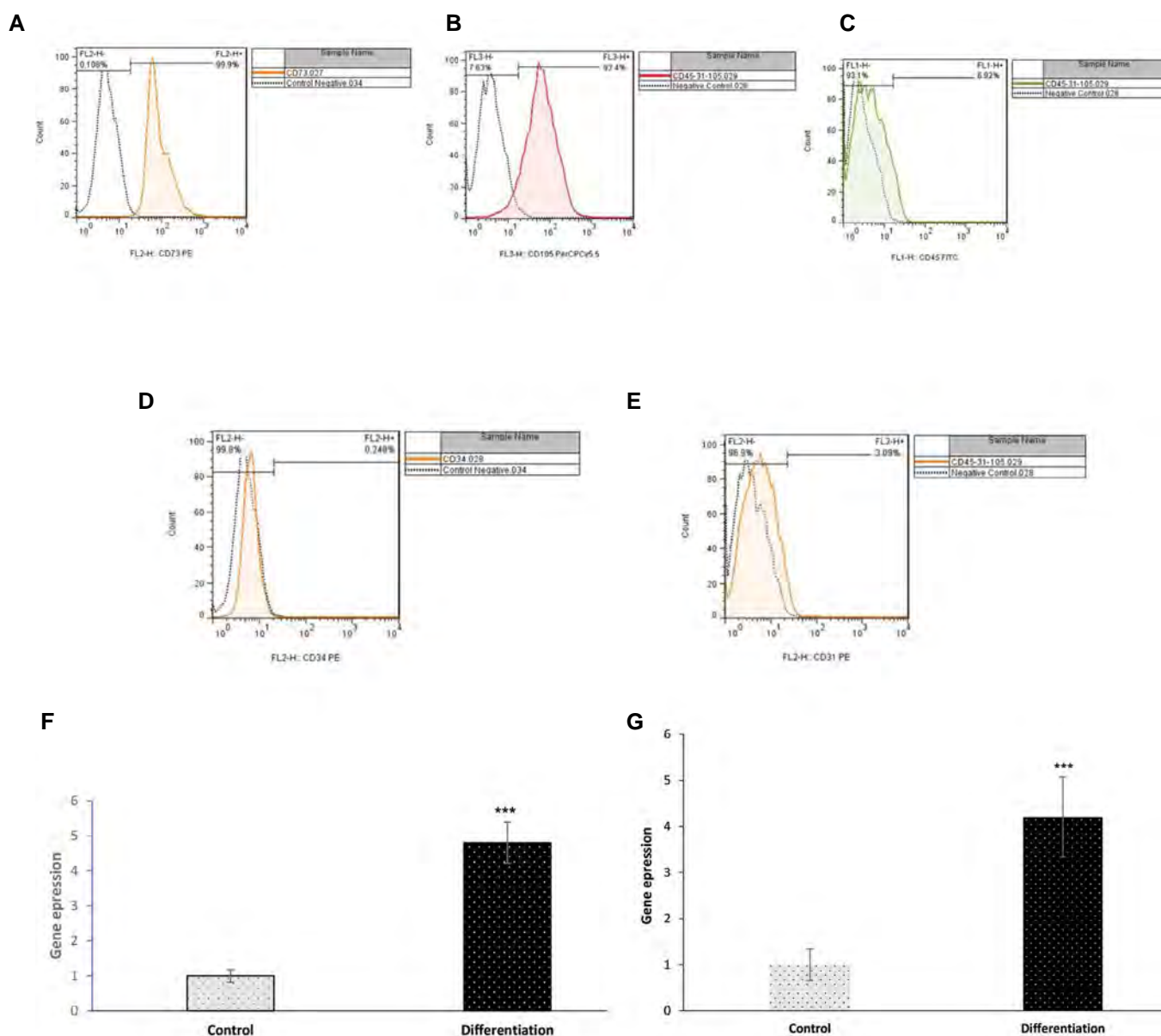


**Fig.1:** Confirmation of bone marrow mesenchymal stem cells (MSCs). **A.** CD73 surface marker diagram. about 99.9% of the cells expressed CD73 marker. **B.** CD105 surface marker diagram. About 92.4% of the cells expressed marker CD105. **C.** CD45 surface marker diagram. A total of 6.92% of the cells expressed marker CD45. **D.** CD34 surface marker diagram. only about 0.2% of the cells expressed marker CD34. **E.** CD31 surface marker diagram. About 3% of the cells expressed marker CD31. Results of **F.** Osteocalcin and **G.** Osteopontin expression in MSCs. As is observed, there is a significant increase in the expression of osteocalcin and osteopontin in the differentiation group compared to the control group. All experiments were repeated three times, each in triplicate. One-way ANOVA test was used for statistical analysis. \*\*\*, P<0.001 compared to the control.



**Results of exosomes isolated from bone marrow mesenchymal stem cells by dynamic light scattering**

The results of this experiment confirmed that the particles extracted using ultracentrifugation from bone marrow stem cells had a diameter from 60-170 nm and the exosome was extracted (Fig.2A).

**Results obtained from the atomic force microscopy of exosomes**

According to the reports published in many articles, the average diameter of exosomes is about 20-200 nm. The results of AFM showed presence of the exosomes with an average diameter of approximately 170 nm (Fig.2B, C).

**Electron scanning microscope results**

SEM images showed presence of the exosomes with an approximate diameter of 50 nm (Fig.2D, E).

**Transmission electron microscopy results**

Morphology of the exosomes was examined using TEM. Findings showed spherical membrane vesicles with less than 100 nm width (Fig.2F).

**Results of granulosa cell confirmation**

Considering GCs have FSH receptors, AMH specific staining was performed by immunohistochemistry to confirm the presence of GCs. The results confirmed presence if these cells (Fig.3).

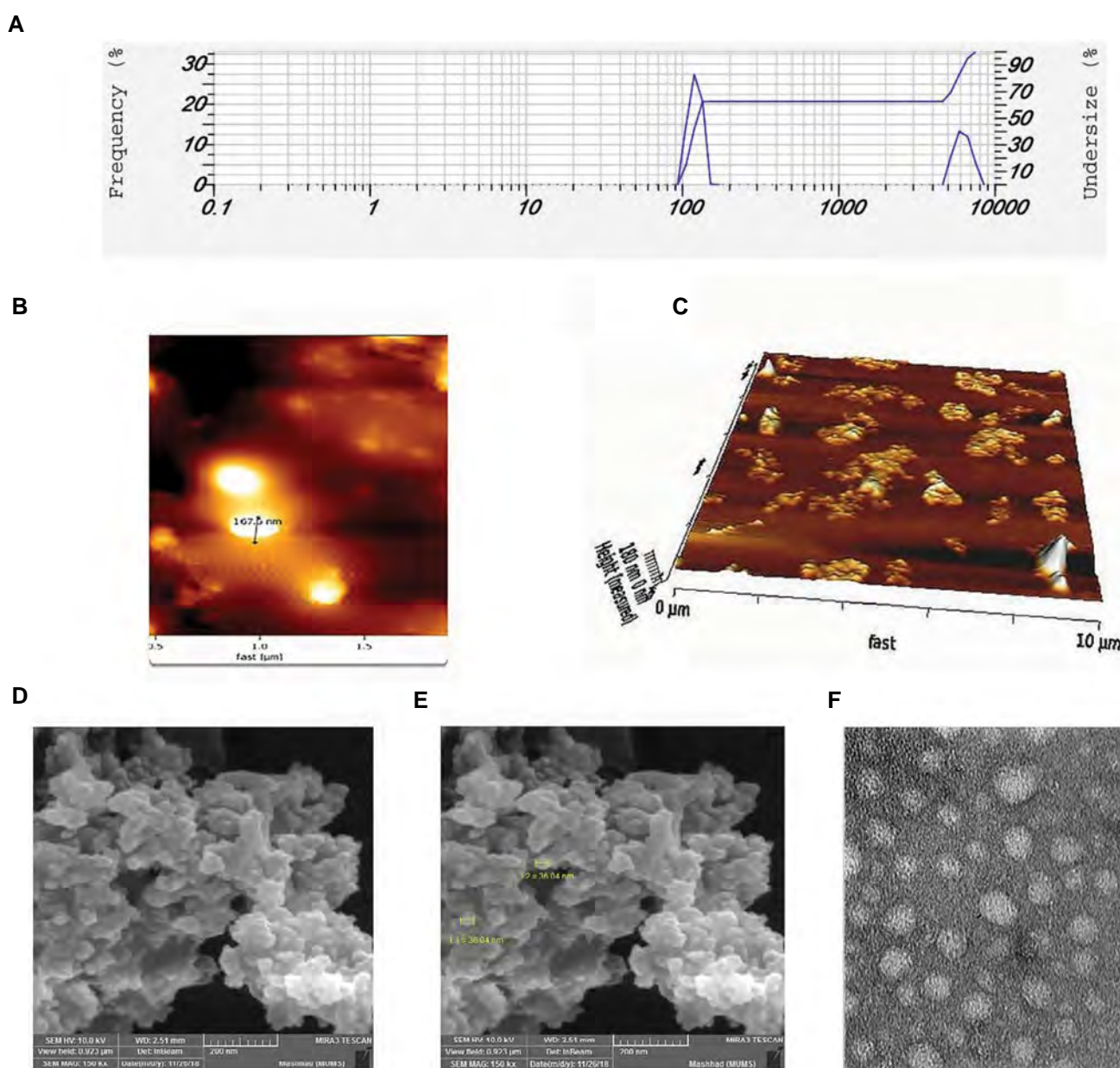


**Fig.2:** Characterization of exosomes. **A.** Exosome diameter measurement by DLS. **B.** The exosome with size of 167-nm is visible in an AFM image. **C.** An exosome with a diameter of around 170 nm is depicted in the AFM output diagram. **D.** SEM image that shows a mass of exosomes. **E.** The same image whereby the approximate dimensions of exosome are specified. **F.** TEM micrograph of the isolated exosomes derived from bone marrow MSCs describes spherical membrane vesicles with the diameters less than 100 nm (scale bar: 50 µm). DLS; Dynamic light scattering, AFM; Atomic force microscopy, SEM; Scanning electron microscopy, TEM; Transmission electron microscopy, and MSCs; Mesenchymal stem cells.

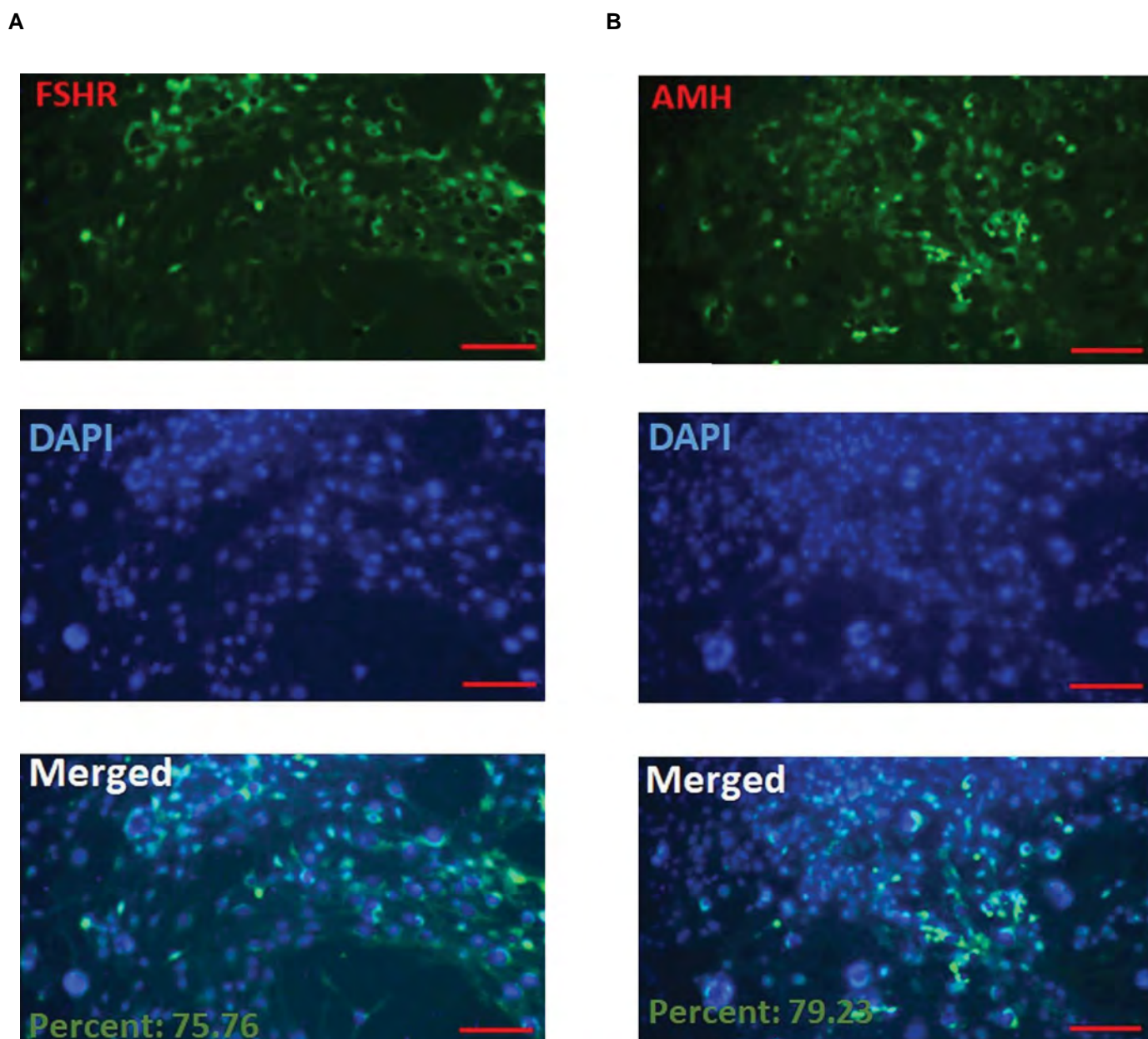


**Fig.3:** Immunofluorescence staining for granulosa cells. **A.** FSHR (green color) and **B.** AMH (green color) and nuclei staining by DAPI (blue color) (scale bar: 100 μm).

### Results of exosome cellular uptake by granulosa cells

PKH26 staining was used to ensure exosome cellular uptake by GCs. The results showed exosome uptake by GCs. The figure displays how tagged exosomes are absorbed by cells. Presence of fluorescent red light in the cytoplasm of GCs shows that they have taken up significant quantities of exosomes from bone marrow-derived stem cells (Fig.4A).

### Results of viability assay

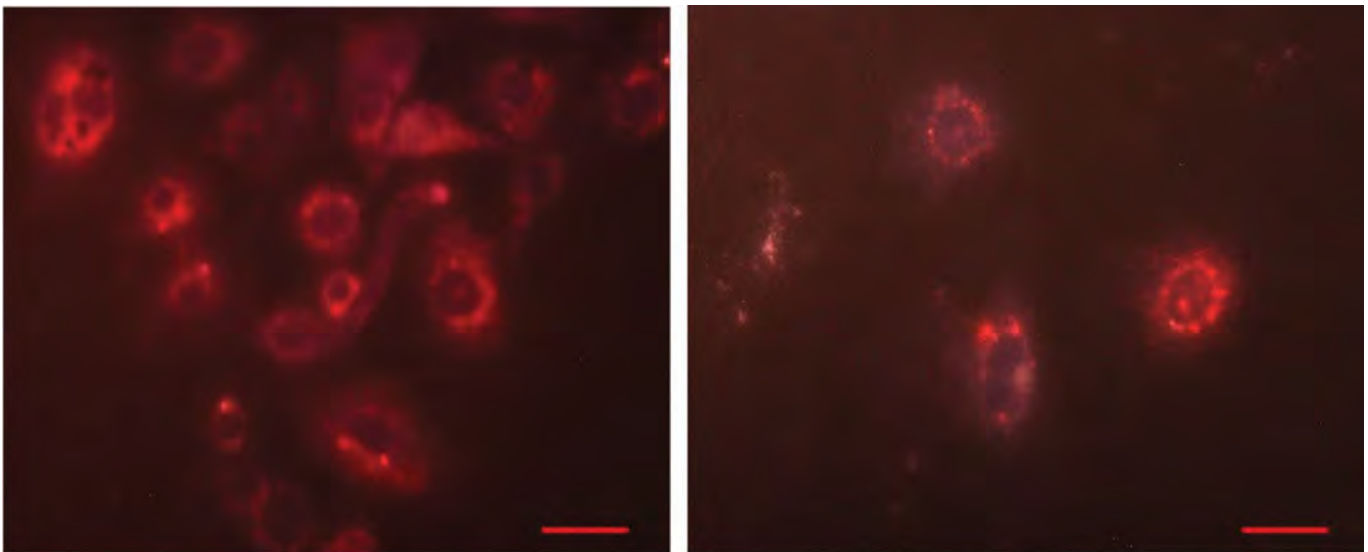
By increasing quantity of exosomes from 25 μg/ml to 50 and 100 μg/ml, viability assay results showed a substantial increase in the cell treated for in 24 hours

and 48 hours compared to the control group ( $P < 0.001$ , Fig.4B).

### Results of Annexin-V assay on granulosa cells

Following the exosome treatment at dosages of 25, 50 and 100 μg/ml, GCs were assessed using the annexin kit in accordance with the corresponding protocol to determine rate of necrosis and apoptosis. Findings demonstrated that, increasing the exosome dose caused dropping GCs levels in the apoptotic treatment groups compared to the control group. Cell viability was roughly 96, 97, and 99.6 in the 25, 50 and 100 μg/ml treated groups, respectively, while it was roughly 90% in the control group (Fig.5).

A



B

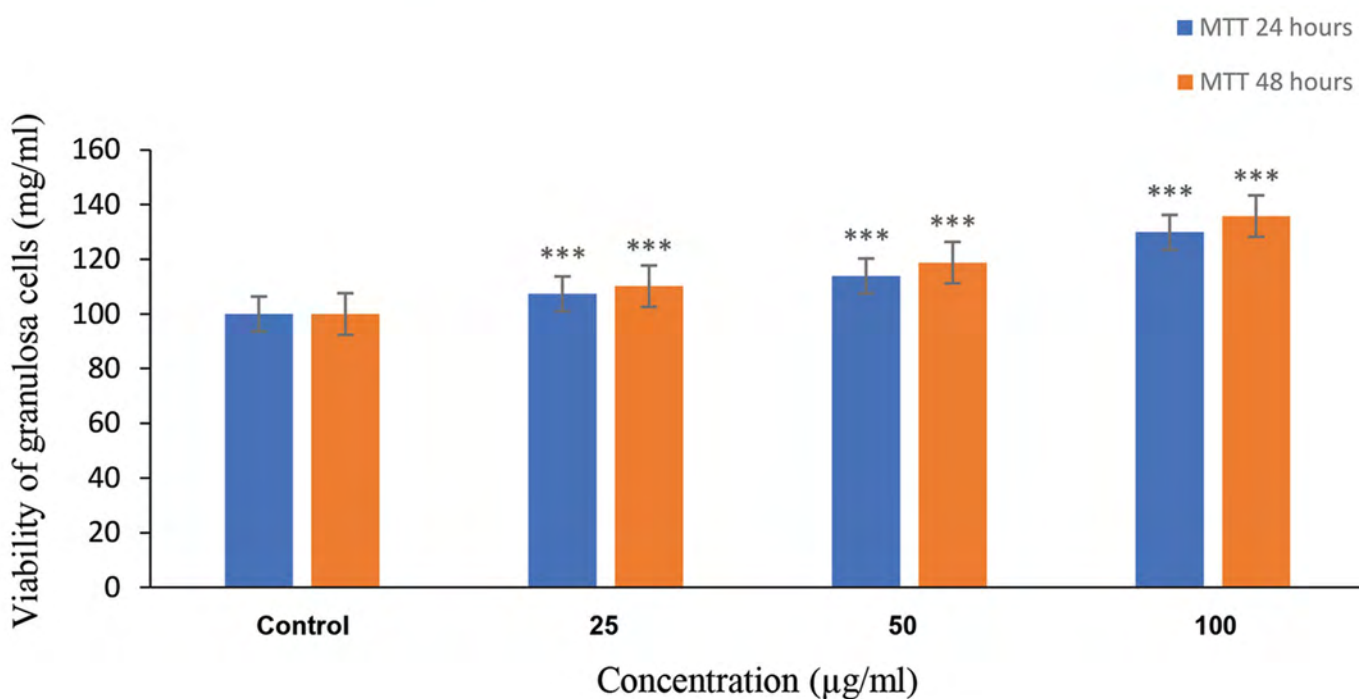


**Fig.4:** Cellular internalization of exosomes and viability of granulosa cells (GCs). **A.** Uptake of the PKH26-labeled exosomes (red) in GCs (scale bar: 100 µm). **B.** Viability diagram of the exosome-treated GCs at 24 and 48 hours. Exosomes were treated in three concentrations of 25, 50 and 100 µg/ml. All three treatment groups are significantly different from the control. Data are represented as the mean ± SD. All experiments were repeated three times, each in triplicate. Statistical One-way ANOVA was used (\*\*\*) P<0.001).

### Results of *GDF-9*, *BMP-15* and *BMP-7* expression levels in granulosa cells

In the groups treated with 50 and 100 µg/ml exosome, *BMP-15* expression levels were increased significantly (P<0.001) compared to the control group. There was no significant change in 25 µg/ml treated group compared to the control group. *BMP-7* gene expression level in GCs showed that in the groups treated with 50 and 100

µg/ml exosome, expression levels of this gene were increased significantly (P<0.001) compared to the control group. There was no significant change in the 25 µg/ml treated group compared to the control group. The results showed that in the groups treated with 50 and 100 µg/ml exosome, *GDF-9* expression level was significantly increased (P<0.001) compared to the control group. There was no significant change in the 25 µg/ml treated group compared to the control group (Fig.6).

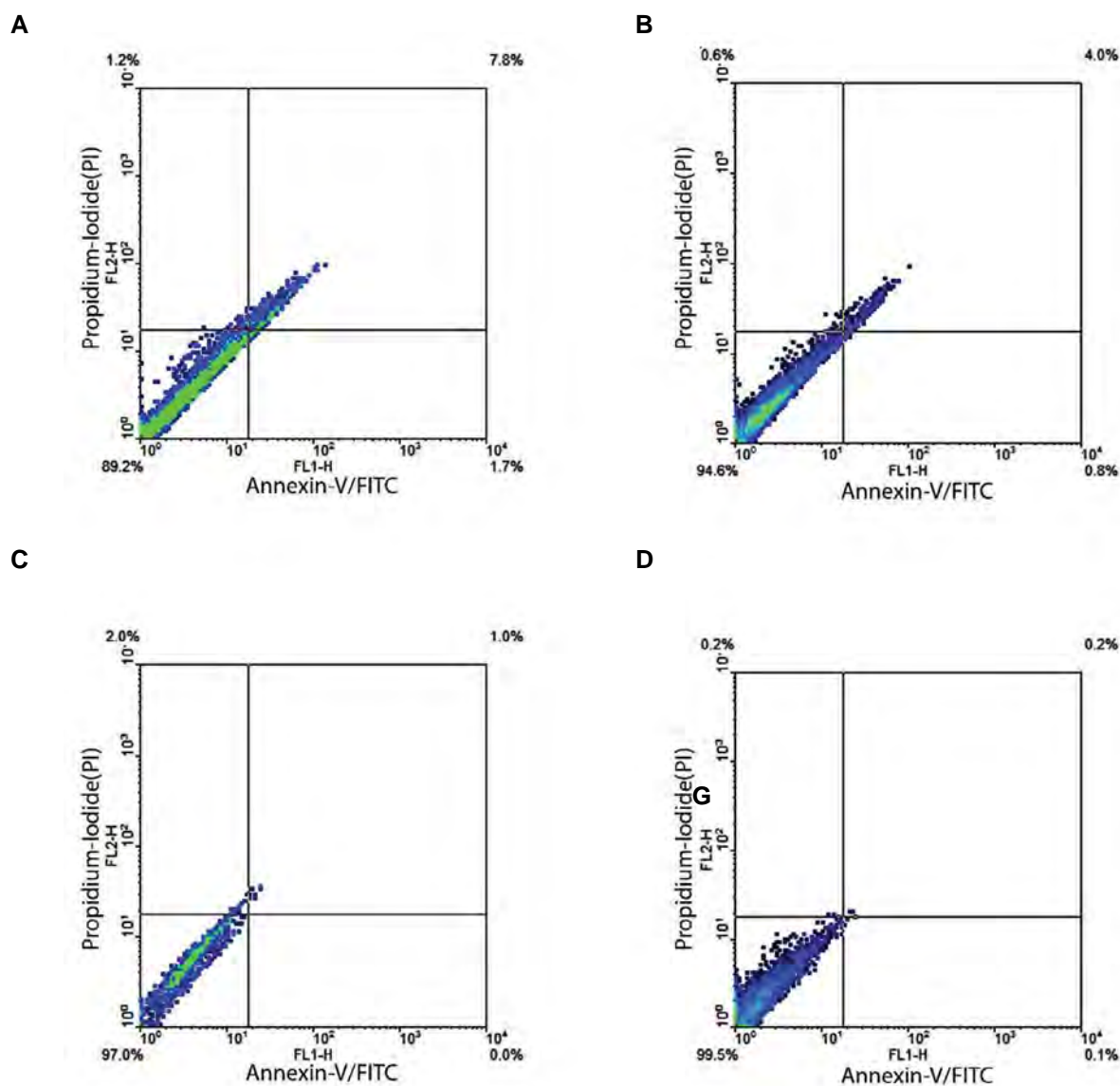


**Fig.5:** Impact of exosomes on granulosa cell (GC) death. Proportion of apoptosis was measured by flow cytometry and Annexin V/PI. **A.** Control group: about 90% of GCs are still alive. **B.** GCs treated group 25 µg/ml: 94.6% of cells are alive. **C.** GCs treated group 50 µg/ml: 97% of cells are alive. **D.** GC treated group 100 µg/ml: 99.5% of cells are alive.

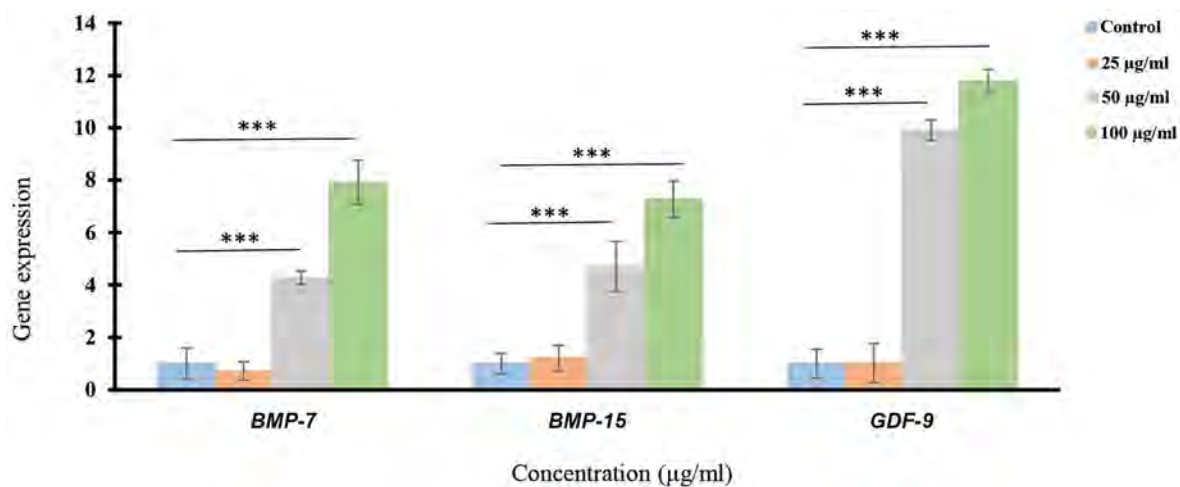


**Fig.6:** Evaluation of *GDF-9*, *BMP-15*, *BMP-7* genes expression in granulosa cells (GCs). Results of *BMP-7*, *GDF-9* and *BMP-15* expression levels in GCs. All experiments were repeated three times, each in triplicate. Statistical One-way ANOVA test was used. \*\*\*, P<0.001 compared to the control.

## Discussion

The most common causes of infertility are ovulation disorders, male factor infertility, and fallopian tube disease. Infertility can indicate a related underlying chronic disease (29). Oocytes, GCs, and theca cells are the main components of follicles (7). Proliferation, differentiation, ovulation, luteinization, and atresia that occur during follicular processes, which comprise these follicular processes, affect GCs, one of the most significant ovarian cells, may result in physiological and morphological alterations. Oocyte development and maturation are impacted by GCs (4). The main function of GCs is to induce production of various sex hormones, and peptides required for folliculogenesis and ovulation (9). The most commonly employed cell phenotype for treatment is MSCs. Numerous secreted molecules have been identified as factors influencing the MSCs purely biological effects. It is thought that paracrine signals play a major role in mediating the effects MSCs. Numerous studies have demonstrated that microvesicles removed from MSCs' culture medium can mimic the regenerative effects of these cells (30). Exosomes are the most significant type of these microvesicles (31). Exosomes are used as carriers for various cellular cargoes. Exosomes' primary job is to transport RNA, miRNA, hormones, proteins, carbohydrates, and other intracellular materials from one cell to another (5). The target cell's behaviour and function may be regulated and altered by the transfer of these chemicals (3).

Findings of the current *in vitro* investigation demonstrated that exosomes are present in the bone marrow MSCs' (BMSCs') supernatant as they develop. Vitality of the GCs was improved by these exosomes, which decreased the incidence of apoptosis in the treated groups. These exosomes were demonstrated to have a favourable impact on the expression of genes related to folliculogenesis.

Flow cytometry was used to prove presence of stem cells in order to investigate cell surface markers. Surface markers that are responsible to identify MSCs include CD44, CD90, CD73 and CD105, while CD11b, CD31, CD34, CD45 markers are not expressed in these cells (32). Results of the present study showed that, CD73 was expressed by more than 99.9% of the cells, CD105 was expressed by more than 92.4%, but CD45 was only present in 6.92% CD34 was only present in 0.2% and also CD31 was only present in 3% of the indicated cells.

Chuo et al. (32) demonstrated to identify various microvesicles secreted by cells, such as exosomes, SEM is an appropriate and important method. In this study, presence of exosomes in the supernatant of stem cells was confirmed using SEM. In the study aimed to identify exosomes, van der Pol et al. (33) showed that one of the approaches to identify exosomes was the DLS method. In the present study, DLS method showed that the approximate exosome diameter is about 50-170 nm.

Results of this study's showed that the exosome extracted from bone marrow cells caused proliferation of GC cells so that bioavailability of GCs at exosome dosage of 25, 50 and 100 µg/ml was increased compared to the control group and there was reduction in the incidence rate of the treated GCs compared to the control group. Yang et al. (34) used Annexin-V apoptosis assay, and showed that T24-derived exosomes of bladder cancer cells could significantly inhibit apoptosis in T24 and 5637 of patients with bladder cancers in a dose-dependent manner.

PKH26 fluorescent dye was used to ensure that the exosomes were absorbed by the GCs and the results showed that this dye was adsorbed by these cells. Salek et al. (21) showed exosome uptake by spermatogenic cells. They labeled the exosomes with the PKH-26 fluorescent dye, and then confirmed that the exosomes entered to cells. The results of this study confirmed the uptake of exosomes by GCs.

According to Maumus et al. (35), these effects of MSCs on immune responses and tissue repair are attributable to the nature and delivery of paracrine signals. These cells transport therapeutic elements and transfer them to the site of injury, which makes them implicated in a variety of physiological and pathological processes (30). They participate in a number of biological activities, including angiogenesis, blood clotting, tissue generalization, immunity, inflammation, and pregnancy (3). It is generally recognized that the chemicals transported by exosomes have the ability to mediate specific physiological pathways and functions in cells. Exosomes, in particular, mediate the interaction between endocrine, paracrine, and juxtacrine glands for cell growth, maintenance, and regeneration (31). Many studies were conducted to find factors that improve the growth and differentiation of follicles cultured *in vitro* in the recent years, and the use of growth-promoting compounds *in vitro* maturation (IVM) has attracted much attention. For example, interleukin-1 (IL-1) regulated the proliferation of bovine and rat GCs *in vitro*. IL-1 also stimulated ovarian cell proliferation and suppresses apoptosis and follicular growth (36). IL-1 beta acted for the synthesis and regulation of steroids and ovulation in GCs and theca cells of rats (21). This cytokine also improved germinal vesicle breakdown (GVBD) in rabbit ovaries and stimulated meiosis and oocyte maturation in female horses (26).

Pashoutan Sarvar et al. (37) reported that exosomes acted as biological mediators produced under physiological and pathological conditions and it included mRNAs, siRNAs, lipids, ribosomal RNAs. In fact, it was shown that they have a supportive function like mesenchymal cells and suppressed inflammatory responses. They also have tissue repair factors in order to repair tissue damage (27). FSH stimulated estradiol production, and researchers reported when the antral follicle phase occurs naturally in the body, it had a significant effect on oocyte meiosis. FSH was proposed to stimulate GC proliferation, while estradiol increased cell size (28). Based on the results of the previous studies, estradiol can have a positive effect

on the growth of preantral follicles (29). The results of qRT-PCR test showed an increase in *BMP-15*, *BMP-7* and *GDF-9* expression levels of GCs treated with exosome dosages of 25, 50 and 100 µg/ml. Similarly, Ghorbani et al. (38) found that treatment of GCs with Barijeh plant extract increased *BMP-15*, *BMP-7* and *GDF-9* expression levels that are effective in folliculogenesis.

## Conclusion

Results obtained from this study indicated that BMSCs derived exosomes of mice had positive effects on the bioavailability of GCs and reduced apoptosis in these cells. Furthermore, since exosomes increased expression levels of *BMP-15*, *BMP-7* and *GDF-9* genes, they had a positive effect on improving the folliculogenesis and GC growth. Nevertheless, further clinical studies are recommended.

## Acknowledgments

The Applied Biology Research Centre for Animal Development, which was instrumental in the success of the current work, is acknowledged by the authors. There is no financial support and conflict of interest in this study.

## Author's Contributions

S.F.; Formal analysis, Writing - the original draft, Analysis and interpretation of data, Drafting of the manuscript, Critical revision of the manuscript for important intellectual content, and Statistical analysis. J.B.; Formal analysis, writing – the original draft, Study concept and design, Analysis and interpretation of data, Drafting of the manuscript, Critical revision of the manuscript for important intellectual content, and Statistical analysis. A.E.; Critical revision of the manuscript for important intellectual content, Statistical analysis critical revision of the manuscript for important intellectual content. N.H.R.; Formal analysis, Analysis and interpretation of data, Critical revision of the manuscript for important intellectual content. All authors read and approved the final manuscript.

## References

1. Nguyen HP, Simpson RJ, Salamonsen LA, Greening DW. Extracellular vesicles in the intrauterine environment: challenges and potential functions. *Biol Reprod.* 2016; 95(5): 109.
2. Di Pietro C. Exosome-mediated communication in the ovarian follicle. *J Assist Reprod Genet.* 2016; 33(3): 303-311.
3. Shomali N, Hemmatzadeh M, Yousefzadeh Y, Soltani-Zangbar MS, Hamdi K, Mehdizadeh A, et al. Exosomes: emerging biomarkers and targets in folliculogenesis and endometriosis. *J Reprod Immunol.* 2020; 142: 103181.
4. Baharara J, Farrokhyar S, Eidi A, Hayati N. The effect of exosomes derived from bone marrow stem cells on the levels of estradiol and testosterone secreted from the ovarian granulosa cells of immature NMRI mice. *Dev Biol.* 2021; 12(4): 1-8.
5. Esmati PZ, Baharara J, Negah SS, Nejad K. Leukemia-derived exosomes induce migration and tumor initiating in astrocytes from human brain tissue. *Int J Pediatr.* 2021; 9(10): 14540-14548.
6. Greening DW, Nguyen HP, Elgass K, Simpson RJ, Salamonsen LA. Human endometrial exosomes contain hormone-specific cargo modulating trophoblast adhesive capacity: insights into endometrial-embryo interactions. *Biol Reprod.* 2016; 94(2): 38.
7. Matsuno Y, Onuma A, Fujioka YA, Yasuhara K, Fujii W, Naito K, et al. Effects of exosome-like vesicles on cumulus expansion in pigs in vitro. *J Reprod Dev.* 2017; 63(1): 51-58.
8. Yang Y, Zhou Y, Li X, He Y, Bai Y, Wang B, et al. Transcriptome profiling reveals transcriptional regulation of Protegrin-1 on immune defense and development in porcine granulosa cells. *Gene.* 2024; 890: 147819.
9. Abedel-Majed MA, Romereim SM, Davis JS, Cupp AS. Perturbations in lineage specification of granulosa and theca cells may alter corpus luteum formation and function. *Front Endocrinol (Lausanne).* 2019; 10: 832.
10. Jeon MJ, Choi YS, Yoo JJ, Atala A, Jackson JD. Optimized culture system to maximize ovarian cell growth and functionality in vitro. *Cell Tissue Res.* 2021; 385(1): 161-171.
11. Ma Y, Jiang XD, Zhang DW, Zi XD. Molecular characterization and effects of the TGIF1 gene on proliferation and steroidogenesis in yak (*Bos grunniens*) granulosa cells. *Theriogenology.* 2023; 211: 224-231.
12. Divya D, Bhattacharya TK. Bone morphogenetic proteins (BMPs) and their role in poultry. *Worlds Poult Sci J.* 2021; 77(3): 539-564.
13. Yang F, He L, Luo B, Ye F, Cui C, Yu X, et al. Effect of bone morphogenetic protein 6 (bmp6) on chicken granulosa cells proliferation and progesterone synthesis. *Braz J Poult Sci.* 2019; 21(2): 1-8.
14. Wan HY, Shin RLY, Chen JCH, Assunção M, Wang D, Nilsson SK, et al. Dextran sulfate-amplified extracellular matrix deposition promotes osteogenic differentiation of mesenchymal stem cells. *Acta Biomater.* 2022; 140: 163-177.
15. Gurunathan S, Kang MH, Jeyaraj M, Qasim M, Kim JH. Review of the Isolation, characterization, biological function, and multifarious therapeutic approaches of exosomes. *Cells.* 2019; 8(4): 307.
16. Zhang X, Yuan X, Shi H, Wu L, Qian H, Xu W. Exosomes in cancer: small particle, big player. *J Hematol Oncol.* 2015; 8: 83.
17. Yurtsever A, Yoshida T, Badami Behjat A, Araki Y, Hanayama R, Fukuma T. Structural and mechanical characteristics of exosomes from osteosarcoma cells explored by 3D-atomic force microscopy. *Nanoscale.* 2021; 13(13): 6661-6677.
18. Nikdel N, Baharara J, Zakerbostanabad S, Tehranipour M. The effect of exosomes derived from human ovarian epithelial cancer cells on the secretion of AMH and Inhibin in granulosa cells. *NBR.* 2021; 8(1): 31-38.
19. Garcia-Contreras M, Brooks RW, Boccuzzi L, Robbins PD, Ricordi C. Exosomes as biomarkers and therapeutic tools for type 1 diabetes mellitus. *Eur Rev Med Pharmacol Sci.* 2017; 21(12): 2940-2956.
20. Tabak S, Schreiber-Avissar S, Beit-Yannai E. Influence of anti-glaucoma drugs on uptake of extracellular vesicles by trabecular meshwork cells. *Int J Nanomedicine.* 2021; 16: 1067-1081.
21. Salek F, Baharara J, Shahrokhbabadi KN, Amini E. The guardians of germ cells; Sertoli-derived exosomes against electromagnetic field-induced oxidative stress in mouse spermatogonial stem cells. *Theriogenology.* 2021; 173: 112-122.
22. Wang Q, Li X, Wang Q, Xie J, Xie C, Fu X. Heat shock pretreatment improves mesenchymal stem cell viability by heat shock proteins and autophagy to prevent cisplatin-induced granulosa cell apoptosis. *Stem Cell Res Ther.* 2019; 10(1): 348.
23. Monsefi M, Nadi A, Alinejad Z. The effects of *Salvia officinalis* L. on granulosa cells and in vitro maturation of oocytes in mice. *Int J Reprod Biomed.* 2017; 15(10): 649-660.
24. Dominkuš P P, Stenovec M, Sitar S, Lasič E, Zorec R, Plemenitaš A, et al. PKH26 labeling of extracellular vesicles: Characterization and cellular internalization of contaminating PKH26 nanoparticles. *Biochim Biophys Acta Biomembr.* 2018; 1860(6): 1350-1361.
25. Dehghani M, Gulvin S M, Flax J, Gaborski T R. Exosome labeling by lipophilic dye PKH26 results in significant increase in vesicle size. *Sci Rep.* 2020; 9533(10).
26. El-Saghir J, Nassar F, Tawil N, El-Sabban M. ATL-derived exosomes modulate mesenchymal stem cells: potential role in leukemia progression. *Retrovirology.* 2016; 13(1): 1-13.
27. Fan Y, Chang Y, Wei L, Chen J, Li J, Goldsmith S, et al. Apoptosis of mural granulosa cells is increased in women with diminished ovarian reserve. *J Assist Reprod Genet.* 2019; 36(6): 1225-1235.
28. De Los Reyes M, Palomino J, Araujo A, Flores J, Ramirez G, Paraguez VH, et al. Cyclooxygenase 2 messenger RNA levels in canine follicular cells: interrelationship with GDF-9, BMP-15, and progesterone. *Domest Anim Endocrinol.* 2021; 74: 106529.
29. Carson SA, Kallen AN. Diagnosis and management of infertility: a review. *JAMA.* 2021; 326(1): 65-76.

30. Fierabracci A, Del Fattore A, Luciano R, Muraca M, Teti A, Muraca M. Recent advances in mesenchymal stem cell immunomodulation: the role of microvesicles. *Cell Transplant*. 2015; 24(2): 133-149
  31. Soria FN, Pampliega O, Bourdenx M, Meissner WG, Bezdard E, Dehay B. Exosomes, an unmasked culprit in neurodegenerative diseases. *Front Neurosci*. 2017; 11: 26.
  32. Chuo ST, Chien JC, Lai CP. Imaging extracellular vesicles: current and emerging methods. *J Biomed Sci*. 2018; 25(1): 91
  33. van der Pol E, Hoekstra AG, Sturk A, Otto C, van Leeuwen TG, Nieuwland R. Optical and non-optical methods for detection and characterization of microparticles and exosomes. *J Thromb Haemost*. 2010; 8(12): 2596-607.
  34. Yang L, Wu XH, Wang D, Luo CL, Chen LX. Bladder cancer cell-derived exosomes inhibit tumor cell apoptosis and induce cell proliferation in vitro. *Mol Med Rep*. 2013; 8(4): 1272-1278.
  35. Maumus M, Jorgensen C, Noël D. Mesenchymal stem cells in regenerative medicine applied to rheumatic diseases: role of secretome and exosomes. *Biochimie*. 2013; 95(12): 2229-2234.
  36. Passos JR, Costa JJ, da Cunha EV, Silva AW, Ribeiro RP, de Souza GB, et al. Protein and messenger RNA expression of interleukin 1 system members in bovine ovarian follicles and effects of interleukin 1 $\beta$  on primordial follicle activation and survival in vitro. *Domest Anim Endocrinol*. 2016; 54: 48-59.
  37. Pashoutan Sarvar D, Shamsasenjan K, Akbarzadehlaleh P. Mesenchymal stem cell-derived exosomes: new opportunity in cell-free therapy. *Adv Pharm Bull*. 2016; 6(3): 293-299.
  38. Ghorbani M, Baharara J, Eidi A, Namvar F. Green biosynthesis of ZnO nano-particles, inhibited development of pre-antral follicles. *Arch Pharma Pract*. 2019; 10(1): 38-49.
-

# A Mutational Hotspot in The *LAMP2* Gene: Unravelling Intrafamilial Phenotypic Variation and Global Distribution of The c.877C>T Variant: A Descriptive Study

Saeideh Kavousi, Ph.D.<sup>1</sup>, Mohammad Dalili, M.D.<sup>2</sup>, Bahareh Rabbani, Ph.D.<sup>3</sup>, Mehrdad Behmanesh, Ph.D.<sup>4</sup>, Mehrdad Noruzinia, M.D., Ph.D.<sup>1\*</sup> , Nejat Mahdieh, Ph.D.<sup>5\*</sup> 

1. Department of Medical Genetics, Faculty of Medical Sciences, Tarbiat Modares University, Tehran, Iran  
2. Rajaie Cardiovascular Medical and Research Centre, Iran University of Medical Sciences, Tehran, Iran  
3. Growth and Development Research, Tehran University of Medical Sciences, Tehran, Iran  
4. Department of Genetics, Faculty of Biological Sciences, Tarbiat Modares University, Tehran, Iran  
5. Cardiogenetic Research Centre, Rajaie Cardiovascular Medical and Research Centre, Iran University of Medical Sciences, Tehran, Iran

## Abstract

**Objective:** Danon disease is defined by a clinical trio of cardiomyopathy, skeletal myopathy, and cognitive impairment. It results from the lysosomal-associated membrane protein-2 (*LAMP2*) gene variants. The aim of study is determination of genotype and phenotype of a newly diagnosed Iranian family with a unique phenotype due to a pathogenic variant of the *LAMP2* gene along with a phenotypic comparison of all reported patients.

**Materials and Methods:** In this descriptive study, we evaluated the demographic data, clinical features, management procedures, as well as genetic analysis of both patients in this newly diagnosed family. Whole genome sequencing (WGS) and in silico structural and functional predictions were applied. A comprehensive search of the c.877C>T variant in *LAMP2* was conducted using the PubMed, Google Scholar, VarSome, ClinVar, Human Gene Mutation Database (HGMD), and Franklin databases to identify any genotype-phenotype correlations.

**Results:** Nine patients were carriers of the c.877C>T variant. All patients were male, and displayed variable degrees of left ventricular hypertrophy (LVH) that ranged from mild to severe. All patients exhibited typical cardiac conduction abnormalities consistent with Danon disease. Four underwent heart transplants and survived. Skeletal muscle involvement and cognitive impairment were observed in four patients each. The mean age of onset was 14 years. The proband in this study exhibited an earlier onset of cardiac symptoms.

**Conclusion:** Genetic analysis is the preferred diagnosis approach for Danon disease and can assist families in managing affected patients, identify carriers, and assist with future family planning. This study highlights the intrafamilial phenotypic variability of Danon disease. It is possible that variants of this gene may be frequent in Iran.

**Keywords:** Danon Disease, Next-Generation Sequencing, Cardiomyopathy

**Citation:** Kavousi S, Dalili M, Rabbani B, Behmanesh M, Noruzinia M, Mahdieh N. A mutational hotspot in the *LAMP2* gene: unravelling intrafamilial phenotypic variation and global distribution of the c.877C>T variant: a descriptive study. *Cell J.* 2024; 26(1): 39-50. doi: 10.22074/CELLJ.2023.2007469.1372  
This open-access article has been published under the terms of the Creative Commons Attribution Non-Commercial 3.0 (CC BY-NC 3.0).

## Introduction

Danon disease (OMIM#300257) is a rare X-linked disorder that results from an abnormality in the lysosomal-associated membrane protein-2 (*LAMP2*) gene. While the prevalence of Danon disease is not accurately estimated, recent advancements in genetic testing have improved the diagnosis of disorders with substantial genetic components. The *LAMP2* gene (OMIM#309060) encodes a 410 amino acid protein. Its luminal domain is encoded by exons 1 to 8 and a portion of exon 9. The remainder of exon 9 contains the encoding for a transmembrane domain and a short cytoplasmic tail that contains the signal for targeting to the lysosomal membrane.

The *LAMP2* protein is the principal regulator of autophagosome maturation, which maintains homeostasis by balancing the synthesis, degradation, and recycling of cellular substances. It facilitates the fusion and degradation of autophagosomes with lysosomes, resulting in autolysosome formation (1, 2).

Mutations in the *LAMP2* gene can hinder autophagy leading to impairments in lysosome maturation and biogenesis. Pathogenic variants in this gene may produce a nonfunctional or insufficient amount of the *LAMP2* protein, which results in various problems depending on the affected cells. In Danon disease, the *LAMP2* protein is

Received: 22/July/2023, Revised: 14/September/2023, Accepted: 08/November/2023

\*Corresponding Addresses: P.O.Box: 14115-111, Department of Medical Genetics, Faculty of Medical Sciences, Tarbiat Modares University, Tehran, Iran  
P.O.Box: 1996911151, Cardiogenetic Research Centre, Rajaie Cardiovascular Medical and Research Centre, Iran University of Medical Sciences, Tehran, Iran  
Emails: noruzinia@modares.ac.ir, nmahdieh@rhc.ac.ir



Royan Institute  
Cell Journal (Yakhteh)



often absent in muscle and heart cells, and leads to muscle weakness and heart abnormalities. Symptoms can vary widely among affected individuals even with the same variant; male patients are typically more severely affected and are often the proband of Danon disease. Although hemizygous males may indicate a loss of function, it is likely that the dominant effect of the mutations is primarily attributable to haploinsufficiency. This means that the protein produced by the unaffected, wild-type allele remains below the normal threshold level (3).

The classic clinical hallmark of Danon disease in males consists of severe cardiomyopathy, skeletal myopathy, and intellectual disability, whereas cardiac disease may be the most prominent symptom in females. Involvement of other organs, such as the liver, lungs, and retina, has also been reported in males with this multisystem disorder. Cardiomyopathy, particularly hypertrophic cardiomyopathy (HCM) in men and dilated cardiomyopathy (DCM) in women, are the most common and life-threatening symptoms. Electrocardiogram abnormalities are also observed in most patients, with ventricular pre-excitation in females and Wolf-Parkinson-White (WPW) syndrome primarily observed in males. Although cardiac symptoms typically appear during infancy, childhood, or adolescence, there is slower progression and later onset in women. Without a heart transplant, the condition rapidly advances to end-stage heart failure, and men typically die in their 30s and women in their 40s or 50s. Due to its similarity with sarcomeric HCM, an accurate diagnosis of Danon disease is critical to ensure appropriate management strategies (4, 5).

The diagnosis of Danon disease is gradually increasing due to advancements in genetic testing methods. Whole exome sequencing, as the most common genetic test, can identify genetic variants in a significant fraction of patients. However, whole genome sequencing (WGS), the most comprehensive genetic testing method, has a higher diagnostic sensitivity for identifying rare and common genetic variants in patients with HCM (6).

This study presents the genotype-phenotype relationship of well-characterised cases of Danon disease due to the c.877C>T variant. Also, a detailed genetic and clinical report on an Iranian family with two affected individuals, a 13-year-old boy and his mother, is also presented.

## Materials and Methods

### Data extraction

In this descriptive study, we conducted a comprehensive review of the c.877C>T (p.Arg293Ter) variant in PubMed and Google Scholar using the keywords: "LAMP2 gene", "c.877C>T", "p.Arg293Ter", "mutation", and "Danon disease". In addition, ClinVar (<https://www.ncbi.nlm.nih.gov/clinvar/>), Leiden Open Variation Database (LOVD) (<https://www.lovd.nl/>), VarSome (<https://varsome.com/>), and the Human Gene Mutation Database (HGMD) (<https://www.hgmd.cf.ac.uk/ac/index.php>) databases were searched to identify all published papers that pertain to

patients who carry this variant. The data from individuals with the p.Arg293Ter variant were extracted. Notably, a review article listed this variant in a table of LAMP2 gene variants reported in the last ten years (7); in one article, specific clinical details for the two families were not provided (8). We excluded these two articles from the clinical review of variant carriers. Characteristics extracted from the published articles included patient demographics, reporting countries, publication year, clinical characteristics (heart, skeletal muscle, cognitive function, and other organs), patient management procedures [implantable cardioverter-defibrillators (ICD) and heart transplants], as well as genetic analysis of both the patients and their families.

In this study, we conducted a clinical and genetic examination of an Iranian family with two patients who referred to Rajaei Hospital Cardiovascular Medical and Research Centre, which represented the second reported family of this variant in Iran, as we previously reported the first family (9). The proband (case III-1) and mother (case II-5) underwent clinical evaluations that included laboratory tests and various cardiovascular examinations such as echocardiography, electrocardiography, Holter monitoring, electrophysiology study, paediatric percutaneous angiography, multi-slice computed tomography (CT) scan of the brain and thorax, and transabdominal ultrasound. The patients underwent cardioverter-defibrillator, ablation, cardioversion and drug therapy, as clinical interventions.

### Genetic analysis

#### Whole genome sequencing and data processing

DNA samples were extracted from the patients' family members according to salting out standard protocols. High-quality DNA from the proband was assessed by WGS, achieving 30-fold coverage with  $\geq 95\%$  of bases sequenced at  $8\times$  or higher coverage using an Illumina NovaSeq 6000 sequencer (Dante Labs, Inc., L'Aquila, Italy). DRAGEN™ Bio-IT Platform was employed to generate raw data files, including FASTQ R1, FASTQ R2, BAM and VCF files of single nucleotide polymorphisms (SNPs), indels, and CNVs.

GATK variant recalibrator was employed to implement Variant Quality Score Recalibration (VQSR) for SNPs and indels at 99.5% and 99.0% sensitivity thresholds, with additional criteria of GQ ( $\geq 20X$ ) and DP ( $\geq 10X$ ). VCF files were annotated using the Ensembl Variant Effect Predictor (VEP) command line tool (<https://github.com/Ensembl/ensembl-vep>).

Potentially pathogenic SNP and indel variants were identified by considering the minor allele frequency (typically  $<0.01-1\%$ ), Combined Annotation Dependent Depletion (CADD) score  $>10$ , non-benign predictions in CLIN\_SIG, and deleterious effects using IMPACT (categorised as high, moderate, modifier, and low) filtration. Subsequently, restricted analysis was carried out following American College of Medical

Genetics (ACMG) guidelines and integrated data from the HGMD, HPO, OMIM and PubMed databases, and scholarly articles. Significant CNVs were detected and genotyped through read-depth (RD) analysis using CNVnator.

### Pathogenicity interpretation

In silico prediction scores were obtained as follows to study the pathogenicity of the different variants: MutationTaster (<http://www.mutationtaster.org/>) (10), Mutation Assessor (<http://mutationassessor.org/>) (11), CADD (<https://cadd.gs.washington.edu/>) (12), deleterious annotation of genetic variants using deleterious annotation of genetic variants using neural networks.

(DANN) ([https://cbcl.ics.uci.edu/public\\_data/DANN/](https://cbcl.ics.uci.edu/public_data/DANN/)) (13), Polymorphism Phenotyping v2 (PolyPhen2) (<http://genetics.bwh.harvard.edu/pph2/>) (14), Sorting Intolerant From Tolerant (SIFT) (<https://sift.bii.a-star.edu.sg/>) (15), Functional Analysis through Hidden Markov Models (FATHMM-MKL) (<http://fathmm.biocompute.org.uk/fathmmMKL.htm>) (16), likelihood-ratio test (LRT) ([http://genetics.wustl.edu/jflab/lrt\\_query.html](http://genetics.wustl.edu/jflab/lrt_query.html)), (17) and BayesDel (<https://fengbj-laboratory.org/BayesDel/BayesDel.html>) (18).

Genomic conservation scores were obtained from following programs: Phylogenetic p-value from the Phylogenetic Analysis with Space/Time models (PHAST) package (<http://compgen.cshl.edu/phast/>) for multiple alignments of 99 vertebrate genomes to the human genome (phyloP100way Vertebrate) (19) and Genomic Evolutionary Rate Profiling (GERP) (<http://mendel.stanford.edu/SidowLab/downloads/gerp/>) (20).

The frequency of the variant in the population was evaluated by comparison with variants from the following databases: dbSNP (<https://www.ncbi.nlm.nih.gov/snp/>), Genome Aggregation Database (gnomAD) (<https://gnomad.broadinstitute.org/>), and Iranome (<http://www.iranome.ir/>).

ClinVar (<https://www.ncbi.nlm.nih.gov/clinvar/>) and HGMD (<http://www.hgmd.cf.ac.uk/ac/index.php>) were used to identify previously reported variants. Candidate variants were assessed for pathogenicity according to ACMG criteria (21).

### Family screening and Sanger sequencing

In order to verify the candidate p.Arg293Ter variant, we designed a specific set of primers using Primer3 (<https://bioinfo.ut.ee/primer3-0.4.0/>). The forward primer LAMP2-F (5'-ccttcagggaatccacagtc-3') and reverse primer LAMP2-R (5'-gcagtttattctaccgatg-3') were utilised to amplify target sequences that contained the variant. The Sanger sequencing protocol used in this study was obtained from our previous publication (22).

The obtained sequencing results were then analysed

using 4Peaks and compared with the *LAMP2* gene sequence from the NCBI database (NM\_002294.3).

### In silico protein structure prediction and visualisation

The protein sequence of LAMP2 was aligned using UniProtKB/Swiss-Prot P13473. The Simple Modular Architecture Research Tool (SMART) ([https://smart.embl.de/smart/show\\_motifs.pl?ID=P11532](https://smart.embl.de/smart/show_motifs.pl?ID=P11532)) and the protein families database (Pfam) (<http://pfam.xfam.org/protein>) were used to determine the LAMP2 protein domains.

There are only two experimental structures of the LAMP2 protein in the Protein Data Bank (PDB) that are related to the transmembrane domain. In the SWISS-MODEL repository, four models are available; however, none of them cover all 410 amino acids. The complete structure of the LAMP2 protein (AF-P13473-F1-model-v4) is available in the AlphaFold Protein Structure Database with high confidence.

Homology/analogy recognition engine V2.0 (Phyre2) (23) and Deep-learning based Iterative Threading ASSEMBLY Refinement (D-I-TASSER) were utilised to determine the effect of the candidate variant on the protein structure and function predictions. The three-dimensional (3D) structure of the wild-type and mutant LAMP2 protein visualised by D-I-TASSER (24). Additionally, the conservation study was conducted via the ConSurf server (25).

### Pathogenic/likely pathogenic variants

Pathogenic/likely pathogenic variants in the *LAMP2* gene were systematically reviewed across multiple databases, including UniProt, ClinVar, VarSome, PubMed, and HGMD to identify all the published and unpublished variants up to March 2023. A literature review of *LAMP2* gene pathogenic variants in PubMed was performed using the keywords "Danon disease, *LAMP2*, variant, pathogenic, likely pathogenic, and gene". The mentioned databases were investigated, and duplicate records were excluded to avoid errors of overrepresentation. All variants were named according to the Human Genome Variation Database (HGVS). The ClinVar variation ID and submissions, as well as publication ID, were collected in the Table S1 (See Supplementary Online Information at [www.celljournal.org](http://www.celljournal.org)).

### Ethics approval and consent to participate

The study portion that involved human participants was carried out in accordance with the ethical standards set by the Ethics Committee of Tarbiat Modares University, Tehran, Iran (IR.MODARES.REC.1399.253). The study followed the ethical guidelines set forth in the latest update of the World Medical Association Declaration of Helsinki. Informed consent was acquired from all adult participants and,

for minors, consent was obtained from their parents or legal guardians for the genetic analysis. These procedures were carried out in accordance with national ethics regulations.

## Results

### Distribution of the p.Arg293Ter variant

We identified eight articles that pertained to the p.Arg293Ter variant. From these, six contained comprehensive clinical data and were selected for comparative analysis (Table 1). Nine patients carry the p.Arg293Ter variant, which is a germline pathogenic variant associated with Danon disease in the ClinVar database. The variant has been submitted to ClinVar five times (accession number: VCV000163812.12) between 2017 and 2020 by reputable submitters of ClinVar.

The cohort consisted of eight male patients and one female patient, consistent with the inheritance pattern and nature of Danon disease. Although the age of onset was not considered, the age range during the study was reported to be between 7 and 44 years for male patients and 35 years for the sole female patient. Three patients were from the United States of America, three cases were from Iran (the studied family), and the remaining individuals were from Italy, Greece, and Spain.

### Iranian patients

#### Previously reported case

In 2018, Amin et al. (9) reported the case of a 30-year-old Iranian male who presented to Rajaie Hospital Cardiovascular Medical and Research Centre with exertional dyspnoea and a family history of cardiac failure in two older brothers. The patient had no notable musculoskeletal complaints, and normal mental health and speech. Electrocardiography revealed left axis deviation and left bundle branch block, whereas the echocardiography showed severe papillary muscle hypertrophy and mild left ventricular hypertrophy (LVH) with an ejection fraction (EF) of 45%. Initially, the patient received treatment for sarcomeric HCM, including an ICD. His condition deteriorated, with cardiomegaly and visible pulmonary congestion on chest X-ray. Progressive symptoms, such as peripheral oedema, ascites and muscle involvement, prompted genetic testing and muscle biopsy. Sequence analysis identified the p.Arg293Ter variant in the *LAMP2* gene, which confirmed Danon disease. Unfortunately, despite standard heart failure therapy, the patient succumbed to respiratory infection and cardiac pump failure.

#### Case (III-1), proband

A 9-year-old proband (III-1) male referred to Rajaie Cardiovascular Medical and Research Hospital due to recurrent chest pain, exertional dyspnoea, and palpitations. He had a history of myopia corrected with glasses and

mild intellectual disability, including learning difficulties at school (not formally tested).

Physical examinations revealed normal tone, power, reflexes, and gait. However, his family reported mildly severe symptoms that consisted of difficulty walking, leg deformity, and proximal muscle weakness that occurred just before the patient's condition worsened in subsequent years. Clinical laboratory examinations that included blood counts, serum creatinine, and serum electrolyte levels were all within the normal range. Paediatric transthoracic echocardiography revealed severe LVH that caused a collapsed right ventricle (RV) due to interventricular septum hypertrophy (IVS >3 cm). Other findings included mild tricuspid regurgitation, severe diastolic dysfunction, and a left ventricular ejection fraction (LVEF) of 60%. HCM was diagnosed based on the echocardiogram and clinical indications, which led to treatment with a single-chamber ICD implantation.

Over the following years, despite standard heart failure treatments, the patient's condition deteriorated. Electrocardiogram abnormalities indicated LV hypertrophic remodelling, atrial rhythm issues, bi-atrial enlargement, and borderline long QT interval. Holter monitoring recorded various cardiac rhythms, including wide QRS tachycardia, supraventricular tachycardia, and premature beats. Subsequent echocardiography revealed severe atrial and ventricular enlargement, concentric LVH, severe right ventricular hypertrophy (RVH) with dysfunction, severe valves regurgitation and reduced LVEF (10-15%). The patient underwent two electrophysiology studies and ablation procedures. Despite interventions, the patient's condition worsened, and imaging studies showed cardiomegaly, hepatomegaly, and pulmonary abnormalities. Unfortunately, the patient passed away due to heart failure at the age of 14 despite medical efforts.

#### Case (II-5), mother

The mother of case III-1, a 35-year-old female, had a distinctly different heart condition, specifically DCM and left ventricular non-compaction cardiomyopathy (LVNC). Her echocardiogram indicated mildly enlarged LV (dilation), mildly reduced systolic function (EF: 35-40%) and global hypokinesia. She exhibited normal motor performance and muscle strength, with clinical laboratory test results within normal ranges. During 24-hour Holter monitoring, the patient experienced palpitations and dizziness, along with frequent premature ventricular contractions and short episodes of nonsustained ventricular tachycardia. External cardioversion was performed twice to restore normal sinus rhythm. Case II-5 experienced recurrent hospitalisations for decompensated heart failure over the years. She received an ICD and was in stable condition, having successfully delivered a child in the last three years.

**Table 1:** Reported clinical characteristics of individuals that carry the p.Arg293Ter variant

Origin	Gender	Age (Y)	First refer	Echocardiography results	Creatine kinase (U/L)	Cardiac conduction impairments	CMR	ICD	HTx	Extracardiac manifestations	Histopathology	Variant status	Reference
Italy	Male	12	Heart failure	Dilated LV Concentric hypertrophy Impaired systolic function	Increased (638 U/L)	-	-	-	Yes	-	Yes	De novo	(26)
USA	Male	19	Dyspnoea Chest pain	-	Increased (500 U/L)	-	-	--	Yes	Myopathy Cognitive impairment	Yes	Mother's death due to heart failure	(27)
USA	-	-	-	-	-	-	-	-	-	-	-	-	(8)
Spain	Male	44	-	Myocardial fibrosis EF 30%	-	Yes	-	-	-	-	-	De novo	(28)
USA	Male	15	Syncope Muscle weakness after HTx	Dilated LV Concentric hypertrophy EF 25%	Increased (660 U/L)	Yes	-	Yes	Yes	Myopathy Seizure Cognitive impairment	Yes	Mother's death due to heart failure (age 30 years)	(29)
Iran	Male	30	Dyspnoea	Severe hypertrophy Valves regurgitation EF 45%.	-	Yes	Cardiomegaly Prominent right heart Pulmonary congestion	Yes	-	Myopathy	-	2 older brothers died from heart failure	(9)
Greece	Male	-	Syncope Dyspnoea Chest pain	Concentric hypertrophy	Increased (267 U/L)	Yes	Extensive LGE of all myocardial walls sparing only the IVS	Yes	Yes	Cognitive impairment	-	Sister sudden death (age 1 year)	(30)
Iran	Male	7	Chest pain Dyspnoea Palpitations	Severe LVH Severe IVS hypertrophy Collapsed RV Valves regurgitation Impaired diastolic function EF 60% ----- Bilateral/biventricular enlargement Concentric hypertrophy Severe IVS hypertrophy Severe RVH Impaired systolic/diastolic function Valves regurgitation Pulmonary insufficiency EF 10%–15%	-	Yes	Cardiomegaly Pulmonary congestion	Yes	-	Following walking difficulty, leg deformity, and proximal muscle weakness (mild severity) Mild cognitive impairment	-	Mother's cardiac symptoms	Case (III-1)*
Iran	Female	35	DCM LVNC	LV dilation Impaired systolic function Valves regurgitation Global hypokinesia EF: 35%–40% ----- LV enlargement Impaired systolic/diastolic function Mild RV enlargement Valves regurgitation Pulmonary/aortic insufficiency Mild to moderate pulmonic/aortic insufficiency Global hypokinesia EF: 20%	-	Yes	-	Yes	-	-	-	Son's death due to heart failure	Case (II-5)*

The results of echocardiography are presented for both the initial visit and the most recent examination. ICD; Implantable cardioverter-defibrillator, HTx; Heart transplantation, LGE; Late gadolinium enhancement, DCM; Dilated cardiomyopathy, LVNC; Left ventricular non-compaction cardiomyopathy, EF; Ejection fraction, LV; Left ventricle, RV; Right ventricle, IVS; Interventricular septum, LVH; Left ventricular hypertrophy, RVH; Right ventricular hypertrophy, and \*; Shows the variant carriers within the family we investigated in this study.

## Genotype-phenotype architecture

Patients with the p.Arg293Ter variant were systematically categorised according to the following parameters: publication source, patient demographics, referral concerns, cardiac assessments, laboratory values, conduction abnormalities, imaging reports, interventions, clinical manifestations, histopathology, genetic test results, family screening, and mortality details (Table 1).

Nine patients harboured the c.877C>T variant, with no reported ethnic associations, except for the two patients from Iran. The mean age of onset was approximately 14 years, consistent with previous findings for male patients with *LAMP2* variants. However, the proband in this study exhibited an earlier onset of cardiac symptoms, with a reported age of onset of seven years. Clinical presentations, cardiac exam results, and age at mortality differed between the two Iranian patients who had the same variant. One patient died in their 30s, while the proband passed away at age 14. All previously reported patients were male and presented with varying degrees of concentric LVH and the typical cardiac conduction abnormalities seen in Danon disease.

Of the nine patients, four underwent heart transplants and survived. Despite receiving preventive treatments, the two male patients from Iran ultimately experienced heart failure and were unable to receive a heart transplant, resulting in fatal outcomes.

Four male patients showed elevated serum creatine kinase levels and skeletal myopathy in their proximal and distal muscles, which was not age-related. Notably, three cases did not present noticeable skeletal myopathy symptoms at disease onset. The p.Arg293Ter variant was associated with a range of neurological symptoms, with varying severities. Four cases reported cognitive impairment, while one reported seizures. Typically, these neurological symptoms were mild, as observed in the proband in this study (Table 1).

## Cardiac features

Dyspnoea was the most common cardiac complication in four patients at their initial visit, whereas chest pain was the most common cardiac complication reported by three patients at their first visit. Furthermore, two cases of episodic syncope and one case of early-onset heart failure were the first referral symptoms. Additionally, a female patient exhibited symptoms of DCM and LVNC. Cardiac hypertrophy patterns included four cases of concentric LVH, and ranged from mild to severe. LVEF ranged from 10 to 60%, and varied according to gender, age, and disease progression.

Systolic dysfunction was noted in three patients and two patients exhibited diastolic dysfunction. The proband and mother in the studied family displayed concurrent

impairments in both systolic and diastolic function.

Cardiovascular guidance abnormalities were found in six patients, and the reported values were consistent with previous articles and guidelines. However, each patient exhibited a distinct phenotypic pattern (Table 1).

Cardiac imaging tools, such as MRI/chest X-rays revealed cardiomegaly and pulmonary congestion in two patients, and one patient exhibited a specific Danon-related pattern of extensive late gadolinium enhancement (LGE) that involved all myocardial walls except the interventricular septum.

Treatment involved the use of an ICD in five patients, while four patients underwent cardiac transplantation as the most aggressive intervention.

Regarding genetic status, two patients had de novo variants, while six had suspected family histories that included five with heart failure and one case of sudden death in first-degree relatives (Table 1).

## Muscular and neurological involvement

Elevated creatine kinase levels were detected in four male patients, but not all cases were associated with myopathy symptoms. Nonetheless, the involvement of skeletal muscles was evident from the disease onset and continued late into disease progression in four patients. Skeletal disorders were characterised by diffuse myopathy in proximal and distal muscles, difficulty walking, leg deformities, and proximal muscle weakness.

Neurological manifestations were observed in four male patients, including cognitive impairment in three cases and rare occurrences of seizures and mental retardation reported in one patient.

## Variant validation and familial segregation

### Case (III-1), proband

The *LAMP2*:c.877C>T (p.Arg293Ter) variant was validated by Sanger sequencing and confirmed the hemizygous state and X-linked dominant inheritance. This variant led to a null variant (stop gain, nonsense) in the *LAMP2* gene. Loss-of-function is a well-established mechanism of this disease (Fig.1).

### Case (II-5)

Familial segregation analysis indicated that the *LAMP2*:c.877C>T (p.Arg293Ter) variant originated from the proband's mother. The X-linked dominant inheritance was also confirmed by the heterozygous state of the mother, which corresponds to her phenotypic pattern.

The absence of p.Arg293Ter variant in clinically unaffected family members (father and sister) was confirmed by Sanger sequencing (Fig.1).

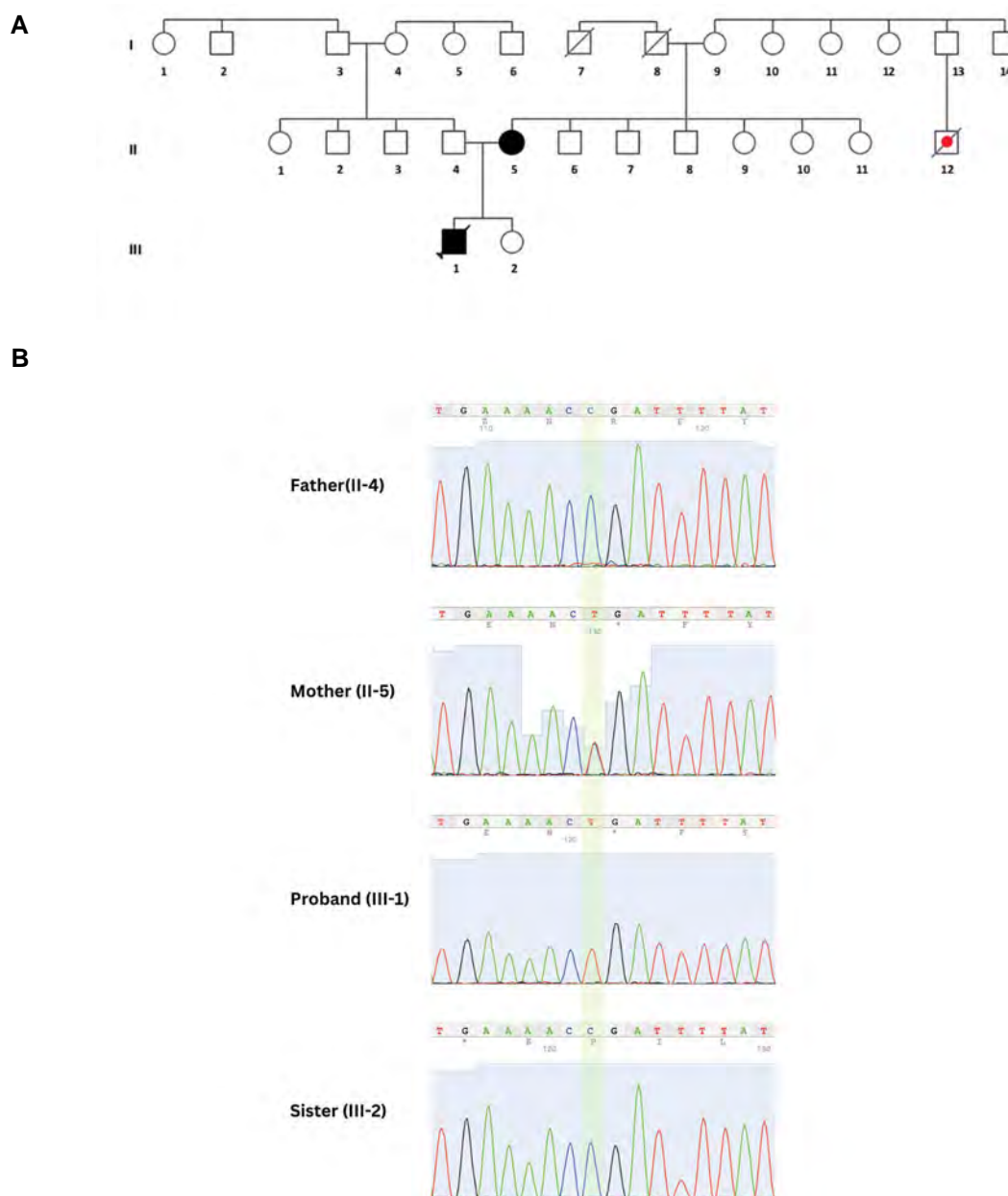


**Fig.1:** Family pedigree and genetic analysis results. **A.** Pedigree of the family with the lysosomal-associated membrane protein-2 (*LAMP2*) variant. The proband (III-1) is indicated by the arrow. Slashed symbols indicate the deceased members. **B.** The nonsense variant, c.877C>T in exon 7 of the *LAMP2* gene, is located at the hemizygous state in proband (III-1) and the heterozygous state in his mother (II-5). The proband's father and sister carry a normal allele. Circles; Females, Squares; Males, Black-filled shapes; Danon disease phenotype-positive subjects, Empty shapes; Unaffected subjects, and Red dot; Cardiac disorders.

### Bioinformatic analysis p.Arg293Ter

Conservation analysis utilising PhyloP100way (value 3.7), showed conservation of the p.Arg293Ter variant. However, bioinformatics analysis of the p.Arg293Ter variant was predicted the variant to be damaging by BayesDel (addAF and noAF), FATHMM-MKL, GenoCanyon and MutationTaster, while other tools indicated varied interpretations. CADD predicted a PHRED score of 43, which indicated that these variants rank in the top 1% for deleteriousness in the human genome (Table 2). The ACMG guidelines (21) showed the candidate variant to be classifiable as “pathogenic”

based on PVS1, PP5 and PM2 criteria.

### *In silico* protein analyses of p.Arg293Ter

The human *LAMP2* gene spans 1233 nucleotides and is divided into 9 exons, encoding a 410 amino acid protein. Structurally, *LAMP2* consists of three domains. The first is the lysosome-luminal domain, which includes exons 1 to 8 and a portion of exon 9. These domains are interconnected by a hinge region notable for its high proline content. There are two conserved disulfide bonds in each of the duplicated domains. The second is a transmembrane region (the remaining part of exon 9

encodes the transmembrane domain). The third is a short cytoplasmic tail at the C-terminal extremity.

The p.Arg293Ter variant occurs within the second luminal domain, specifically at position 229-375 of the LAMP2 protein.

**Table 2:** Bioinformatics tools and prediction scores of the *LAMP2*: c.877C>T (p.Arg293Ter) variant

Bioinformatics tools	Prediction	Score
BayesDel addAF	Damaging	0.618
BayesDel noAF	Damaging	0.649
CADD	Pathogenic	43
DANN	Uncertain	0.9982
FATHMM-MKL	Damaging	0.8429
Frequency in gnomAD	Not found	Not found
GenoCanyon	Deleterious	1
GERP	Uncertain	5.3
Iranome	Not found	Not found
LRT	Neutral	0.002944
Mutation Assessor	N/A	-
Mutation Taster	Disease causing	1
PhyloP100way	Conserve	9.5
PolyPhen2	N/A	-
SIFT	N/A	-
Splice AI	Splice-altering/moderate	0.21
SNP ID	rs727503118	-

LAMP2; Lysosomal-associated membrane protein-2, CADD; Combined annotation dependent depletion, DANN; Deleterious annotation of genetic variants using neural networks, FATHMM-MKL; Functional analysis through hidden markov models, GERP; Genomic evolutionary rate profiling, gnomAD; Genome aggregation database, LRT; Likelihood-ratio test, PolyPhen2; Polymorphism phenotyping v2, SIFT; Sorting intolerant from tolerant, and SNP; Single nucleotide polymorphism.

Using the Phyre2 web portal, LAMP2 was modelled based on the PDB entry 5gv0(A), and it represents the

local structural environment of the Arg293 residue with 34% identity and 100% confidence. Secondary structure analysis revealed that the  $\beta$ -strand at amino acid 293 was predicted to be disordered and altered with a high score, which indicated reduced flexibility, dynamics, and extension. According to secondary structure model analysis, the p.Arg293Ter variant was predicted to alter the N-terminal  $\beta$ -strands, causing destruction of the second luminal domain ends, and the cytoplasmic tail of LAMP2 led to drastic conformational change.

The D-I-TASSER server ranked 5gv0A as the optimal output model, primarily due to the Arg293 location. The secondary structure for the normal sequence was predicted to be a strand, whereas it was predicted to be a coil in the Arg293 mutant, which resulted from the stop codon. The solvent accessibility prediction changed from a score of 3 (normal) to 8 (mutant), and indicated that the mutated protein at this position is more exposed than the normal sequence. The scores range from 0 to 8, with higher values indicative of greater exposure. The B-factor profile values showed a significant change, from -0.07 for the normal sequence at Arg293 (indicating a strand and being exposed) to 2.14 in the mutant sequence, which was predicted to be unstable, coiled, and highly exposed.

The enzyme function remained unchanged, with a C-score<sub>EC</sub> of 0.060 (scores range from 0 to 1, with higher values indicative of more reliable predictions). Predicted active site residues were not identified by D-I-TASSER analysis. Gene ontology (GO) values (C-score<sub>GO</sub>) showed slight changes in biological processes, molecular functions, and cellular components (Data not shown). Additionally, downstream residues of exon 7 were found to be highly conserved using the ConSurf web server. Mutant and wild-type 3D structures, generated by D-I-TASSER, exhibited significant structural alterations in line with the secondary structure analysis from Phyre2 (Fig.2).

*LAMP2* is associated with Danon disease through 137 documented pathogenic LOF variants, which indicates a well-established loss-of-function mechanism. Among these variants, Arg293Ter, found in exon 7, significantly impacts the 'second luminal domain' of the UniProt protein LAMP2\_HUMAN. This alteration is predicted to cause nonsense mediated decay. Exon 7 contains seven pathogenic variants, while the truncated region includes 39 pathogenic variants, which supports a pathogenic criterion (PVS1) for this particular variant.

According to Uniport information, Arg293 is a monomethylation site identified in vivo (epithelial cells) via mass spectrometry. Sites modified by arginine monomethylation, like Arg293Ter, are known hotspots for disease-related mutations. Additionally, downstream of Arg293, there are N-Glycosylation sites at positions 300, 307, 312, 317, and 356, a disulfide

bond at position 331-368, and Phosphorylation sites at 304, 309, and 407. Disruption of these elements significantly impacts the protein's 3D conformation. LAMP2 functions as a receptor in the lysosomal membrane, and facilitates the degradation of substrate proteins like *GAPDH*, *NLRP3*, and *MLLT1*. Notably,

four amino acids (GLKHHHAGYEQF) in the cytosolic tail are essential for binding to substrate proteins (Fig.2). The Arg293Ter variant disrupts this critical binding site, which results in the loss of LAMP2's proper cellular functionality and the development of Danon disease.

A



B

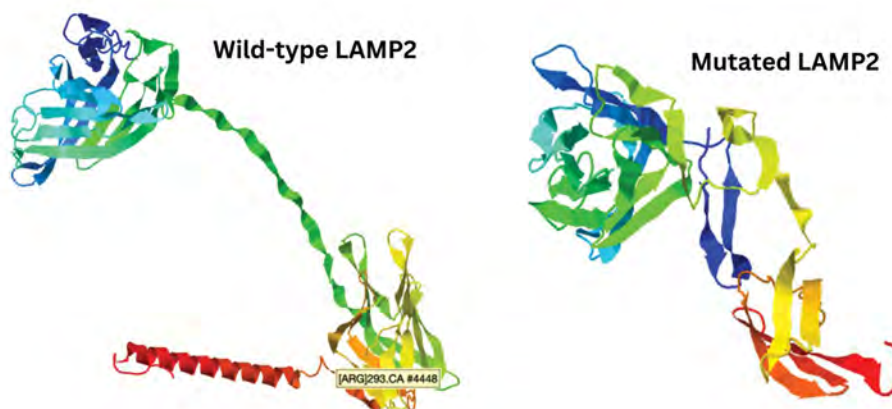


**Fig.2:** In-silico structural modeling of the identified mutation. **A.** Secondary structure model analysis of the lysosomal-associated membrane protein-2 (LAMP2) protein using Homology/analogY Recognition Engine V2.0 (PHYRE2). The left column indicates the protein sequence, secondary structure, and disorder for each line of the wild-type LAMP2 protein (left) and the mutated (p.Arg293Ter) protein (right). The confidence value score for each item is determined by the confidence key colour palette. Destruction of the end of the second luminal region, the cytoplasmic tail, and the alternation of the N-terminal  $\beta$ -strands lead to visible secondary structure changes. The boxes on the right side show the altered regions of the protein after the variant. **B.** Three-dimensional (3D) structure of wild-type (left) and mutated (right) LAMP2 as generated by Deep-learning based Iterative Threading ASSEMBly Refinement (D-I-TASSER) software.



### Pattern of the *LAMP2* pathogenic/likely pathogenic variant

At the time of this consideration, 145 pathogenic/likely pathogenic *LAMP2* variants have been reported based on published and unpublished databases (Table S1, See Supplementary Online Information at [www.celljournal.org](http://www.celljournal.org)).

Although pathogenic variants occur in all exons, they are most frequent in the last exon. Frameshift indels followed by nonsense variants are the majority (~85%) of pathogenic truncating variants that are predicted to cause the loss of the transmembrane region and cytoplasmic tail, both of which are critical domains for *LAMP2* protein structure. Large pathogenic deletions are mainly found in exon 8, followed by exons 1 and 6, while one pathogenic duplication, 199bp, has been reported in exon 4. The splicing variants, either in the splice site or not within 2 bp of a splicing junction region, that cause *LAMP2* deficiency have also been described in most of the exons. The five missense variants are only identified in exons 7 and 8, with the most common pathogenic variant belonging to p.Val310 (Table S1, See Supplementary Online Information at [www.celljournal.org](http://www.celljournal.org)). It has been reported as pathogenic in nine submissions in ClinVar and various reports in the LOVD databases, as well as in nine articles published in PubMed until February 2023.

### Discussion

Diagnosis and management of cardiac diseases can be difficult due to multiple non-cardiac symptoms and variable clinical presentations. Danon disease is a prime example of this challenge, as an accurate diagnosis is essential to prevent potentially severe complications. The significant heterogeneity in clinical manifestations and genetic variants associated with this disease further complicates its diagnosis and management. Herein, we report the first well-characterised family with Danon disease in Iran. In this study, bioinformatic analysis revealed that the p.Arg293Ter variant creates a premature translational stop signal, disrupts the consensus splice site in the *LAMP2* gene through changes in RNA splicing and ultimately affects protein structure, which results in an absent or disrupted protein product. Prior research has indicated that most *LAMP2* gene variants result in protein deficiency, including nonsense mutations, frame-shift deletions/insertions, and splicing site variants. In contrast, missense mutations and large rearrangements that impact one or more exons are infrequent. Notably, missense variants have a lower incidence of cardiomyopathy, while truncation variants have the earliest onset, followed by splicing and missense variants. While there is no established genotype-phenotype correlation in Danon disease, null variants lead to non-functional proteins, while other variants impact protein function (8, 31).

Our research contributes significantly to our understanding by assessing the prevalence of all pathogenic

variants in the *LAMP2* gene, notably the p.Arg293Ter variant, which serves as a mutational hotspot linked to a range of clinical phenotypes. Among the more than 145 pathogenic variants identified in the *LAMP2* gene, c.926G>A and c.877C>T are two of the most frequently observed.

Significant disparities in disease outcomes and symptoms have been noted among different patients (5). The proband's mother in this study (case II-5) is the first female with the variant that has both LVNC and DCM. This specific cardiac phenotype, also known as dilated LVNC, has been previously found in disorders associated with the Titin (TTN), Lamin A/C (LMNA), and RNA binding motif protein 20 (RBM20) genes (32). The presence of non-compaction cardiomyopathy in Danon disease is unusual, with limited previous reports; to the best of our knowledge, this is the first documented instance of both DCM and LVNC that occur together (29, 33).

Clinical heterogeneity between genders could stem from the varying extent of X-chromosome inactivation, including random and skewed, which occur in female cells (34). Furthermore, it could also be due to the effect of oestrogen on autophagy and the lysosomal pathway (35). The phenotype of Danon disease in female patients remains inadequately elucidated relative to males, and leads to many undiagnosed cases in females. Lack of early diagnosis can cause uncompensable costs and lost opportunities for heart transplantation (HTx).

Female patients typically have milder symptoms and a later onset, with an average onset age of 19 years (8). Cardiac disease is an isolated clinical feature in 73% of female patients, but its severity is equal to that of males. HCM is the most commonly observed type of cardiomyopathy in both males and females. However, it is noteworthy that females have a lower prevalence of HCM and a higher prevalence of DCM compared to males (5).

Males with Danon disease experience a multisystem disorder that presents with cardiomyopathy, cognitive impairment, and skeletal myopathy, usually occurring around the age of 13 years. Other organs, including the retina and liver, may also be affected. Studies have indicated that 80-100% of male patients experience skeletal myopathy. However, the symptoms may not always be obvious; in some cases, the disease may progress and result in severe manifestations (36). In a review of patients with the p.Arg293Ter variant, four male patients showed a significant increase in serum creatine kinase and skeletal myopathy. However, no significant symptoms of skeletal myopathy were noted at the onset of the disease in three cases, including the two Iranian patients and a 44-year-old patient with end-stage HCM.

Studies have shown that 70-100% of patients have mild to moderate cognitive disabilities. Paediatric patients have

reported mild speech delay, attention deficits, autism, and behavioural problems. Brain CT scans and MRI imaging studies have indicated the involvement of the central nervous system (37). The p.Arg293Ter variant is linked to a range of neurological symptoms that are often mild and may only be noticeable to close family members, as seen in the case under examination in this study. The c.877C>T variant may arise from an ancestry in our population such as variants in other genes; however, further studies are required to prove a founder effect about this variant (38, 39).

An isolated cardiac phenotype has been reported in 18% of male cases, with HCM in 96% of affected patients. Conduction abnormalities have also been observed in up to 80% of cases. The most common electrocardiography finding is pre-excitation, specifically WPW syndrome, which occurs in approximately 48% of affected male (5, 8).

Echocardiography often reveals concentric LVH, especially in childhood-onset cases and this necessitates a heart transplant. In males, there is a rapid progression towards end-stage heart failure in their third decade of life, while females may experience this in their forties to fifties if the condition is not treated. Four patients with the p.Arg293Ter variant underwent heart transplants and survived. Despite preventive treatments, two patients from Iran eventually experienced heart failure and died.

A prevalence of 60% of Danon disease patients have ocular involvement that include strabismus, myopia, and retinopathy. Hepatomegaly has been observed in 36% of cases, often accompanied by elevated liver enzymes since childhood (40). Gastrointestinal complaints have been reported by 77% of individuals (8). The proband in this study had myopia and hepatomegaly, which aligns with these clinical findings. Advancements in genetic testing have led to a precise diagnosis of Danon disease, which is often initially misdiagnosed in HCM. Next-generation sequencing technology and bioinformatics have enabled the development of cost-effective and accurate diagnostic tools for genetic disorders such as cardiomyopathies. WGS analysis of intronic regions and the mitochondrial genome may also help identify pathogenic variants in 9% of HCM patients with a familial history and no causative variant identified through initial genetic testing (6).

The discovery prompted a genetic evaluation and cascade screening for the patient's family, which revealed the patient's mother as a carrier with compatible clinical manifestations. On the other hand, the intergender phenotypic variability in Danon disease underscores the importance of precise genetic analysis to prevent false negative results. An accurate phenotype characterisation that incorporates WGS along with complimentary copy number variation genetic analysis can offer the best possible care for affected families and enable family planning for their offspring.

Our inability to perform histopathological examinations of the proband's skeletal muscle and heart in our case series, given that the proband was deceased, is recognized as a limitation of this study.

## Conclusion

This study provides important insights into the diagnosis and genetic analysis of Danon disease in Iran. Through a detailed case report and bioinformatic analysis, we shed light on the impact of the p.Arg293Ter variant in the *LAMP2* gene on protein structure and function. Our findings also highlight the high frequency of this variant among individuals with Danon disease. Overall, this study enhances our understanding of the disease and may help improve the diagnosis and management of affected individuals.

## Acknowledgements

This work was conducted at Tarbiat Modares University, Tehran, Iran. We express our sincere appreciation to the family members of the proband who graciously consented to participate in this research study. We also thank the Medical and Laboratory staff of Rajaie Hospital who assisted with the diagnosis and treatment of the patient. This research was financially supported by the Department of Medical Genetics, Tarbiat Modares University, Tehran, Iran. The authors have no competing of interest to declare.

## Authors' Contributions




M.N., N.M.; Conceptualisation, Study design, Critical supervision of the manuscript, Data analysis, and Interpretation validation. S.K.; Experiment investigation, Performed formal analysis, Interpretation of data, and Writing- original draft preparation. M.D.; Surveyed the patients clinically and Participated in collecting clinical data of the patients. B.R.; Counselling and Participated in collecting clinical data of the patients. M.B.; Counselling and Research plan management. All authors read and approved the final manuscript.

## References

1. Khandia R, Dadar M, Munjal A, Dhama K, Karthik K, Tiwari R, et al. A comprehensive review of autophagy and its various roles in infectious, non-infectious, and lifestyle diseases: current knowledge and prospects for disease prevention, novel drug design, and therapy. *Cells*. 2019; 8(7): 674.
2. Endo Y, Furuta A, Nishino I. Danon disease: a phenotypic expression of LAMP-2 deficiency. *Acta Neuropathol*. 2015; 129(3): 391-398.
3. Sugie K, Koori T, Yamamoto A, Ogawa M, Hirano M, Inoue K, et al. Characterization of Danon disease in a male patient and his affected mother. *Neuromuscul Disord*. 2003; 13(9): 708-711.
4. Maron BJ, Roberts WC, Arad M, Haas TS, Spirito P, Wright GB, et al. Clinical outcome and phenotypic expression in LAMP2 cardiomyopathy. *JAMA*. 2009; 301(12): 1253-1259.
5. Brambatti M, Caspi O, Maolo A, Koshi E, Greenberg B, Taylor MRG, et al. Danon disease: Gender differences in presentation and outcomes. *Int J Cardiol*. 2019; 286: 92-98.
6. Bagnall RD, Ingles J, Dinger ME, Cowley MJ, Ross SB, Minoche AE, et al. Whole genome sequencing improves outcomes of genetic testing in patients with hypertrophic cardiomyopathy. *J Am Coll Cardiol*. 2018; 72(4): 419-429.
7. Cheng Z, Fang Q. Danon disease: focusing on heart. *J Hum Genet*. 2012; 57(7): 407-410.
8. Boucek D, Jirikowic J, Taylor M. Natural history of Danon disease. *Genet Med*. 2011; 13(6): 563-568.
9. Amin A, Khoshavi M, Taghavi S, Naderi N, Mahdieh N, Emkanjoo Z, et al. Danon disease: a challenging case with diagnosis of hy-

- peritrophic cardiomyopathy. *Multidiscip Cardio Annal*. 2019; 10(1): e87232.
10. Schwarz JM, Cooper DN, Schuelke M, Seelow D. MutationTaster2: mutation prediction for the deep-sequencing age. *Nat Methods*. 2014; 11(4): 361-362.
  11. Reva B, Antipin Y, Sander C. Determinants of protein function revealed by combinatorial entropy optimization. *Genome Biol*. 2007; 8(11): R232.
  12. Kircher M, Witten DM, Jain P, O’Roak BJ, Cooper GM, Shendure J. A general framework for estimating the relative pathogenicity of human genetic variants. *Nat Genet*. 2014; 46(3): 310-315.
  13. Quang D, Chen Y, Xie X. DANN: a deep learning approach for annotating the pathogenicity of genetic variants. *Bioinformatics*. 2015; 31(5): 761-763.
  14. Adzhubei IA, Schmidt S, Peshkin L, Ramensky VE, Gerasimova A, Bork P, et al. A method and server for predicting damaging missense mutations. *Nat Methods*. 2010; 7(4): 248-249.
  15. Ng PC, Henikoff S. SIFT: predicting amino acid changes that affect protein function. *Nucleic Acids Res*. 2003; 31(13): 3812-3814
  16. Shihab HA, Gough J, Cooper DN, Stenson PD, Barker GL, Edwards KJ, et al. Predicting the functional, molecular, and phenotypic consequences of amino acid substitutions using hidden Markov models. *Hum Mutat*. 2013; 34(1): 57-65.
  17. Chun S, Fay JC. Identification of deleterious mutations within three human genomes. *Genome Res*. 2009; 19(9): 1553-1561.
  18. Feng BJ. PERCH: A unified framework for disease gene prioritization. *Hum Mutat*. 2017; 38(3): 243-251.
  19. Hubisz MJ, Pollard KS, Siepel A. PHAST and RPHAST: phylogenetic analysis with space/time models. *Brief Bioinform*. 2011; 12(1): 41-51.
  20. Davydov EV, Goode DL, Sirota M, Cooper GM, Sidow A, Batzoglou S. Identifying a high fraction of the human genome to be under selective constraint using GERP++. *PLoS Comput Biol*. 2010; 6(12): e1001025.
  21. Richards S, Aziz N, Bale S, Bick D, Das S, Gastier-Foster J, et al. Standards and guidelines for the interpretation of sequence variants: a joint consensus recommendation of the American College of Medical Genetics and Genomics and the Association for Molecular Pathology. *Genet Med*. 2015; 17(5): 405-424.
  22. Kavousi S, Pourahmadiyan A, Soleymani F, Noruzinia M. Identification of a novel de novo splicing mutation in duchenne muscular dystrophy gene in an iranian family. *Mol Syndromol*. 2023; 14(4): 331-340.
  23. Kelley LA, Sternberg MJ. Protein structure prediction on the Web: a case study using the Phyre server. *Nat Protoc*. 2009; 4(3): 363-371.
  24. Zheng W, Zhang C, Li Y, Pearce R, Bell EW, Zhang Y. Folding non-homologous proteins by coupling deep-learning contact maps with I-TASSER assembly simulations. *Cell Rep Methods*. 2021; 1(3): 100014.
  25. Ashkenazy H, Abadi S, Martz E, Chay O, Mayrose I, Pupko T, et al. ConSurf 2016: an improved methodology to estimate and visualize evolutionary conservation in macromolecules. *Nucleic Acids Res*. 2016; 44(W1): W344-50.
  26. Iacone M, Iacovoni A, Marchetti D, Ferrazzi P. Novel human pathological mutations. *Hum Genet*. 2008; 123(5): 537-555.
  27. Katzberg H, Karamchandani J, So YT, Vogel H, Wang CH. End-stage cardiac disease as an initial presentation of systemic myopathies: case series and literature review. *J Child Neurol*. 2010; 25(11): 1382-1388.
  28. Garcia-Pavia P, Vázquez ME, Segovia J, Salas C, Avellana P, Gómez-Bueno M, et al. Genetic basis of end-stage hypertrophic cardiomyopathy. *Eur J Heart Fail*. 2011 Nov; 13(11): 1193-1201.
  29. Van Der Starre P, Deuse T, Pritts C, Brun C, Vogel H, Oyer P. Late profound muscle weakness following heart transplantation due to Danon disease. *Muscle Nerve*. 2013; 47(1): 135-137.
  30. Miliou A, Antonopoulos AS, Kouris N, Lazaros G, Tsioufis K, Vlachopoulos C. Danon cardiomyopathy: specific imaging signs. *JACC Case Rep*. 2022; 4(22): 1496-1500.
  31. Yang Z, Funke BH, Cripe LH, Vick GW 3rd, Mancini-Dinardo D, Peña LS, et al. LAMP2 microdeletions in patients with Danon disease. *Circ Cardiovasc Genet*. 2010; 3(2): 129-137.
  32. Sedaghat-Hamedani F, Haas J, Zhu F, Geier C, Kayvanpour E, Liss M, et al. Clinical genetics and outcome of left ventricular non-compaction cardiomyopathy. *Eur Heart J*. 2017; 38(46): 3449-3460.
  33. Arbustini E, Favalli V, Narula N, Serio A, Grasso M. Left ventricular noncompaction: a distinct genetic cardiomyopathy? *J Am Coll Cardiol*. 2016; 68(9): 949-966.
  34. Hedberg Oldfors C, Máthé G, Thomson K, Tulinius M, Karason K, Östman-Smith I, et al. Early onset cardiomyopathy in females with Danon disease. *Neuromuscul Disord*. 2015; 25(6): 493-501.
  35. Su JW, Li SF, Tao JJ, Xu YY, Wang K, Qian XW, et al. Estrogen protects against acidosis-mediated articular chondrocyte injury by promoting ASIC1a protein degradation. *Eur J Pharmacol*. 2021; 908: 174381.
  36. Bui YK, Renella P, Martinez-Agosto JA, Verity A, Madikians A, Alejos JC. Danon disease with typical early-onset cardiomyopathy in a male: focus on a novel LAMP-2 mutation. *Pediatr Transplant*. 2008; 12(2): 246-250.
  37. Kashio N, Usuki F, Akamine T, Nakagawa S, Higuchi I, Nakahara K, et al. Cardiomyopathy, mental retardation, and autophagic vacuolar myopathy. Abnormal MRI findings in the head. *J Neurol Sci*. 1991; 105(1): 1-5.
  38. Davoudi-Dehaghani E, Zeinali S, Mahdih N, Shirkavand A, Bagherian H, Tabatabaiefar MA. A transversion mutation in non-coding exon 3 of the TMC1 gene in two ethnically related Iranian deaf families from different geographical regions; evidence for founder effect. *Int J Pediatr Otorhinolaryngol*. 2013; 77(5): 821-6.
  39. Mahdih N, Mahmoudi H, Ahmadzadeh S, Bakhtiyari S. GJB2 mutations in deaf population of Ilam (Western Iran): a different pattern of mutation distribution. *Eur Arch Otorhinolaryngol*. 2016; 273(5): 1161-5.
  40. Cenacchi G, Papa V, Pegoraro V, Marozzo R, Fanin M, Angelini C. Review: Danon disease: Review of natural history and recent advances. *Neuropathol Appl Neurobiol*. 2020; 46(4): 303-322.

# Candidate Biomarkers for Targeting in Type 1 Diabetes; A Bioinformatic Analysis of Pancreatic Cell Surface Antigens

Hamed Dabiri, Ph.D.<sup>1,2</sup>, Mahdi Habibi-Anbouhi, Pharm.D., Ph.D.<sup>3\*</sup> , Vahab Ziaei, Pharm.D., Ph.D.<sup>3</sup>, Zahra Moghadasi, M.Sc.<sup>3</sup>, Majid Sadeghizadeh, Ph.D.<sup>1\*</sup> , Ensiyeh Hajizadeh-Saffar, M.D., Ph.D.<sup>4,5\*</sup> 

1. Department of Genetics, Faculty of Biological Sciences, Tarbiat Modares University, Tehran, Iran
2. Department of Stem Cells and Developmental Biology, Cell Science Research Center, Royan Institute for Stem Cell Biology and Technology, ACECR, Tehran, Iran
3. National Cell Bank of Iran, Pasteur Institute of Iran, Tehran, Iran
4. Department of Regenerative Medicine, Cell Science Research Center, Royan Institute for Stem Cell Biology and Technology, ACECR, Tehran, Iran
5. Advanced Therapy Medicinal Product Technology Development Center (ATMP-TDC), Royan Institute for Stem Cell Biology and Technology, ACECR, Tehran, Iran

## Abstract

**Objective:** Type 1 diabetes (T1Ds) is an autoimmune disease in which the immune system invades and destroys insulin-producing cells. Nevertheless, at the time of diagnosis, about 30-40% of pancreatic beta cells are healthy and capable of producing insulin. Bi-specific antibodies, chimeric antigen receptor regulatory T cells (CAR-Treg cells), and labeled antibodies could be a new emerging option for the treatment or diagnosis of type I diabetic patients. The aim of the study is to choose appropriate cell surface antigens in the pancreas tissue for generating an antibody for type I diabetic patients.

**Materials and Methods:** In this bioinformatics study, we extracted pancreas-specific proteins from two large databases; the Human Protein Atlas (HPA) and Genotype-Tissue Expression (GTEx) Portal. Pancreatic-enriched genes were chosen and narrowed down by Protter software for the investigation of accessible extracellular domains. The immunohistochemistry (IHC) data of the protein atlas database were used to evaluate the protein expression of selected antigens. We explored the function of candidate antigens by using the GeneCards database to evaluate the potential dysfunction or activation/hyperactivation of antigens after antibody binding.

**Results:** The results showed 429 genes are highly expressed in the pancreas tissue. Also, eighteen genes encoded plasma membrane proteins that have high expression in the microarray (GEO) dataset. Our results introduced four structural proteins, including NPHS1, KIRREL2, GP2, and CUZD1, among all seventeen candidate proteins.

**Conclusion:** The presented antigens can potentially be used to produce specific pancreatic antibodies that guide CAR-Treg, bi-specific, or labeling molecules to the pancreas for treatment, detection, or other molecular targeted therapy scopes for type I diabetes.

**Keywords:** Bioinformatics, Cell Surface Antigens, Molecular Targeted Therapies, Pancreatic Islets, Type 1 Diabetes

**Citation:** Dabiri H, Habibi-Anbouhi M, Ziaei Y, Moghadasi Z, Sadeghizadeh M, Hajizadeh-Saffar E. Candidate biomarkers for targeting in type 1 diabetes; a bioinformatic analysis of pancreatic cell surface antigens: a prospective study. Cell J. 2024; 26(1): 51-61. doi: 10.22074/CELLJ.2023.1996297.1262  
This open-access article has been published under the terms of the Creative Commons Attribution Non-Commercial 3.0 (CC BY-NC 3.0).

## Introduction

While Type 1 diabetes (T1D) is a mostly T-cell-mediated autoimmune disease, it is defined as a destruction of pancreatic beta-cells by autoreactive immune cells. This destruction event results in lifelong exogenous insulin dependency. The T1D development is complicated by immunological regulations

and responses, that are accompanied by the key role of cellular immunity. More precisely, the destruction of pancreatic beta cells is caused by the invasion of multiple cells, including clusters of differentiation 4 positive [CD4<sup>+</sup>] and CD8<sup>+</sup> T lymphocytes, B lymphocytes, natural killer cells, dendritic cells, and other immune cells, which leads to the incidence of T1D (1). While immunosuppressive

Received: 26/March/2023, Revised: 27/August/2023, Accepted: 24/October/2023

\*Corresponding Addresses: P.O.Box: 66492-595, National Cell Bank of Iran, Pasteur Institute of Iran, Tehran, Iran

P.O. Box: 14115-175, Department of Genetics, Faculty of Biological Sciences, Tarbiat Modares University, Tehran, Iran

P.O.Box: 16635-174, Department of Regenerative Medicine and Advanced Therapy Medicinal Product Technology Development Center (ATMP-TDC), Cell Science Research Center, Royan Institute for Stem Cell Biology and Technology, ACECR, Tehran, Iran

Emails: [habibi\\_m@pasteur.ac.ir](mailto:habibi_m@pasteur.ac.ir), [sadeghma@modares.ac.ir](mailto:sadeghma@modares.ac.ir), [en.hajizadeh@royan-rc.ac.ir](mailto:en.hajizadeh@royan-rc.ac.ir)



medications are used to treat autoimmune diseases, they are not only partially efficient (2), but also they cause a general immune response attenuation, increasing susceptibility to infections and malignancies (3). In most cases, in type I diabetic patients, the balance between regulatory T cell functions or numbers is upset. Around a third of pancreatic beta cells are intact and capable of producing insulin at the time of diagnosis, therefore it would be a notable strategy to induce a T-cell tolerance for specific beta-cell antigens (Ag) to prevent further disease development that is a useful strategy for identification of individuals at risk of diabetes (4). It seems that the Bispecific antibodies and chimeric antigen receptor regulatory T cells (CAR-Treg cells) are two new implements to reach this goal.

Bispecific antibodies (bsAb) significantly have two antigen-binding sites. They are made up of two separate Fragment antigen-binding (Fab) arms or two different antibodies (Abs) joined by a common Fragment crystallizable (Fc) region (5). In autoimmune conditions, bsAbs can be utilized to: i. Deactivate multiple cytokines or receptors at the same time, ii. Drive cell-cell contacts between different immune cell populations, and iii. Cause receptor co-localization on the cell surface (5, 6). Blinatumomab, a CD19- and CD3-bispecific recombinant antibody, was the first bsAb to be used in clinical trials for the treatment of non-Hodgkin's B cell lymphoma. A Blinatumomab causes B cells to engage with cytotoxic T cells. As a result of the interaction between two cells by bsAb, B lymphoma cells are effectively eliminated, protective T lymphocytes are expanded, and the majority of patients have a longer life expectancy (5, 7). In the same way, pancreatic cell surface antigens can be effective for producing and using bsAb for the type I diabetic remission.

The immune system has a remarkable capacity to scan tissues and recognize and clear aberrant and malignant cells. In contrast, many immune system components, such as regulatory T cells, can locally modulate the aberrant immune response against the body's own cells. Adoptive immunotherapies utilize and improve the strength of our immune system against cancerous cells and aberrant immune responses. Among the various techniques, chimeric antigen receptors, or CARs, have recently been of large interest. Recently, many studies have been developed for using polyclonal Tregs in cell treatment approaches. They are now being studied in transplant recipients and patients with autoimmune disorders, especially in T1D (8). This method has some limitations, including a few numbers of Treg cells in the peripheral blood in comparison to other common T cells such as effector or cytotoxic ones. The use of antigen-specific modified Tregs has acceptable patient outcomes, because of their higher ability to generate a response and their requirement to fewer cells due to their local activity.

Animal model studies have been revealed that antigen-specific Tregs are functionally superior to polyclonal Tregs. Currently, in a few investigations genetic engineering has been used for expressing CAR in Tregs, as it has been

used for hematological malignancies. Multiple studies have used various methods to confer antigen specificity to Tregs, with a focus on CAR-Treg cells. According to these investigations, CAR-Treg cells are preferable for type I diabetic patients. The local activity of CAR-Tregs in the pancreas provides a significant response and needs fewer cells (9-11). Hence, the pancreatic cell surface antigens can be used for the production of pancreas-specific CAR-Treg cells following the generation of appropriate antibodies (scFvs).

The appropriate beta-cell mass (BCM) is a valuable indication of the pancreatic proper function. Beta-cells are destroyed in the T1Ds, leading to a significant drop of BCM. Due to peripheral insulin resistance and increasing insulin demand, the BCM decreases slowly and steadily in people with type 2 diabetes. Surface antigens of beta cells can be recruited to evaluate the BCM as well as pancreatic proper function in a non-invasive manner. Some antigens have been studied in the human brain and pancreas, [11C] dihydrotetabenazine (2-hydroxy-3-isobutyl-9-[11C] methoxy-10-methoxy-1,2,3,4,6,7-hexahydro-11bH-benzo[a]quinolizine), commonly known as [11C] DTBZ, was used to investigate the BCM with a positron emission tomography (PET) in a non-invasive in vivo method. In another study, researchers showed that the specific antibodies were bound to beta cells in normal mice but not to mice administered with streptozotocin (STZ) which induced BCM loss and diabetes (12). Consequently, the appropriate beta cell surface antigens accompanied by their specific antibodies can be used for monitoring BCM changes in diabetic patients.

As mentioned above, the most preliminary step for the production of bi-specific antibodies, CAR-Treg cells, or labeled antibodies for T1Ds is choosing the appropriate cell surface antigen in the pancreas tissue. The selection of surface antigens is sensitive from different viewpoints. First, the cell surface antigen should have an acceptable expression level in pancreatic cells. This is an influential event for the potential binding of antibodies or CAR-Treg cell receptors to the antigen. The antigen frequency can be surveyed in two levels of RNA expression and protein expression. Second, according to the length and three-dimensional structure of the polypeptide chain in the plasma membrane, the antigen should have enough accessible extracellular domains. Accessible domains are important for the potential binding activity of antibodies or CAR-Treg cells. Third, antigen enrichment in the pancreas in comparison to other body tissues is another aspect that should be considered in this regard. This feature is important in order to make antigens, the least off-target effect for final products. According to the binding of antibodies or CAR-Treg cells to other tissues, off-target events decrease pancreas accumulation of the final products leading to a decrease their effectiveness. Moreover, gathering final products in other tissues causes unpleasant side effects as well. Fourth, the function of the surface antigen is vital for the pancreatic cells in terms of inactivation or activation/hyperactivation after antibody

binding.

In the present study, we investigated important features of pancreatic surface antigens from the genes preferentially expressed in the pancreas tissues. To reach the best candidate antigens, we categorized them into two distinct groups according to their functions: "Structural proteins" that do not alter their activity after antibody binding, and "Functional proteins" which can be divided into two subgroups, water channels and signaling proteins. Water channels may have less impact on cell behavior upon antibody binding. In contrast, signaling proteins, which may bring about substantial changes in normal cell function due to the gain of function or loss of functions.

## Materials and Methods

### Data mining

In this bioinformatics study, to find the genes that are preferentially expressed in the pancreas tissue, candidate genes were extracted from two different sources, the Human Protein Atlas (HPA, Karolinska Institutet, 2023, Sweden) and the Genotype-Tissue Expression (GTEx) project (Broad Institute, 2021, USA) (13). The protein atlas database has an RNA dataset that was utilized to group genes based on their expression in different tissues. The clustering of 19019 genes which are expressed in different tissues led to obtain 87 expression groups. The groups were manually annotated to explain functional and specificity properties. The HPA is divided into 10 parts, each of which focuses on a different component of the genome-wide investigation of human proteins.

The protein distribution throughout all major tissues and organs in the human body is shown in the Tissue section of Protein Atlas tool (<https://www.proteinatlas.org/humanproteome/tissue>). Pancreas high-expressed genes as well as genes that are only detected in the pancreas tissue were extracted from the Protein Atlas database.

The GTEx project is a long-term program aimed at preparing a comprehensive free source for investigating gene expression in body tissues as well as their gene regulations. Nearly 1000 people had samples taken from 54 non-diseased tissue locations, largely for molecular omics such as Whole Genome and Exome Sequencing (WGS and WES), and RNA-Seq data. The GTEx Biobank has also the remainder of the samples. The GTEx Portal makes data available such as gene expression, QTLs, and histology pictures. The 100 top genes expressed in the pancreas were got from GTEx and added to the genes which were extracted from the protein atlas database. The names of candidate genes were converted to ensemble ID by BioMart (<https://www.ensembl.org/biomart>) and prepared in the Ext. data format. The files were used as input materials for the consequent analysis (14).

### Calculating tissue-specific gene enrichment using "TissueEnrich" tool

The TissueEnrich is an R-based package that finds gene

enrichment in the body tissues from a set of input genes. Using TissueEnrich, tissue-specific genes were identified through the HPA methodology to analyze RNA-Seq data from the Human Protein Atlas, GTEx, and ENCODE projects (15). To evaluate if tissue-specific genes were enriched among the input genes, the hypergeometric test was performed. In addition, the TissueEnrich package also was used to identify enrichment through user-supplied expression datasets, which subsequently led to computing tissue-specific gene enrichment parameters such as exact P values.

The TissueEnrich package uses RNA Sequencing results from the HPA, GTEx, and ENCODE database to identify gene enrichments in tissues. This package only employed tissues with two biological replicates to have strong estimating. The following datasets were employed in this tool: i. RNA Sequencing results from human tissues (n=35) in the HPA Database, ii. RNA sequencing results from human tissues (n=29) in the GTEx Database, and iii. RNA sequencing results from mouse tissues (n=17) in the Mice ENCODE Dataset (16).

Tissue-specific genes definition in HPA were categorized as follows:

Genes having an expression level greater than one [Transcript Per Million (TPM) or Fragments per kilobase of transcript per million mapped fragments (FPKM)] as well as minimum five-fold expression levels in a specific tissue in comparison to all body tissues were referred to as "TissueEnriched". Genes having an expression level of more than 1 (TPM or FPKM) that also had at minimum five-fold expression levels in comparison to all body tissues were considered to as "Group Enriched". Genes having an expression level over 1 (TPM or FPKM) and minimum five-fold expression levels in a specific tissue in comparison with the average levels in all body tissues but were non-TissueEnriched or non-Group Enriched was referred as a "TissueElevated". To employ the TissueEnrich package, the R programming language (R v4.1.1 for Windows) and RStudio-Integrated Development Environment (IDE)- (RStudio 1.2.5042) were installed. The package was acquired from the Bioconductor version, Release 3.14, and added to the R program. Four hundred twenty-nine input genes were prepared as an Ext. data format and located in the program work directory (setwd). The command codes were written and run in the RStudio environment. Just the Tissue Enrich function of the software was used for a gene expression analysis. The resulting data were evaluated according to the suggested pipeline.

### Evaluation RNA expression level of transmembrane proteins by using microarray analysis from the GEO dataset

The Output of the Tissue Enrich tool was analyzed to select the genes that encode plasma transmembrane proteins which can be targeted as pancreatic cell surface antigens. For this aim, the information on total human

transmembrane proteins was extracted from the HPA (Karolinska Institutet, 2023, Sweden). The correspondence between the total transmembrane and output proteins of Tissue Enrich was achieved using the Barc software (Bioinformatics and Research Computing, Massachusetts Institute of Technology, 2023, USA). To confirm the expression of plasma membrane genes in beta and acinar cells, microarray data of 3 samples were investigated again. For this aim, microarray raw data of acinar and beta cells, adipose tissue, heart, small intestine, diaphragm tissues, bone marrow, and spleen were downloaded from the GEO dataset (accession No. GSE24207). Data were analyzed by using "affy", "Affymetrix HG-U133A" and "annotate" packages from Bioconductor version Release 3.14 in the R programming language (R v4.1.1 for Windows).

### Evaluation of accessible extracellular domains

To evaluate the accessible extracellular domains of the plasma membrane proteins, PROTTER (<http://wlab.ethz.ch/protter/#>), an interactive protein feature visualization software (ETH University, 2023, Switzerland), was used (17).

### Evaluation of gene expression at the protein level

To confirm the protein expression of the candidate genes, besides the RNA expression, the pancreatic human proteome of the Protein Atlas database (<https://www.proteinatlas.org/ENSG00000138161> and <https://www.proteinatlas.org/ENSG00000164756-SLC30A8/tissue/pancreas#img> - available from v21.0.proteinatlas.org) was used (18, 19). In this database, a protein profiling has been done through the immunohistochemistry (IHC) method and the final images have been deposited. To obtain the human proteome, protein expression data were extracted from 44 normal human tissue types. All primary pictures of the normal tissues IHC profile, as well as scientific annotations of protein expression stages, have been provided. The databank has been included 15323 genes (76%) that antibodies were accessible. The IHC process has been done according to the standard protocol of the Protein Atlas database. Briefly, Paraffin slides have been dried at room temperature overnight (20).

The slides have been deparaffinized in xylene (Cat No. 22-050-283, Thermo Fisher Scientific, Germany) and graded ethanol (Cat No. 64-17-5, Sigma, USA) to distilled water before immunostaining. Endogenous peroxidase has been blocked with 0.3% H<sub>2</sub>O<sub>2</sub> plus 95% ethanol. The Heat-Induced Epitope Retrieval (HIER) has been performed by heating the slides immersed in the antigen retrieval buffer (Cat No. ab93684, Abcam, UK) for 4 minutes at 125°C. When the boiling step has been done, the immunohistochemical staining program has been run by Autostainer 480® instrument (AUTOSTAINER 480S-2D 220-240., ThermoFisher Scientific, Runcorn, UK). The slides have been cleaned in the washing buffer (Cat No. ab206977, Abcam, UK) and incubated with Ultra V Block (TA-060-UB, ThermoFisher Scientific, UK) for 5 minutes. After that, the slides were washed in the

washing buffer (2X) Or a washing solution (Cat No. ab252273, Abcam, UK), then incubated with primary antibody (Thermo Fisher Scientific, Germany) for 30 minutes, and consequently rinsed in the wash buffer (3X) (Cat No. ab252273, Abcam, UK). Then, the slides were incubated with labeled HRP antibodies (Cat No. ab102890, Abcam, UK) for 30 minutes and cleaned in the wash buffer (2X) solution (Cat No. ab252273, Abcam, UK). Moreover, slides have been incubated in 3,3'-Diaminobenzidine (DAB) solution for 5 minutes and bleached in hematoxylin for 7.5 minutes. In the next step, slides were washed in the lithium carbonate water (Cat No. ab235613, Abcam, UK) and diluted in 1:5 in the saturated PBS solution for 1 minutes. Finally, the slides have been dehydrated in graded ethanol and followed by coverslips mounted. All reagents are applied at a volume of 300 µl per slide and antibody concentrations have been optimized based on their manufacture data sheets (20). The DAB labeled antibodies have been used to stain tissue microarrays, which have been then counterstained with hematoxylin (Cat No. ab220365, Abcam, UK). With the exception of the endometrium, skin, soft tissue and stomach, which are each represented by samples from six people, each tissue type is represented by samples from three individuals. Additional tissues have been stained for chosen proteins, including mouse brain, human samples of different tissues, including lactating breast, eye, thymus, and extended adrenal gland, skin, and brain. Immunohistochemical staining slides from tissue microarrays have been digitized and uploaded to the HPA online portal for analysis and presentation. All tissue samples have been obtained from the Department of Clinical Pathology, Uppsala University Hospital, Uppsala, Sweden, as part of the sample collection managed by the Uppsala Biobank and have been collected and handled in compliance with Swedish laws and regulations. All tissue samples have been anonymized in compliance with the Uppsala Ethical Review Board's permission and advisory report. Finally, selected genes were searched by gene names and IHC images and appendix data were extracted from the pancreas tissue section.

### Investigation of antigen functions using the GeneCards database

Some cell surface antigens become inactivated or activated/hyperactivated after targeting. Hence, natural functions or homeostasis of the target cells can be altered after binding the antibodies to their surface antigens. For investigating the functions of selected antigens, the GeneCards database was employed. Using the GeneCards database, the candidate proteins were divided into two groups according to their functional or structural roles.

### Statistical analysis

To better discover the tissue enrichment of total extracted genes, the analysis of the genes was carried out using the TissueEnrich package. According to the standard protocol, One-way ANOVA was employed to





**Eighteen genes encoded plasma membrane proteins that have enough expression level microarray data analysis based on GEO database**

The output of the TissueEnrich tool, a group of 68 genes, was analyzed to select the genes that encoded plasma membrane proteins and could be considered as a pancreatic cell surface antigen. The results showed that eighteen genes were encoded proteins that were single or multiple-pass trans plasma-membrane as well as anchored membrane proteins (Table 1). To confirm the expression of these genes in the islet and acinar cells, microarray data (accession No. GSE24207) of 3 samples were analyzed separately for multiple tissues including islet cells of the pancreas, acinar cells of the pancreas, adipose tissue, heart, small intestine, diaphragm tissues, bone marrow, and spleen. The results revealed that 8 genes have high RNA expression levels in islets in comparison with the insulin gene, as a positive control gene of pancreatic beta cells. Also, the results showed that 8 genes have a good expression level in the pancreatic islet cells. Interestingly, 5 genes that exhibit a strong RNA expression level in the

pancreatic islet cells also have high RNA expression levels in the pancreatic acini cells in comparison to other tissues (Fig.3).

**Except for *SLC30A8*, all seventeen candidate genes encode plasma membrane proteins with enough accessible extracellular domains**

The appropriate cell surface antigen should have enough accessible extracellular domains for the production of specific antibodies. Evaluating these extracellular domains of the plasma membrane proteins, the Protter software, an interactive protein feature visualization, was employed. The results showed that most of the plasma membrane proteins had accessible extracellular domains for targeting antibodies except for *SLC30A8*. The *SLC30A8* protein just had intracellular and transmembrane domains without sufficient extracellular regions and had to be omitted from the candidate gene list (Fig.4, Supplementary File 2, See Online Information at [www.celljournal.org](http://www.celljournal.org)).

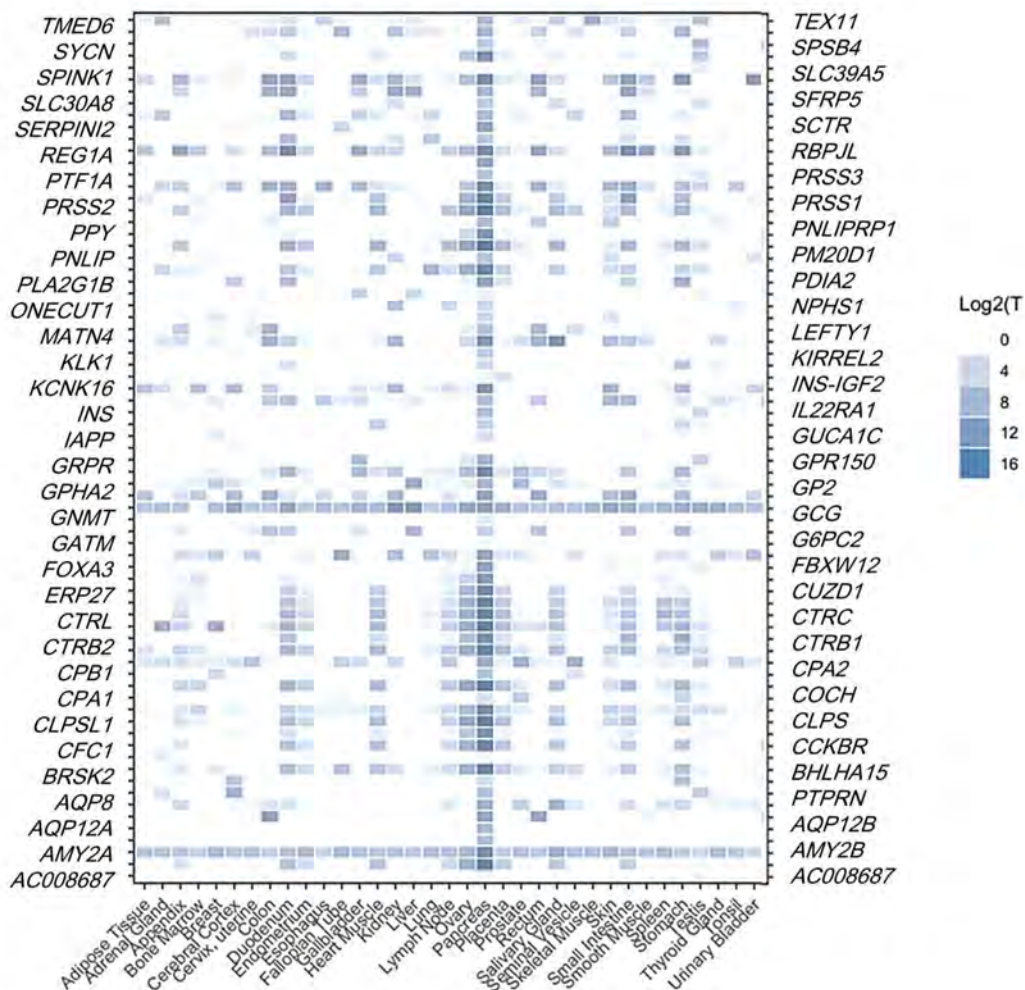


**Fig.2:** The Heatmap plot of pancreas enriched expression genes. The plot showed all 68 genes have a high preferential expression level in the pancreas. Some genes, such as insulin (*INS*), were only detected in the pancreas, and some others, such as Glycine Amidinotransferase (*GATM*), had a basic expression level in other body tissues.

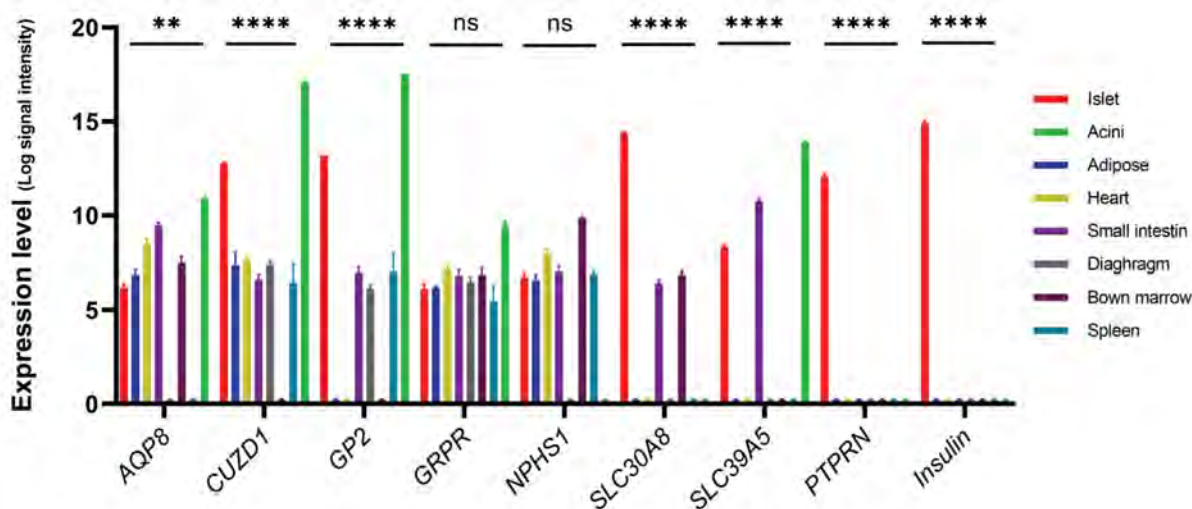


**Fig.3:** RNA expression level of plasma membrane proteins of the pancreatic islet cells and other tissues. Islets of the pancreas, acinar cells of the pancreas, adipose tissue, heart, small intestine, diaphragm tissues, bone marrow, and spleen tissues were evaluated by microarray data analysis (accession No. GSE24207). All 8 candidate genes have acceptable expression levels in the Pancreas beta cells. Five genes also have a good expression level in the Pancreas acini cells. The results showed that *AQP8*, *CUZD1*, *GP2*, *SLC30A8*, *SLC39A5*, and *PTPRN* genes were significantly expressed in the Pancreatic islet and acini cells. Also, the data showed that *GRPR* and *NPHS1* were not significantly expressed in the Pancreas islets and acini cells in comparison with other tissues. According to the results of analysis, P Value of *AQP8*, *CUZD1*, *GP2*, *SLC30A8*, *SLC39A5*, and *PTPRN* genes were  $3 \times 10^{-3}$ ,  $5 \times 10^{-5}$ ,  $7 \times 10^{-5}$ ,  $3 \times 10^{-5}$  and  $2 \times 10^{-5}$ , respectively. \*\*\*\*;  $P < 0.0001$ , \*\*,  $P < 0.01$ , and ns; Not significant.

**Table 1:** Different functional and structural proteins among selected pancreatic surface antigens

Functional proteins		Structural proteins	
Gene name	Function in the pancreas	Gene name	Function in the pancreas
<i>SLC39A5</i>	Zinc transporters	<i>NPHS1</i>	Cell adhesion molecules
<i>SLC30A8</i>	Zinc-efflux transporter	<i>KIRREL2</i>	Cell adhesion molecules. The encoded protein localizes to adherent junctions in pancreatic beta cells and regulates insulin secretion.
<i>SCTR</i>	G protein-coupled receptor and belongs to the glucagon-VIP-secretin receptor	<i>GP2</i>	Integral membrane protein associates with the plasma membrane via glycosylphosphatidylinositol (GPI) linkage
<i>KCNK16</i>	Potassium channel proteins	<i>CUZD1</i>	Localized to zymogen granules, where it functions in trypsinogen activation (by similarity). May indirectly regulate cell motility, cell-cell and cell/extracellular matrix interactions
<i>IL22RA1</i>	Cytokine receptor		
<i>GRPR</i>	Receptor for gastrin-releasing peptide		
<i>GPR150</i>	Rhodopsin-like family of G-protein-coupled receptors		
<i>CFC1</i>	Member of the epidermal growth factor which are involved in signaling during embryonic development		
<i>CCKBR</i>	G-protein coupled receptor for gastrin and cholecystinin (CCK)		
<i>AQP8</i>	Aquaporins facilitate the transport of water and small neutral solutes across cell membranes		
<i>AQP12B</i>	Aquaporin		
<i>AQP12A</i>	Aquaporin		
<i>PTPRN</i>	Protein tyrosine phosphatase receptor type N		

**Seventeen candidate proteins are highly expressed in the pancreatic tissue and localized in the cytoplasm/plasma membrane area**

To validate the expression of the candidate antigens at the protein level, the IHC data of the pancreatic tissue from the HPA database were used. The results of normal pancreas tissue sections illustrated that five genes of these ten genes, including *GP2*, *CUZD1*, *AQP12A*, *AQP12B*, and *SCTR*, had a high protein expression level in the exocrine cells of the pancreas. In addition, three genes, including *CFC1*, *KIRREL2*, and *PTPRN*, showed a high expression level in the pancreatic endocrine cells. Based on the IHC data from the protein atlas database, three other genes, including *GPR150*, *AQP8*, and *NPHS1*, were highly or moderately expressed in both endocrine and exocrine cells at the protein level. Interestingly, IHC data revealed that all selected antigens were localized in the

cytoplasm or plasma-membrane (Fig.5, Supplementary File 3, See Online Information at [www.celljournal.org](http://www.celljournal.org)).

**Four structural proteins were among all seventeen candidate proteins**

After interaction with antibodies, several cell surface proteins become inactivated or activated/hyperactivated. As a result, the target cells homeostasis, and regular functions were disrupted. However, appropriate surface antigens should not have vital functions for natural cells. For the investigation of the functions of the candidate antigens, the GeneCards database was used. Finally, the antigens were categorized into two groups "Functional genes" and "Structural genes". Among all antigens, *NPHS1*, *KIRREL2*, *GP2*, and *CUZD1* were structural proteins that will be less affected after an antibody binding.

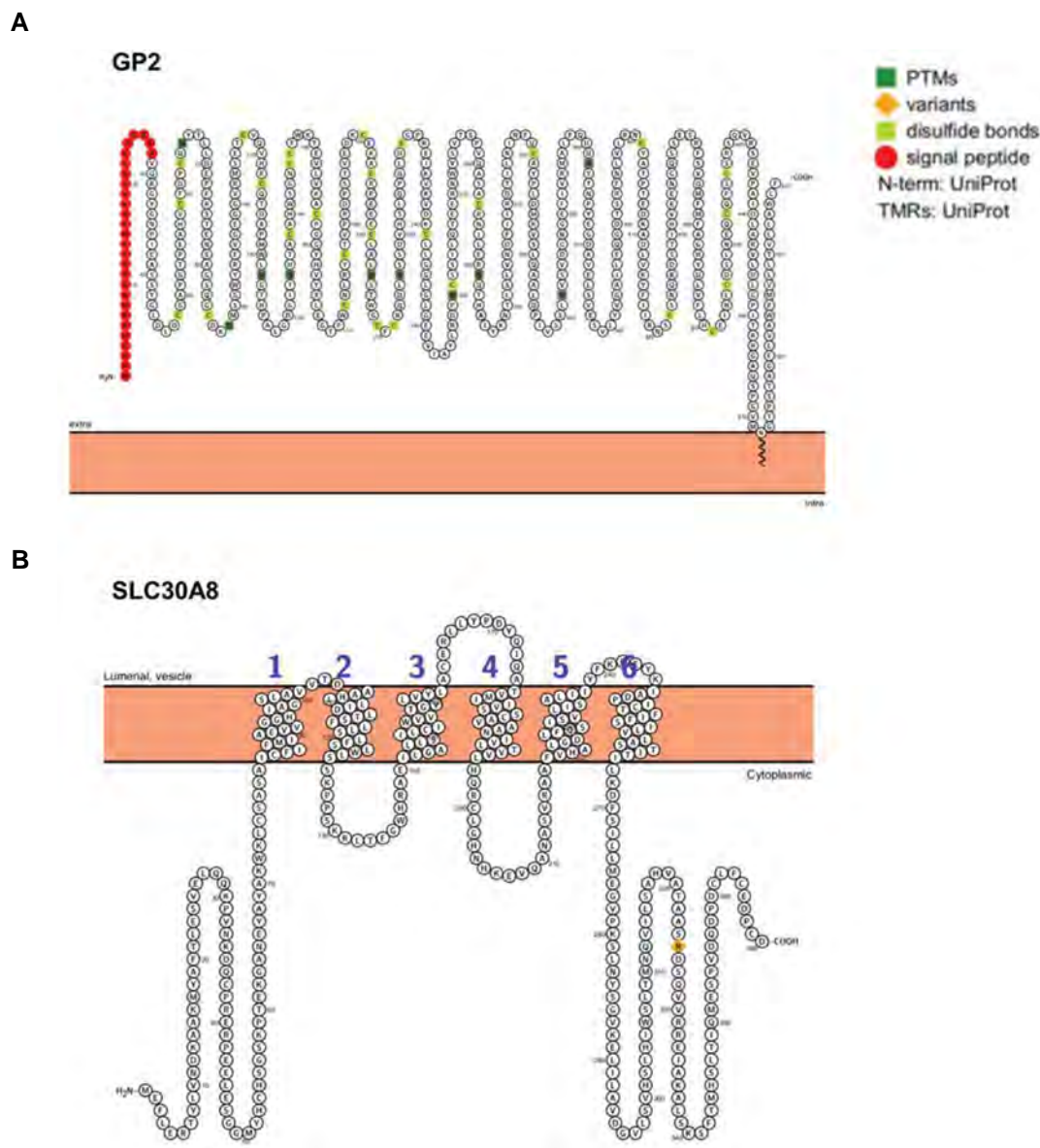


**Fig.4:** Two examples of the Protter outputs of candidate plasma membrane antigens. **A.** The results showed that glycoprotein 2 (GP2) had an extracellular domain of about 510 amino acids which binds to the plasma membrane by a glycosylphosphatidylinositol (GIP) anchor. **B.** In comparison, the SLC30A8 protein did have not an adequate extracellular domain (just about 15 amino acids) for being targeted by antibodies or immune Treg cells.

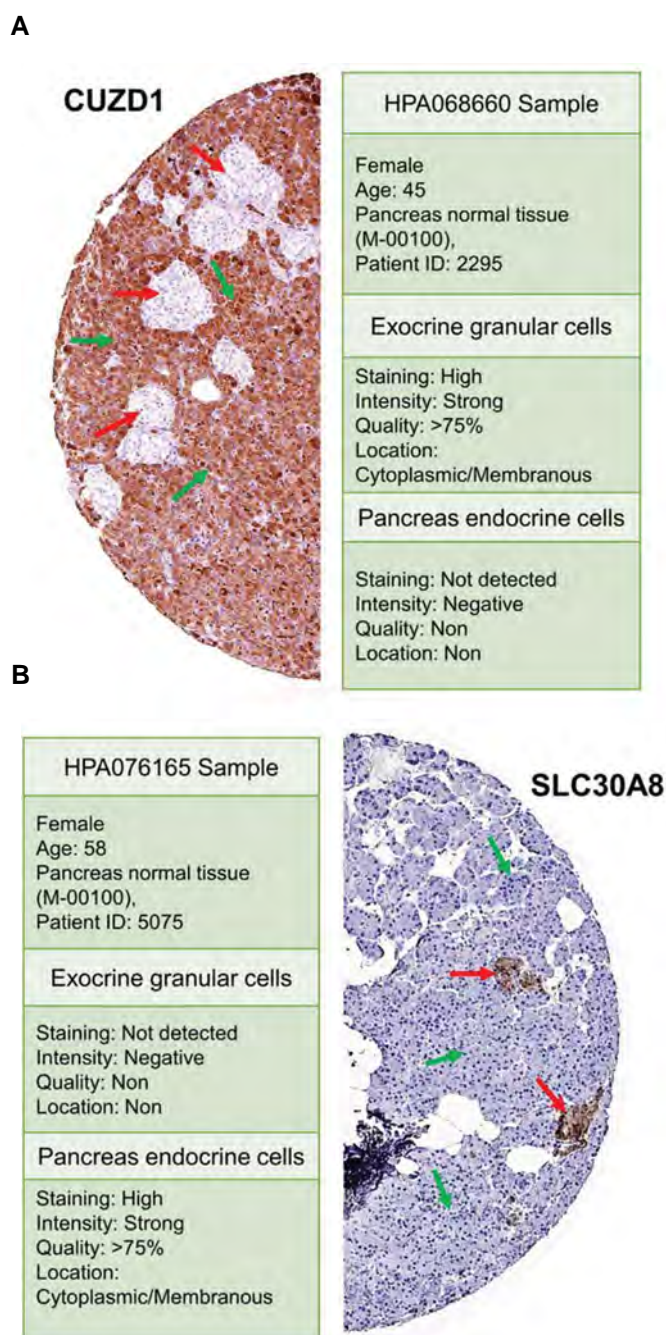


**Fig.5:** Two examples of immunohistochemistry (IHC) images and localized area for candidate antigens. **A.** IHC data showed that the CUZD1 protein had a high expression in the pancreas exocrine cells and displayed a cytoplasmic/membranous subcellular localization. **B.** IHC data showed that the SLC30A8 protein had a high expression in the pancreatic islet endocrine cells and showed a cytoplasmic/membranous subcellular localization. Red arrows indicate the islets of Langerhans, endocrine cells including insulin-producing beta cells, and green arrows reveal the exocrine cells, including acini.

## Discussion

As mentioned earlier, in T1Ds, insulin-producing beta cells are destroyed by the patient's immune cells. Since in most cases, about one-third of beta cells are healthy at diagnosis, preventing immune system attack can lead to the disease avert through repairing pancreatic tissue. Some strategies have been proposed and used to suppress the immune system in T1Ds, but approaches that do it

locally are preferred. Therefore, one of the main strategies is targeting pancreatic cells which become desirable recently and is of significant importance (24). In this study, to investigate comprehensively the total antigens of pancreatic tissues to achieve the appropriate surface antigen to target beta cells in T1Ds, bioinformatics systems, and comprehensive databases were employed. Overall, a suitable antigen should have three main features, as follows: i. Having high and preferential expression in pancreatic cells, ii. Having enough accessible extracellular domains, and iii. Not having any critical function that affects the natural behavior of the cells after being targeted. It can be said with almost certainty that there is no antigen in the body tissues that possesses all the desired features (25). So, the candidate antigens should be investigated more carefully in different aspects.

Muraro et al. (26) developed a platform that captured the transcriptomes of pancreatic cells obtained from dead organ donors by using FACS and the CEL-Seq2 protocol. They presented the top 10 expressed genes in islet cells, including alpha, beta, delta, and PP cells. Among all 40 genes that Muraro et al. (26) presented, 8 genes were contained within our list of 429 genes set. The other 32 genes they presented were either intracellular or expressed in other body tissues. Therefore, they were not appropriate biomarker as specific surface antigens. Other authors also used a single-cell RNA sequencing approach to assess the transcriptomes of 12,000 separate pancreatic cells from four different human pancreases. They represented 15 pancreas marker genes, five of which are included in our list of 429 genes set. The remaining 10 proteins (10/15) were intracellular or expressed in other body tissues. Hence, as before, they were not suitable as specific surface antigens (27).

The SLC30A8, also known as ZnT8, is a transporter protein efflux zinc. In the secretory granules of insulin, the encoded protein co-localizes with an insulin structure in beta cells. Having multi-pass transmembrane helices and not having any accessible extracellular domains make this antigen unsuitable for targeting by antibodies (27). The *NPHS1* gene encodes a protein for cell adhesion from the immunoglobulin family that plays a role in the kidney's glomerular filtration barrier. Based on the protein atlas database, the protein expression level of *NPHS1* antigen was low in the pancreas but high in kidney tissues, particularly in the glomeruli cells (28). Due to the potential the antibodies of the renal off-target, it is less suitable. The *KIRREL2* gene also encodes a transmembrane protein which is one of the immunoglobulin superfamily of cell adhesion molecules (29). This protein controls the insulin secretion by binding to adherent junctions in the pancreatic beta cells. The protein expression level of this gene, based on the protein atlas database, for pancreatic exocrine glandular cells is high, although in the kidney tissue, particularly in the tubule cells, is low. Therefore, it seems to be a more suitable biomarker than *NPHS1* for the pancreatic tissue targeting. The *GP2* gene encodes an inherent plasma membrane protein that forms a

glycosylphosphatidylinositol (GPI) connection with the plasma membrane (30). According to our IHC finding of the protein atlas database, the GP2 has a high protein expression level in the pancreas tissue. It seems to be a suitable aim for acinar cells targeting in comparison with other antigens in the pancreas. The CUZD1 is a protein found in zymogen granules that aids in the activation of trypsinogen (31). Cell motility, cell-cell, and cell-extracellular matrix interactions may all be influenced indirectly. Based on pancreatic expression protein levels, it is another suitable potential target of exocrine cells in the pancreas.

Several studies by subjects similar to the present investigation were done yet. One of them is the research that was completed by Bausch-Fluck et al. (32). They employed a machine-learning method that find specific domains of proteins to make a prediction software based on the transmembrane topology that predicts the surface proteins (33). Their goal was only highlighting overexpressed surface proteins of cancer cells. They developed an RNA sequencing analyser software named Qsurface that extracts the data from the Cancer Genome Atlas (TCGA) database as inputs and at the end presents surface proteins. The limitation of their method was that the Qsurface just uses gene expression at RNA levels and doesn't regard protein expression since it is a more important attribute. Two other similar studies were done by Pont et al. (34) and Orentas et al. (35). In the first gene expression effort from microarray, databases were employed to find surface antigens for the Hematological Malignancies immunotherapy. In the second, an algorithm was written based on the tumour cell gene expression to capture the surface antigens of cancerous cells. Both investigations were about cancers, not normal tissues, and used just RNA expression, not proteins. In the present study, about some gene cases such as *AQP8*, *CUZD1*, *GP2* and *SLC39A5*, it seems to be a mismatched expression in protein and RNA levels. This matter can be due to many causes. The stability of the transcript, translation rate of the transcript, stability of translated polypeptide as well as the association of multi-subunit protein components are the main reasons for different RNA and protein expression of the same genes. Our results showed that *PTPRN* and *SLC30A8* genes have RNA expression just in islet cells. Our present finding revealed that *AQP8*, *CUZD1*, *GP2*, and *SLC39A5* genes express in the RNA level in both islets and acini cells. It seems that the only transcript of these genes is functional protein in the cells, although their amount is not enough for an IHC assay. The affinity of a specific antibody which used in the IHC assay also is important to detect the low-level expression of the proteins in the cells. On the other hand, several studies confirmed the RNA expression of *AQP8*, *CUZD1*, *GP2*, and *SLC39A5* genes in both islets and acini cells (36).

There are some limitations to the pipeline introduced in the presented study. One of them is that the *PTPRN* protein plays a role in vesicle-mediated secretory processes and was categorized as a "functional" group

antigen, hence it is "structural" group antigen after the fusion of vesicles to the plasma membrane. On the other hand, what makes this protein less suitable antigen, as a surface antigen, is that the most of its extracellular domains are cut and separated before the vesicle fuses with the plasma membrane. This cutting phenomenon can be found just in the literature but not in expression databases. Evaluating all features of selected antigens for future practical investigations, the literature should be considered besides the bioinformatics (37). Another limitation of this investigation is that the categorizing of the candidate antigens was not absolute. Hence, among functional proteins, there were antigens that were less affected when were banded, and conversely, antigens that were highly affected. For example, receptors involved in signaling pathways or G protein-like receptors (e.g., SCTR, GPR150, CCKBR), hormone or cytokine receptors (e.g., IL22RA1, GRPR, CFC1, and CCKBR), and specific ion transporters or channels (e.g., SLC39A5, SLC39A8, and KCNK16) are greatly affected if targeted by antibodies. In contrast, water channels (e.g., Aquaporin), since they are more abundant, may not cause major problems upon some of them being blocked by binding antibodies in their overall function of the cells (38). Hence, the proteins just categorized as two 'Functional' and 'Structural' groups that should be evaluated in more detail in individual cases. However, the candidate surface antigens presented in this study can be recruited to develop the potential monoclonal antibodies as well as recombinant antibody fragments such as scFvs for binding to the pancreatic beta cells in the strategies to overcome type I diabetes disease.

## Conclusion

One effective way to treat the T1Ds is a local suppression of the immune system to prevent it from invading insulin-producing cells. The first and perhaps most important step in local inhibition is to find the proper antigens to target pancreatic tissue cells. Therefore, in this study, we evaluated the antigens of pancreatic tissue cells comprehensively. Based on our results, 18 genes encoded plasma membrane proteins on pancreatic cells, of which, NPHS1, KIRREL2, GP2, and CUZD1 antigens are structural and probably more suitable for targeting. In addition, water channel proteins (Aquaporins), despite being a functional channel protein, can be used as target antigens. However, the proposed antigens or any other antigen needs to be verified using experimental and laboratory work to prove that the antigen is suitable for targeting. In addition, the antibody type, affinity, and specificity are very important factors for developing an efficient treatment.

## Acknowledgements

Dr. Javad Zahiri, Dr. Maryam Hasanlou, Dr. Ali Fasihi and Dr. Hadi Najafi have helped us in the microarray data analysis, which we appreciate greatly. The research reported in this publication was supported by the Elite

Researcher Grant Committee under award number [989951] from the National Institute for Medical Research Development (NIMAD), Tehran, Iran. This project was also financially supported by Iran National Science Foundation (INSF, Grant No. 97011360). There is no conflict of interest in this study.

## Authors' Contributions

H.D., M.H.-A., V.Z., Z.M., M.S., E.H.-S.; Conceptualization, Methodology, Resources, Visualization, Supervision, and Funding acquisition. All authors read and approved the final manuscript.

## References

- Ilonen J, Lempainen J, Veijola R. The heterogeneous pathogenesis of type 1 diabetes mellitus. *Nat Rev Endocrinol*. 2019; 15(11): 635-650.
- Paschou SA, Papadopoulou-Marketou N, Chrousos GP, Kanakagantenbein C. On type 1 diabetes mellitus pathogenesis. *Endocr Connect*. 2018; 7(1): R38-R46.
- Jwad SM, AL-Fatlawi HY. Types of diabetes and their effect on the immune system. *J Adv Pharm Pract*. 2022; 4(1): 21-30.
- Perry JS, Hsieh CS. Development of T-cell tolerance utilizes both cell-autonomous and cooperative presentation of self-antigen. *Immunol Rev*. 2016; 271(1): 141-155.
- Labrijn AF, Janmaat ML, Reichert JM, Parren PW. Bispecific antibodies: a mechanistic review of the pipeline. *Nat Rev Drug Discov*. 2019; 18(8): 585-608.
- Kufer P, Lutterbüse R, Baeuerle PA. A revival of bispecific antibodies. *Trends Biotechnol*. 2004; 22(5): 238-244.
- Topp MS, Stelljes M, Zugmaier G, Barnette P, Heffner LT Jr, Trippett T, et al. Blinatumomab retreatment after relapse in patients with relapsed/refractory B-precursor acute lymphoblastic leukemia. *Leukemia*. 2018; 32(2): 562-565.
- Balcerak J, Shy BR, Putnam AL, Masiello LM, Lares A, Dekovic F, et al. Polyclonal regulatory T cell manufacturing under cGMP: a decade of experience. *Front Immunol*. 2021; 12: 744763.
- Mohseni YR, Tung SL, Dudreuilh C, Lechler RI, Fruhwirth GO, Lombardi G. The future of regulatory T cell therapy: promises and challenges of implementing CAR technology. *Front Immunol*. 2020; 11: 1608.
- Tarbell KV, Yamazaki S, Olson K, Toy P, Steinman RM. CD25+ CD4+ T cells, expanded with dendritic cells presenting a single autoantigenic peptide, suppress autoimmune diabetes. *J Exp Med*. 2004; 199(11): 1467-1477.
- Tang Q, Henriksen KJ, Bi M, Finger EB, Szot G, Ye J, et al. In vitro expanded antigen-specific regulatory T cells suppress autoimmune diabetes. *J Exp Med*. 2004; 199(11): 1455-1465.
- Chopra A, Shan L, Eckelman WC, Leung K, Latterner M, Bryant SH, et al. Molecular imaging and contrast agent database (MICAD): evolution and progress. *Mol Imaging Biol*. 2012; 14(1): 4-13.
- Sjöstedt E, Zhong W, Fagerberg L, Karlsson M, Mitsios N, Adori C, et al. An atlas of the protein-coding genes in the human, pig, and mouse brain. *Science*. 2020; 367(6482): eaay5947.
- Cunningham F, Amode MR, Barrell D, Beal K, Billis K, Brent S, et al. Ensembl 2015. *Nucleic Acids Res*. 2015; 43(Database issue): D662-D669.
- Karlsson M, Zhang C, Méar L, Zhong W, Digre A, Katona B, et al. A single-cell type transcriptomics map of human tissues. *Sci Adv*. 2021; 7(31): eabh2169.
- Rosenbloom KR, Sloan CA, Malladi VS, Dreszer TR, Learned K, Kirkup VM, et al. ENCODE data in the UCSC Genome Browser: year 5 update. *Nucleic Acids Res*. 2013; 41(Database issue): D56-D63.
- Omasits U, Ahrens CH, Müller S, Wollscheid B. Protter: interactive protein feature visualization and integration with experimental proteomic data. *Bioinformatics*. 2014; 30(6): 884-886.
- Thul PJ, Åkesson L, Wiking M, Mahdessian D, Geladaki A, Ait Blal H, et al. A subcellular map of the human proteome. *Science*. 2017; 356(6340): eaal3321.
- Karlsson M, Zhang C, Méar L, Zhong W, Digre A, Katona B, et al. A single-cell type transcriptomics map of human tissues. *Sci Adv*. 2021; 7(31): eabh2169.
- Kampf C, Olsson I, Ryberg U, Sjöstedt E, Pontén F. Production of tissue microarrays, immunohistochemistry staining and digitalization within the human protein atlas. *J Vis Exp*. 2012; (63): 3620.
- Peng S, Zhou Y, Xiong L, Wang Q. Identification of novel targets and pathways to distinguish suicide dependent or independent on depression diagnosis. *Sci Rep*. 2023; 13(1): 2488.
- Kuo L, Yu F, Zhao Y. Statistical methods for identifying differentially expressed genes in replicated microarray experiments: a review. *Stat Adv Biomed Science*. 2008: 341.
- Cramer AO, van Ravenzwaaij D, Matzke D, Steingroever H, Wetzel R, Grasman RP, et al. Hidden multiplicity in exploratory multi-way ANOVA: Prevalence and remedies. *Psychon Bull Rev*. 2016; 23(2): 640-647.
- von Scholten BJ, Kreiner FF, Gough SCL, von Herrath M. Current and future therapies for type 1 diabetes. *Diabetologia*. 2021; 64(5): 1037-1048.
- Haen SP, Löffler MW, Rammensee HG, Brossart P. Towards new horizons: characterization, classification and implications of the tumour antigenic repertoire. *Nat Rev Clin Oncol*. 2020; 17(10): 595-610.
- Muraro MJ, Dharmadhikari G, Grün D, Groen N, Dielen T, Jansen E, et al. A single-cell transcriptome atlas of the human pancreas. *Cell Syst*. 2016; 3(4): 385-394. e3.
- Kawasaki E. ZnT8 and type 1 diabetes. *Endocr J*. 2012; 59(7): 531-537.
- Zhuo L, Huang L, Yang Z, Li G, Wang L. A comprehensive analysis of NPHS1 gene mutations in patients with sporadic focal segmental glomerulosclerosis. *BMC Med Genet*. 2019; 20(1): 111.
- Korshunov A, Okonechnikov K, Stichel D, Schrimpf D, Delaidelli A, Tonn S, et al. Gene expression profiling of Group 3 medulloblastomas defines a clinically tractable stratification based on KIRREL2 expression. *Acta Neuropathol*. 2022; 144(2): 339-352.
- Lin Y, Nakatochi M, Hosono Y, Ito H, Kamatani Y, Inoko A, et al. Genome-wide association meta-analysis identifies GP2 gene risk variants for pancreatic cancer. *Nat Commun*. 2020; 11(1): 3175.
- Rygiel AM, Unger LS, Sörgel FL, Masson E, Matsumoto R, Ewers M, et al. Variants in the pancreatic CUB and zona pellucida-like domains 1 (CUZD1) gene in early-onset chronic pancreatitis - A possible new susceptibility gene. *Pancreatology*. 2022; 22(5): 564-571.
- Bausch-Fluck D, Goldmann U, Müller S, van Oostrum M, Müller M, Schubert OT, et al. The in silico human surfaceome. *Proc Natl Acad Sci USA*. 2018; 115(46): E10988-E10999.
- Hong Y, Park C, Kim N, Cho J, Moon SU, Kim J, et al. QSurface: fast identification of surface expression markers in cancers. *BMC Syst Biol*. 2018; 12 Suppl 2: 17.
- Pont MJ, Honders MW, Kremer AN, van Kooten C, Out C, Hiemstra PS, et al. Microarray gene expression analysis to evaluate cell type specific expression of targets relevant for immunotherapy of hematological malignancies. *PLoS One*. 2016; 11(5): e0155165.
- Orentas RJ, Yang JJ, Wen X, Wei JS, Mackall CL, Khan J. Identification of cell surface proteins as potential immunotherapy targets in 12 pediatric cancers. *Front Oncol*. 2012; 2: 194.
- Magaki S, Hojat SA, Wei B, So A, Yong WH. An introduction to the performance of immunohistochemistry. *Methods Mol Biol*. 2019; 1897: 289-298.
- Toledo PL, Vazquez DS, Gianotti AR, Abate MB, Wegbrod C, Torkko JM, et al. Condensation of the  $\beta$ -cell secretory granule luminal cargoes pro/insulin and ICA512 RESP18 homology domain. *Protein Sci*. 2023; 32(6): e4649.
- da Silva IV, Soveral G. Aquaporins in immune cells and inflammation: new targets for drug development. *Int J Mol Sci*. 2021; 22(4): 1845.

# The Neuroprotective Effects of Curcumin Nanoparticles on The Cerebral Ischemia-Reperfusion Injury in The Rats-The Roles of The Protein Kinase RNA-Like ER Kinase/Extracellular Signal-Regulated Kinase and Transcription Factor EB proteins

Yalda Saghari, Ph.D.<sup>1</sup>, Monireh Movahedi, Ph.D.<sup>1</sup>, Majid Tebianian, Ph.D.<sup>2</sup>, Maliheh Entezari, Ph.D.<sup>3,4\*</sup> 

1. Department of Biochemistry, Faculty of Biological Sciences, North Tehran Branch, Islamic Azad University, Tehran, Iran

2. Department of Biotechnology, Razi Vaccine and Serum Research Institute, Karaj, Tehran, Iran

3. Department of Genetics, Advanced Science and Technology, Tehran Medical Sciences, Islamic Azad University, Tehran, Iran

4. Farhikhtegan Medical Convergence Sciences Research Center, Farhikhtegan Hospital Tehran Medical Sciences, Islamic Azad University, Tehran, Iran

## Abstract

**Objective:** Reduction of cerebral ischemia-reperfusion injury (IRI)/re-oxygenation injury, is defined as the paradoxical exacerbation of the cellular dysfunction and death, following restoration of the blood flow to previously ischemic tissues. The re-establishment of blood flow is essential to salvage the ischemic tissues. As a result, the treatment of IRI with novel therapies, which have fewer side effects, are of great importance. Therefore, this study aimed to investigate the effects of curcumin nanoparticle (CN) pre-treatment on the cerebral I/R rat model.

**Materials and Methods:** In this experimental study, CN was administered to rats orally five days before the bilateral common carotid artery occlusion (BCCAO) and continued for three days. The intensity of oxidative stress, the activities of antioxidant enzymes, glutathione (GSH) content, the activity of mitochondrial enzymes, including succinate dehydrogenase (SDH), malate dehydrogenase (MDH) and lactate dehydrogenase (LDH), curcumin bioavailability, pERK/ERK expression ratio and TFEB protein were studied. Data analysis was performed using Graphpad Prism V.8 software, one-way analysis of variance (ANOVA) with the statistical package for the social sciences (SPSS V.26 software).

**Results:** Cerebral IRI-damage significantly increased the oxidative stress ( $P=0.0008$ ) and decreased the activity of the antioxidant enzymes including catalase (CAT) ( $P<0.001$ ), super oxide dismutase (SOD) ( $P<0.001$ ), reduced GSH ( $P<0.001$ ), mitochondrial enzymes, pERK/ERK expression ratio ( $P=0.002$ ) and TFEB protein ( $P=0.005$ ) in rats' brains. In addition, the pre-treatment of the rats with CN resulted in a decrease in the reactive oxygen species (ROS), and an increase in the activities of antioxidants and mitochondrial enzymes. This in turn up-regulated the pERK/ERK expression ratio and TFEB expression.

**Conclusion:** CN has neuroprotective effects on the cerebral IRI condition due to its antioxidant properties and is able to overexpress the pERK and TFEB proteins; thus, it can be considered as a suitable treatment option during and after the incidence of stroke.

**Keywords:** Curcumin, Ischemia, Lactate Dehydrogenase, Malate Dehydrogenase, Succinate Dehydrogenase

**Citation:** Saghari Y, Movahedi M, Tebianian M, Entezari M. The neuroprotective effects of curcumin nanoparticles on the cerebral ischemia-reperfusion injury in the rats-the roles of the protein kinase RNA-like ER kinase/extracellular signal-regulated kinase and transcription factor EB proteins. Cell J. 2024; 26(1): 62-69. doi: 10.22074/CELLJ.2023.1995696.1257

This open-access article has been published under the terms of the Creative Commons Attribution Non-Commercial 3.0 (CC BY-NC 3.0).

## Introduction

Ischemia-reperfusion injury (IRI)/re-oxygenation injury damage following brain ischemic stroke leads to worsening of the condition and reduces the survival rate (1). During the IRI damage, large amounts of free radicals are generated and the brain is exposed to oxidative stress (2). Unfortunately, despite many advances in reducing the IRI damage, no effective drug has yet been found to treat this disease. Recently, however, the use of antioxidants has been suggested as a suitable new strategy because of

their neuroprotective effects (3).

Curcumin, with the chemical formula of  $C_{21}H_{20}O_6$ , is the active ingredient in the rhizome of turmeric plant *Curcuma longa*, and it is a dietary compound with potent anti-inflammatory, antioxidant, and anti-apoptotic properties. Nonetheless, due to its low aqueous solubility, low bioavailability, and rapid first-pass hepatic metabolism, curcumin is limited in therapeutic applications (4). It has been stated that this compound plays an important role

Received: 19/March/2023, Revised: 31/October/2023, Accepted: 11/November/2023

\*Corresponding Address: P.O.Box: 1477899679, Farhikhtegan Medical Convergence Sciences Research Center, Farhikhtegan Hospital Tehran Medical Sciences, Islamic Azad University, Tehran, Iran

Email: entezari@iautmu.ac.ir



Royan Institute  
Cell Journal (Yakhteh)

in protecting against oxidative damage by scavenging the activity of reactive oxygen species (ROS) (5). Its antioxidant effect is attributed to the phenolic groups or the CH<sub>2</sub> group of the β-diketone moiety. In addition, its neuroprotective effects against ischemic brain injury have been reported. However, the blood brain barrier (BBB) appears to prevent free curcumin (FC) from reaching the brain to exert its effects, which in turn reduces the bioavailability of this molecule (6). One possible way to bypass the BBB is the formulation of curcumin nanoparticles, which are proposed to have the capability of crossing the BBB and therefore increasing the concentration of curcumin in the brain.

The mitogen activated protein kinases (MAPK) signaling pathway has been extensively studied in recent years. This pathway plays a critical role in signal transduction in enzymes ranging from protein kinases to protein phosphatases. The most well-known kinase in this pathway is the protein kinase RNA-like ER kinase (ERK). The ERK signaling pathway contains important modulators that are involved in the growth, proliferation, differentiation, aging, and apoptosis of the cells (7). This pathway is activated by growth factors, oxidative stress, an increase in the intracellular calcium level and the stimulation of glutamate receptors. The absence of oxygen leads to ERK up-regulation (8). This kinase is phosphorylated by a three-part MAPK activity, which is required for the inhibition of skeletal muscle differentiation by insulin-like growth factor 1 or fibroblast growth factor 2. In addition, ERK usually increases after the cerebral IRI injury and this may be either protective or destructive (9). Inhibition of ERK phosphorylation stops ischemic injury (10). It has been shown that ERK activation protects neurons under pathological conditions, such as seizures, Alzheimer's disease, cerebral ischemia, or deprivation of neurotrophic factors (11).

The role of transcription factor EB protein (TFEB) as a critical regulator in the autophagy process is well documented (12). Likewise, TFEB is a branch of the unfolded protein response that confers neuroprotection in ischemic stroke by suppressing protein synthesis. Studies also show that TFEB has beneficial effects on degenerative disorders such as Huntington's and Parkinson's diseases (13). Furthermore, the anti-apoptotic role of TFEB in the heart, as well as inhibition of atherosclerosis are also reported (14). TFEB is shown to affect endothelial cell function and regulate angiogenesis after ischemia (15).

This study aimed to investigate the antioxidant and neuroprotection effects of the curcumin nanoparticles (CN) and their impacts on mitochondrial enzymes and ERK and TFEB signaling pathways in the ischemic brains of rats. The reason for investigating the expression levels of TFEB and ERK proteins was their involvement in the autophagy pathway.

## Materials and Methods

### Animals

For this experimental study, specific pathogen-free

(SPF) male Wistar rats, aged 30-45 days and weighed approximately 250 to 300 g, were obtained from the Pasteur Institute of Iran. The animals were kept at 25 ± 1.5°C and 65% relative humidity with a 12-hour dark/light cycle condition and free access to water and food. Before starting the experiments, the animals were allowed to adapt to the laboratory environment. All experimental protocols were approved by the Ethics Committee of the Tehran Medical Sciences Department of the Islamic Azad University (IR.IAU.TNB.REC.1400.022).

### Materials

CN were purchased from the Exir Nano Sina Company, Iran. Other materials were of analytical grade and purchased from the Merck Company, Germany.

### Induction of the cerebral ischemia/reperfusion

The induction of the cerebral stroke was conducted by the bilateral common carotid artery occlusion (BCCAO) method (16). Firstly, the rats were anesthetized by ketamine (50 mg/kg, Cat# 1867-66-9) and xylazine (2-8 mg/kg, Cat# 23076-35-9), a sagittal incision was made through the neck midline (1 cm in length), and then both carotid arteries were carefully separated from the respective vagal nerves. A 5-0 silk suture loop was made around each CCA, and then all CCAs were occluded by clamps for 10 minutes followed by a 72-hour reperfusion. After the reperfusion step, the wounds were sutured. The sham group underwent surgery without BCCAO. During this period, the animals were examined for rectal temperature of 37°C, a cornea reflex on exposure to light and maintenance of dilated pupils. Animals that did not meet these criteria or developed seizures were excluded from the study. After the period of reperfusion, the animals were sacrificed to remove their brains.

### Animals grouping

A total of 48 rats were divided into 5 groups: Group I: Healthy control rats (n=9), Group II: Sham rats (the animals underwent surgery without BCCAO) (n=9), Group III: Cerebral IRI rats (n=10), Groups IV: Cerebral IRI rats receiving FC orally through gavage everyday (25 mg/kg, n=10), and Group V: Cerebral IRI rats receiving 25 mg/kg CN orally through gavage everyday (n=10). FC and CN administrations were started 5 days before the induction of the cerebral IRI and continued until three days after the BCCAO.

### Separation of the mitochondria from the brain

Brain homogenization was performed according to the method of Navarro and Boveris (17), using a buffer containing 10 mM KCl, 1.5 mM MgCl<sub>2</sub>, 0.1 mM Phenylmethylsulfonyl fluoride (PMSF), 20 mM Hepes-KOH and protease inhibitor. The prepared homogenate was centrifuged at 1000 g for 5 minutes at 4°C and then the supernatant was centrifuged at 35000 g for 60 minutes. The resulting pellet containing mitochondria was



collected and re-suspended in the same buffer.

### **The bioavailability of free curcumin and curcumin nanoparticles**

After the administration of the last doses of FC or CN, the brain homogenates were prepared at 1, 2, 4, 8, 16, 24, 48, and 72 hour(s) post-treatment to measure the brain concentrations of the FC and CN in the rats. According to the method of Shinde and Devarajan (18), curcumin was extracted from the brain homogenates using the coupled high-performance liquid chromatography (HPLC) with 2487 Dual Absorbance Detector and Waters 515 Pump Reversed Phase C18 Column. The peaks were read at 425 nm.

Interestingly, HPLC has become a routine tool for the separation of complex mixtures. However, the ability to obtain structural information on substances separated using HPLC is limited by the online detector systems and, in most applications, full structural elucidation is performed off-line following separation.

### **Lipid peroxidation, reactive oxygen species level, succinate dehydrogenase, lactate dehydrogenase and malate dehydrogenase assays**

Malondialdehyde (MDA) content, as an indicator of lipid peroxidation, was determined using the method explained by Dhindsa et al. (19). Conversion of the cell-permeant 2',7'-dichlorodihydrofluorescein diacetate (H<sub>2</sub>DCFDA) (also known as dichlorofluorescein diacetate) to DCFDA, is used to detect the generation of reactive oxygen intermediates in cells. In the current study, the conversion of H<sub>2</sub>DCFDA to DCFDA, which detected by spectrometers at 499 nm and 520 nm, respectively, was used as an indicator to measure the ROS levels in brain mitochondria after normalization. The ROS content was expressed as percentages (20).

The measurements of succinate dehydrogenase (SDH) (EC 1.3.5.1, Succinate Dehydrogenase Assay Kit, Cat#MAK197), MDA (EC 1.1.1.37, Malate Dehydrogenase Activity Assay Kit, Cat# MAK196) and lactate dehydrogenase (LDH) (EC 1.1.1.27, LDH Assay kit, Cat# MAK066) were performed using the Sigma-Aldrich kits (St. Louis, Missouri, United States) according to the manufacturer's instructions.

### **The measurement of catalase, reduced glutathione and superoxide dismutase activities**

The measurement of glutathione (GSH) content was done by the method of Jollow et al. (21); the SOD activity was evaluated by the Kono's method (22) and the catalase (CAT) activity was estimated by the Greenwald's method (23).

### **Western blot analysis**

The brain tissue was isolated from the rats, and subsequently rinsed with cold phosphate-buffered saline

(PBS, pH=7.4), and then crushed and homogenized with 1 ml radio immunoprecipitation assay (RIPA) buffer (Cat#ab206996, Abcam, Cambridge, UK) supplemented with 1% protease inhibitor (Cat#P8340, Sigma, St. Louis, Missouri, USA). After centrifugation at 13000g for 15 minutes, the supernatant was collected and the protein concentration was determined using the BCA Kit (Cat#23227, Thermo, Waltham, Massachusetts, USA). 60 µg of the total protein was electrophoresed on 10% polyacrylamide gel at a constant voltage of 80 V for 35 minutes and then 120 V for 45 minutes. The electrophoresed proteins were then transferred to the Polyvinylidene Fluoride (PVDF) paper and incubated with ERK (Cat#9102, Cell Signaling, Danvers, Massachusetts, USA), TFEB (Cat# 4240, Cell Signaling, Danvers, Massachusetts, USA) and beta-actin (β-actin) monoclonal antibodies at 4°C overnight. PBS tween-20 (PBST) solution containing 0.1% Tween-20 was used to wash the membrane and then horseradish peroxidase rabbit (HRP-rabbit) anti-rat secondary antibody (1:10000) against the primary antibodies was incubated on shaker for 190 minutes and washed again. Finally, by adding the Electrochemical Luminescence (ECL) (Cat# WBULS0100, Sigma, St. Louis, Missouri) to PVDF paper, the presence of ERK and TFEB proteins in the samples were investigated. In addition to the samples, the negative control sample (without the primary antibodies) was also electrophoresed with the same protein concentrations. Western blot results were analyzed using the Image-Pro Plus 6.0 software (Media Cybernetics, Bethesda, MD, USA).

### **Statistical analysis**

Data analyzing and figure plotting were carried out using the Graphpad Prism V.8 software (Dotmatics, USA). One way analysis of variance (ANOVA) unpaired t test was used to analyze the data (n=6) and post hoc test was done based on the Tukey's and Duncan's multiple range tests at a significant level of P<0.05. Data was presented as mean ± SEM.

## **Results**

### **Bioavailability of curcumin in the brain**

The amounts of FC and CN were measured in the rat brain homogenates over time and the outcome showed an increase in the concentration of curcumin in the brain homogenates up to 8 hours after administration. No curcumin was found in the brain homogenates past 48 or 72 hours of curcumin administration. However, the concentration of CN was higher in the brain homogenates compared to the FC and showed an increasing trend for up to 24 hours. After 24 hours, a decreasing trend of CN concentration was observed. However, the presence of CN was observed in the brain homogenates 72 hours after administration (Table 1).

### **Mitochondria function**

The ROS were overproduced in the cerebral IRI

rats. However, a sharp decrease in the ROS production was observed in the cerebral IRI rats receiving CN compared to rats receiving FC. Therefore, it seems that CN is very effective in reducing oxidative stress due to IRI damage. High lipid peroxidation was observed in the cerebral IRI group compared to the control group, indicating damage to the mitochondrial membrane due to the cerebral IRI. However, administration of CN significantly reduced the lipid peroxidation of mitochondrial membranes, and therefore, CN appeared to have stronger protective effects against the cerebral IRI damage compared to FC. Induction of the cerebral IRI in the rats lowered the activities of SDH, MDH and LDH enzymes, which indicates decreased respiratory activity in these rats. However, pre-treatment of the rats with CN increased the activities of these enzymes (Table 2).

### Antioxidant enzyme activities and reduced glutathione content

A sharp reduction in the activity of antioxidant enzymes CAT and superoxide dismutase, as well as a decrease in the reduced GSH content due to the cerebral IRI damage, were observed in the rats ( $P < 0.001$ ). However, pre-treatment of CN in the rats with the cerebral IRI recovered the activities of these enzymes

to their levels in the healthy control rats, indicating a significant amplification in the antioxidant capacity and an increase in the GSH content, due to the CN administration (Fig.1).

### TFEB and pERK/ERK protein expression levels

Induction of the IRI brain injury significantly down-regulated the TFEB protein expression in the rat brain compared with the control group ( $P = 0.005$ ). FC and CN both showed positive effects on the TFEB over expression, so that the expression of TFEB protein in the brains of rats receiving CN did not show a significant difference, compared with the control group. Therefore, our data confirm that CN has the ability to up-regulate the TFEB protein expression insignificantly (Fig.2).

This study also showed that the induction of the cerebral IRI in rats leads to the dephosphorylation of the ERK protein. However, FC and CN administration increased the levels of pERK and subsequently lead to an increase in the pERK/ERK ratio (Fig.3). However, insignificant difference was observed in the brain tissues of the rats receiving only CN concerning the pERK/ERK expression ratio compared to the control group ( $P = 0.243$ ).

**Table 1:** The concentration-time bioavailability of FC and CN in the rat brain homogenate (25 mg/kg, n=3)

Treatment	1 hour	2 hours	4 hours	8 hours	16 hours	24 hours	48 hours	72 hours
FC	0.12 ± 0.01	0.16 ± 0.03	0.29 ± 0.04	0.68 ± 0.06	0.26 ± 0.03	0.09 ± 0.05	Undetectable	Undetectable
NC	1.22 ± 0.11 <sup>#</sup>	1.89 ± 0.19 <sup>#</sup>	3.11 ± 0.53 <sup>#</sup>	4.25 ± 0.62 <sup>#</sup>	10.88 ± 0.86 <sup>#</sup>	14.75 ± 0.93 <sup>#</sup>	5.85 ± 0.37 <sup>#</sup>	1.78 ± 0.33 <sup>#</sup>

Data are presented as mean ± SD. FC; Free curcumin, CN; Curcumin nanoparticles, and #; Shows significant differences, based on the unpaired t test at the probability level of  $P < 0.0001$ .

**Table 2:** The effects of FC and CN on the mitochondria ROS generation, activities of SDH, MDH and LDH in the rat brain homogenate (25 mg/kg, n=5)

Group	ROS	Lipid peroxidation (μM)	SDH activity (U/mg protein/minutes)	MDH activity (U/mg protein/minutes)	LDH activity (U/mg protein/minutes)
Control	106 ± 5 <sup>c</sup>	3.23 ± 0.56 <sup>b</sup>	5.48 ± 0.53 <sup>a</sup>	5.98 ± 0.37 <sup>a</sup>	5.07 ± 0.54 <sup>a</sup>
Sham	112 ± 6 <sup>c</sup>	3.44 ± 0.63 <sup>b</sup>	5.42 ± 0.58 <sup>a</sup>	5.84 ± 0.32 <sup>a</sup>	4.85 ± 0.51 <sup>a</sup>
Cerebral IRI	274 ± 18 <sup>a</sup>	6.23 ± 0.78 <sup>a</sup>	2.88 ± 0.28 <sup>b</sup>	3.42 ± 0.21 <sup>c</sup>	3.27 ± 0.25 <sup>c</sup>
FC	243 ± 16 <sup>b</sup>	5.78 ± 0.73 <sup>a</sup>	3.42 ± 0.31 <sup>b</sup>	3.88 ± 0.34 <sup>b</sup>	3.58 ± 0.39 <sup>b</sup>
NC	131 ± 14 <sup>c</sup>	3.65 ± 0.53 <sup>b</sup>	5.22 ± 0.43 <sup>a</sup>	5.42 ± 0.44 <sup>ab</sup>	4.86 ± 0.42 <sup>a</sup>

Data are presented as mean ± SD. Different letters show significant differences, based on the Duncan's multiple range test, Sham group underwent surgery without BCCAO. FC; Free curcumin at the concentration of 25 mg/kg, CN; Curcumin nanoparticles at the concentration of 25 mg/kg, ROS; Reactive oxygen species, SDH; Succinate dehydrogenase, MDH; Malate dehydrogenase, LDH; Lactate dehydrogenase, BCCAO; Bilateral common carotid artery occlusion, and IRI; Ischemia-reperfusion injury.

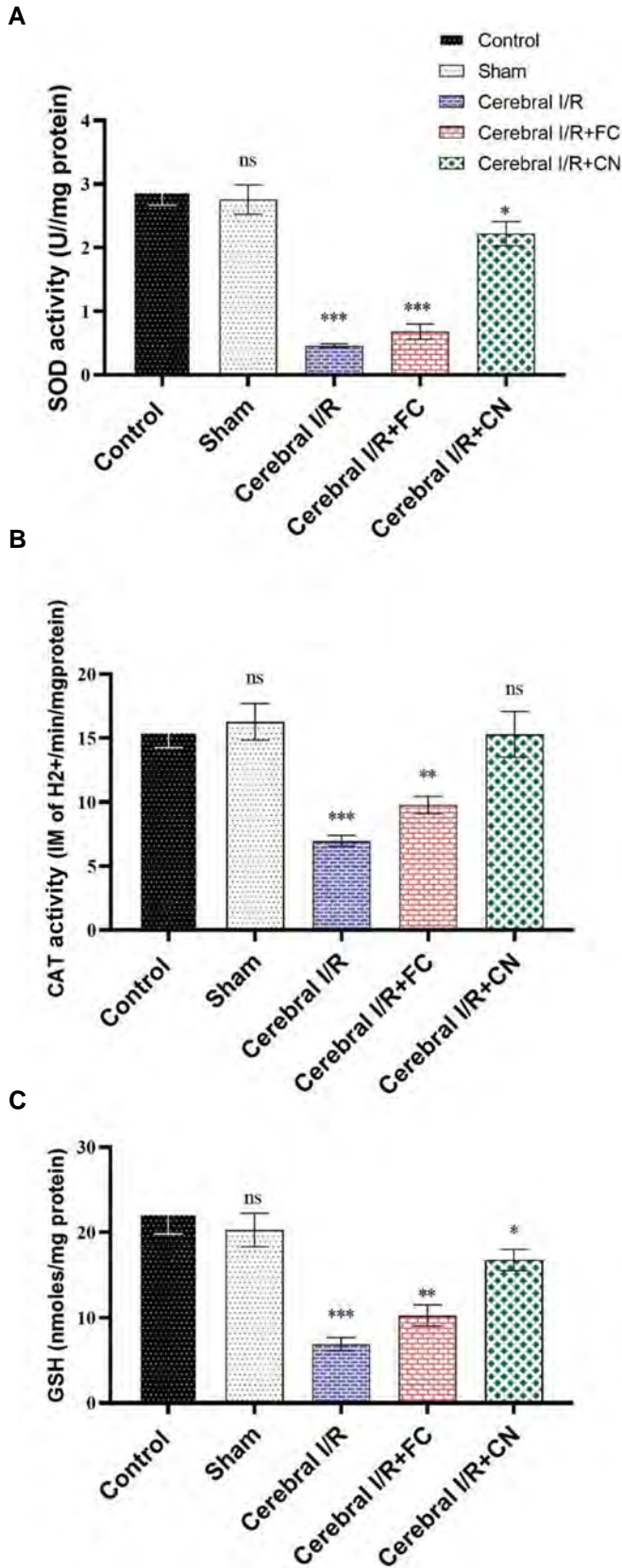


**Fig.1:** The changes in anti-oxidant enzymes activities in the rats' brain after pretreatment with 25/mg/kg FC and CN (n=6). **A.** SOD, **B.** CAT, and **C.** Reduced GSH. FC; Free curcumin, CN; Curcumin nanoparticles, SOD; Superoxide dismutase, CAT; Catalase, GSH; Glutathione, BCCAO; Bilateral common carotid artery occlusion, IRI; Ischemia/reperfusion injury, ns; Not significant, \*, \*\*, and \*\*\*; Significant differences at the probability levels of P<0.05, P<0.01 and P<0.001, respectively. Sham group underwent surgery without BCCAO.

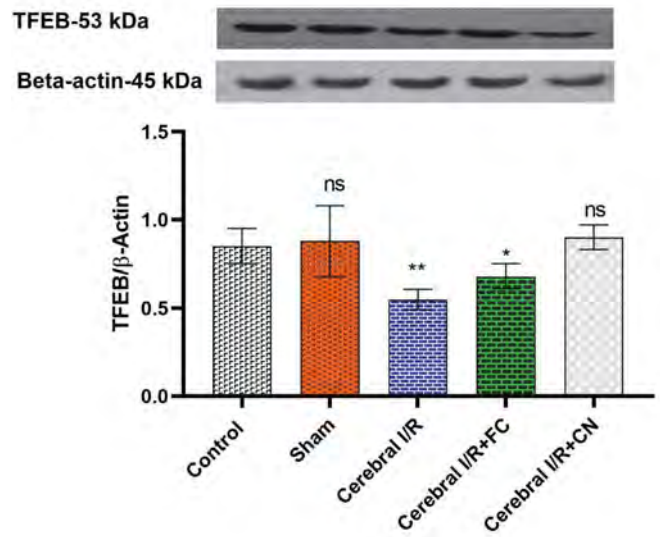


**Fig.2:** The expression levels of the TFEB/β-Actin proteins in the rat brain homogenate pre-treated with FC (25 mg/kg) and CN (25 mg/kg). FC; Free curcumin, CN; Curcumin nanoparticles, BCCAO; Bilateral common carotid artery occlusion, IRI; Ischemia/reperfusion injury, ns; Not significant, \*, and \*\*; Significant differences at the probability levels of P<0.05 and P<0.01, respectively. Sham group underwent surgery without BCCAO.

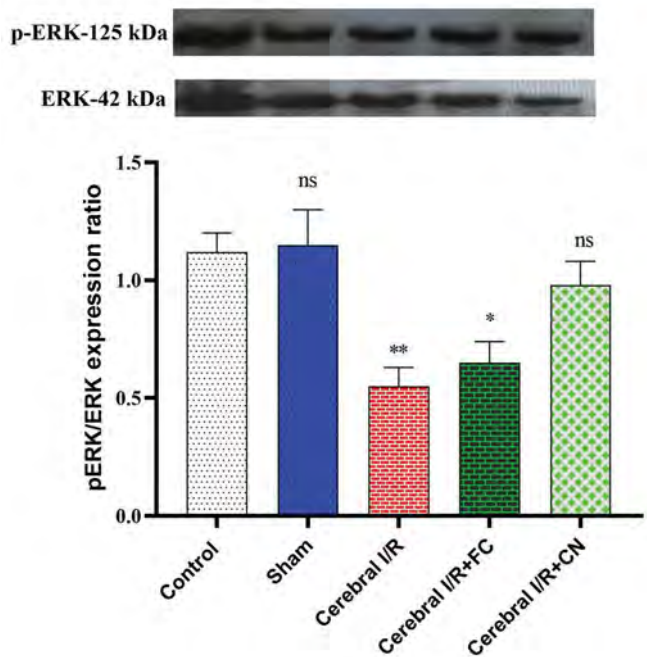


**Fig.3:** The pERK/ERK expression ratio in the rat brain homogenate pre-treated with FC (25 mg/kg) and CN (25 mg/kg), (n=3). FC; Free curcumin, CN; Curcumin nanoparticles, BCCAO; Bilateral common carotid artery occlusion, IRI; Ischemia/reperfusion injury, ns; Not significant, \*, and \*\*; Significant differences at the probability levels of P<0.05 and P<0.01, respectively. The sham group underwent surgery without BCCAO.

## Discussion

This study aimed to investigate the antioxidant and neuroprotection effects of CN, and its effects on the

mitochondrial enzymes, ERK and TFEB signaling pathways in ischemic brains of rats, as IRI models. This study investigated the effects of pretreatment with FC and CN on the cerebral IRI in rats. The results showed promising positive effects of CN in reducing oxidative stress, increasing the activities of antioxidant enzymes and GSH content, recovering SDH, LDH and MDH activities in mitochondria and overexpressing TFEB proteins and increasing pERK/ERK ratio in the brain.

Increased oxidative stress in IRI is commonly reported in different studies and especially during the reperfusion stage, high levels of damage due to oxidative stress is very likely (24). Therefore, pretreatment with antioxidant compounds can be very effective in reducing the fatal effects of the oxidative stress in the reperfusion phase (25). The protective role of curcumin against ischemic injury is reported in previous studies. However, due to the low bioavailability of this compound, its use has been limited (26). Therefore, due to their small sizes, the use of curcumin nanoparticles may be a solution to this problem. Numerous studies have shown that curcumin nanoparticles successfully cross the BBB (27). This study showed that when CN was given to the rats, even 48 hours after administration, significant amounts of curcumin were still found in the rat brain homogenate samples. This confirms both CN passage through the BBB as well as sustained release of curcumin from the CN. Therefore, CN can be considered as a good therapeutic approach in prevention of oxidative stress induced by the cerebral IRI.

The activities of antioxidant enzymes are highly sensitive to the ROS content, as high ROS levels leads to their inactivation and rapid consumption in the body (28). The human brain contains high levels of polyunsaturated fatty acids (PFA), therefore it is highly sensitive to oxidative stress compared to other tissues. Also, in the incidence of oxidative stress, lipid peroxidation in the brain occurs to a large extent (29). In this study, it was observed that the cerebral I/R damage increased the ROS production and consequently, lipid peroxidation increased sharply. However, when CN was given to the rats, the ROS content and lipid peroxidation in the brain were severely reduced, indicating a strong antioxidant consequence of CN administration. The antioxidant effects of CN have been reported in other previous studies (30). In this study, the decrease in the activities of CAT and SOD antioxidant enzymes after the cerebral I/R injury may be attributed to the increase in the endogenous ROS content. The function of CAT is to inactivate  $H_2O_2$  radicals in the cell and SOD is involved in scavenging the superoxide radicals (31). Therefore, the observed decrease in the ROS in the present study is due to the pre-treatment of rats with CN, and can be attributed to increases in the activities of antioxidant enzymes, which in turn affect the GSH content in a similar fashion.

In this study, decreases in the activities of SDH, MDH and LDH enzymes were observed after the occurrence of cerebral IRI in the rat brain mitochondria, indicating

impairment in the electron transfer chain and oxidative phosphorylation. However, in pre-treated rats with CN, slight decreases in the activities of these enzymes were observed, suggesting a protective role for FC from the mitochondrial respiratory function after the I/R injury. The cerebral I/R damage leads to mitochondrial dysfunction, and ROS produced by complexes I and II plays an important role in this damage (32). Our findings also revealed that administration of CN to the rats prevented the reduction of SDH, MDH and LDH enzymes in the cerebral I/R rats. The antioxidant properties of curcumin and its role in increasing the activities of antioxidant enzymes appear to play an important role in prevention of the mitochondrial and respiratory chain damages. Impaired mitochondrial respiration is associated with the oxidative stress, and the results of this study showed that CN has a protective role on the mitochondrial function in cerebral I/R condition.

The Mitogen-activated protein kinases (MAPK) signaling pathway plays an important role in the signal transduction of protein kinases and phosphatases (33). The most important kinase of this pathway is ERK, which contains important modulators for cell growth and proliferation. Induction of the cerebral ischemia is reported to rapidly activate the MAPKs in different areas of the brain, causing phosphorylation and activation of ERKs, thus protecting neurons under the pathological conditions. The neuronal protection mechanism of ERK has been attributed to the activation of tyrosine kinase receptors, induction of B-cell lymphoma 2 (Bcl-2), BCL2-associated agonist of cell death (Bad) and nuclear factor kappa-light-chain-enhancer of activated B cells (NF- $\kappa$ B) expressions, or inhibition of cytochrome C release (34). A reduction in the pERK/ERK ratio was observed after reperfusion in the brain homogenates, indicating a decrease in the neuronal protection. However, CN significantly increased the pERK/ERK expression ratio, compared to the I/R group rats, suggesting a neuroprotective role for CN. Nonetheless, the role of ERK in the ischemia model has been controversial; ERK activity has been shown in both neuronal protection and worsening of the ischemic injury. It has been suggested that its activity may exacerbate inflammation and necrosis by up regulating the expression of interleukin-1beta (IL-1 $\beta$ ) (35).

Nevertheless, another report stated that ERK positively regulates caspase-3 expression in the brain after ischemia, leading to cell death (36). In the present study, we observed that up regulation of pERK and down regulation of ERK in the cerebral I/R rats receiving CN played an important role in protecting against neurodegeneration. However, more research is needed in this area to better understand the mechanism of this phenomenon. Elevated levels of phosphorylated ERK proteins have been reported following curcumin treatment in depressive conditions (37), indicating the anti-inflammatory effects of this secondary metabolite. However, since the neuroprotective effects of curcumin

depends on crossing the BBB, size reduction due to the application of nano-formulation intensifies the protective effects of neurons. It is therefore reasonable to conclude that this experiment had a sound internal and external validity.

The main regulator of autophagy-lysosomal pathway (ALP) is TFEB, which upon expression leads to increased lysosome biogenesis. The therapeutic role of this protein has been reported in various studies, in all of which it has been stated that this protein has a protective effect on neurons by clearing proteins involved in the neurodegenerative diseases, such as Parkinson's and Alzheimer's diseases (38). The results of our study also showed that the expression levels of the TFEB protein were downregulated in the cerebral I/R rats. This is not a desirable sign, because this protein plays a role in lysosomal biogenesis and autophagy in the cerebral IRI conditions. Nevertheless, administration of CN was significantly up-regulated TFEB protein expression. As mentioned earlier, the role of TFEB in prevention of the accumulation of autophagosomes and protein clearance has been reported. Collectively, this protein is located inside the cytosol at the lysosomal surface, where it interacts with the mammalian target of rapamycin (mTOR) (39). Under stressful conditions, this protein is transported into the nucleus, where it activates the genes involved in autophagy, which is important in the survival of nerve cells due to the clearance of defective mitochondria (40). Therefore, up-regulation of the TFEB protein expression in the IRI rats receiving CN can be extremely important as it leads to increased autophagy of defective mitochondria.

The first limitation of this study, was the use of an animal model, which required clinical studies to confirm the protective effects of the CN and FC. The second was a limited sample size. The strength point of this study is the neuroprotective effects of the CN and FC in the cerebral IRI of the rats.

## Conclusion

The results of this study suggest that CN has strong neuroprotective effects in the cerebral IRI conditions due to its antioxidant properties and ability to upregulate the pERK/ERK and TFEB protein expressions, and therefore, may be considered as a suitable adjuvant therapy option in stroke conditions.

## Acknowledgements

The authors would like to express their sincere gratitude to the members of the Faculty of the Biological Sciences, Tehran Islamic Azad University, for their generous assistance. There is no financial support and conflict of interest in this study.

## Authors' Contributions

Y.S.; Writing original draft, Methodology, and Software.


M.E.; Writing-Reviewing and Supervision. M.M., M.T.; Software and Validation. All authors read and approved the final draft of the manuscript.

## References

- Zhang DM, Zhang T, Wang MM, Wang XX, Qin YY, Wu J, et al. TIGAR alleviates ischemia/reperfusion-induced autophagy and ischemic brain injury. *Free Radic Biol Med.* 2019; 137: 13-23.
- Janyou A, Wicha P, Jittiwat J, Suksamrarn A, Tocharus C, Tocharus J. Dihydrocapsaicin attenuates blood brain barrier and cerebral damage in focal cerebral ischemia/reperfusion via oxidative stress and inflammatory. *Sci Rep.* 2017; 7(1): 10556.
- Malekiyan R, Abdanipour A, Sohrabi D, Jafari Anarkooli I. Antioxidant and neuroprotective effects of lycopene and insulin in the hippocampus of streptozotocin-induced diabetic rats. *Biomed Rep.* 2019; 10(1): 47-54.
- Abrahams S, Haylett WL, Johnson G, Carr JA, Bardien S. Antioxidant effects of curcumin in models of neurodegeneration, aging, oxidative and nitrosative stress: a review. *Neuroscience.* 2019; 406: 1-21.
- Malik P, Singh M. Study of curcumin antioxidant activities in robust oil-water nanoemulsions. *New J Chem.* 2017; 41(21): 12506-12519.
- Velásquez-Jiménez D, Corella-Salazar DA, Zuñiga-Martínez BS, Domínguez-Avila JA, Montiel-Herrera M, Salazar-López NJ, et al. Phenolic compounds that cross the blood-brain barrier exert positive health effects as central nervous system antioxidants. *Food Funct.* 2021; 12(21): 10356-10369.
- Wang YC, Li X, Shen Y, Lyu J, Sheng H, Paschen W, et al. PERK (Protein Kinase RNA-Like ER Kinase) branch of the unfolded protein response confers neuroprotection in ischemic stroke by suppressing protein synthesis. *Stroke.* 2020; 51(5): 1570-1577.
- Chen L, Liu L, Xie ZY, Wang F, Zhu L, Zhang C, et al. Protein kinase RNA-like ER kinase/eukaryotic translation initiation factor 2 $\alpha$  pathway attenuates tumor necrosis factor alpha-induced apoptosis in nucleus pulposus cells by activating autophagy. *J Cell Physiol.* 2019; 234(7): 11631-11645.
- Xu D, Kong T, Zhang S, Cheng B, Chen J, Wang C. Orexin-A protects against cerebral ischemia-reperfusion injury by inhibiting excessive autophagy through OX1R-mediated MAPK/ERK/mTOR pathway. *Cell Signal.* 2021; 79: 109839.
- Mohamed SK, Ahmed AAE, Elmorsy EM, Nofal S. ERK activation by zeranol has neuroprotective effect in cerebral ischemia reperfusion. *Life Sci.* 2019; 227: 137-144.
- Wiciński M, Socha M, Malinowski B, Wódkiewicz E, Walczak M, Górski K, et al. Liraglutide and its neuroprotective properties-focus on possible biochemical mechanisms in alzheimer's disease and cerebral ischemic events. *Int J Mol Sci.* 2019; 20(5): 1050.
- Nnah IC, Wang B, Saqçena C, Weber GF, Bonder EM, Bagley D, et al. TFEB-driven endocytosis coordinates MTORC1 signaling and autophagy. *Autophagy.* 2019; 15(1): 151-164.
- Pantiya P, Thonusin C, Chattipakorn N, Chattipakorn SC. Mitochondrial abnormalities in neurodegenerative models and possible interventions: focus on Alzheimer's disease, Parkinson's disease, Huntington's disease. *Mitochondrion.* 2020; 55: 14-47.
- Zhou P, Xie W, Luo Y, Lu S, Dai Z, Wang R, et al. Inhibitory effects of ginsenoside Rb1 on early atherosclerosis in ApoE<sup>-/-</sup> mice via inhibition of apoptosis and enhancing autophagy. *Molecules.* 2018; 23(11): 2912.
- Fan Y, Lu H, Liang W, Garcia-Barrio MT, Guo Y, Zhang J, et al. Endothelial TFEB (Transcription Factor EB) positively regulates postischemic angiogenesis. *Circ Res.* 2018; 122(7): 945-957.
- Saghari Y, Movahedi M, Tebianian M, Entezari M. The neuroprotective effect of betanin nanoparticles on brain ischemia-reperfusion injury. *Animal Gene.* 2023; 27: 200145.
- Navarro A, Boveris A. Rat brain and liver mitochondria develop oxidative stress and lose enzymatic activities on aging. *Am J Physiol Regul Integr Comp Physiol.* 2004; 287(5): R1244-R1249.
- Shinde RL, Devarajan PV. Docosahexaenoic acid-mediated, targeted and sustained brain delivery of curcumin microemulsion. *Drug Deliv.* 2017; 24(1): 152-161.
- Dhindsa RS, Plumb-Dhindsa P, Thorpe TA. Leaf senescence: correlated with increased levels of membrane permeability and lipid peroxidation, and decreased levels of superoxide dismutase and catalase. *J Exp Bot.* 1981; 32(1): 93-101.

20. Batandier C, Fontaine E, Kériel C, Leverve XM. Determination of mitochondrial reactive oxygen species: methodological aspects. *J Cell Mol Med*. 2002; 6(2): 175-187.
21. Jollow DJ, Mitchell JR, Zampaglione N, Gillette JR. Bromobenzene-induced liver necrosis. Protective role of glutathione and evidence for 3,4-bromobenzene oxide as the hepatotoxic metabolite. *Pharmacology*. 1974; 11(3): 151-169.
22. Kono Y. Generation of superoxide radical during autoxidation of hydroxylamine and an assay for superoxide dismutase. *Arch Biochem Biophys*. 1978; 186(1): 189-195.
23. Greenwald RA. *Handbook methods for oxygen radical research*. 1<sup>st</sup> ed. Boca Raton: CRC Press; 2017.
24. Zhou H, Toan S. Pathological roles of mitochondrial oxidative stress and mitochondrial dynamics in cardiac microvascular ischemia/reperfusion injury. *Biomolecules*. 2020; 10(1): 85.
25. Torki A, Khalaji-Pirbalouty V, Lorigooini Z, Rafeian-Kopaei M, Sadeghimanesh A, Rabiei Z. *Anchusa italica* extract: phytochemical and neuroprotective evaluation on global cerebral ischemia and reperfusion. *BJPS*. 2018; 54(1): 1-9.
26. Rahmati F. Microencapsulation of *Lactobacillus acidophilus* and *Lactobacillus plantarum* in Eudragit S100 and alginate chitosan under gastrointestinal and normal conditions. *Appl Nanosci*. 2020; 10(9): 391-399.
27. Barbara R, Belletti D, Pederzoli F, Masoni M, Keller J, Ballestrazzi A, et al. Novel curcumin loaded nanoparticles engineered for Blood-Brain Barrier crossing and able to disrupt Aβ aggregates. *Int J Pharm*. 2017; 526(1-2): 413-424.
28. Bodega G, Alique M, Puebla L, Carracedo J, Ramírez RM. Microvesicles: ROS scavengers and ROS producers. *J Extracell Vesicles*. 2019; 8(1): 1626654
29. Raefsky SM, Furman R, Milne G, Pollock E, Axelsen P, Mattson MP, et al. Deuterated polyunsaturated fatty acids reduce brain lipid peroxidation and hippocampal amyloid β-peptide levels, without discernable behavioral effects in an APP/PS1 mutant transgenic mouse model of Alzheimer's disease. *Neurobiol Aging*. 2018; 66: 165-176.
30. Huang X, Huang X, Gong Y, Xiao H, McClements DJ, Hu K. Enhancement of curcumin water dispersibility and antioxidant activity using core-shell protein-polysaccharide nanoparticles. *Food Res Int*. 2016; 87: 1-9.
31. Rahmati F, Hosseini SS, Mahuti Safai S, Asgari Lajayer B, Hatami M. New insights into the role of nanotechnology in microbial food safety. *3 Biotech*. 2020; 10(10): 425.
32. Angelova PR, Abramov AY. Role of mitochondrial ROS in the brain: from physiology to neurodegeneration. *FEBS Lett*. 2018; 592(5): 692-702.
33. Klemm C, Bruchhagen C, van Krüchten A, Niemann S, Löffler B, Peters G, et al. Mitogen-activated protein kinases (MAPKs) regulate IL-6 over-production during concomitant influenza virus and *Staphylococcus aureus* infection. *Sci Rep*. 2017; 7: 42473.
34. Tiong YL, Ng KY, Koh RY, Ponnudurai G, Chye SM. Melatonin prevents oxidative stress-induced mitochondrial dysfunction and apoptosis in high glucose-treated schwann cells via upregulation of Bcl2, NF-κB, mTOR, Wnt signalling pathways. *Antioxidants (Basel)*. 2019; 8(7): 198.
35. Wang Y, Che M, Xin J, Zheng Z, Li J, Zhang S. The role of IL-1β and TNF-α in intervertebral disc degeneration. *Biomed Pharmacother*. 2020; 131: 110660.
36. Zhang D, Han S, Wang S, Luo Y, Zhao L, Li J. cPKCγ-mediated down-regulation of UCHL1 alleviates ischaemic neuronal injuries by decreasing autophagy via ERK-mTOR pathway. *J Cell Mol Med*. 2017; 21(12): 3641-3657.
37. Fan C, Li Y, Lan T, Wang W, Mao X, Yu SY. Prophylactic treatment of curcumin in a rat model of depression by attenuating hippocampal synaptic loss. *Food Funct*. 2021; 12(22): 11202-11213.
38. Lindestam Arlehamn CS, Garretti F, Sulzer D, Sette A. Roles for the adaptive immune system in Parkinson's and Alzheimer's diseases. *Curr Opin Immunol*. 2019; 59: 115-120.
39. Rabanal-Ruiz Y, Korolchuk VI. mTORC1 and nutrient homeostasis: the central role of the lysosome. *Int J Mol Sci*. 2018; 19(3): 818.
40. Damme M, Suntio T, Saftig P, Eskelinen EL. Autophagy in neuronal cells: general principles and physiological and pathological functions. *Acta Neuropathol*. 2015; 129(3): 337-362.

# Fabrication of Rosuvastatin-Incorporated Polycaprolactone -Gelatin Scaffold for Bone Repair: A Preliminary *In Vitro* Study

Maliheh Gharibshahian, Ph.D.<sup>1</sup>, Morteza Alizadeh, Ph.D.<sup>2</sup>, Mohammad Kamalabadi Farahani, Ph.D.<sup>2</sup>,  
Majid Salehi, Ph.D.<sup>2, 3, 4\*</sup> 

1. Student Research Committee, School of Medicine, Shahroud University of Medical Sciences, Shahroud, Iran
2. Department of Tissue Engineering, School of Medicine, Shahroud University of Medical Sciences, Shahroud, Iran
3. Tissue Engineering and Stem Cells Research Centre, Shahroud University of Medical Sciences, Shahroud, Iran
4. Sexual Health and Fertility Research Centre, Shahroud University of Medical Sciences, Shahroud, Iran

## Abstract

**Objective:** Rosuvastatin (RSV) is a hydrophilic, effective statin with a long half-life that stimulates bone regeneration. The present study aims to develop a new scaffold and controlled release system for RSV with favourable properties for bone tissue engineering (BTE).

**Materials and Methods:** In this experimental study, high porous polycaprolactone (PCL)-gelatin scaffolds that contained different concentrations of RSV (0 mg/10 ml, 0.1 mg/10 ml, 0.5 mg/10 ml, 2.5 mg/10 ml, 12.5 mg/10 ml, and 62.5 mg/10 ml) were fabricated by the thermally-induced phase separation (TIPS) method. Mechanical and biological properties of the scaffolds were evaluated by Fourier transform infrared spectroscopy (FTIR), scanning electron microscope (SEM), compressive strength, porosity, MTT, alkaline phosphatase (ALP) activity, water contact angle, degradation rate, pH alteration, blood clotting index (BCI), and hemocompatibility.

**Results:** SEM analysis confirmed that the porous structure of the scaffolds contained interconnected pores. FTIR results showed that the RSV structure was maintained during the scaffold's fabrication. RSV (up to 62.5 mg/10 ml) increased compressive strength ( $16.342 \pm 1.79$  MPa), wettability (70.2), and degradation rate of the scaffolds. Scaffolds that contained 2.5 mg/10 ml RSV had the best effect on the human umbilical cord mesenchymal stem cell (HUC-MSCs) survival, hemocompatibility, and BCI. As a sustained release system, only  $31.68 \pm 0.1\%$  of RSV was released from the PCL-Gelatin-2.5 mg/10 ml RSV scaffold over 30 days. In addition, the results of ALP activity showed that RSV increased the osteogenic differentiation potential of the scaffolds.

**Conclusion:** PCL-Gelatin-2.5 mg/10 ml RSV scaffolds have favorable mechanical, physical, and osteogenic properties for bone tissue and provide a favorable release system for RSV. They can be mentioned as a promising strategy for bone regeneration that should be further assessed in animals and clinical studies.

**Keywords:** Bone, Gelatin, Polycaprolactone, Regeneration, Rosuvastatin

**Citation:** Gharibshahian M, Alizadeh M, Kamalabadi Farahani M, Salehi M. Fabrication of rosuvastatin-incorporated polycaprolactone -gelatin scaffold for bone repair: a preliminary in vitro study. Cell J. 2024; 26(1): 70-80. doi: 10.22074/CELLJ.2023.2009047.1391  
This open-access article has been published under the terms of the Creative Commons Attribution Non-Commercial 3.0 (CC BY-NC 3.0).

## Introduction

One of the vital clinical needs of tissue engineering is the reconstruction of fractures and congenital and trauma-induced bone defects that are larger than the critical size. These fractures and defects can lead to permanent functional disability if they do not fully heal (1). Tissue engineering can be used to design and manufacture biodegradable and biocompatible scaffolds in combination with various types of cells and biochemical agents to stimulate local bone formation and decrease healing time (2). The selection of appropriate materials is one of the main requirements to encourage optimal osteoblastic adhesion and differentiation for bone scaffolds (3, 4).

Various polymers are used in bone tissue engineering (BTE). Among them, polycaprolactone (PCL) is a

linear aliphatic polyester and a hydrophobic synthetic polymer approved by the United States Food and Drug Administration that has attracted much attention (5). PCL is a biocompatible, flexible, thermoplastic, and biodegradable polymer. It has suitable stiffness and mechanical properties for bone applications. This polymer is affordable, easy to process, not carcinogenic, and has low immunogenicity. However, due to the slow degradation rate of PCL (about 2-4 years), lack of osteogenesis potential, and its hydrophobic nature, the PCL composite is generally used with other polymers and growth factors (6, 7).

Gelatin is a natural, hydrophilic polymer obtained from the incomplete hydrolysis of collagen. Properties of this polymer include low antigenicity, rapid degradation, favourable biocompatibility, availability,

Received: 11/August/2023, Revised: 16/November/2023, Accepted: 05/December/2023

\*Corresponding Address: P.O.Box: 3614773943, Department of Tissue Engineering, School of Medicine, Shahroud University of Medical Sciences, Shahroud, Iran

Email: Salehi.m@shmu.ac.ir



Royan Institute  
Cell Journal (Yakhteh)

cost-effectiveness, and the presence of an Arg–Gly–Asp (RGD) sequence (7, 8). Gelatin reinforces cell adhesion due to these RGD sequences. Although gelatin has good cell adhesion, proliferation and differentiation properties (9), its use in tissue engineering applications has been restricted by low mechanical strength and rapid breakdown (7).

Statins are specific inhibitors of 3-hydroxy-2-methylglutaryl coenzyme A (HMG-CoA) reductase (an enzyme that limits the rate of cholesterol synthesis) that play a role in the treatment of hyperlipidaemia and atherosclerosis. Various studies have reported the effects of statins for osteoporosis, angiogenesis, osteogenesis, and modulation of inflammation (10, 11). Rosuvastatin (RSV) is a group of second-generation hydrophilic statins that play a role in reducing fat and preventing cardiovascular disorders (12). Due to its hydrophilic nature, RSV does not easily penetrate the bilayer lipid membrane of the cell and needs special carriers to enter the cells. In addition to its anti-inflammatory effects, RSV can stimulate osteogenesis, differentiate osteoblastic cells, and reduce oxidative stress (13). This statin helps to reduce inflammation by increasing nitric oxide production and inhibiting phosphorus selectin synthesis (14). RSV decreases the activity of osteoclasts, stimulates the differentiation of osteoblasts, and increases bone mineralisation. It increases bone morphogenetic protein (BMP)-2 expression and alkaline phosphatase (ALP) activity (10). BMP-2, as a bone-inducing factor, helps bone formation by increasing the transcription of bone-inducing genes and stimulates the differentiation of immature mesenchymal cells, including osteoblasts. Therefore, their use will be more favourable than expensive growth factors with a short half-life that may lead to immune stimulation (due to high molecular weight) (10, 15).

Various studies have shown the effect of oral administration of RSV on bone repair; however, due to its primary metabolism in the liver and low bioavailability (less than 20%), oral use of RSV does not provide a suitable effect on bone formation and sometimes leads to autoimmune myopathy, rhabdomyolysis, nausea, and hepatic injury (10). Therefore, RSV should be incorporated into scaffolds/carriers to optimize its efficiency (16). Monjo et al. (13) used a collagen sponge that contained RSV and obtained the release of more than 50% of RSV within three hours. Rezazadeh et al. (15) applied chitosan/chondroitin sulphate nanoparticles that contained RSV and integrated these nanoparticles into a heat-sensitive Pluronic F127/hyaluronic acid hydrogel to create an optimal release system for RSV. Their results showed that more than 60% of the drug was released within 48 hours and had a positive effect on the survival and proliferation of osteoblasts in the culture medium. Ibrahim and Fahmy (17) used RSV-containing collagen sponges to repair bone defects created in rat femurs. They observed the formation of new bone with higher mineral density in the rats.

The thermally-induced phase separation (TIPS) method is a desirable technique for the fabrication of bone scaffolds with interconnected pores. The basis of this process is the use of a change in thermal energy to convert the thermodynamically homogeneous polymer solution into polymer- and solvent-rich phases. Finally, a porous structure with interconnected pores is fabricated by extracting the solvent (18). Scaffolds with different morphologies can be obtained by controlling various parameters of the TIPS method, such as polymer type, solvent type, polymer concentration, temperature, and solvent or non-solvent ratio (8).

The present study aims to fabricate a novel scaffold and release system for sustained release of RSV. For this purpose, we intend to fabricate a PCL-gelatin composite scaffold that contains different concentrations of RSV using the TIPS method and evaluate the role of various RSV concentrations on the physical, mechanical, and cell behaviour properties of these scaffolds. Our results can provide an acceptable platform for BTE research.

## Materials and Methods

In this experimental study, the chemicals used for the fabrication of the scaffolds included: PCL (mw: 80 000 g/mol, Sigma-Aldrich Company, St. Louis, MO, USA), gelatin type B (mw: 180.155 g/mol, DNA Biotech Company, Tehran, Iran), and 1,4-dioxane (mw: 88.11 g/mol, DNA Biotech Company, Tehran, Iran).

The Ethical Committee of Shahrood University of Medical Sciences, Shahrood, Iran approved this research (IR.SHMU.REC.1401.078).

### Scaffold preparation

The TIPS method was used to fabricate the scaffolds. For this purpose, we prepared a 5% (W/V) solution of PCL in 1,4-dioxane. Gelatin powder (25% W/W PCL) was added to the above solution. The resultant solution was stirred for 24 hours and sonicated for 20 minutes. Then, this homogenous solution was divided into six equal parts, and we separately added various amounts of RSV powder (0 mg/10 ml, 0.1 mg/10 ml, 0.5 mg/10 ml, 2.5 mg/10 ml, 12.5 mg/10 ml, and 62.5 mg/10 ml) to the solution. The solutions were stirred for 4 hours. In order to perform an optimal phase separation, the above solutions were flash-frozen below the dioxane freezing point in a nitrogen tank, stored at -80°C for 24 hours, and then freeze-dried for 48 hours to form porous scaffolds by solvent sublimation.

### Scaffold characterization

#### Fourier transform infrared spectroscopy analysis

Functional groups or surface chemical bonds on the scaffolds and the stability of RSV during the fabrication process were analysed using Fourier transform infrared (FTIR) spectroscopy. For this purpose, an FTIR



spectrophotometer (WQF-510A, Rayleigh, China) was used at a wavelength range of 1000–4000  $\text{cm}^{-1}$ .

### Scanning electron microscope

The KYKY Technology scanning electron microscope (SEM, Beijing, China) was used to evaluate scaffold morphology. A coating of gold was applied on the scaffolds using a sputter cutter for 90 seconds at a current of 18 mA. Then, the samples were observed by SEM with an accelerating voltage of 18 kV. At least 20 random measurements and their frequencies in each SEM image were checked by the ImageJ software (National Institutes of Health, Bethesda, MD, USA) to determine the pore size.

### Porosity assessment

The scaffolds were immersed in 10 ml of ethanol. Scaffold porosity was calculated using the liquid displacement method and the following equation:

$$\text{porosity} = (v_1 - v_3) / (v_2 - v_3) \times 100$$

Where  $V_1$  is the initial volume of absolute ethanol,  $V_2$  is the volume of ethanol after immersing the scaffold, and  $V_3$  is the remaining volume of ethanol after removing the scaffold. Each scaffold was evaluated in triplicate (18).

### Weight loss assessment

The biodegradability of the scaffolds was evaluated by measuring their weight loss after 30 days. Scaffolds that had the same dimension (1  $\text{cm}^3$ ) were weighed and immersed in 10 ml of phosphate-buffered saline (PBS) at 37°C. Then, at specified time points, the scaffolds were extracted from the PBS, dried, and weighed. The amount of weight loss was calculated using the following equation:

$$\text{Weight-loss (\%)} = (w_1 - w_2) / w_1 \times 100$$

Where  $W_1$  is the initial weight of the sample, and  $W_2$  is their dry weight after extraction from PBS. The average values of three samples were considered for each group (19).

### Wettability evaluation

A static contact angle measuring device (KRÜSS GmbH, Germany) was used to determine the wettability of the scaffolds. The average water contact angle values were recorded using deionized water (sessile drop method) in three parts of each scaffold after 10 seconds at room temperature (6).

### Assessment of pH changes

Different scaffolds with the same weights were immersed in simulated body fluid (SBF) at 37°C and pH=7.4 for one month. The pH of the solution was measured at different time intervals (7, 14, 21, and 30 days) using a Mettler Toledo pH metre (Greifensee, Switzerland) (6).

### Hemocompatibility

Fresh human blood (2 ml) that contained the appropriate anticoagulant was diluted with normal saline (2.5 ml) to evaluate the blood compatibility of the scaffold. Three replications of each sample were placed in 96-well plate. Diluted blood (0.2 ml) was added to each well and the plate was placed in an incubator at 37°C for one hour. In the next step, the plate was centrifuged for 10 minutes at 1500  $\times g$ . The absorbance of the sample was measured at 545 nm using an Anthos Microplate Reader (Biochrom, Berlin, Germany) by transferring the supernatant to a different 96-well plate. Normal saline (4 ml) with diluted blood (0.2 ml) was used as the negative control. The positive control sample consisted of 4 ml of distilled water with 0.2 ml of diluted blood (20). The following equation was used to calculate hemolysis:

$$\text{Hemolysis \%} = (Dt - Dnc) / (Dpc - Dnc) \times 100$$

Where Dt, Dpc, and Dnc are the absorption of the sample, positive control, and negative control, respectively.

### Blood clotting index

The samples were cut into disk shapes and placed in beakers. Then, the beakers were placed in a 37°C water bath for one hour. Next, we added 100  $\mu\text{l}$  of blood that contained the anticoagulant to each sample. After five minutes, 20  $\mu\text{l}$  of 0.2 mol/l calcium chloride solution was added. After five minutes, 25 ml of distilled water was gently added to the samples. The samples were kept at 37°C for five minutes. Finally, their absorbance was measured at 545 nm. The control group included 100  $\mu\text{l}$  of blood along with 25 ml of distilled water (no sample). The blood clotting index (BCI) was calculated according to the following equation:

$$\text{BCI} = A_{\text{sample}} / A_{\text{control}} \times 100\%$$

Where  $A_{\text{sample}}$  is the absorbance value of each sample and  $A_{\text{control}}$  is the absorbance value of the control group (21).

### Compressive strength evaluation

The mechanical properties of the scaffolds were measured under dry and wet conditions at room temperature using a mechanical testing machine (Zwick Roell, Germany) with a 2N load cell and a speed of one mm/minute. The scaffolds were immersed in phosphate-buffered saline (PBS) for one hour to evaluate the mechanical properties under wet conditions. The samples were subjected to an increasing load until the strain reached 30%. The samples were cut into cylinders with a diameter and height of eight mm. Each test was repeated three times (22).

### In vitro release profile of rosuvastatin

We evaluated the RSV release profile by placing the scaffolds in 10 ml of SBF on a shaker located in an incubator at 37°C. At specific time points (1, 2, 3, 6,

12, 18, and 30 days), the supernatants were collected and the same volume of fresh SBF was added to the scaffolds. The concentration of RSV was measured using a UV spectrophotometer (Cole-Parmer UV/Visible spectrophotometer, USA) at a wavelength of 240 nm (10).

### MTT assay

The direct MTT test was used to evaluate the cytotoxicity of the scaffolds. The scaffolds were sterilized by ultraviolet radiation at 254 nm (20 minutes on each side). Human umbilical cord mesenchymal stem cells (HUC-MSCs) were isolated from umbilical cord blood bags according to a previous study procedure (23) and used for this experiment. We placed the sterile scaffolds (with three replicates) in 96-well plate and then added  $1 \times 10^4$  cells to each well. The cells were incubated for 24 and 72 hours at 37°C. The MTT solution in PBS (5 mg/ml) was added to each well at a specific time point and the plates were incubated at 37°C for 4 hours. A total of 150  $\mu$ l of DMSO was added to each well to dissolve the formazan. Again, the plate was placed in a shaker incubator (in the dark) at 37°C for 20 minutes. A microplate reader (Biochrom GmbH, Berlin, Germany) set at a wavelength of 570 nm was used to record the absorbance of the resultant solution in each well (10). The following formula was used to calculate the survival percentage:

$$\text{survival percentage} = \text{ODe} / \text{ODb} \times 100$$

Where ODe is the optical density of the sample, and ODb is the optical density of the blank.

### Alkaline phosphatase activity

ALP is a biochemical marker of osteoblasts that increases after osteogenic differentiation of HUC-MSCs (19). The scaffolds were sterilized with ultraviolet radiation at 254 nm (20 minutes on each side) and placed in 48-well plate. Then,  $10^4$  cells per well of HUC-MSCs were seeded on the scaffolds. The scaffolds were incubated in osteogenic medium (Bio Idea Company, Tehran, Iran) for 21 days. This medium includes dexamethasone, sodium pyruvate, beta glycerol phosphate, and ascorbic acid in Dulbecco's Modified Eagle's Medium-Low Glucose medium that contained foetal bovine serum. The cells were continuously checked and the medium was replaced. ALP activity was evaluated according to the manufacturer's instructions in the ALP kit (Delta. DP, Tehran, Iran). Briefly, on day 21, the scaffolds were washed twice with PBS and placed in 500  $\mu$ l TritonX-100 (1%) for 30 minutes at 37°C. The cell lysate was collected and centrifuged at  $3000 \times g$  at 4°C for 15 minutes. Then, 100  $\mu$ l of the supernatant was transferred to a new microtube and the ALP premix solution (4:1 ratio of A:B solution) was added. After one- and 30-minutes incubation at 37°C, the absorbance of each sample was measured by a microplate reader at 405 nm. The amount of total protein was measured by the Bicinchoninic Acid Assay kit (BCA, DNA Biotech, Tehran, Iran) according to the manufacturer's protocol. We placed 25  $\mu$ l of each sample in the wells of 96-well plate

(three duplications), and 75  $\mu$ l of reagent (1:49 copper reagent to BCA reagent) was added. The plate was slowly shaken and incubated at 60°C for 60 minutes. The plates were cooled to room temperature, and the absorbance was measured at 562 nm. ALP activity values were normalized in terms of total protein.

### Statistical analysis

GraphPad Prism software version 9 (GraphPad Software, Inc., USA) was used for statistical analysis. Data analysis was performed with one-way ANOVA, two-way ANOVA, and Tukey's post hoc test for different groups (with three repetitions).  $P < 0.05$  indicate statistical significance. Low variables are described with mean and standard deviation.

## Results

### Fourier transform infrared spectroscopy

Figure 1 shows the Fourier transform infrared spectroscopy (FTIR) spectra for the scaffolds. The PCL-Gelatin-0 mg/10 ml RSV scaffold (black spectra) revealed characteristic peaks of PCL and gelatin: a peak at 2956  $\text{cm}^{-1}$  ( $\text{CH}_2$  asymmetrical stretching), 2863  $\text{cm}^{-1}$  ( $\text{CH}_2$  symmetrical stretching), 1731  $\text{cm}^{-1}$  (carbonyl group), 1642  $\text{cm}^{-1}$  (amide I bond), and 1260-1400  $\text{cm}^{-1}$  (hydroxyl group). The addition of RSV revealed characteristic peaks at 3372  $\text{cm}^{-1}$  (hydroxyl stretching), 1554  $\text{cm}^{-1}$  (aromatic  $\text{c}=\text{c}$  stretching), and 1440 and 1370  $\text{cm}^{-1}$  (C-H bending) in the scaffolds that had various concentrations of RSV. This indicates the preservation of the RSV structure during the manufacturing process. The RSV bands became sharper with increasing concentrations of RSV. In addition, the position and intensity of the peaks also changed due to the hydrogen bond between the scaffold's components and RSV.

### Scanning electron microscope

Figure 2 shows SEM images of the scaffolds' cross-sections. The scaffolds had well-defined internal geometry, highly porous structure, and proper pore connectivity. The pore size of the scaffolds increased with increased RSV concentration, from  $34 \pm 4 \mu\text{m}$  in the PCL-Gelatin-0 mg/10 ml RSV scaffold to  $81 \pm 1.8 \mu\text{m}$  in the PCL-Gelatin-62.5 mg/10 ml RSV scaffold.

### Porosity assessment

Table 1 shows the percent of porosity of all the assessed scaffolds. The presence of the RSV did not cause any significant change in the percent of porosity of the scaffolds. In general, the scaffolds have sufficient porosity for the migration, growth, and proliferation of bone cells.

### Weight loss assessment

Figure 3A shows the results of the degradation rate of various scaffolds at 7, 14, 21, and 30 days. The results show an increase in degradation rate over time. In addition, increasing the concentration of RSV, which is hydrophilic, can increase the degradation rate. However, the lower concentrations of RSV did not have a significant effect on the degradation rate.

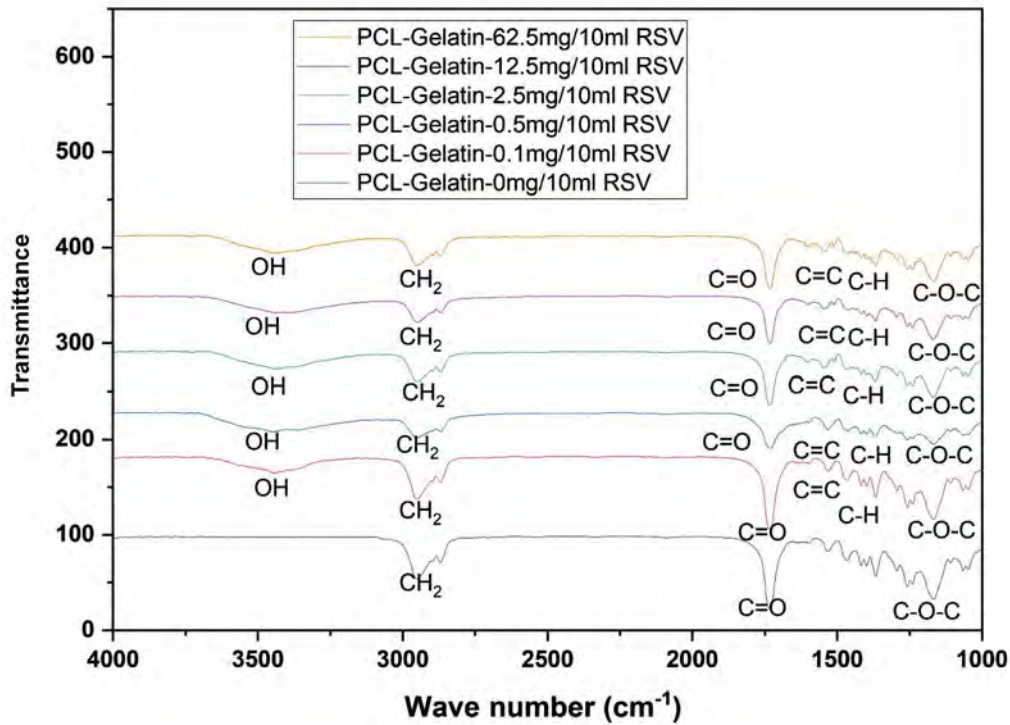


**Fig.1:** Functional groups or surface chemical bonds on the scaffolds. FTIR spectra of the PCL-Gelatin-0 mg/10 ml RSV (black spectra), PCL-Gelatin-0.1 mg/10 ml RSV (red spectra), PCL-Gelatin-0.5 mg/10 ml RSV (blue spectra), PCL-Gelatin-2.5 mg/10 ml RSV (green spectra), PCL-Gelatin-12.5 mg/10 ml RSV (purple spectra), and PCL-Gelatin-62.5 mg/10 ml RSV (orange spectra) scaffolds. The presence of gelatin, PCL, and the RSV functional groups indicates the stability of the components during the fabrication process. FTIR; Fourier transform infrared spectroscopy, PCL; Polycaprolactone, and RSV; Rosuvastatin.

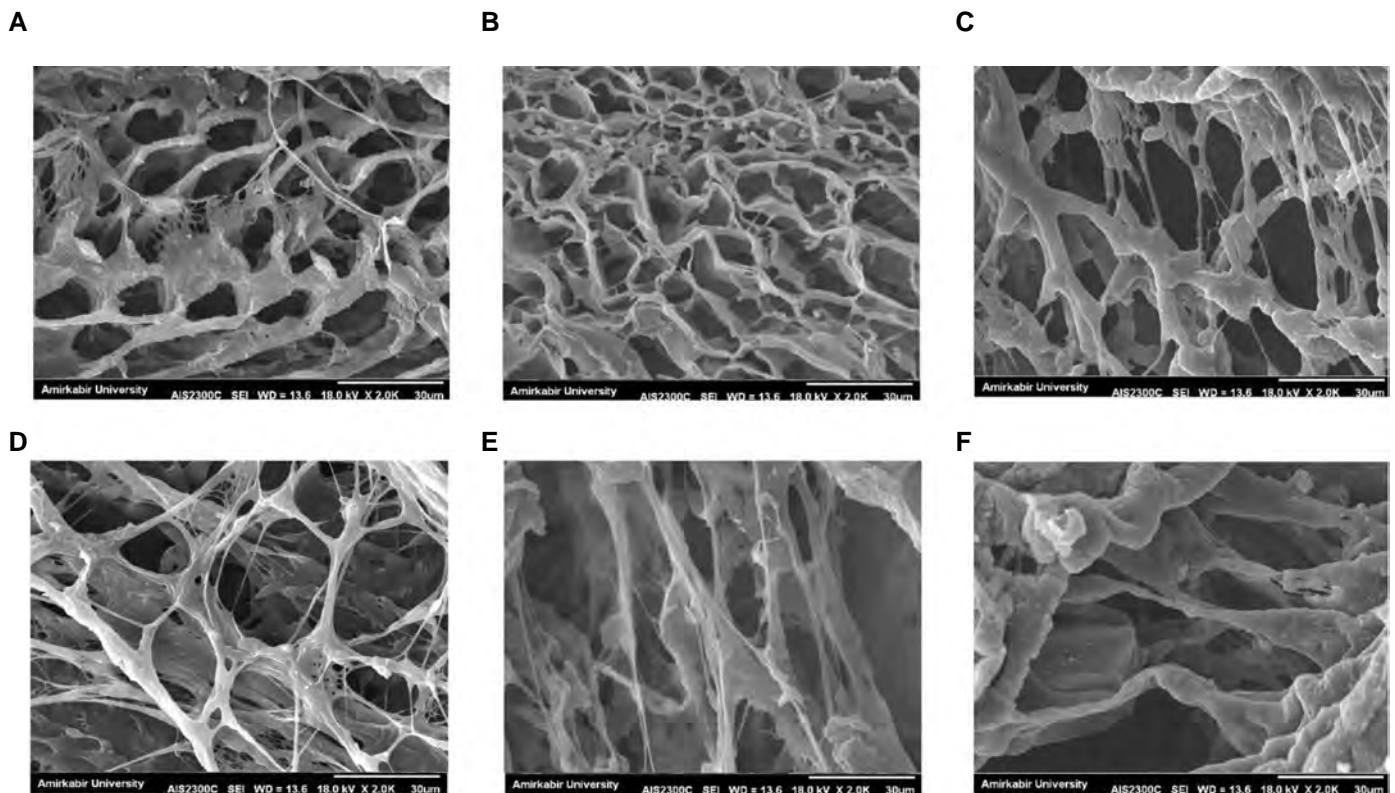


**Fig.2:** Morphological evaluation of scaffolds. **A.** SEM images of the PCL-Gelatin-0 mg/10 ml RSV, **B.** PCL-Gelatin-0.1 mg/10 ml RSV, **C.** PCL-Gelatin-0.5 mg/10 ml RSV, **D.** PCL-Gelatin-2.5 mg/10 ml RSV, **E.** PCL-Gelatin-12.5 mg/10 ml RSV, and **F.** PCL-Gelatin-62.5 mg/10 ml RSV scaffolds. Increases in the RSV concentration cause an increase in pore size. SEM; Scanning electron microscope, PCL; Polycaprolactone, and RSV; Rosuvastatin.

**Table 1:** Physical characteristics of the scaffolds

Sample	Porosity (%)	Compressive strength	Young's modulus	Compressive strength	Young's modulus	Pore size ( $\mu\text{m}$ )
		Dry (MPa)	Dry (MPa)	Wet (MPa)	Wet (MPa)	
PCL-Gelatin-0 mg/10 ml RSV	78 $\pm$ 1.4	5.8 $\pm$ 0.34	5.33 $\pm$ 1.5	5.68 $\pm$ 0.47	4.9 $\pm$ 0.98	34 $\pm$ 4
PCL-Gelatin-0.1 mg/10 ml RSV	78 $\pm$ 3.2	6.19 $\pm$ 1.35	5.39 $\pm$ 0.89	6.01 $\pm$ 0.14	4.9 $\pm$ 0.37	34.12 $\pm$ 2.1
PCL-Gelatin-0.5 mg/10 ml RSV	78 $\pm$ 6.7	6.72 $\pm$ 0.97	7 $\pm$ 0.2	6.34 $\pm$ 0.67	6.1 $\pm$ 1.21	37.92 $\pm$ 0.35
PCL-Gelatin-2.5 mg/10 ml RSV	79 $\pm$ 0.3	11.23 $\pm$ 0.47	10.22 $\pm$ 2.63	10.34 $\pm$ 1.02	9.76 $\pm$ 0.9	46 $\pm$ 5.4
PCL-Gelatin-12.5 mg/10 ml RSV	79 $\pm$ 0.87	14.264 $\pm$ 2.1	18.37 $\pm$ 0.95	12.02 $\pm$ 2.12	17.03 $\pm$ 0.81	62.11 $\pm$ 2.78
PCL-Gelatin-62.5 mg/10 ml RSV	79 $\pm$ 2.2	16.342 $\pm$ 1.79	24 $\pm$ 0.14	13.86 $\pm$ 2.62	22.73 $\pm$ 0.15	81 $\pm$ 1.8

Data are presented as mean  $\pm$  SD. PCL; Polycaprolactone and RSV; Rosuvastatin.

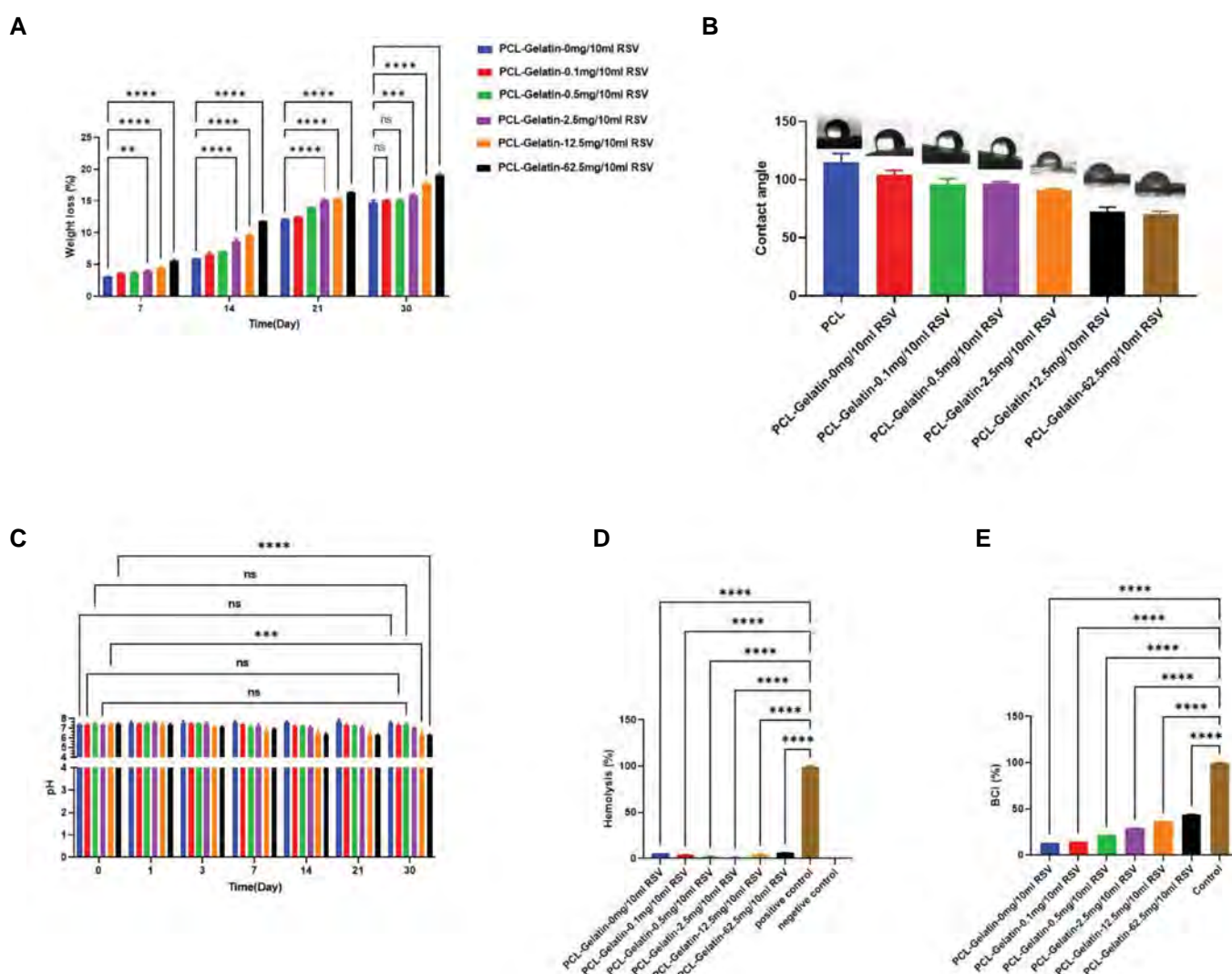


**Fig.3:** Evaluation of RSV effect on various properties of scaffolds. **A.** Evaluation of the scaffold degradation rate after 7, 14, 21, and 30 days. **B.** The contact angle of the PCL-gelatin scaffolds that contain different concentrations of RSV. **C.** pH changes of aqueous media in contact with the scaffolds after 7, 14, 21, and 30 days. **D.** Hemolysis percent and **E.** BCI of the scaffolds (mean  $\pm$  standard deviation, \*\*,  $P < 0.05$ , \*\*\*,  $P < 0.001$ , and \*\*\*\*,  $P < 0.0001$ ). RSV improved the degradation rate, wettability, and hemocompatibility of the scaffolds in a concentration-dependent manner. PCL; Polycaprolactone, RSV; Rosuvastatin, and BCI; Blood clotting index.

### Wettability evaluation

As shown in Figure 3B, the addition of gelatin (as a hydrophilic component) to PCL decreased its contact angle from 118 to 101.7 degrees. In addition, the addition of RSV to the PCL-gelatin scaffold also reduced the contact angle in a concentration-dependent manner so that the PCL-Gelatin-62.5 mg/10 ml RSV scaffold had a contact angle equal to 70.2 degrees.

### Assessment of pH changes

Figure 3C shows the pH changes of the aqueous medium (SBF) in contact with the scaffold after 7, 14, 21, and 30 days. More rapid pH changes occurred during the first two weeks, followed by a decreased rate of change. RSV acidified the pH of the environment, and this opposed the alkaline nature of gelatin.

### Hemocompatibility

Figure 3D shows the hemolysis percent of the scaffolds. The hemolysis percent of all groups was significantly lower than the positive control, which indicated their hemocompatibility. The addition of up to 2.5 mg/10 ml RSV decreased hemolysis from 5.47 to 1.43%, which improved the hemocompatibility of the scaffolds. Higher amounts of RSV decreased the hemocompatibility.

### Blood clotting index

Figure 3E shows the coagulation effect of the scaffolds according to the BCI. A lower BCI indicates a better coagulation effect and a faster coagulation rate. The drug-free scaffold had a BCI of 13.11. The addition of RSV (up to 62.5 mg/10 ml) increased this value to 43.8.

### Compressive strength

The stress-strain curve and mechanical properties of the scaffolds are presented in Figure 4A and Table 1, respectively. Our results indicated that the RSV had a positive effect on the compressive strength of the scaffolds under both dry and wet conditions. The compressive strength increased from  $5.8 \pm 0.34$  MPa for the PCL-Gelatin-0 mg/10 ml RSV scaffold to  $16.342 \pm 1.79$  MPa for the PCL-Gelatin-62.5 mg/10 ml scaffold.

### In vitro release profile of rosuvastatin

Figure 4B shows the RSV-release profile of the PCL-Gelatin-62.5 mg/10 ml RSV and PCL-Gelatin-2.5 mg/10 ml RSV scaffolds at 1, 2, 3, 6, 12, 18, and 30 days. According to the graph, there was a continuous release of RSV from the scaffold for 30 days; only  $37 \pm 0.68\%$  (62.5 mg/10 ml RSV) and  $31.68 \pm 1.02\%$  (2.5 mg/10 ml RSV) of the drug was released during this period. The scaffolds had a burst release during the first 12 days, which was related to the drug released in the surface pores of the scaffold. After that, the release continued gradually

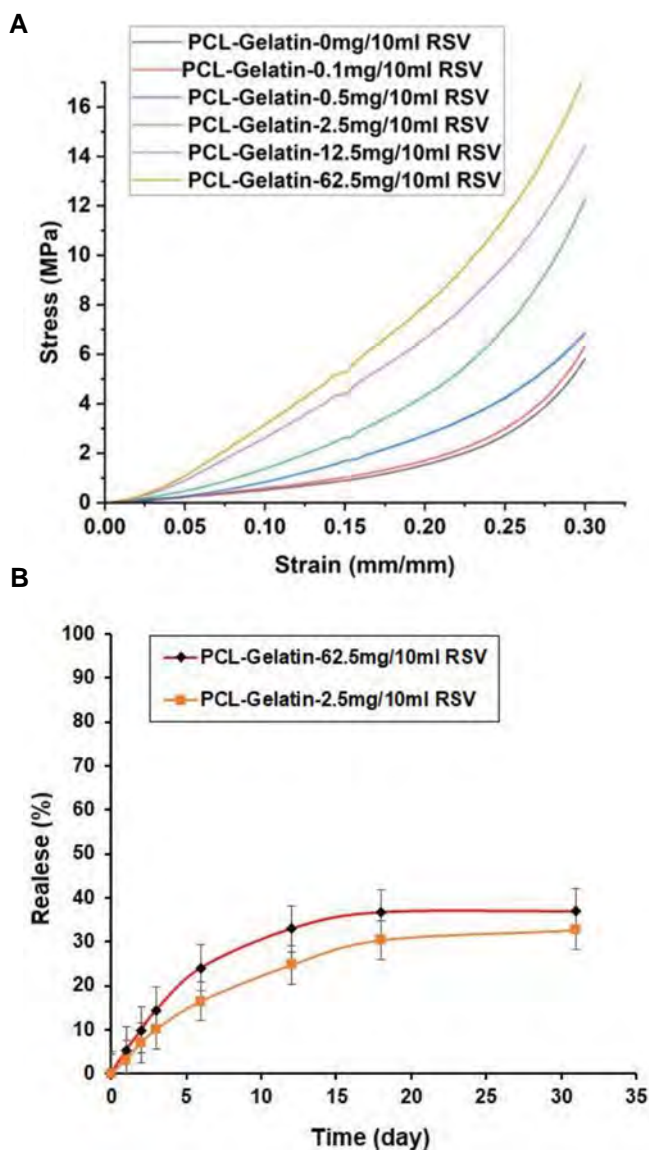


**Fig.4:** Evaluation of RSV effect on various properties of scaffolds. **A.** Stress-strain curves of the PCL-Gelatin-0 mg/10 ml RSV (black spectra), PCL-Gelatin-0.1 mg/10 ml RSV (red spectra), PCL-Gelatin-0.5 mg/10 ml RSV (blue spectra), PCL-Gelatin-2.5 mg/10 ml RSV (green spectra), PCL-Gelatin-12.5 mg/10 ml RSV (purple spectra), and PCL-Gelatin-62.5 mg/10 ml RSV (orange spectra) scaffolds under dry conditions indicate a positive effect of RSV on compressive strength. **B.** RSV release profile from the PCL-Gelatin-62.5 mg/10 ml RSV and PCL-Gelatin-2.5 mg/10 ml RSV scaffold within 30 days indicate sustained release of RSV (n=3). RSV: Rosuvastatin and PCL: Polycaprolactone.

We evaluated the data using different formulas and mathematical models related to each kinetic (zero-order, first-order, and Higuchi). Our results indicated that the kinetics of drug release was attributed to the zero-order model, in which the amount of RSV released at a certain time ( $Q_t$ ) is calculated based on the initial amount of RSV in the solution ( $Q_0$ ) according to the following equation:

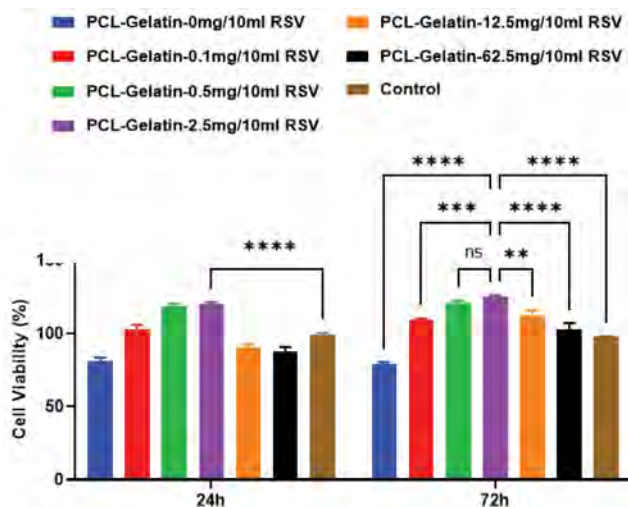
$$Q_t = Q_0 + k_0 t$$

Where  $k_0$  is a rate constant. Zero-order kinetics results indicated that a constant amount of drug was released from the surface of the scaffold per unit of time. The release graph shows a straight line with a positive slope.

## MTT assay

The cytotoxicity effect of these scaffolds on the survival of HUC-MSCs is shown in Figure 5A. We noted that increasing the amount of RSV to 2.5 mg/10 ml resulted in an increase in cell survival rate after 24 and 72 hours compared to the scaffolds without drugs. However, the 12.5 mg/10 ml and 62.5 mg/10 ml concentrations of RSV slightly reduced cell survival.

A



B

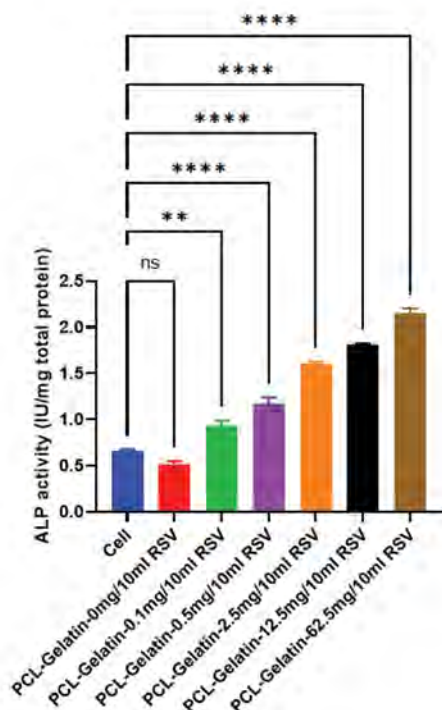


**Fig.5:** Evaluation of RSV effect on biological properties of scaffolds. **A.** Cell viability assay of HUC-MSCs cultured on the scaffolds after 24 and 72 hours. **B.** ALP activity of MSCs after 21 days of culture with PCL-gelatin scaffolds that contain different concentrations of RSV (mean  $\pm$  standard deviation, \*\*,  $P < 0.05$ , \*\*\*,  $P < 0.001$ , and \*\*\*\*,  $P < 0.0001$ ). RSV improves the ALP activity of scaffolds in a concentration-dependent manner. MSCs; Mesenchymal stem cells, PCL; Polycaprolactone, RSV; Rosuvastatin, and ALP; Alkaline phosphatase.

## Alkaline phosphatase activity

We evaluated the ALP activity to determine the osteogenic differentiation ability of the scaffolds that contained RSV. Figure 5B showed more ALP activity in the scaffolds that contained RSV compared to those without RSV and the sample without scaffold. Increasing RSV from 0.1 mg/10 ml to 62.5 mg/10 ml caused an approximately five-fold increase in ALP activity. RSV significantly increased osteogenic differentiation of the HUC-MSCs.

## Discussion

The present study evaluated the PCL-gelatin-RSV scaffolds for use as a valuable tool for bone defect regeneration. We used the TIPS method to fabricate PCL-gelatin scaffolds that had different concentrations of RSV to assess the role of RSV in these scaffold characteristics.

RSV is a second-generation statin with seven to eight times the effectiveness of simvastatin and few side effects. It improves BMP-2 expression, ALP activity and bone formation, and delays osteoblastic apoptosis (17, 24). However, the primary metabolism of RSV in the liver has reduced its bioavailability after oral administration to less than 20%, and this does not have a good effect on osteogenesis. High doses of RSV cause an inflammatory response, cytotoxicity, and slow bone regeneration (11). Therefore, the preparation of suitable carriers for local administration of RSV can help to improve its performance, reduce side effects, and reduce the required dose.

In the present study, we used a PCL-gelatin composite as an RSV carrier for bone defect regeneration to take advantage of the positive effect of both components on bone tissue regeneration and ECM simulation. PCL is an inexpensive polymer with favourable mechanical properties of bone tissue, which is not desirable for use alone due to its hydrophobicity and low decomposition rate (7). Therefore, we used the PCL-gelatin combination to improve cell attachment and cell infiltration into the scaffold (more than 100  $\mu$ m), create structures similar to trabecular bone, increase angiogenesis, and differentiate pre-osteoblast cells (8).

SEM images showed that the scaffolds had optimal interconnectivity and pore size to assist nutrient exchange, remove metabolites, and migrate bone cells. These scaffolds had about 78-79% porosity, which was in the range for cancellous bone (75-85%) and allowed the trabeculae matrix to penetrate the scaffold (25). The compressive strengths of the scaffolds were  $5.8 \pm 0.34$  to  $16.342 \pm 1.79$  MPa, which is in the optimal range for cancellous bone (1.5-45 MPa) and could prevent irritations and environmental damage (26).

The results of the drug release profile showed that only  $31.68 \pm 0.1\%$  of the drug was released from the PCL-Gelatin-2.5 mg/10 ml RSV scaffold after 30 days, which indicated the potential of this system for slow,

local release of RSV. Therefore, these scaffolds could help bone regeneration during this period by making available a sufficient amount of RSV to the cells in the defect area. The resulting scaffolds had interconnected pores and uniform pore size, which made it possible to control degradation rate, porosity, pH changes, and pore size by changing the ratio of the components (PCL-gelatin) (6). The scaffolds created a desirable tool for the continuous release of RSV; however, previous studies did not achieve this release profile. Monjo et al. (13) used a resorbable collagen sponge impregnated with RSV, which was fixed in the defect by a titanium implant in order to repair bone defects in rabbit tibia. The collagen sponges released 82.5% of the drug in only 24 hours, which caused toxicity and reduced bone volume at higher doses and caused insufficient drug availability to the healing cells during the treatment period. The high concentrations of released RSV caused an excessive increase in BMP-2 expression and accelerated bone turnover, which did not leave enough time for bone mineralisation. Ibrahim and Fahmy (17) used polyelectrolyte sponges that consisted of chitosan-xanthan gum, polycarbophil, Carbopol®, and sodium alginate as a carrier for RSV to repair bone defects in rat femurs. They reported the release of 80% RSV from this carrier within eight hours.

We performed a cytotoxicity test to determine the biological effectiveness and optimal concentration of RSV loaded in the PCL-gelatin scaffolds because of the slow-release rate of RSV from these scaffolds. The results showed that the slow-release profile of RSV and its beneficial effects resulted in cell survival after 72 hours. However, concentrations above 2.5 mg/10 ml decreased cell survival. High concentrations of RSV prevent cholesterol production, which is an essential element for the maintenance of cell membrane integrity (16). Previous studies have shown that statins stimulate a cellular response and osteointegration, and their release kinetics can affect osteoblast differentiation (15). In agreement with our results, other groups have reported that concentrations of RSV greater than 10  $\mu$ M reduced cell survival (24).

In addition, our results showed that ALP activity in the HUC-MSCs increased with increasing RSV concentration, which confirmed the findings of previous studies (13). In their study, Monjo et al. (13) removed the collagen sponge from the rabbit tibia to examine ALP activity in the wound fluid. The results showed that the increase in RSV concentration increased ALP activity. Since the chemical composition and biological abilities of the scaffold affect cell behaviour, it can be stated that increasing the amount of RSV by improving the wettability of the scaffold would increase cell adhesion and differentiation (27). In addition, increasing the amount of RSV leads to improvements in the mechanical performance and stiffness of the scaffold, which facilitates osteogenic differentiation (28). In addition, RSV uses the Wnt/ $\beta$ -catenin pathway for osteogenic differentiation of bone marrow-MSCs (in osteoporotic rats), which results in increased ALP activity.

RSV reduces the breakdown of  $\beta$ -catenin, increases its accumulation in cells, and stimulates the proliferation of osteoblasts (29). High ALP activity indicates early mineralisation and remodelling of bone tissue, and it decreases with the cessation of bone matrix deposition and mineralisation in mature osteocytes.

The results of the weight loss analysis indicate that the hydrophilic nature of RSV enables more water to penetrate the scaffold and increase hydrolysis (30). After one month, 62.5 mg/10 ml RSV increased the rate of scaffold degradation from  $14.5 \pm 0.68\%$  to  $19.8 \pm 1.37\%$ . The scaffold degradation rate should be proportional to the bone regeneration rate (three months) and pure PCL has a degradation rate of 1.4% within 28 days (31), which may inhibit bone growth. Therefore, the presence of RSV could improve and impact the scaffold degradation rate.

The contact angle (wettability) of the scaffold is a critical parameter that determines the interaction of the scaffold with cells and proteins. According to previous studies, PCL has a high contact angle of about 118 degrees. Our results show that the addition of both gelatin and RSV, two hydrophilic components, to this scaffold helps to improve the contact angle and reduce the scaffold contact angles to 70.2 degrees, which enhances the cell-scaffold interaction.

Our evaluation of pH changes in this study showed the effect of the residues released from the scaffold during degradation on the surrounding environment. If these changes are excessive, they cannot be adjusted by the cells and result in toxicity (32). Our results showed drastic changes in pH in the first two weeks due to the release of di-hydroxy monocarboxylic acid (RSV) present in the surface pores. The presence of RSV partially neutralized the alkaline nature of the gelatin. During the initial days of bone mineralization, the accumulation of acidic metabolites results in a decrease in the pH of the tissue to less than normal serum. Then, with the precipitation of minerals and increasing calcium, the pH becomes more alkaline (33). By taking into consideration the essential role of tissue pH in bone repair and mineralisation, the residues released from the scaffold should not cause severe pH changes. In addition to its biocompatibility and favourable degradation rate, the scaffold that contained 2.5 mg/10 ml RSV also had small pH changes, which made it acceptable for bone tissue repair.

The amount of hemoglobin in the samples indicates the degree of red blood cell (RBC) membrane destruction. The hemolysis percent has an inverse relationship with the level of the scaffold's hemocompatibility. Generally, hemolysis up to 5% is acceptable for scaffolds (34). Previous studies have shown that statins can cause acute hemolysis, but RSV does not lead to hemolysis due to its structural difference with other statins (Atorvastatin and Lovastatin) (35). This is compatible with our results that showed a decrease in hemolysis with the addition of up to 2.5 mg/10 ml RSV. However, our results showed that higher amounts of RSV could increase hemolysis. The

cholesterol content of the RBC membrane is a factor that determines the mechanics of RBCs and the behaviour of their membranes. Statins can affect the cholesterol content of the RBC membrane, and their high amounts cause cell membrane rupture and increase hemolysis. In the case of atorvastatin, it has been proven that this statin can soften RBCs and increase the risk of hemolysis due to its shape and charge (36).

Blood coagulation on the implanted scaffold is one of the critical parameters in tissue regeneration. In damaged bone repair, the clot creates a temporary matrix that helps with cell absorption, migration, and bone repair. Blood clots induce maturation, differentiation, and repair of bone tissue (37). Our results show that high concentrations of RSV can reduce the rate of clot formation. Statins, as a weak anticoagulant factor, cause downregulation of the coagulation cascade and reduce the expressions of tissue factors and thrombin production. By inhibiting HMG-CoA reductase, they disrupt the coagulation reactions by this enzyme and activate the protein C anticoagulant pathway (38). However, the presence of PCL-gelatin moderates its effect to some extent by controlling the drug release rate and its coagulation properties. Tran (39) showed that the blood cells penetrated the PCL scaffold and caused clot strengthening. Furthermore, the new bone is also formed from the edge of the defect towards the centre of the scaffold, which shows the role of clot guidance. In total, the BCI index of the scaffolds that contained the highest concentration of RSV was 57% lower compared to the control group, which indicated that the scaffolds increased the blood coagulation rate, but low concentrations of RSV could be more effective.

## Conclusion

This study evaluated the properties of PCL-gelatin scaffolds with different concentrations of RSV on bone healing. Our results show that the RSV had a dose-dependent positive effect on hydrophilicity, pore size, porosity, mechanical properties, weight loss, and hemocompatibility. The PCL-Gelatin-2.5 mg/10 ml RSV scaffolds have the best characteristics for BTE. The PCL-gelatin combination provides a favourable release system for RSV and greater bioavailability than free RSV.

## Acknowledgements

This article was extracted from a Ph.D. dissertation and it was supported by grant no. 14010015 (Shahroud University of Medical Sciences). We sincerely thank Dr. Amir Atashi for supplying the MSCs for this research. There is no conflict of interest in this study.

## Authors' Contributions

M.Gh.; Conceptualization, Formal analysis, Visualization, Resources, and Writing-original draft. M.A.; Conceptualization, Supervision, Investigation methodology, and Writing-original draft. M.K.F.; Resources, Investigation, and Writing-original draft.

M.S.; Conceptualization, Investigation, Methodology, Project administration, Supervision, and Writing-original draft. All of the authors have read and approved the paper for publication.




## References

1. Ranjbarnejad F, Khazaei M, Shahryari A, Khazaei F, Rezakhani L. Recent advances in gene therapy for bone tissue engineering. *J Tissue Eng Regen Med*. 2022; 16(12): 1121-1137.
2. Murugan S, Parcha SR. Fabrication techniques involved in developing the composite scaffolds PCL/HA nanoparticles for bone tissue engineering applications. *J Mater Sci Mater Med*. 2021; 32(8): 93.
3. Gharibshahian M, Salehi M, Beheshtizadeh N, Kamalabadi-Farahani M, Atashi A, Nourbakhsh MS, et al. Recent advances on 3D-printed PCL-based composite scaffolds for bone tissue engineering. *Front Bioeng Biotechnol*. 2023; 11: 1168504.
4. Jang JW, Min KE, Kim C, Shin J, Lee J, Yi S. Scaffold characteristics, fabrication methods, and biomaterials for the bone tissue engineering. *Int J Precis Eng Manuf*. 2023; 24(3): 511-529.
5. Malikmammadov E, Tanir TE, Kiziltay A, Hasirci N. Preparation and characterization of poly( $\epsilon$ -caprolactone) scaffolds modified with cell-loaded fibrin gel. *Int J Biol Macromol*. 2019; 125: 683-689.
6. Hashemi SF, Mehrabi M, Ehterami A, Gharravi AM, Bitaraf FS, Salehi M. In-vitro and in-vivo studies of PLA/PCL/gelatin composite scaffold containing ascorbic acid for bone regeneration. *J Drug Deliv Sci Technol*. 2021; 61(4): 102077.
7. Ren K, Wang Y, Sun T, Yue W, Zhang H. Electrospun PCL/gelatin composite nanofiber structures for effective guided bone regeneration membranes. *Mater Sci Eng C*. 2017; 78: 324-332.
8. Sultana N, Hassan MI, Ridzuan N, Ibrahim Z, Soon CF. Fabrication of gelatin scaffolds using thermally induced phase separation technique. *Int J Eng*. 2018; 31(8): 1302-1307.
9. Wang CY, Hong PD, Wang DH, Cherng JH, Chang SJ, Liu CC, et al. Polymeric gelatin scaffolds affect mesenchymal stem cell differentiation and its diverse applications in tissue engineering. *Int J Mol Sci*. 2020; 21(22): 8632.
10. Akbari V, Rezazadeh M, Ebrahimi Z. Comparison the effects of chitosan and hyaluronic acid-based thermally sensitive hydrogels containing rosuvastatin on human osteoblast-like MG-63 cells. *Res Pharm Sci*. 2020; 15(1): 97-106.
11. Türer A, Coşkun Türer Ç, Durmuşlar MC, Ballı U, Önger ME. The influence of oral administration of rosuvastatin on calvarial bone healing in rats. *J Craniomaxillofac Surg*. 2016; 44(9): 1327-1332.
12. Türer A, Türer ÇÇ, Ballı U, Durmuşlar MC, Önger ME, Çelik HH. Effect of local rosuvastatin administration on calvarial bone defects. *J Craniofac Surg*. 2016; 27(8): 2036-2040.
13. Monjo M, Rubert M, Wohlfahrt JC, Rønold HJ, Ellingsen JE, Lyngstadaas SP. In vivo performance of absorbable collagen sponges with rosuvastatin in critical-size cortical bone defects. *Acta Biomater*. 2010; 6(4): 1405-1412.
14. Fan CH, Hao Y, Liu YH, Li XL, Huang ZH, Luo Y, et al. Anti-inflammatory effects of rosuvastatin treatment on coronary artery ectasia patients of different age groups. *BMC Cardiovasc Disord*. 2020; 20(1): 330.
15. Rezazadeh M, Parandeh M, Akbari V, Ebrahimi Z, Taheri A. Incorporation of rosuvastatin-loaded chitosan/chondroitin sulfate nanoparticles into a thermosensitive hydrogel for bone tissue engineering: preparation, characterization, and cellular behavior. *Pharm Dev Technol*. 2019; 24(3): 357-367.
16. Kalani MM, Nourmohammadi J, Negahdari B. Osteogenic potential of Rosuvastatin immobilized on silk fibroin nanofibers using argon plasma treatment. *Biomed Mater*. 2018 Dec 7; 14(2):025002.
17. Ibrahim HK, Fahmy RH. Localized rosuvastatin via implantable bioerodible sponge and its potential role in augmenting bone healing and regeneration. *Drug Deliv*. 2016; 23(9): 3181-3192.
18. Ehterami A, Abbaszadeh-Goudarzi G, Haghi-Daredeh S, Niyakan M, Alizadeh M, JafariSani M, et al. Bone tissue engineering using 3-D polycaprolactone/gelatin nanofibrous scaffold containing berberine: In vivo and in vitro study. *Polym Adv Technol*. 2022; 33(2): 672-681.
19. Kang YG, Wei J, Kim JE, Wu YR, Lee EJ, Su J, et al. Characterization and osteogenic evaluation of mesoporous magnesium-calcium silicate/polycaprolactone/polybutylene succinate composite scaffolds fabricated by rapid prototyping. *RSC Adv*. 2018; 8(59): 33882-33892.
20. Chi Perera CJ, Castillo Baas MG, Alcocer Lara GA, Ramos Borges



- SI, Rodríguez Guzmán AL, Fernández Cervantes I, et al. Characterization and hemocompatibility assessment of porous composite scaffolds with a biomimetic human clavicle macrostructure. *Health Technol.* 2020; 10: 423-428.
21. Zhang D, Hu Z, Zhang L, Lu S, Liang F, Li S. Chitosan-based thermo-sensitive hydrogel loading oyster peptides for hemostasis application. *Materials.* 2020; 13(21): 5038.
  22. Park HJ, Lee OJ, Lee MC, Moon BM, Ju HW, Lee Jm, et al. Fabrication of 3D porous silk scaffolds by particulate (salt/sucrose) leaching for bone tissue reconstruction. *Int J Biol Macromol.* 2015; 78: 215-223.
  23. Ajami M, Soleimani M, Abroun S, Atashi A. Comparison of cord blood CD34+stem cell expansion in coculture with mesenchymal stem cells overexpressing SDF-1 and soluble /membrane isoforms of SCF. *J Cell Biochem.* 2019; 120(9): 15297-15309.
  24. Monjo M, Rubert M, Ellingsen JE, Lyngstadaas SP. Rosuvastatin promotes osteoblast differentiation and regulates SLCO1A1 transporter gene expression in MC3T3-E1 cells. *Cell Physiol Biochem.* 2010; 26(4-5): 647-656.
  25. Novitskaya E, Chen PY, Lee S, Castro-Ceseña A, Hirata G, Lubarda VA, et al. Anisotropy in the compressive mechanical properties of bovine cortical bone and the mineral and protein constituents. *Acta Biomater.* 2011; 7(8): 3170-3177.
  26. Ait Said H, Noukrati H, Oudadesse H, Ben Youcef H, Lefevre B, Hakkou R, et al. Formulation and characterization of hydroxyapatite-based composite with enhanced compressive strength and controlled antibiotic release. *J Biomed Mater Res A.* 2021; 109(10): 1942-1954.
  27. Ghasemi-Mobarakeh L, Prabhakaran MP, Tian L, Shamirzaei-Jeshvaghani E, Dehghani L, Ramakrishna S. Structural properties of scaffolds: Crucial parameters towards stem cells differentiation. *World J Stem Cells.* 2015; 7(4): 728-744.
  28. Wang S, Hashemi S, Stratton S, Arinze TL. The effect of physical cues of biomaterial scaffolds on stem cell behavior. *Adv Healthc Mater.* 2021; 10(3): e2001244.
  29. Wang BX, Li KP, Yu T, Feng HY. Rosuvastatin promotes osteogenic differentiation of mesenchymal stem cells in the rat model of osteoporosis by the Wnt/ $\beta$ -catenin signal. *Eur Rev Med Pharmacol Sci.* 2019; 23(22): 10161-10168.
  30. Stewart SA, Domínguez-Robles J, McIlorum VJ, Gonzalez Z, Utomo E, Mancuso E, et al. Poly(caprolactone)-based coatings on 3D-printed biodegradable implants: a novel strategy to prolong delivery of hydrophilic drugs. *Mol Pharm.* 2020; 17(9): 3487-3500.
  31. Wu F, Wei J, Liu C, O'Neill B, Ngothai Y. Fabrication and properties of porous scaffold of zein/PCL biocomposite for bone tissue engineering. *Compos B Eng.* 2012; 43(5): 2192-2197.
  32. Sung HJ, Meredith C, Johnson C, Galis ZS. The effect of scaffold degradation rate on three-dimensional cell growth and angiogenesis. *Biomaterials.* 2004; 25(26): 5735-5742.
  33. Berkmann JC, Herrera Martin AX, Ellinghaus A, Schlundt C, Schell H, Lippens E, et al. Early pH changes in musculoskeletal tissues upon injury-aerobic catabolic pathway activity linked to inter-individual differences in local pH. *Int J Mol Sci.* 2020; 21(7): 2513.
  34. Archana D, Singh BK, Dutta J, Dutta PK. In vivo evaluation of chitosan-PVP-titanium dioxide nanocomposite as wound dressing material. *Carbohydr Polym.* 2013; 95(1): 530-539.
  35. Moghadasi M, Maghsoomi Z. Statins can lead to acute hemolysis. *Cardiovasc Hematol Agents Med Chem.* 2018; 16(2): 123.
  36. Sheikh-Hasani V, Babaei M, Azadbakht A, Pazoki-Toroudi H, Mashaghi A, Moosavi-Movahedi AA, et al. Atorvastatin treatment softens human red blood cells: an optical tweezers study. *Biomed Opt Express.* 2018; 9(3): 1256-1261.
  37. Milillo L, Cinone F, Lo Presti F, Lauritano D, Petrucci M. The role of blood clot in guided bone regeneration: biological considerations and clinical applications with titanium foil. *Materials (Basel).* 2021; 14(21): 6642.
  38. Stępień K, Siudut J, Koniecznyńska M, Nowak K, Zalewski J, Undas A. Effect of high-dose statin therapy on coagulation factors: Lowering of factor XI as a modifier of fibrin clot properties in coronary artery disease. *Vascul Pharmacol.* 2023; 149: 107153.
  39. Tran PA. Blood clots and tissue regeneration of 3D printed dual scale porous polymeric scaffolds. *Mater Lett.* 2021; 285: 129184.

# Effects of Streptozotocin Induced Diabetes on One-Carbon Cycle and Sperm Function

Farnaz Pouriayevali, D.V.M.<sup>1</sup>, Marziyeh Tavalaei, Ph.D.<sup>1\*</sup> , Fatemeh Kazeminasab, Ph.D.<sup>2</sup>,  
Maurizio Dattilo, Ph.D.<sup>3\*</sup> , Mohammad Hossein Nasr-Esfahani, Ph.D.<sup>1\*</sup> 

1. Department of Animal Biotechnology, Reproductive Biomedicine Research Center, Royan Institute for Biotechnology, Isfahan, Iran
2. Department of Physical Education and Sport Sciences, Faculty of Humanities, University of Kashan, Kashan, Iran
3. Parthenogen, R&D Department, Lugano, Switzerland

## Abstract

**Objective:** Diabetic men suffer an increased risk of infertility associated with signs of oxidative damage and decreased methylation in sperm pointing to a deficit of the one-carbon cycle (1CC). We aimed to investigate this deficit using mice models (type 1 and 2) of streptozotocin-induced diabetes.

**Materials and Methods:** In this experimental study, 50 male mice, aged eight weeks, were divided randomly into four groups: sham, control, type 1 diabetes mellitus (DM1), and DM2. The DM1 group was fed a normal diet (ND) for eight weeks, followed by five consecutive days of intraperitoneal administration of Streptozotocin (STZ, 50 mg/kg body weight). The DM2 group was fed a high-fat diet (HFD) for eight weeks, followed by a single intraperitoneal injection of STZ (100 mg/kg). After twelve weeks, all the mice were euthanized, and study parameters assessed. In the sham group, citrate buffer as an STZ solvent was injected.

**Results:** Both types of diabetic animals had serious impairment of spermatogenesis backed by increased DNA damage ( $P=0.000$ ) and decreased chromatin methylation (percent:  $P=0.019$ ; intensity:  $P=0.001$ ) and maturation ( $P=0.000$ ). The 1CC was deeply disturbed with increased homocysteine ( $P=0.000$ ) and decreased availability of carbon units [methionine ( $P=0.000$ ), serine ( $P=0.088$ ), folate ( $P=0.016$ ), B12 ( $P=0.025$ )] to feed methylations.

**Conclusion:** We have observed a distinct impairment of 1CC within the testes of individuals with diabetes. We speculate that this impairment may be linked to inadequate intracellular glucose and diminished carbon unit supply associated with diabetes. As a result, interventions focusing on enhancing glucose uptake into sperm cells and providing supplementary methyl donors have the potential to improve fertility issues in diabetic patients. However, additional clinical testing is required to validate these hypotheses.

**Keywords:** Chromatin, Diabetes, Glucose, Methylations, Spermatogenesis

**Citation:** Pouriayevali, F, Tavalaei M, Kazeminasab F, Dattilo M, Nasr-Esfahani MH. Effects of streptozotocin induced diabetes on one-carbon cycle and sperm function. Cell J. 2024; 26(1): 81-90. doi: 10.22074/CELLJ.2023.2010652.1399

This open-access article has been published under the terms of the Creative Commons Attribution Non-Commercial 3.0 (CC BY-NC 3.0).

## Introduction

Diabetes is a chronic metabolic disorder characterized by high blood sugar levels, resulting from impaired insulin secretion and/or action. There are three main types of diabetes: type 1, type 2, and gestational diabetes. Type 1 diabetes is an autoimmune disease in which the immune system attacks and destroys insulin-producing beta cells in the pancreas, leading to insulin deficiency. Type 2 diabetes is a metabolic disorder characterized by the pancreas being unable to secrete adequate insulin due to the development of insulin resistance (1). There is a well-established association with oxidative stress in the context of diabetes, characterized by an imbalance between the production of reactive oxygen species (ROS) and the body's antioxidant defense mechanisms. This imbalance

in oxidative homeostasis can contribute significantly to the development and progression of diabetes-related complications. Hence, maintaining a harmonious equilibrium between ROS generation and elimination, known as redox homeostasis, is crucial for cellular functionality and overall health. Disturbances in redox homeostasis, such as oxidative stress and reductive stress, can lead to heightened levels of ROS, resulting in cellular damage and compromised physiological function (2-4). Previous studies have shown a correlation between all types of diabetes and increased ROS, which can damage cellular proteins, lipids, DNA, and ultimately, cell death (4, 5). Additionally, excessive ROS can directly disrupt the insulin signaling pathway and hinder glucose uptakes in peripheral tissues, such as adipose tissue and muscles

Received: 02/September/2023, Revised: 25/November/2023, Accepted: 23/December/2023

\*Corresponding Addresses: P.O.Box: 8165131378, Department of Animal Biotechnology, Reproductive Biomedicine Research Center, Royan Institute for Biotechnology, Isfahan, Iran  
Parthenogen, R&D Department, Lugano, Switzerland  
Emails: m.tavalaei@royan-rc.ac.ir, maurizio.dattilo@parthenogen.ch, mh.nasr-esfahani@royaninstitute.org



Royan Institute  
Cell Journal (Yakhteh)

(6, 7), in part mediated by the release of inflammatory cytokines like tumor necrosis factor-alpha (TNF- $\alpha$ ).

The one-carbon cycle (1CC) is a crucial metabolic cycle playing a vital role in maintaining the cellular redox state. This metabolic pathway, responsible for the synthesis and metabolism of various biomolecules such as amino acids, nucleotides, and lipids, is a complex network of interconnected reactions and necessitates adequate availability of several enzymes, cofactors, and vitamins, including folate, vitamin B12, and betaine, to ensure proper functioning (8, 9). The 1CC plays a vital role in generating the antioxidant glutathione protecting cells from oxidative damage (10). Briefly, the 1CC product S-adenosylmethionine (SAM), besides acting as the universal methyl donor for DNA methylation and other cellular processes, is also the activator of cystathionine beta-synthase (CBS), the regulating enzyme for de-novo Glutathione (GSH) synthesis (11). In turn, oxidative damages can hamper DNA methylation, making the 1CC a pivotal pathway connecting epigenetic programming and redox regulation (9, 12).

Previous studies have demonstrated that infertile men exhibit lower levels of sperm DNA methylation, increased oxidative stress, and elevated DNA damage compared to fertile men (13, 14). Dattilo et al. (15) further emphasized that impaired DNA methylation and/or the oxidation of methyl imprints could result in abnormal sperm chromatin condensation. The disruption of redox homeostasis and DNA methylation, which are characteristic of sperm damage in both clinical and experimental diabetes (16), may also be influenced by disturbances in the 1CC. In this study, we aimed to investigate the involvement of the 1CC in male reproductive impairments using a mouse model of both type 1 and type 2 diabetes.

## Material and Methods

### Ethical committee approval

This experimental study was conducted in compliance with ARRIVE guidelines (17) and received approval from the Scientific Ethics Committee of Royan Institute (IR.ACECR.ROYAN.REC.1399.072). The mice used in the study were housed at the Royan Institute for Animal Biotechnology in Isfahan, Iran.

### Study design

A total of 50 male C57 mice (8-week-old, 25-30 g) were housed in special cages under normal light conditions with a 12-hour light-dark cycle, a temperature of  $23 \pm 1^\circ\text{C}$ , and a moisture level of 45-60%. The mice were provided with ad libitum access to pellet rodent diet and water throughout the study. The entire study was conducted by a single person. After a one-week acclimatization period, the mice were randomly assigned to one of four groups: sham (n=10), control (n=10), type 1 diabetes mellitus (DM1, n=15), or DM2 (n=15). The allocation to each group was done randomly.

The sham group received a normal diet (ND) and a single intraperitoneal (i.p) injection of sodium citrate buffer dissolved in double distilled water (1.47 g/kg in double distilled water, pH=4.5) after 8 weeks from the start of the study. The control group was fed an ND without any injection. The DM1 group was fed an ND for 8 weeks and then intraperitoneally administered Streptozotocin (STZ, Sigma-Aldrich, St Louis, MO) dissolved in citrate buffer (pH=4.5) at a dose of 50 mg/kg body weight (b.w.) for 5 consecutive days. Afterwards, the mice were fed an ND for 4 weeks. The DM2 group was fed a high-fat diet (HFD-60% kcal from fat) for 8 weeks and then received a single intraperitoneal injection of STZ (100 mg/kg, dissolved in 0.1 M sodium citrate buffer). The mice were then fed an HFD for 4 weeks.

After twelve weeks from the start of the study, a glucose tolerance test (GTT) was performed in all groups to confirm diabetes induction. Subsequently, all mice were euthanized, and blood samples collected via cardiac puncture. The serum was then separated from the blood and evaluated for sex hormone factors [luteinizing hormone (LH), follicle-stimulating hormone (FSH), and testosterone] as well as methionine, homocysteine, ferritin, and amino acids involved in the one-carbon cycle. The testes, epididymides, pancreas, liver, and kidneys were removed, dissected, and weighed. Testicular morphometric parameters, such as width, length, and thickness, were also measured. Furthermore, the testicular volume was calculated using the formula:  $\text{length} \times \text{width}^2 \times 0.52$  (18).

Portions of all organ tissues were fixed in 10% formalin solution and stained with hematoxylin and eosin (H&E) after preparing paraffin sections. The spermatogenesis process in the testicular tissue sections was evaluated based on three criteria: Johnson scores, tubular differentiation index (TDI), and spermatogenesis index (SPI) (19). The cauda epididymis was dissected and cut into small pieces. These pieces were incubated in VitaSperm washing medium (Inoclon, Iran) supplemented with 10% serum for 30 minutes at  $37^\circ\text{C}$ , and the extracted sperm was used to assess the study parameters.

### Glucose tolerance test

A GTT was performed by fasting the mice for 4-5 hours, followed by an intraperitoneal injection of 2 g/kg D-glucose in 30% phosphate-buffered saline (PBS). Blood glucose levels were measured at 0, 30, 60, 90, and 120 minutes after injection (20) using a glucometer (EASY Gluco Auto-coding TM).

### Serum analyses

To evaluate the main components of the 1CC and testosterone levels, high-performance liquid chromatography (HPLC) and ELISA techniques were used. All parameters were assessed by an expert in a clinical laboratory following standard procedures. ELISA kits (Elecsys 2010 and Cobas e411 analyzers) were used

to assess the levels of testosterone (Testosterone II, Roche, Switzerland), folate (Folate III, Roche, Switzerland), and vitamin B12 (Vitamin B12 II, Roche, Switzerland) by the manufacturer's protocol. The serum levels of methionine, homocysteine, serine, lysine, glycine, threonine, aspartic acid, and other factors were analyzed using HPLC. In addition, LH (Luteinizing hormone, Roche, Switzerland) and FSH (Follicle stimulating hormone, Roche, Switzerland) were evaluated by an ELISA kit (Elecysys 2010 and Cobas e 411 analysers).

### Assessment of sperm parameters, and sperm function

Briefly, sperm concentration and sperm motility were by evaluated using a sperm counting chamber (Sperm meter, Sperm Processor, Aurangabad, India), under a light microscope with 40x magnification. Sperm abnormal morphology was assessed through Eosin/Nigrosine staining. In addition, sperm functional tests were conducted including aniline blue staining to assess sperm retained histones, chromomycin A3 staining to determine protamine deficiency, acridine orange staining to evaluate sperm DNA damage, BODIPY C11 Probe to measure lipid peroxidation, and Dichloro-dihydro-fluorescein diacetate (DCFH-DA) to assess cytosolic ROS, based on the methodology described by Pouriayevali et al (21).

### Assessment of sperm chromatin maturation (protamine deficiency, and sperm persistent histones)

The assessment of excessive retained histones was conducted by using aniline blue staining, which selectively binds to lysine residues on histones. To perform the test, a smear of 20 microliters of extracted epididymal spermatozoa was air-dried and fixed for 2 hours in a 3% glutaraldehyde solution in 0.2 M phosphate buffer at pH=7.2. Subsequently, the prepared slides were dried and subjected to staining with a 5% aqueous solution of aniline blue in 4% acetic acid at pH=3.5 for 90 minutes. Under a light microscope (100x magnification, CX31 OLYMPUS, Japan), a random count of 200 spermatozoa was performed for each sample, and those exhibiting a dark blue stain were considered positive for aniline blue (AB+), indicating abnormal chromatin compaction (21).

The effectiveness of protamine substitution was evaluated using CMA3 staining competing with protamines for DNA binding. Briefly, extracted epididymal spermatozoa in PBS buffer (20 microliters) smeared on slides and fixed with Carnoy's solution (methanol/acetic acid, 3:1, Merck, Darmstadt, Germany) for 5 minutes at a temperature of -4°C. Subsequently, the slides stained with 100 µl of a 0.25 mg/ml chromomycin A3 solution (Sigma Chemical Co., St. Louis, USA) for 1 hour. Following staining, the slides washed twice with PBS, air-dried, and covered with a coverslip. A minimum of 200 spermatozoa on each slide were examined by using a fluorescent microscope (Olympus, BX51, Tokyo, Japan) equipped with the appropriate filters (460-470 nm). Spermatozoa displaying bright yellow staining (CMA3 positive or indicative of protamine deficiency) were recorded (21).

### Assessment of sperm DNA methylation

Sperm DNA methylation was evaluated by using a 5-methylcytosine (5-mc) antibody by flowcytometry. Briefly, two million sperm cells mixed with PBS, and fixed with 96% acetone-alcohol. The mixture then kept at 4°C for 30 minutes. After that, the samples were washed with PBS and centrifuged at 500 g for 5 minutes. The supernatant then discarded. In order to decondense the sperm head, a mixture of Triton x-100 and dithiothreitol (DTT) in PBS slowly added to the sperm pellet and the mixture kept in the dark room for 20 minutes. The samples were then washed with PBS and centrifuged at 500 g for 5 minutes.

To block non-specific binding, a solution of 6% normal goat serum (NGS+PBS) was added directly to each sample, and incubated at 25°C for 30 minutes. The samples were then centrifuged at 500 g for 5 minutes, and the primary antibody [5-methylcytosine Antibody (5-mc); Eurogentec; Belgium; Cat. No. BI-MECY-0100, 1:400] added to the sperm pellet in PBS containing 3% NGS and 0.1% Triton x-100 followed by overnight incubation at 4°C. On the following morning, the samples were incubated for one hour at 37°C, then washed and incubated in a darkroom with the secondary antibody (Goat Anti-Mouse IgG (H&L) FITC; Chemicon; USA; Cat. No. AP124F; Lot number: 0605029979) at a dilution of 1:200 for two hours. Afterwards, the samples were rinsed twice with PBS and analyzed using a flow cytometer (FACS Caliber; Becton Dickinson, San Jose, CA, USA). The same method was employed for the isotype control tube of each sample with an isotype antibody (Mouse IgG Negative Control Antibody; Chemicon; Japan; Cat. No. CBL600, 1:300) as the primary antibody. For each sample, the percentage and intensity of sperm DNA methylation was reported.

### Statistical analysis

Results were reported as mean ± standard error, and the significance between study groups was determined using Tukeys post hoc multiple comparison test, following a one-way analysis of variance. A P<0.05 was considered highly statistically significant.

## Results

### Confirmation of diabetic models

After a 12-hour fasting period, mice were injected intraperitoneally with 2 g/kg D-glucose in 30% PBS, and their glucose tolerance was tested at 0, 30, 60, 90, and 120 minutes. Figure 1 shows that the blood sugar levels in both type 1 and type 2 diabetic mice were higher than in the control and sham groups. The mean fasting blood sugar (FBS) was significantly higher in both the type 1 (DM1) and type 2 (DM2) diabetic groups compared to the control and sham groups (P<0.05). Thereafter, a significant difference was observed in diabetic mice at 60,

90, and 120 minutes compared to control and sham mice.

**Spermatogenesis indexes were reduced in the type 1, and type 2 diabetic mice in the testicular tissue**

We evaluated the spermatogenesis process in mice testis using the Johnsen score system, TDI, and SPI criteria, and compared the results within the control, sham, type 1, and

type 2 diabetic groups. As shown in Figure 2, the mean Johnsen score was significantly lower in type 1 and type 2 diabetic mice compared to the control ( $P=0.002$ ) whereas the means of TDI ( $P=0.001$ ) and SPI ( $P=0.007$ ) were significantly lower in type 1 and type 2 diabetic mice compared to both control and sham groups. We illustrated these results schematically in a section of the testicular tissue of all studied groups using H&E staining.

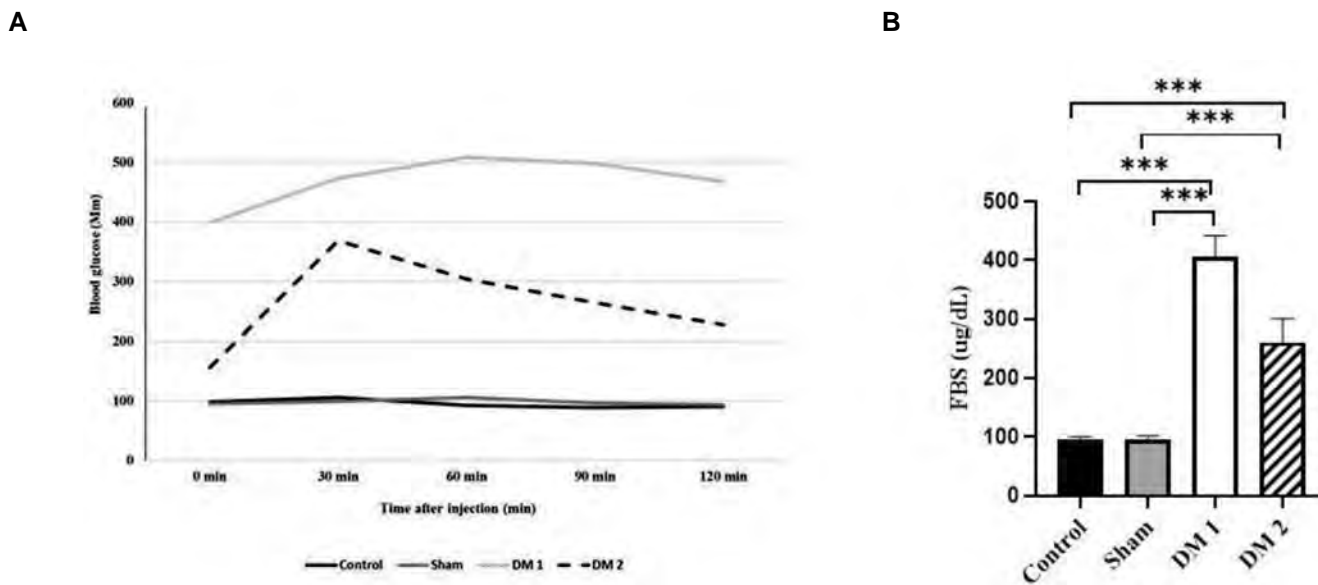


**Fig.1:** Assessment of glucose tolerance test (GTT) and fasting blood sugar (FBS) to confirm the type 1 and type 2 diabetic models. **A.** GTT was evaluated by intraperitoneally injecting 3% glucose at 0, 30, 60, 90, and 120 minutes. **B.** FBS was assessed in the control (n=10), sham (n=10), type 1 (DM1, n=15), and type 2 (DM2, n=15) diabetic groups. \*\*\*;  $P<0.001$ .

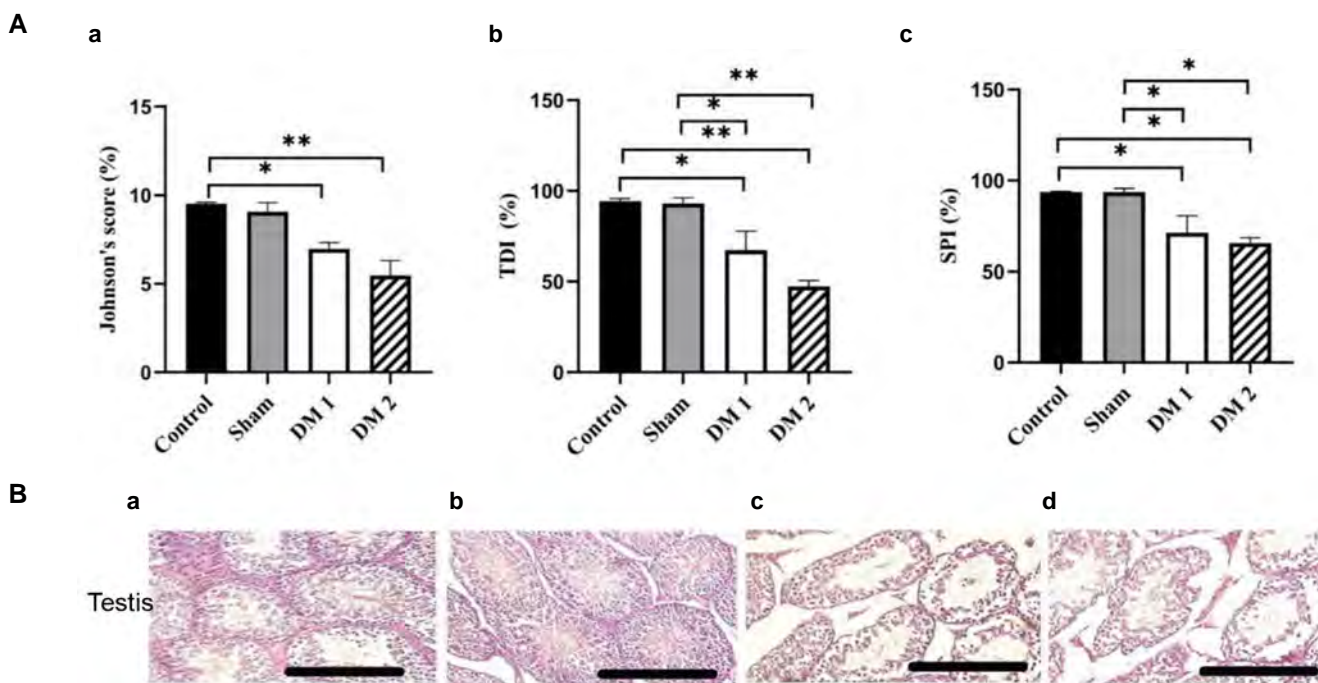


**Fig.2:** Assessment of testicular morphometric parameters in study groups. **A.** Comparison of spermatogenesis results using the Johnsen score system (a), Z tubular differentiation index (TDI, b), and spermatogenesis index (SPI, c) within the testicular tissues of control, sham, type 1 (DM1), and type 2 (DM2) diabetic mice. **B.** The pattern of these results was illustrated in the section prepared from the testicular tissue of each group using H&E staining (a-d, scale bar: 200  $\mu$ m). \*;  $P<0.05$  and \*\*;  $P<0.01$  [Sham (n=3), Control (n=3), DM1 (n=3), and DM2 (n=3)].

Body weight, and the weight of organs such as the liver, pancreas and kidneys reduced in the type 1, and type 2 diabetic mice.

As shown in Figure 3, the body weight was decreased in type 1 and type 2 diabetic groups compared to control and sham groups, but this decrease was significant only between type 1 diabetic mice and the control group (P=0.000). The weight of organs such as the liver (P=0.005), pancreas (P=0.000) and kidneys (left kidney: P=0.000; right kidney: P=0.001) were also significantly decreased compared to either controls or sham groups.

### Testicular weight reduced in the type 1, and type 2 diabetic mice

The mean testicular volume did not show any significant difference between the groups. However, the mean testicular weight was significantly lower in the diabetic groups compared to the control group. The epididymal fat, as shown in Figure 3, was significantly lower in the type 1 diabetic mice compared to controls (P<0.001) and sham (P<0.05) and to type 2 diabetes (P<0.001).

### The quality of sperm parameters and sperm function reduced in the type 1, and type 2 diabetic mice

Sperm parameters (Fig.4): Sperm concentration was significantly lower in type 1 and type 2 diabetic mice

compared to the control and sham groups (P=0.000). Sperm motility was not different among groups whereas we observed a significant reduction in the mean percentage of progressive motility in the type 1 and type 2 diabetic groups as well as in the sham group compared to the control group (P=0.017). Furthermore, there was a significant increase in the percentage of sperm abnormal morphology in type 1 and type 2 diabetic mice compared to the control group (P=0.003).

Sperm functional tests (Fig.4): The mean values of sperm lipid peroxidation and intracytoplasmic ROS were significantly higher in type 1 and type 2 diabetic groups compared to control and sham groups (P=0.000). In addition, the means of sperm DNA damage as well as sperm chromatin maturation (protamine deficiency, and sperm persistent histones) were significantly higher in type 1 and type 2 diabetic groups compared to the control and sham groups (P=0.000).

### The level of sex hormonal factors altered in the type 1, and type 2 diabetic mice

Unlike LH which only showed a significant decrease in type 2 diabetic mice compared to the control group (P=0.028), the mean levels of FSH (P=0.003) and testosterone (P=0.000) were significantly lower in both type 1 and 2 diabetic mice compared to the control and sham groups (Fig.5).

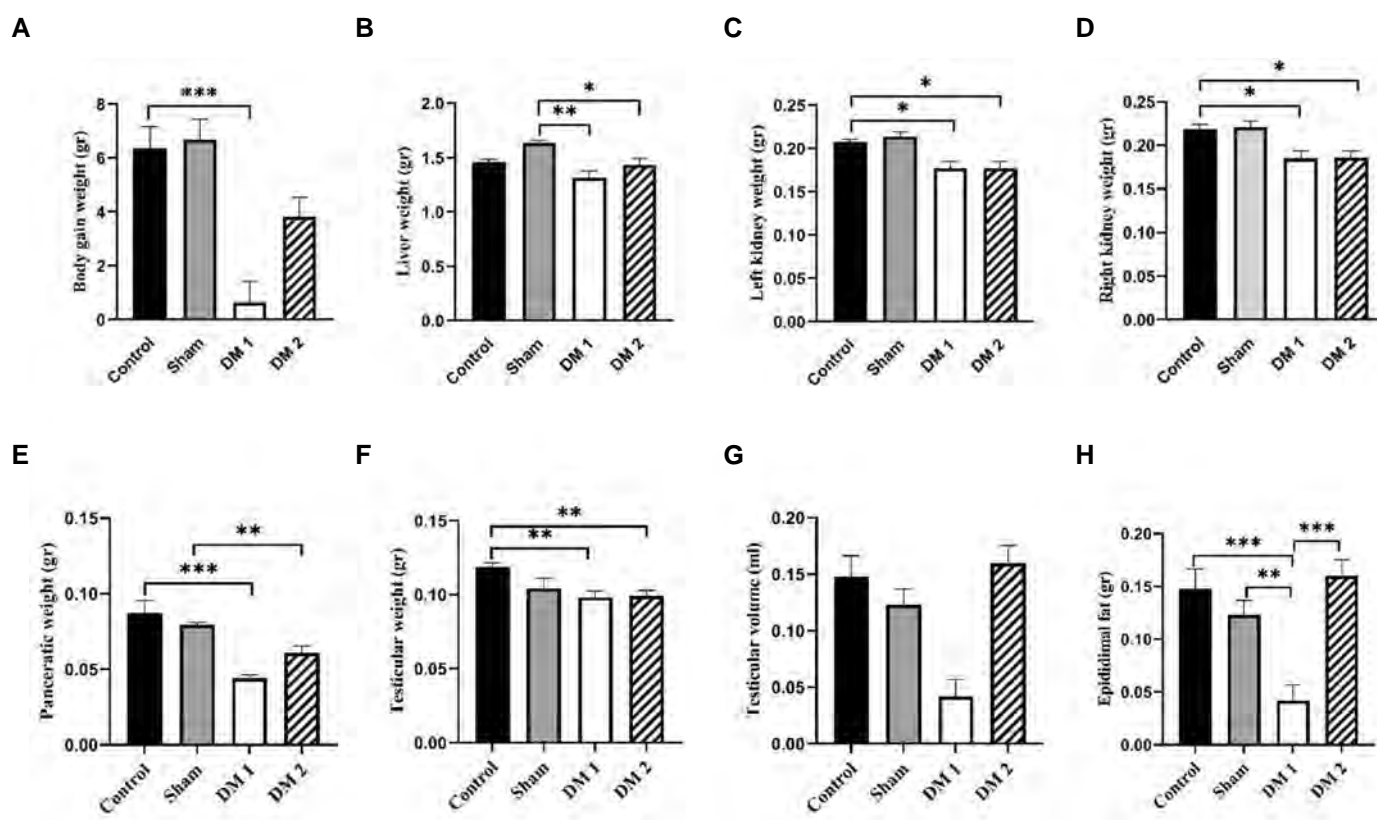


**Fig.3:** Comparison of body weight, and organs weight within groups. **A.** Body weight, **B.** Liver weight, **C, D.** Right and left kidney weight, **E.** Pancreas weight, **F.** Testicular weight, **G.** Testicular volume, and **H.** Epididymal fat. Control (n=10), Sham (n=10), Type 1 (DM1, n=15), and Type 2 (DM2, n=15) diabetic groups. \*, P<0.05, \*\*, P<0.01, and \*\*\*, P<0.001.

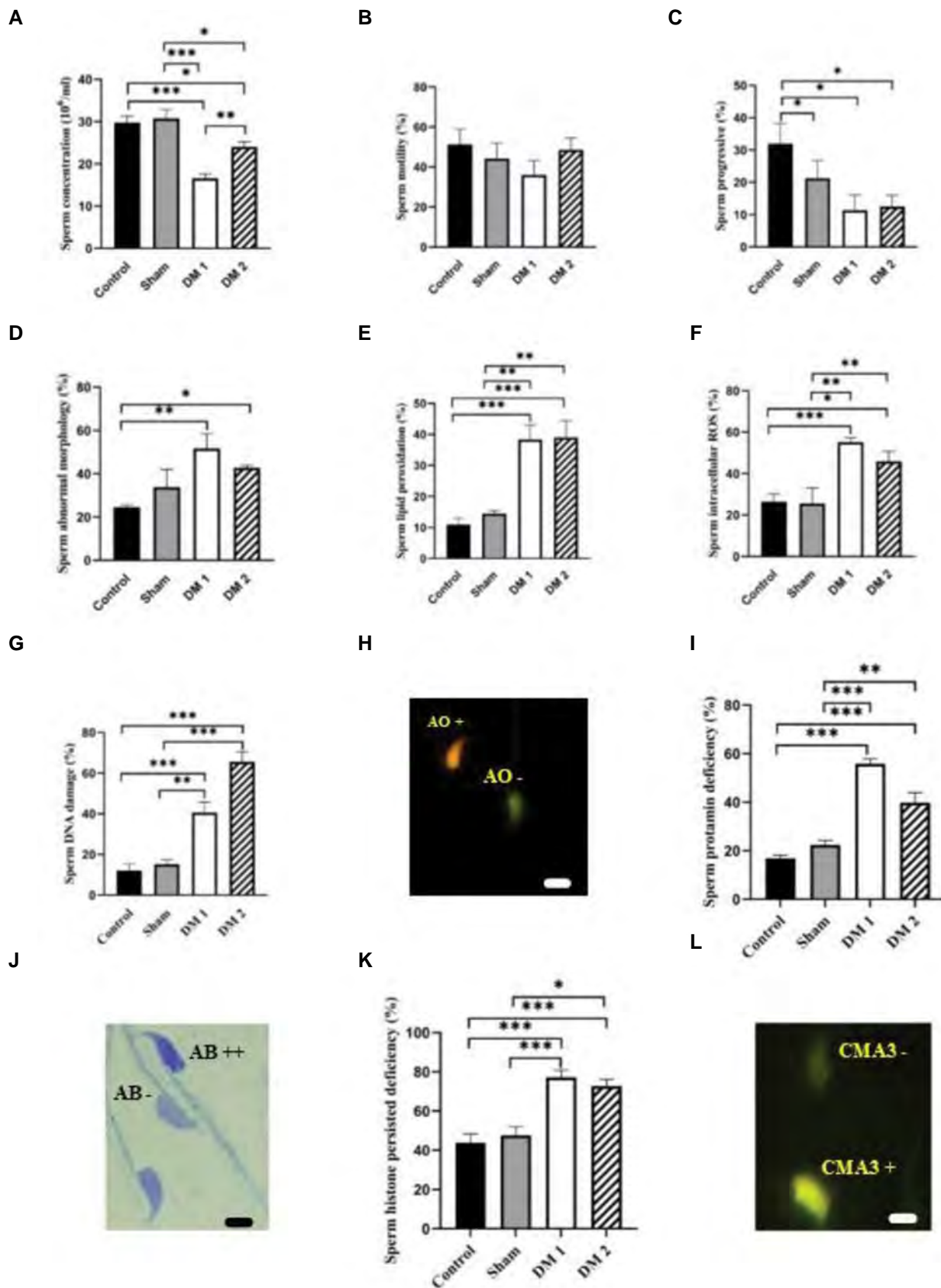


**Fig.4:** Comparison of sperm parameters and sperm functional tests within groups. **A-D.** Comparison of sperm parameters, and **E-L.** Sperm functional tests within the control, sham, type 1 (DM1), and 2 (DM2) diabetic groups. Sperm lipid peroxidation and sperm intracytoplasmic ROS were assessed by BODIPY and dichlorofluorescein diacetate (DCF-DA) staining, respectively by flow cytometry. In addition, sperm DNA damage, protamine deficiency, and sperm persistent histones were evaluated by acridine orange (orange and yellow sperm as DNA damaged sperm while green sperm were considered to have intact DNA), chromomycin A3 staining (CMA3 positive sperm as sperm with protamine deficient while negative sperms were ranked as sperm with normal protamine content), and aniline blue staining (depending on the intensity of the blue color, dark blue sperm have persistent histones, while pale blue sperm or colorless have a normal level of histone remaining in the sperm), respectively. \*,  $P < 0.05$ , \*\*,  $P < 0.01$ , and \*\*\*,  $P < 0.001$  [Sham (n=10), Control (n=10), DM1 (n=15), and DM2 (n=15) (scale bar: 50  $\mu$ m)].

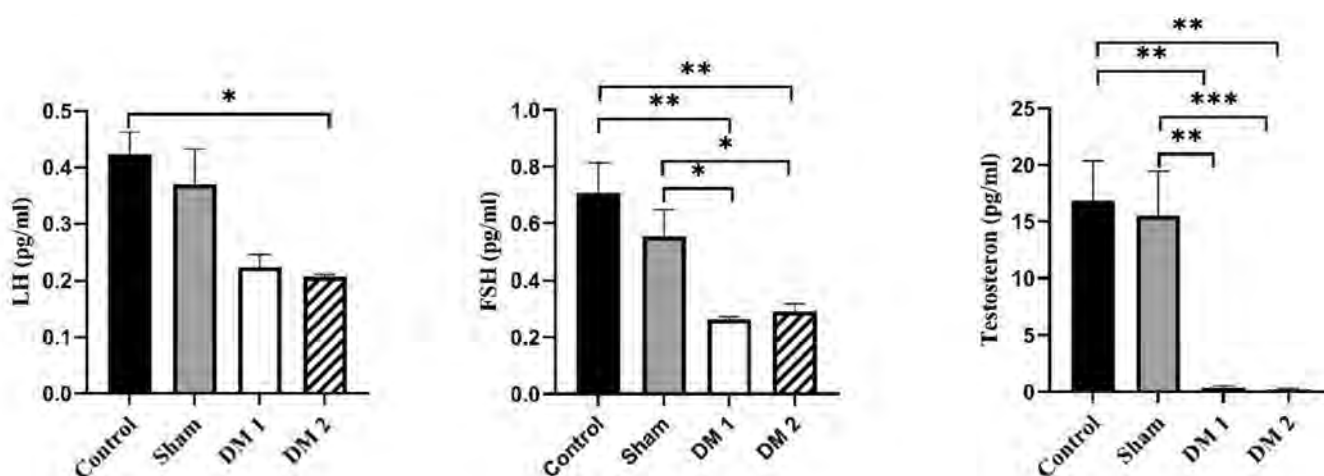
**The level of the main factors involved in the one-carbon cycle altered in the type 1, and type 2 diabetic mice**

The levels of the main factors involved in the 1CC such as methionine, homocysteine, serin, lysin, folate, ferritin, and vitamin B12 were compared among study groups. As shown in Figure 6, the mean serum levels of methionine were significantly lower in both type 1 and 2 diabetic groups compared to the control and sham groups (P=0.000). The mean levels of serum homocysteine and ferritin were significantly higher in both diabetic groups compared to the control and sham groups (P=0.000). Vitamin B12 was significantly lower only in the type 1 diabetic group compared to control and sham groups (P=0.025). Serum folate and serine were significantly reduced in the type

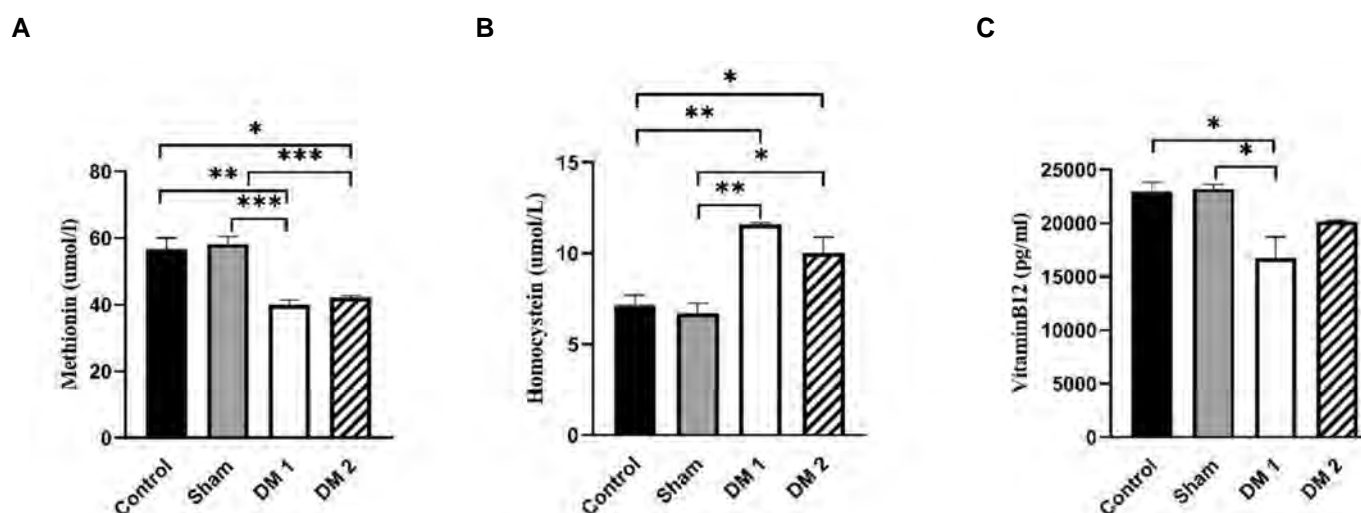
1 diabetic group when compared, respectively, to the control group (P=0.030) and the sham (P=0.048) group. Additionally, the mean levels of lysine were significantly lower in both diabetic groups compared to the sham group (P=0.006). Changes in other metabolites involved in the 1CC are reported in Fig.S1 (See Supplementary Online Information at [www.celljournal.org](http://www.celljournal.org)).

**Sperm DNA methylation was reduced in the type 1, and type 2 diabetic mice**

As illustrated in Figure 6, the mean percentages and intensities of sperm DNA methylation were significantly lower in both type 1 and 2 diabetic groups compared to the control and sham groups (P<0.001).



**Fig.5:** Comparison of serum sex hormonal factors (LH, FSH, and testosterone) among control (n=3), sham (n=3), type 1 (DM1, n=3), and 2 (DM2, n=3) diabetic groups. LH; Luteinizing hormone, FSH; Follicle-stimulating hormone, \*, P<0.05, \*\*, P<0.01, and \*\*\*, P<0.001.





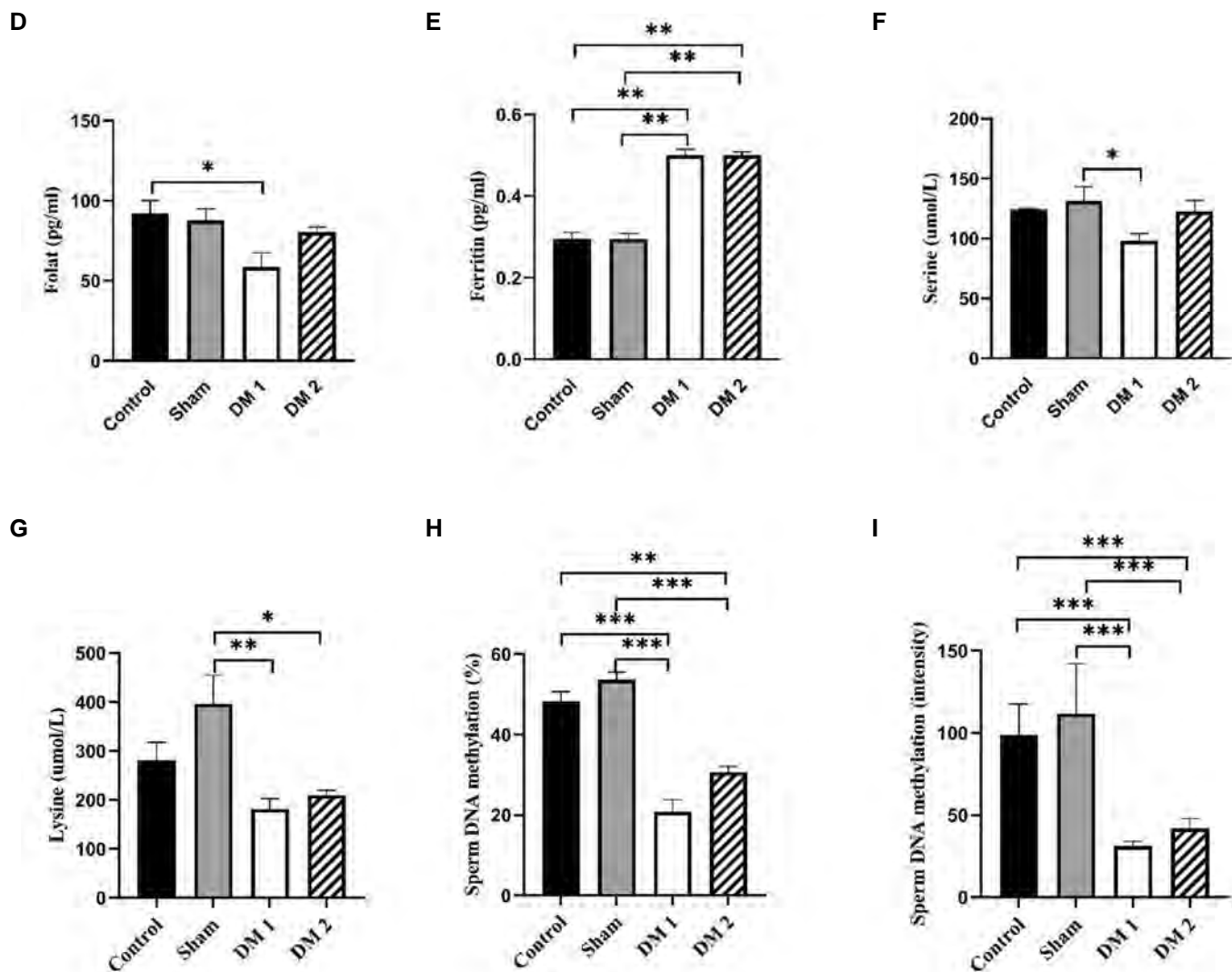


**Fig. 6:** Comparison of the main serum factors involved in One-carbon cycle, and sperm DNA methylation among the various study groups. **A.** Methionine, **B.** Homocysteine, **C.** Vitamin B12, **D.** Folate, **E.** Ferritin, **F.** Serine, **G.** Lysin, **H.** and **I.** Sperm DNA methylation. For assessment of folate, ferritin, serine, and lysine, we used three samples for each group while, for assessment of sperm DNA methylation (% and intensity), 10 samples were used for each of the control and sham groups and 15 samples were used for each of DM1, and DM2 groups. DM1; Diabetes mellitus type 1, DM2; Diabetes mellitus type 2, \*;  $P < 0.05$ , \*\*;  $P < 0.01$ , and \*\*\*;  $P < 0.001$ .

## Discussion

Diabetes has been shown to have adverse effects on male fertility, with diabetic men experiencing lower sperm quality and higher rates of infertility (22, 23) and such damage is linked to a perturbation of both redox homeostasis and DNA methylation (16). The above functions strictly depend on the correct functioning of the ICC, therefore we aimed to investigate the perturbations of the ICC using both type 1 and type 2 diabetes models in mice.

As already shown with similar models (24), both our type 1 and type 2 diabetes mice suffered testicular alterations, defective spermatogenesis and sperm motility, sperm oxidative damage, and defective nuclear maturation baked by a deep suppression of testosterone and FSH. These damages were associated in our animals with significantly increased ROS and oxidative damage to both lipids and

DNA together with defective DNA methylation, all pointing to an improper function of the ICC.

Accordingly, the ICC was deeply disturbed in our diabetic animals. In their serum we found a sharp increase of homocysteine, likely reflecting defective re-methylation to methionine, which was indeed decreased together with the other source of carbon units, serine, and with a discrete decrease of the methyl donors necessary for homocysteine re-methylation, folate and B12. Chen et al. (25), working on hepatic tissue samples, had already shown that STZ-induced diabetes is associated with deep perturbations of the ICC within the liver, therefore changes in liver metabolism might as well explain our findings in serum. However, the above ICC-defective metabolic fingerprint was associated in our animals with decreased sperm methylation, which is a strictly intra-testicular process, proving that the ICC defect occurred

directly within the testes. This might be dependent on the lower availability of folates and B12 in serum, however, their decrease was modest compared to very evident defects in sperm methylation, so a direct interference of streptozotocin diabetes with the ICC within the testicular metabolism was likely in place.

The derangement of the ICC in our animals is unlikely to depend on a direct effect of STZ. Indeed, we found ICC defect, i.e. lower DNA methylation, within the testes whereas STZ enters the cells via GLUT2 (26) and therefore affects tissues with a high density of GLUT2, like the pancreas and liver, which is not the case of testes that mostly rely on GLUT8 (27). More importantly, in STZ-induced diabetes, the administration of insulin reverts the increase of homocysteine (28), which points to a direct role of glucose in the impairment of the ICC. However, the sperm was shown to be very resistant to extra-cellular glycemia with no negative effects up to 50 millimolar D-glucose whereas the shortage of intracellular glucose was more likely to hamper (29).

Indeed, the specific importance of glucose for sperm metabolism and function is well known (30). Whether it is due to a lack of insulin (type 1) or defective insulin signaling (type 2), diabetes may have caused a defect in intracellular glucose in our mice. Within cells, besides being oxidized to produce energy, glucose can also be used by the serine synthesis pathway (SSP) to generate serine and thereafter methionine, at least in conditions of low methionine (31), thus feeding carbon units to the ICC. This would not happen in diabetes where intracellular glucose is in shortage and unlikely to feed the above pathway. Thus, the impairment of the ICC in our animals may directly depend on the shortage of intracellular glucose and the significant reduction of serum serine in our type 1 diabetes group seems to endorse this interpretation.

Whatever the mechanisms, the defect in methylations may easily explain the oxidative damage to the sperm of our diabetic animals. First, the defective homocysteine re-methylation leads to a shortage of SAM, necessary to activate GSH de novo synthesis (11) and antioxidant defences, which may explain the increase of ROS and the activation of lipoperoxidation. Second, the defect in methylation may cause histone retention and protamine defect (32), both reducing the efficacy of the protamine shield and thus increasing the exposure of sperm DNA to ROS insult explaining the increased DNA damage.

The present study reveals a significant difference in the mean levels of valine and glycine between mice with type 1 and type 2 diabetes. This distinction may be attributed to various potential causes and mechanisms. These include dysregulation of specific metabolic pathways involved in amino acid metabolism, such as the branched-chain amino acid (BCAA) pathway, as well as impaired insulin signaling and insulin resistance observed in type 2 diabetes (33, 34). These factors can impact the metabolism of amino acids, including valine and glycine. A study by Vangipurapu et al. (34) demonstrated that nine amino acids (phenylalanine, tryptophan, tyrosine, alanine, isoleucine, leucine, valine,

aspartate, and glutamate) were significantly associated with decreased insulin secretion (disposition index) and elevated fasting or 2-hour glucose levels. Among these amino acids, five (tyrosine, alanine, isoleucine, aspartate, and glutamate) were also significantly associated with an increased risk of developing type 2 diabetes. However, no studies have compared these amino acids between type 1 and type 2 diabetes, necessitating further investigation.

In summary, we are showing that both type 1 and type 2 STZ diabetes models in mice result in deep disturbance of the ICC within the testes leading to defective sperm nuclear maturation and increased oxidative damage. Based on our findings, the most likely reason for these damages is the shortage of intracellular glucose that, besides bioenergetic problems, may generate a reduced flux of carbon units to feed the methylation metabolism. Due to the high relevance of methylations in sperm maturation, the impairment of the ICC is likely involved in the decreased fertility of diabetic patients.

One of the notable innovations of this research is the concurrent assessment of the fundamental components of the 1-carbon cycle and sperm function investigated in both type 1 and type 2 diabetes conditions. The main limitation of the present study is that we could not measure GSH, therefore we cannot confirm that the methylation defect resulted in a shortage of antioxidant defences in our animals. Moreover, we neither measured intracellular glucose nor did we assess the markers of glycolysis to show a reduced activity, therefore the shortage of intracellular glucose that we claim, although very likely to be in place, remains speculative.

However, our findings may have wider implications. Based on our interpretation, the well-known activation of oxidative damage in diabetes seems to be a secondary phenomenon linked to a deficit of the ICC and may have little chance of being corrected by oral antioxidants that, moreover, cannot remedy the defect of methylations. These concerns may explain the conflicting and non-conclusive clinical benefits of dietary or supplemented antioxidants in clinical diabetes (35). The same concerns apply to the effect of metformin on sperm function. Metformin mainly works by decreasing the synthesis of glucose and, although decreasing glycemia, may therefore further decrease the feed of carbon units from glucose and, hence, the sperm methylation defects. Metformin assumption by fathers in the three months before conception was reported to increase by 40% the risk of birth defects in the offspring (36) fitting with a methylation deficit and epigenetic derangement.

## Conclusion

We have observed a distinct impairment of ICC within the testes of individuals with diabetes. We speculate that this impairment may be linked to inadequate intracellular glucose and diminished carbon unit supply associated with diabetes. As a result, interventions focusing on enhancing glucose uptake into sperm cells and providing supplementary methyl donors have the potential to improve fertility issues

in diabetic patients. However, additional clinical testing is required to validate these hypotheses.

## Acknowledgements

We would like to express our gratitude to the staff of the Department of Animal Biotechnology, Reproductive Biomedicine Research Center, Royan Institute for Biotechnology, ACECR, Isfahan, Iran. In addition, we would like to acknowledge the contribution of the chat-based artificial intelligence tool in editing this article. While the content and writing of this article were primarily done by the authors themselves, chat-based AI was only used for editing purposes to enhance the clarity and coherence of the text. The authors declare that they have no competing interests, or financial and personal association with people or organizations that can inappropriately impact this work. There is no professional or other personal interest of any nature or kind in any product, service, and/or company that could be construed as influencing the content of this paper.

## Authors' Contributions

F.P.; Sample preparation, Conduction of experiment, and Data collection. F.K.; Induction of diabetes. M.T., M.D., M.H.N.-E.; Study design, Statistics analysis, Writing the original draft Review, and Editing. All authors have read and approved the final manuscript.

## References

- Diabetes Canada Clinical Practice Guidelines Expert Committee; Punthakee Z, Goldenberg R, Katz P. Definition, classification and diagnosis of diabetes, prediabetes and metabolic syndrome. *Can J Diabetes*. 2018; 42 Suppl 1: S10-S15.
- Caroppo E, Dattilo M. Sperm redox biology challenges the role of antioxidants as a treatment for male factor infertility. *Fertil Steril Rev*. 2022; 3(1): 90-104.
- Marengo B, Nitti M, Furfaro AL, Colla R, Ciucis CD, Marinari UM, et al. Redox homeostasis and cellular antioxidant systems: crucial players in cancer growth and therapy. *Oxid Med Cell Longev*. 2016; 2016: 6235641.
- Yan LJ. Pathogenesis of chronic hyperglycemia: from reductive stress to oxidative stress. *J Diabetes Res*. 2014; 2014: 137919.
- Yang H, Jin X, Kei Lam CW, Yan SK. Oxidative stress and diabetes mellitus. *Clin Chem Lab Med*. 2011; 49(11): 1773-1782.
- Fazakerley DJ, Krycer JR, Kearney AL, Hocking SL, James DE. Muscle and adipose tissue insulin resistance: malady without mechanism? *J Lipid Res*. 2019; 60(10): 1720-1732.
- Sahakyan G, Vejux A, Sahakyan N. The role of oxidative stress-mediated inflammation in the development of T2DM-induced diabetic nephropathy: possible preventive action of tannins and other oligomeric polyphenols. *Molecules*. 2022; 27(24): 9035.
- Rubini E, Bajens IMM, Horánszky A, Schoenmakers S, Sinclair KD, Zana M, et al. Maternal one-carbon metabolism during the periconceptual period and human foetal brain growth: a systematic review. *Genes (Basel)*. 2021; 12(10): 1634.
- Clare CE, Brassington AH, Kwong WY, Sinclair KD. One-carbon metabolism: linking nutritional biochemistry to epigenetic programming of long-term development. *Annu Rev Anim Biosci*. 2019; 7: 263-287.
- Tiwari BK, Pandey KB, Abidi AB, Rizvi SI. Markers of oxidative stress during diabetes mellitus. *J Biomark*. 2013; 2013: 378790.
- Ereño-Orbea J, Majtan T, Oyenarte I, Kraus JP, Martínez-Cruz LA. Structural insight into the molecular mechanism of allosteric activation of human cystathionine  $\beta$ -synthase by S-adenosylmethionine. *Proc Natl Acad Sci USA*. 2014; 111(37): E3845-E3852.
- Menezo YJ, Silvestris E, Dale B, Elder K. Oxidative stress and alterations in DNA methylation: two sides of the same coin in reproduction. *Reprod Biomed Online*. 2016; 33(6): 668-683.
- Bahreini M, Tavalae M, Abbasi H, Kiani-Esfahani A, Shiravi AH, Nasr-Esfahani MH. DNA hypomethylation predisposes sperm to DNA damage in individuals with varicocele. *Syst Biol Reprod Med*. 2015; 61(4): 179-186.
- Tunc O, Tremellen K. Oxidative DNA damage impairs global sperm DNA methylation in infertile men. *J Assist Reprod Genet*. 2009; 26(9-10): 537-544.
- Dattilo M, D'Amato G, Caroppo E, Ménézo Y. Improvement of gamete quality by stimulating and feeding the endogenous antioxidant system: mechanisms, clinical results, insights on gene-environment interactions and the role of diet. *J Assist Reprod Genet*. 2016; 33(12): 1633-1648.
- Ding GL, Liu Y, Liu ME, Pan JX, Guo MX, Sheng JZ, et al. The effects of diabetes on male fertility and epigenetic regulation during spermatogenesis. *Asian J Androl*. 2015; 17(6): 948-953.
- Kilkenny C, Browne WJ, Cuthill IC, Emerson M, Altman DG. Improving bioscience research reporting: The ARRIVE guidelines for reporting animal research. *J Pharmacol Pharmacother*. 2010; 1(2): 94-99.
- Lin CC, Huang WJ, Chen KK. Measurement of testicular volume in smaller testes: how accurate is the conventional orchidometer? *J Androl*. 2009; 30(6): 685-689.
- Zhang LT, Kim HK, Choi BR, Zhao C, Lee SW, Jang KY, et al. Analysis of testicular-internal spermatic vein variation and the re-creation of varicocele in a Sprague-Dawley rat model. *Andrology*. 2014; 2(3): 466-473.
- Tonne JM, Sakuma T, Munoz-Gomez M, El Khatib M, Barry MA, Kudva YC, et al. Beta cell regeneration after single-round immunological destruction in a mouse model. *Diabetologia*. 2015; 58(2): 313-323.
- Pouriyaveali F, Tavalae M, Taktaz-Hafshejani T, Dattilo M, Nasr-Esfahani MH. Overlapping sperm damages from vitamin B or D deficiency in mice: Insights into the role of clinical supplementations. *Andrologia*. 2022; 54(11): e14592.
- Amaral S, Oliveira PJ, Ramalho-Santos J. Diabetes and the impairment of reproductive function: possible role of mitochondria and reactive oxygen species. *Curr Diabetes Rev*. 2008; 4(1): 46-54.
- Andlib N, Sajad M, Kumar R, Thakur SC. Abnormalities in sex hormones and sexual dysfunction in males with diabetes mellitus: A mechanistic insight. *Acta Histochem*. 2023; 125(1): 151974.
- Dimakopoulou A, Jayasena CN, Radia UK, Algeferi M, Minhas S, Oliver N, et al. Animal models of diabetes-related male hypogonadism. *Front Endocrinol (Lausanne)*. 2019; 10: 628.
- Chen M, Zheng H, Xu M, Zhao L, Zhang Q, Song J, et al. Changes in hepatic metabolic profile during the evolution of STZ-induced diabetic rats via an  $^1\text{H}$  NMR-based metabolomic investigation. *Biosci Rep*. 2019; 39(4): BSR20181379.
- Szkudelski T. The mechanism of alloxan and streptozotocin action in B cells of the rat pancreas. *Physiol Res*. 2001; 50(6): 537-546.
- Mueckler M, Thorens B. The SLC2 (GLUT) family of membrane transporters. *Mol Aspects Med*. 2013; 34(2-3): 121-138.
- Jacobs RL, House JD, Brosnan ME, Brosnan JT. Effects of streptozotocin-induced diabetes and of insulin treatment on homocysteine metabolism in the rat. *Diabetes*. 1998; 47(12): 1967-1970.
- Portela JM, Tavares RS, Mota PC, Ramalho-Santos J, Amaral S. High glucose concentrations per se do not adversely affect human sperm function in vitro. *Reproduction*. 2015; 150(1): 77-84.
- Williams AC, Ford WC. The role of glucose in supporting motility and capacitation in human spermatozoa. *J Androl*. 2001; 22(4): 680-695.
- Sowers ML, Herring J, Zhang W, Tang H, Ou Y, Gu W, et al. Analysis of glucose-derived amino acids involved in one-carbon and cancer metabolism by stable-isotope tracing gas chromatography mass spectrometry. *Anal Biochem*. 2019; 566: 1-9.
- Bao J, Bedford MT. Epigenetic regulation of the histone-to-protamine transition during spermiogenesis. *Reproduction*. 2016; 151(5): R55-R70.
- Newgard CB, An J, Bain JR, Muehlbauer MJ, Stevens RD, Lien LF, et al. A branched-chain amino acid-related metabolic signature that differentiates obese and lean humans and contributes to insulin resistance. *Cell Metab*. 2009; 9(6): 565-566.
- Vangipurapu J, Stancáková A, Smith U, Kuusisto J, Laakso M. Nine amino acids are associated with decreased insulin secretion and elevated glucose levels in a 7.4-year follow-up study of 5,181 Finnish men. *Diabetes*. 2019; 68(6): 1353-1358.
- Barrea L, Vetrani C, Verde L, Frias-Toral E, Ceriani F, Cernea S, et al. Comprehensive approach to medical nutrition therapy in patients with type 2 diabetes mellitus: from diet to bioactive compounds. *Antioxidants (Basel)*. 2023; 12(4): 904.
- Wensink MJ, Lu Y, Tian L, Shaw GM, Rizzi S, Jensen TK, et al. Preconception antidiabetic drugs in men and birth defects in offspring: a nationwide cohort study. *Ann Intern Med*. 2022; 175(5): 665-673.